



Establishing Correlations between the Ruthenium Concentration of Cladded 304L Stainless Steel and its Corrosion Resistance in Acidic Media

MSc (50/50) RESEARCH REPORT

Prepared by

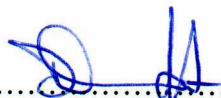
Dominique Tharandt (9507900P)

A research report submitted to the Faculty of Engineering and the Built Environment,
University of the Witwatersrand, Johannesburg, in partial fulfilment of the
requirements for the degree of Master of Science in Engineering

Supervisor: Dr Josias van der Merwe

Johannesburg, October 2015

I, Dominique Tharandt (student number 9507900P), hereby declare that this report is my own unaided work except where references are made and specifically acknowledged below. It is being submitted as a research report for the Master of Science in Engineering to the University of the Witwatersrand, Johannesburg. It has not been submitted previously for any other degree or examination at this or any other university.



.....

On the 14th day of October2015

Abstract

The corrosion behaviour of laser alloyed surface clad 304L stainless steel with ruthenium was evaluated by conducting a series of electrochemical tests including open circuit potential and potentiodynamic polarisation. This research utilised a laser cladding method to obtain an alloyed layer of uniform thickness of various ruthenium concentrations on the 304L stainless steel samples. The resultant compositions of the ruthenium enriched samples were 0.44 wt%, 0.82 wt%, 2.92 wt%, 2.44 wt% and 4.67 wt% ruthenium.

The laser clad samples were exposed to various corrosive agents including sulphuric acid solutions (with and without sodium chloride) as well as hydrochloric acid. The test series was conducted at ambient conditions (25°C) and at elevated temperature (45°C). The corrosion protection offered by the alloyed ruthenium doped samples was compared to that of unclad 304L stainless steel, 316, SAF2205 duplex stainless steel and Hastelloy C276. In this way the most viable application for this form of corrosion protection could be established.

It was observed that the addition of ruthenium showed better results in terms of measured corrosion rates and passivation characteristics compared to the 304L samples without ruthenium. It was also observed that the ruthenium clad samples behaved differently in the different environments and that an optimum ruthenium range exists which was not always at the highest concentrations of the precious metal. A direct correlation of improved corrosion protection with increased ruthenium concentration was more prominently observed in the environments containing chloride; indicating the real benefit of the ruthenium addition.

The introduction of chloride ions to the solution, both via the salt or hydrochloric acid, caused severe attack on the protective layer of the stainless steel and created harsh corrosive conditions that increased the tendency of the sample to corrode and, in the case of hydrochloric acid, introduced pitting corrosion. Higher temperatures had a detrimental effect on all the 304L samples and their alloys.

Passivation was only observed for the 1 M sulphuric acid and 1 M sulphuric acid with 1% sodium chloride solutions at 25°C. It was observed that active corrosion was taking place in all other environments tested. When passivation is achieved, the ruthenium containing samples can compete with commercially available steels providing that the cladding is less than 200 µm thin. Where passivation is not achieved, the SAF2205 and Hastelloy C276 showed equivalent or better corrosion protection.

Acknowledgements

The Department of Science and Technology as well as the National Research Foundation as part of the DST/ NRF Centre of Excellence in Strong Materials funding some of the research that is presented here

The University of the Witwatersrand, School of Chemical and Metallurgical Engineering through which this study was conducted, they supplied all laboratory equipment and facilities required

Dr Josias van der Merwe who is the supervisor for this project, has given me numerous invaluable suggestions and has been most encouraging

Fortunate Moyo who is a fellow student working on her PhD research in a very similar field and who has been most helpful in explaining various concepts as well as equipment set-up issues that could not have been resolved quickly without her

Michael Dinon who is a Principal Materials Engineer for WorleyParsons in Australia and who has had many discussions with me regarding corrosion principals and who most certainly contributed to my understanding of the theory and relating it to my results

Anglo Platinum for sponsoring the ruthenium powder required for preparing the samples being tested

WorleyParsons has been allowing me time and resources for these studies which I appreciate very much

The National Laser Centre, NLC, for preparing all the samples that have been used during this research

Table of Contents

Abstract.....	iii
Acknowledgements.....	iv
List of Figures.....	vii
List of Tables.....	xiii
1. Introduction.....	1
2. Literature Review.....	6
2.1 A phenomenon called Corrosion.....	6
2.2 Corrosion characterisation.....	12
2.3 Stainless Steel.....	21
2.4 Current surface modifying trends for austenitic stainless steels.....	23
2.5 Improvements to the corrosion resistance of stainless steel using Precious Metals.....	27
2.6 Mechanisms to explain why the addition of ruthenium to stainless steels improves corrosion prevention.....	30
2.7 Dissolution behaviour of stainless steels.....	34
3. Experimental Procedure.....	37
3.1 Sample Preparation.....	37
3.2 Laser Surface Alloying Technique.....	38
3.3 Sample Characterisation.....	40
3.3.1 Optical Microscopy.....	41
3.3.2 Scanning Electron Microscopy.....	41
3.4 Corrosion Characterisation.....	42
4. Results.....	48
4.1 Microstructural Characterisation.....	48
4.2 Microstructure Analysis.....	53
4.3 Electrochemical Testing.....	57
4.3.1 1 M H ₂ SO ₄ solution at 25°C.....	57
4.3.2 1 M H ₂ SO ₄ + 1% NaCl solution at 25°C.....	74
4.3.3 1 M H ₂ SO ₄ solution at 45°C.....	93
4.3.4 1 M H ₂ SO ₄ + 1% NaCl solution at 45°C.....	107
4.3.5 1 M HCl solution at 25°C.....	123
4.3.6 Comparisons of the different environments.....	141
5. Discussion.....	148
5.1 Energy Dispersive Spectroscopy.....	148
5.2 Microstructural Analysis.....	150
5.3 Electrochemical Testing.....	153

5.3.1	1 M H ₂ SO ₄ solution at 25°C	154
5.3.2	1 M H ₂ SO ₄ + 1% NaCl solution at 25°C	163
5.3.3	1 M H ₂ SO ₄ solution at 45°C	170
5.3.4	1 M H ₂ SO ₄ + 1% NaCl solution at 45°C	175
5.3.5	1 M HCl solution at 25°C	181
5.3.6	Cost analysis of the ruthenium alloys	186
6.	Conclusion	190
7.	Recommendations.....	193
7.1	Further testwork with the available samples.....	193
7.2	Application method.....	193
7.3	Alternative corrosion prevention to be tested	194
7.4	Industrial applications.....	195
7.5	Analytical questions.....	196
8.	References.....	197
	Appendices.....	206
	Appendix A – Publications and Presentations	206
	Appendix B - Calculations.....	207
	Appendix C - EDS analysis of all samples	208
	Appendix D - 1 M H ₂ SO ₄ solution at 25°C	209
	Appendix E - 1 M H ₂ SO ₄ + 1% NaCl solution at 25°C.....	215
	Appendix F - 1 M H ₂ SO ₄ solution at 45°C.....	220
	Appendix G - 1 M H ₂ SO ₄ + 1% NaCl solution at 45°C	226
	Appendix H - 1 M HCl solution at 25°C	231

List of Figures

Figure 1: Corrosion taking place, rusting of a metal in atmospheric conditions, adopted from Maass (2013) and Ebbing (1990).....	7
Figure 2: Log i vs E diagram showing where corrosion is taking place.....	10
Figure 3: Iron equilibrium diagram, Bradford (2001)	11
Figure 4: Corrosion process showing anodic and cathodic current components, adopted from Stern and Geary (1957).....	13
Figure 5: Typical Polarisation Diagram of a material exhibiting cathodic and anodic regions, adopted from Jones (1996) and Wright (2014).....	15
Figure 6: Polarisation Diagram illustrating change in potential	16
Figure 7: Log i vs E comparison with E vs time curves	17
Figure 8: Schematic diagram of potential controlled polarisation curves - Case 1	18
Figure 9: Schematic diagram of potential controlled polarisation curves - Case 2	18
Figure 10: Schematic diagram of potential controlled polarisation curves - Case 3	19
Figure 11: Schematic diagram of potential controlled polarisation curves - Case 4	19
Figure 12: Schematic diagram of potential controlled polarisation curves - Case 5	20
Figure 13: Schematic diagram of potential controlled polarisation curves - Case 6	20
Figure 14: Microstructure changes based on the addition of nickel to the steel (DSS, 2007).22	
Figure 15: Effect of ruthenium on the corrosion potential of steel (adapted from Potgieter et al., 1990)	32
Figure 16: Potentiodynamic cyclic polarisation curves for various alloys increasing their ruthenium additions and exposure in 2 M HCl solution; taken from Sherif et al. (2009)	36
Figure 17: Graphical application of the laser cladding onto a base plate	39
Figure 18: Samples used for the experimentation where A is the cladded coupon, B is the hot mounted sample for SEM analysis and C is the cold mounted sample for electrochemical testing.....	39
Figure 19: Laser Surface cladding performed at the National Laser Centre	40
Figure 20: Selection of a suitable area for EDS analysis.....	42
Figure 21: Electrochemical Cell used for all electrochemical experimentation	44
Figure 22: Experimental set-up in the university's Corrosion Laboratory	46
Figure 23: Surface view of the blank stainless steel sample.....	49
Figure 24: 0 wt% Ru laser cladded sample, (a) surface view (b) a cross sectional view	50
Figure 25: 2.92 wt% Ru laser cladded sample, (a) surface view and (b) cross-sectional view	50
Figure 26: 2.44 wt% Ru laser cladded sample, (a) surface view and (b) cross-sectional view	51
Figure 27: Higher magnification cross-sectional view of the 2.44 wt% Ru laser cladded sample	51
Figure 28: 4.67 wt% Ru laser cladded sample, (a) surface view and (b) cross-sectional view	52
Figure 29: Higher magnification surface view of the 4.67 wt% Ru laser cladded sample.....	52
Figure 30: Microstructural view of the interface of the 0.44 wt% Ru sample.....	54
Figure 31: Microstructural view of the interface of the 0.82 wt% Ru sample.....	55
Figure 32: Microstructural view of the interface of the 2.44 wt% Ru sample, both images show the samples at different magnifications and different sections of the sample.....	55
Figure 33: Microstructural view of the alloyed section of the 2.44 wt% Ru sample	56
Figure 34: Microstructural view of the interface of the 4.67 wt% Ru sample, both images show the samples at different magnifications and different sections of the sample.....	56

Figure 35: Microstructural view of the interface of the 4.76 wt% Ru sample at higher magnification	57
Figure 36: Log i vs E graphs for the Stainless Steel blank sample in 1 M H ₂ SO ₄ at 25°C.....	58
Figure 37: E vs time graphs for the Stainless Steel blank sample in 1 M H ₂ SO ₄ at 25°C.....	59
Figure 38: Log i vs E graphs for the 0.82 wt% Ru sample in 1 M H ₂ SO ₄ at 25°C.....	60
Figure 39: E vs time graphs for the 0.82 wt% Ru sample in 1 M H ₂ SO ₄ at 25°C.....	60
Figure 40: Log i vs E graphs for the 4.67 wt% Ru sample in 1 M H ₂ SO ₄ at 25°C.....	61
Figure 41: E vs time graphs for the 4.67 wt% Ru sample in 1 M H ₂ SO ₄ at 25°C.....	62
Figure 42: Log i vs E graphs from the exposed surface scan comparing all samples in 1 M H ₂ SO ₄ at 25°C.....	63
Figure 43: Log i vs E graphs from the fresh surface scan comparing all samples in 1 M H ₂ SO ₄ at 25°C.....	64
Figure 44: E vs time graphs comparing all samples in 1 M H ₂ SO ₄ at 25°C.....	65
Figure 45: E _{corr} comparison at various ruthenium compositions for the exposed surface scan in 1 M H ₂ SO ₄ at 25°C	66
Figure 46: i _{corr} comparison at various ruthenium compositions for the exposed surface scan in 1 M H ₂ SO ₄ at 25°C	66
Figure 47: i at 0.2V comparison at various ruthenium compositions for the exposed surface scan in 1 M H ₂ SO ₄ at 25°C	67
Figure 48: Corrosion rate at various ruthenium compositions for the exposed surface scan in 1 M H ₂ SO ₄ at 25°C	67
Figure 49: Polarisation resistance at various ruthenium compositions for the exposed surface scan in 1 M H ₂ SO ₄ at 25°C	68
Figure 50: OCP comparison at various ruthenium compositions from the exposed surface scan in 1 M H ₂ SO ₄ at 25°C	68
Figure 51: E _{corr} comparison at various ruthenium compositions from the fresh surface scan in 1 M H ₂ SO ₄ at 25°C	69
Figure 52: i _{corr} comparison at various ruthenium compositions from the fresh surface scan in 1 M H ₂ SO ₄ at 25°C	70
Figure 53: Corrosion rate comparison at various ruthenium compositions from the fresh surface scan in 1 M H ₂ SO ₄ at 25°C.....	70
Figure 54: Polarisation resistance comparison at various ruthenium compositions from the fresh surface scan in 1 M H ₂ SO ₄ at 25°C.....	71
Figure 55: Log I vs E graphs from the exposed surface scan comparing ruthenium samples to other steels in 1 M H ₂ SO ₄ at 25°C	73
Figure 56: Log i vs E graphs from the fresh surface scan comparing ruthenium samples to other steels in 1 M H ₂ SO ₄ at 25°C	74
Figure 57: Log i vs E graphs for the Stainless Steel blank sample in 1 M H ₂ SO ₄ + 1% NaCl at 25°C.....	75
Figure 58: E vs time graphs for the Stainless Steel blank sample in 1 M H ₂ SO ₄ + 1% NaCl at 25°C.....	76
Figure 59: Log i vs E graphs for the 0.82 wt% Ru sample #1 in 1 M H ₂ SO ₄ + 1% NaCl at 25°C.....	77
Figure 60: Log E vs time graphs for the 0.82 wt% Ru sample #1 in 1 M H ₂ SO ₄ + 1% NaCl at 25°C.....	77
Figure 61: Log i vs E graphs for the 0.82 wt% Ru sample #2 in 1 M H ₂ SO ₄ + 1% NaCl at 25°C.....	78
Figure 62: E vs time graphs for the 0.82 wt% Ru sample #2 in 1 M H ₂ SO ₄ + 1% NaCl at 25°C.....	79

Figure 63: Log i vs E graphs for the 4.67 wt% Ru sample in 1 M H ₂ SO ₄ + 1% NaCl at 25°C	80
Figure 64: E vs time graphs for the 4.67 wt% Ru sample in 1 M H ₂ SO ₄ + 1% NaCl at 25°C	80
Figure 65: Log i vs E graphs from the exposed surface scan comparing all samples in 1 M H ₂ SO ₄ + 1% NaCl at 25°C	81
Figure 66: Log i vs E graphs from the fresh surface scan comparing all samples in 1 M H ₂ SO ₄ + 1% NaCl at 25°C	82
Figure 67: E vs time graphs comparing all samples in 1 M H ₂ SO ₄ + 1% NaCl at 25°C	83
Figure 68: E _{corr} comparison at various ruthenium compositions from the exposed surface scan in 1 M H ₂ SO ₄ + 1% NaCl at 25°C	84
Figure 69: i _{corr} comparison at various ruthenium compositions from the exposed surface scan in 1 M H ₂ SO ₄ + 1% NaCl at 25°C	85
Figure 70: j at 0.1V comparison at various ruthenium compositions from the exposed surface scan in 1 M H ₂ SO ₄ + 1% NaCl at 25°C	85
Figure 71: Corrosion rate comparison at various ruthenium compositions from the exposed surface scan in 1 M H ₂ SO ₄ + 1% NaCl at 25°C	86
Figure 72: Polarisation resistance comparison at various ruthenium compositions from the exposed surface scan in 1 M H ₂ SO ₄ + 1% NaCl at 25°C	86
Figure 73: OCP comparison at various ruthenium compositions from the exposed surface scan in 1 M H ₂ SO ₄ + 1% NaCl at 25°C	87
Figure 74: E _{corr} comparison at various ruthenium compositions from the fresh surface scan in 1 M H ₂ SO ₄ + 1% NaCl at 25°C	88
Figure 75: i _{corr} comparison at various ruthenium compositions from the fresh surface scan in 1M H ₂ SO ₄ + 1% NaCl at 25°C	89
Figure 76: Corrosion rate comparison at various ruthenium compositions from the fresh surface scan in 1 M H ₂ SO ₄ + 1% NaCl at 25°C	89
Figure 77: Polarisation resistance comparison at various ruthenium compositions from the fresh surface scan in 1 M H ₂ SO ₄ + 1% NaCl at 25°C	90
Figure 78: Log I vs E graphs from the exposed surface scan comparing ruthenium samples to other steels in 1 M H ₂ SO ₄ + 1% NaCl at 25°C	92
Figure 79: Log i vs E graphs from the fresh surface scan comparing ruthenium samples to other steels in 1 M H ₂ SO ₄ + 1% NaCl at 25°C	93
Figure 80: Log i vs E graphs for the Stainless Steel blank sample in 1 M H ₂ SO ₄ at 45°C	94
Figure 81: E vs time graphs for the Stainless Steel blank sample in 1 M H ₂ SO ₄ at 45°C	94
Figure 82: Log i vs E graphs for the 0.82 wt% Ru sample in 1 M H ₂ SO ₄ at 45°C	95
Figure 83: E vs time graphs for the 0.82 wt% Ru sample in 1 M H ₂ SO ₄ at 45°C	96
Figure 84: Log i vs E graphs for the 4.67 wt% sample in 1 M H ₂ SO ₄ at 45°C	97
Figure 85: E vs time graphs for the 4.67 wt% Ru sample in 1 M H ₂ SO ₄ at 45°C	97
Figure 86: Log i vs E graphs from the exposed surface scan comparing all samples in 1 M H ₂ SO ₄ at 45°C	98
Figure 87: Log i vs E graphs from the fresh surface scan comparing all samples in 1 M H ₂ SO ₄ at 45°C	99
Figure 88: E vs time graphs comparing all samples in 1 M H ₂ SO ₄ at 45°C	100
Figure 89: E _{corr} comparison at various ruthenium compositions from the exposed surface scan in 1 M H ₂ SO ₄ at 45°C	101
Figure 90: i _{corr} comparison at various ruthenium compositions from the exposed surface scan in 1 M H ₂ SO ₄ at 45°C	102
Figure 91: Current density at 0.1 V comparison at various ruthenium compositions from the exposed surface scan in 1 M H ₂ SO ₄ at 45°C	102

Figure 92: Corrosion rate comparison at various ruthenium compositions from the exposed surface scan in 1 M H ₂ SO ₄ at 45°C.....	103
Figure 93: Polarisation resistance at various ruthenium compositions from the exposed surface scan in 1 M H ₂ SO ₄ at 45°C.....	103
Figure 94: OCP comparison at various ruthenium compositions from the exposed surface scan in 1 M H ₂ SO ₄ at 45°C	104
Figure 95: E _{corr} comparison at various ruthenium compositions from the fresh surface scan in 1 M H ₂ SO ₄ at 45°C	105
Figure 96: i _{corr} comparison at various ruthenium compositions from the fresh surface scan in 1 M H ₂ SO ₄ at 45°C	105
Figure 97: Corrosion rate comparison at various ruthenium compositions from the fresh surface scan in 1 M H ₂ SO ₄ at 45°C.....	106
Figure 98: Polarisation resistance comparison at various ruthenium compositions from the fresh surface scan in 1 M H ₂ SO ₄ at 45°C.....	106
Figure 99: Log i vs E graphs for the Stainless Steel blank sample in 1 M H ₂ SO ₄ + 1% NaCl at 45°C.....	108
Figure 100: E vs time graphs for the Stainless Steel blank sample in 1 M H ₂ SO ₄ + 1% NaCl at 45°C.....	109
Figure 101: Log i vs E graphs for the 0.82 wt% Ru sample in 1 M H ₂ SO ₄ + 1% NaCl at 45°C	110
Figure 102: E vs time graphs for the 0.82 wt% Ru sample in 1 M H ₂ SO ₄ + 1% NaCl at 45°C	110
Figure 103: Log i vs E graphs for the 4.67 wt% Ru sample in 1 M H ₂ SO ₄ + 1% NaCl at 45°C	111
Figure 104: E vs time graph for the 4.67 wt% Ru sample in 1 M H ₂ SO ₄ + 1% NaCl at 45°C	112
Figure 105: Log i vs E graphs from the exposed surface scan comparing all samples in 1 M H ₂ SO ₄ + 1% NaCl at 45°C	113
Figure 106: Log i vs E graphs from the fresh surface scan comparing all samples in 1 M H ₂ SO ₄ + 1% NaCl at 45°C	114
Figure 107: E vs time graphs comparing all samples in 1 M H ₂ SO ₄ + 1% NaCl at 45°C.....	114
Figure 108: E _{corr} comparison at various ruthenium compositions from the exposed surface scan in 1 M H ₂ SO ₄ + 1% NaCl at 45°C	116
Figure 109: i _{corr} comparison at various ruthenium compositions from the exposed surface scan in 1 M H ₂ SO ₄ + 1% NaCl at 45°C	116
Figure 110: Current density at 0.1 V comparison at various ruthenium compositions from the exposed surface scan in 1 M H ₂ SO ₄ + 1% NaCl at 45°C	117
Figure 111: Corrosion rate comparison at various ruthenium compositions from the exposed surface scan in 1 M H ₂ SO ₄ + 1% NaCl at 45°C.....	117
Figure 112: OCP value comparison at various ruthenium compositions from the exposed surface scan in 1 M H ₂ SO ₄ + 1% NaCl at 45°C.....	118
Figure 113: E _{corr} comparison at various ruthenium compositions from the fresh surface scan in 1 M H ₂ SO ₄ + 1% NaCl at 45°C	119
Figure 114: i _{corr} comparison at various ruthenium compositions from the fresh surface scan in 1 M H ₂ SO ₄ + 1% NaCl at 45°C	119
Figure 115: Corrosion rate comparison at various ruthenium compositions from the fresh surface scan in 1 M H ₂ SO ₄ + 1% NaCl at 45°C.....	120
Figure 116: Log i vs E graphs from the exposed surface scan comparing ruthenium samples to other steels in 1 M H ₂ SO ₄ + 1% NaCl at 45°C	122

Figure 117: Log i vs E graphs from the fresh surface scan comparing ruthenium samples to other steels in 1 M H_2SO_4 + 1% NaCl at 45°C	123
Figure 118: Log i vs E graphs for the Stainless Steel blank sample in 1 M HCl at 25°C.....	124
Figure 119: E vs time graphs for the Stainless Steel blank sample in 1 M HCl at 25°C.....	125
Figure 120: Log i vs E graphs for the 0.82 wt% Ru sample in 1 M HCl at 25°C.....	126
Figure 121: E vs time graphs for the 0.82 wt% Ru sample in 1 M HCl at 25°C.....	126
Figure 122: Log i vs E graphs for the 4.67 wt% sample in 1 M HCl at 25°C	127
Figure 123: E vs time graphs for the 4.67 wt% Ru sample in 1 M HCl at 25°C.....	128
Figure 124: Log i vs E graphs from the exposed surface scan comparing all samples in 1 M HCl at 25°C.....	129
Figure 125: Log i vs E graphs from the fresh surface scan comparing all samples in 1 M HCl at 25°C.....	130
Figure 126: E vs time graphs comparing all samples in 1 M HCl at 25°C	131
Figure 127: E_{corr} comparison at various ruthenium compositions from the exposed surface scan in 1 M HCl at 25°C	132
Figure 128: i_{corr} comparison at various ruthenium compositions from the exposed surface scan in 1M HCl at 25°C	133
Figure 129: Current density at 0.1 V comparison at various ruthenium compositions from the exposed surface scan in 1 M HCl at 25°C.....	133
Figure 130: Corrosion rate comparison at various ruthenium compositions from the exposed surface scan in 1 M HCl at 25°C.....	134
Figure 131: Polarisation resistance comparison at various ruthenium compositions from the exposed surface scan in 1 M HCl at 25°C.....	134
Figure 132: E_{corr} comparison at various ruthenium compositions from the fresh surface scan in 1 M HCl at 25°C	135
Figure 133: i_{corr} comparison at various ruthenium compositions from the fresh surface scan in 1 M HCl at 25°C	136
Figure 134: Corrosion rate comparison at various ruthenium compositions from the fresh surface scan in 1 M HCl at 25°C.....	136
Figure 135: Polarisation resistance comparison at various ruthenium compositions from the fresh surface scan in 1 M HCl at 25°C.....	137
Figure 136: Log i vs E graphs from the exposed surface scan comparing ruthenium samples to other steels in 1 M HCl at 25°C	138
Figure 137: Log i vs E graphs from the fresh surface scan comparing ruthenium samples to other steels in 1 M HCl at 25°C	140
Figure 138: E vs time graphs comparing ruthenium samples to other steels in 1 M HCl at 25°C.....	140
Figure 139: Log i vs E graphs from the exposed surface scan comparing the stainless steel blank sample in different environments.....	142
Figure 140: Log i vs E graphs from the fresh surface scan comparing the stainless steel blank sample in different environments.....	143
Figure 141: Log i vs E graphs from the exposed surface scan comparing the 0.82 wt% Ru sample in different environments.....	144
Figure 142: Log i vs E graphs from the fresh surface scan comparing the 0.82 wt% Ru sample in different environments.....	145
Figure 143: Log i vs E graphs from the exposed surface scan comparing the 4.67 wt% Ru sample in different environments.....	146
Figure 144: Log i vs E graphs from the fresh surface scan comparing the 4.67 wt% Ru sample in different environments.....	147

Figure 145: Cross sectional view of the 2.92 wt% Ru sample indicating different surface exposure possibilities	150
Figure 146: Equilibrium Phase Diagram of the Fe-Ru system	153
Figure 147: Log i vs E graphs for the two 0.82 wt% Ru samples in 1 M H ₂ SO ₄ + 1% NaCl at 25°C.....	164
Figure 148: Log i vs E graphs for the 0 wt% Ru sample in 1 M H ₂ SO ₄ at 25°C.....	209
Figure 149: E vs time graphs for the 0 wt% Ru sample in 1 M H ₂ SO ₄ at 25°C	210
Figure 150: Log i vs E graphs for the 0.44 wt% Ru sample in 1 M H ₂ SO ₄ at 25°C.....	210
Figure 151: E vs time graphs for the 0.44 wt% Ru sample in 1 M H ₂ SO ₄ at 25°C.....	211
Figure 152: Log i vs E graphs for the 2.92 wt% Ru sample in 1 M H ₂ SO ₄ at 25°C.....	212
Figure 153: E vs time graphs for the 2.92 wt% Ru sample in 1 M H ₂ SO ₄ at 25°C	212
Figure 154: Log i vs E graphs for the 2.44 wt% Ru sample in 1 M H ₂ SO ₄ at 25°C.....	213
Figure 155: E vs time graphs for the 2.44 wt% Ru sample in 1 M H ₂ SO ₄ at 25°C	213
Figure 156: Log i vs E graphs for the 0 wt% Ru sample in 1 M H ₂ SO ₄ + 1% NaCl at 25°C	215
Figure 157: E vs time graph for the 0 wt% Ru sample in 1 M H ₂ SO ₄ + 1% NaCl at 25°C...	216
Figure 158: Log i vs E graphs for the 2.92 wt% Ru sample in 1 M H ₂ SO ₄ + 1% NaCl at 25°C	217
Figure 159: E vs time graphs for the 2.92 wt% Ru sample in 1 M H ₂ SO ₄ + 1% NaCl at 25°C	217
Figure 160: Log i vs E graphs for the 2.44 wt% Ru sample in 1 M H ₂ SO ₄ + 1% NaCl at 25°C	218
Figure 161: E vs time graphs for the 2.44 wt% Ru sample in 1 M H ₂ SO ₄ + 1% NaCl at 25°C	218
Figure 162: Log i vs E graphs for the 0 wt% Ru sample in 1 M H ₂ SO ₄ at 45°C.....	220
Figure 163: E vs time graphs for the 0 wt% Ru sample in 1 M H ₂ SO ₄ at 45°C	221
Figure 164: Log i vs E graphs for the 2.92 wt% Ru sample in 1 M H ₂ SO ₄ at 45°C.....	222
Figure 165: E vs time graphs for the 2.92 wt% Ru sample in 1 M H ₂ SO ₄ at 45°C	222
Figure 166: Log i vs E graphs for the 2.44 wt% Ru sample in 1 M H ₂ SO ₄ at 45°C.....	223
Figure 167: E vs time graphs for the 2.44 wt% Ru sample in 1 M H ₂ SO ₄ at 45°C.....	224
Figure 168: Log i vs E graphs for the 0 wt% Ru sample in 1 M H ₂ SO ₄ + 1% NaCl at 45°C	226
Figure 169: E vs time graphs for the 0 wt% Ru sample in 1 M H ₂ SO ₄ + 1% NaCl at 45°C.	227
Figure 170: Log i vs E graphs for the 2.92 wt% Ru sample in 1 M H ₂ SO ₄ + 1% NaCl at 45°C	227
Figure 171: E vs time graphs for the 2.92 wt% Ru sample in 1 M H ₂ SO ₄ + 1% NaCl at 45°C	228
Figure 172: Log i vs E graphs for the 2.44 wt% Ru sample in 1 M H ₂ SO ₄ + 1% NaCl at 45°C	229
Figure 173: E vs time graphs for the 2.44 wt% Ru sample in 1 M H ₂ SO ₄ + 1% NaCl at 45°C	229
Figure 174: Log i vs E graphs for the 0 wt% Ru sample in 1 M HCl at 25°C.....	231
Figure 175: E vs time graphs for the 0 wt% Ru sample in 1 M HCl at 25°C	232
Figure 176: Log i vs E graphs for the 2.92 wt% Ru sample in 1 M HCl at 25°C.....	233
Figure 177: E vs time graphs for the 2.92 wt% Ru sample in 1 M HCl at 25°C.....	233
Figure 178: Log i vs E graphs for the 2.44 wt% Ru sample in 1 M HCl at 25°C.....	234
Figure 179: E vs time graphs for the 2.44 wt% Ru sample in 1 M HCl at 25°C	235

List of Tables

Table 1: Samples tested for this research report	38
Table 2: Equivalent weight and current density values	46
Table 3: Composition of the laser alloyed surface of the stainless steel	48
Table 4: Chemical Analysis of the stainless steel base plate	49
Table 5: Chemical Analysis of the laser cladding section of the samples	53
Table 6: Indicators of corrosion rate using average sample measurements from the exposed surface scan in 1 M H ₂ SO ₄ at 25°C	65
Table 7: Indicators of corrosion rate using average sample measurements from the fresh surface scan in 1 M H ₂ SO ₄ at 25°C	69
Table 8: Passivation potential comparison to OCP values at 1 M H ₂ SO ₄ at 25°C	71
Table 9: Indicators of corrosion rate using average sample measurements from the exposed surface scan in 1 M H ₂ SO ₄ + 1% NaCl at 25°C	84
Table 10: Indicators of corrosion rate using average sample measurements from the fresh surface scan in 1M H ₂ SO ₄ + 1% NaCl at 25°C	88
Table 11: Passivation potentials comparison to OCP values in 1 M H ₂ SO ₄ + 1% NaCl at 25°C	91
Table 12: Indicators of corrosion rate using average sample measurements from the exposed surface scan in 1 M H ₂ SO ₄ at 45°C	101
Table 13: Indicators of corrosion rate using average sample measurements from the fresh surface scan in 1 M H ₂ SO ₄ at 45°C	104
Table 14: Passivation potentials comparison to OCP values in 1 M H ₂ SO ₄ at 45°C	107
Table 15: Indicators of corrosion rate using average sample measurements from the exposed surface scan in 1 M H ₂ SO ₄ + 1% NaCl at 45°C	115
Table 16: Indicators of corrosion rate using average sample measurements from the fresh surface scan in 1 M H ₂ SO ₄ + 1% NaCl at 45°C	118
Table 17: Passivation potentials comparison to OCP values in 1 M H ₂ SO ₄ + 1% NaCl at 45°C	120
Table 18: Indicators of corrosion rate using average sample measurements from the exposed surface scan in 1 M HCl at 25°C	132
Table 19: Indicators of corrosion rate using average sample measurements from the fresh surface scan in 1 M HCl at 25°C	135
Table 20: Passivation potentials comparison to OCP values in 1 M HCl at 25°C	137
Table 21: Cost analysis of only the material costs for the different ruthenium claddings in Rand	187
Table 22: EDS Analysis obtained for the 2 nd batch of tested samples	208
Table 23: Results from the exposed surface scan in 1 M H ₂ SO ₄ at 25°C	214
Table 24: Results from the fresh surface scan in 1 M H ₂ SO ₄ at 25°C	214
Table 25: Results from the exposed surface scan in 1 M H ₂ SO ₄ + 1% NaCl at 25°C	219
Table 26: Results from the fresh surface scan in 1 M H ₂ SO ₄ + 1% NaCl at 25°C	219
Table 27: Results from the exposed surface scan in 1 M H ₂ SO ₄ at 45°C	224
Table 28: Results from the fresh surface scan in 1 M H ₂ SO ₄ at 45°C	225
Table 29: Results from the exposed surface scan in 1 M H ₂ SO ₄ + 1% NaCl at 45°C	230
Table 30: Results from the fresh surface scan in 1 M H ₂ SO ₄ + 1% NaCl at 45°C	230
Table 31: Results from the exposed surface scan in 1 M HCl at 25°C	235
Table 32: Results from the fresh surface scan in 1 M HCl at 25°C	236

1. Introduction

Stainless steel is defined as a steel alloy with a minimum chromium content of 10.5 wt%. The quality and grade of the stainless steel determine its corrosion resistance (SSINA, 2014). The base element in stainless steel is iron (Fe) and to this chromium (Cr) is added in order to turn it into a corrosion-resistant alloy. Carbon (C) is always included in stainless steel; small amounts are often included to increase hardness and strength but can have a detrimental effect on the corrosion resistance of the stainless steel, if chrome carbides form it could lead to sensitisation and intergranular corrosion (SSINA, 2014). Nickel (Ni) is the essential alloying element in the 300 series stainless steel grades as it results in the formation of the austenitic structure that gives these grades their ductility and toughness. While the role of nickel has no direct influence on the development of the passive surface layer, it results in significant improvement in resistance to acid attack, particularly in sulfuric acid media (SSINA, 2014). Other alloying elements such as molybdenum (Mo) and titanium (Ti) may be added to improve heat and corrosion-resistant properties. According to the ASSDA (2014) all stainless steels have a high resistance to corrosion: low alloyed grades resist corrosion in atmospheric conditions while highly alloyed grades resist corrosion in most acids, alkaline solutions and chloride bearing environments, even at elevated temperatures and pressures.

Type 304 stainless steels are most commonly used in industrial applications and are relatively inexpensive compared to more corrosion resistant types (ISSF, 2014). According to Crawford (2014) it represented 25.8% of the global stainless steel production in 2013. Thus finding ways to economically improve its corrosion resistance would be of industrial importance. Duplex stainless steels, which are specifically formulated for corrosion protection and added strength, have mixed phases of austenite and ferrite, are expensive and can be up to 65% higher in cost than 304L stainless steel (MacSteel, 2014). Therefore, surface treated 304L stainless steels (UNS designation of the material is UNS S30403) may become economically more attractive where higher strength is not required.

Worldwide the cost of corrosion is significant and certain industries, such as the oil and gas industry, are well known for constantly having to spend large sums of money on corrosion prevention and maintenance. A study conducted in 2012 by the United States (US) Department of Transportation Federal Highway Administration (FHWA) identified their direct cost of corrosion totalling well over \$100 billion (Koch et al., 2014). The authors then

extrapolated these figures to the total US economy to obtain a total cost of corrosion of \$276 billion; which is 3.1 % of the Gross Domestic Product (GDP) of the USA. A study conducted by the University of Witwatersrand in 2004 revealed that the direct cost of corrosion to the South African economy is estimated to be 154 billion Rand every year (Webb, 2011). This is comparable with the rest of the world; De la Fuente et al. (2014) discussed that in Europe corrosion costs 450 billion Euros a year which is between 3 to 5% of their GDP. A study by the US Department of Energy (DOE) showed that more than half of all unplanned power outages are due to corrosion (Rebak and Dolley, 2014). Other studies in different third world countries indicated that between 25% and 30% of water supply is lost in the supply chain due to corrosion. These figures indicate that there is scope to make a significant economic difference in adding to the knowledge of finding more corrosion resistant materials. Several independent studies presented at EuroCorr 2014 (Kajiyama; Diminich et al.; Al Subai et al. and Kittel et al.) showed that 25% of the effects and costs of corrosion can be prevented by applying known corrosion technology, for example, by applying surface coatings to the metal.

Surface treatment techniques are only applied on the surfaces exposed to corrosion attack which makes them less costly and more effective than bulk alloying as the alloying element(s) are kept where they are most required. The research in this report focuses only on corrosion protection on the surface of the austenitic stainless steel 304L since corrosion is a surface dependent degradation method. Corrosion control is primarily an economic problem and the choice of control is therefore determined by the cost saving involved. Although the initial cost of a corrosion protection system, such as proposed by this report, might seem high, it is important to take the entire life cycle of the protected system into account. The benefits of a good corrosion control system include lower maintenance, fewer lost man/machine hours and lower risk due to a reduced probability of a safety related incident occurring.

One of the qualities of stainless steel of interest to metallurgists and chemical engineers is that it is self-repairing. Stainless steels derive their corrosion resistance from a very thin surface layer (1 – 3 nm as per Henkel, 2003) which is formed during the reaction between the alloy and air (specifically the oxygen in the air). The chromium, through passivation, forms an invisible compact adherent layer of chromium oxide (Cr_2O_3) over the iron to protect it from most corrosive environments. If the surface is damaged, chromium would simply form a

new oxide layer in the presence of oxygen. This is why high quality stainless steel will not rust if it were scratched. Streicher (1977) already described that this is not a passive state but a dynamic one and small amounts of continuing metal dissolution are required to maintain it. Certain environments, however, cause permanent breakdown of this passive layer and enhanced corrosion occurs on the unprotected surface. According to Jones (1996), all stainless steels generally show good corrosion resistance in oxidising acids (e.g. HNO₃) but are not always able to retain their passive layer in non-oxidising acids (e.g. HCl). Other studies (Fontana, 1986; Hoyle & Taylor, 1993 and Varga et al., 1997), specifically investigating austenitic stainless steels, confirmed that the ability to form the protective chromium oxide layer is greatly diminished in chloride and reducing acid solutions. This renders the stainless steel susceptible to active corrosion in these environments and therefore limits the application and service life of this group of steels. The demand for stainless steel is ever growing and it is thus of economic importance to improve the corrosion resistance of these alloys through research and development. The evaluation of a more corrosion resistant surface coating for 304L stainless steel is the subject of investigation in this research report.

In general, the ever increasing demand for more corrosion resistant materials in more severe environments in conjunction with global pressures for reducing costs and therefore, structures and plants requiring less maintenance, corrosion resistant materials of construction have always been carefully considered for each application. Tjong et al. (1997) showed an improvement of the corrosion resistance in reducing acids by the addition of small amounts of palladium (Pd) and ruthenium (Ru); 0.2 wt% was sufficient. Ruthenium containing alloys of stainless steel have been gaining focus in recent years by, for example, Potgieter and Brookes (1995), Banda and van der Merwe (2014), Govender (2012), Myburg et al. (1998) and Sherif et al. (2009) clearly stated that it was well known that the corrosion resistance, electrochemical and pitting corrosion, of all types of stainless steels is significantly increased by alloying them with small amounts of Platinum Group Metals (PGMs).

Like the other members of the platinum group metals, ruthenium is inert to most other chemicals. The metal was found to induce passivity of stainless steel in sulphuric acid without compromising resistance to pitting in oxidising chloride environments (Streicher, 1977 and Sherif, 2012). In their proposed surface alloy (0.3 wt% Ru addition tested in 2 M HCl and 0.6 M NaCl), they suggested that ruthenium is the metal that protects the 304L

stainless steel by either providing an inert barrier between the steel and the environment or by catalysing the cathodic evolution of hydrogen, or both.

Ruthenium is by far the cheapest of the PGMs, its value being up to 24 times less than that of platinum (London Metal Exchange, 2014). It is therefore of most interest to industry, from an economic point of view, when investigating its passivation processes on stainless steels and corrosion reducing mechanisms for the purpose of alloying it with stainless steels increasing their benefit of corrosion protection. Nickel, which is less costly, can be substituted for the comparatively expensive ruthenium but larger amounts would be required. Streicher (1977) observed this and reported that “passivity and self-repassivation can also be produced in the 28-4 alloy by addition of 2 per cent nickel to this composition with the same effect on other forms of corrosion attacks at that of the 0.5 per cent ruthenium addition”.

South Africa is the world’s largest producer of Platinum Group Metals and contributed 76% of the world’s 6.06 million Troy ounces (Toz) of Platinum metal produced in 2010 (Butler, 2011). In 2011 alone the PGM mining industry generated 84 billion Rand for the South African economy, accounting for 17% of the country’s total exports (Facts and Figures, 2012). Ruthenium is a byproduct from the mining and refining of platinum and is not mined for its own sake. In 2010 the demand for ruthenium stood at 945 000 Toz and decreased by 14% the year after (Butler, 2012) which keeps its price relatively low. Focusing research on finding a possible application and market for ruthenium may stimulate the interest in the metal and thus has the potential to increase future demands.

It has been observed, by Potgieter et al. (1995) amongst others, that the addition of small amounts of ruthenium improves the corrosion resistance of stainless steel. They stated that during active corrosion, ruthenium additions to stainless steel cause an increase in its resistance to anodic dissolution and lowers its hydrogen over-potential. This implies that ruthenium inhibits the corrosion of the alloy by the combination of the two mechanisms suggested above. They furthermore showed that during active dissolution, ruthenium caused an increase in the corrosion potential and lowered the critical as well as the passivation current densities of the stainless steel. It is understood that stainless steel, alloyed with minor ruthenium additions, passivates spontaneously due to the formation of a stable passive layer of significantly increased corrosion resistance. Their research showed that this shifts the corrosion potential of these alloys towards more noble (more positive) values. They had found in their research that this corrosion phenomenon depends on the medium of exposure.

Bulk alloying is still considered expensive, and since corrosion is a surface phenomenon, recent research (Lekala et al., 2012) indicates a tendency to only add the alloy to the surface where corrosion protection is most required. The investigations by Lekala et al. (2012) sparked interest into laser surface cladding where 316L stainless steel was alloyed with ruthenium and nickel mixtures. The same laser cladding technique and equipment (4.4 kW Rofin Sinar diode pumped Nd:YAG laser) was used in this research to add to the knowledge obtained by the team. Type 304 and 304L, or one of its modifications, is the material specified more than 50% of the time whenever a stainless steel is used (MacSteel, 2014) which is why it was selected for this study. The laser alloyed layer studied by Lekala et al. (2012) consisted of 5 – 10 wt% Ru and 9 – 23 wt% Ni while this research considered 1 wt% to 5 wt% Ru but did not look at altering the nickel composition. The exposure medium studied originally was sulphuric acid only while, during this investigation, the exposure effects of different types of acidic media and salt additions were being studied. Variations of temperature have also been considered in this research broadening the knowledge base in this field significantly. The microstructures of the different laser alloyed zones have been compared and their significance to their corrosion resistance investigated. It was expected that a specific ruthenium composition in the surface cladded layer will give the best results and that these may vary depending on the corrosive media. This is exactly what was observed in this study. The intention of this research report was to evaluate the results from a technical perspective as well as an economic one to achieve maximum corrosion enhancement with minimal cost as industrial applications can only be found if there are economic benefits.

The objectives of this research were:

- a. To characterise the microstructure of the 304L stainless steel laser cladded layer and the effects which varying ruthenium additions (%Ru added: 0.0, 1.0, 2.0, 3.0, 4.0 and 5.0 wt%) have on the phases that form within the surface layer
- b. To investigate how different types of acidic media (H_2SO_4 , H_2SO_4 with NaCl and HCl) and temperatures of exposure ($25^\circ C$ and $45^\circ C$) affect the corrosion resistance of the different stainless steel surfaces
- c. To determine the cost effectiveness of the laser cladding method for actual industrial applications

2. Literature Review

2.1 A phenomenon called Corrosion

Corrosion is the degradation of a material (mostly metals) by its environment: it literally means to ‘gnaw away’ (Jones, 1996) and thus leads to the loss of useful properties. It is further mentioned (Jones, 1996) that pure metals and alloys have a higher energy state than the products formed by their interaction with the natural environment, usually oxides and sulphides, and there is a natural tendency to return to their lowest energy state. The type and rate of corrosion depends upon the type of materials involved and the environment they are exposed to. It can be very rapid in a highly corrosive environment or take thousands of years in an only slightly corrosive environment. Corrosion, whether in the atmosphere, underwater or underground, is caused by the flow of electrons, from one metal to another metal or from one part of the surface of a piece of metal to another part of the same metal (Jones, 1996). For this to occur an electrolyte must be present, this could be an aqueous medium contaminated with salts, so that the flow of electrons can take place. Corrosion therefore involves at least two reactions: oxidation and reduction and it occurs only when the total rate of oxidation equals the total rate of reduction. The three corrosion phenomena expected to occur during this study are:

- Uniform surface attack occurs where the metal/material is almost uniformly removed from the surface. This form of corrosion is also the basis for the determination of the corrosion rate.
- Shallow pit formation is when irregular surface attack forms pits with diameters much larger than their depth.
- Pitting is a form of corrosion with crater-shaped or surface-excavating pits resembling pin pricks. The depth of the pitting spots usually exceeds their diameter. It is very difficult to differentiate between shallow pit formation and pitting.

There are other types of corrosion such as Stress Corrosion Cracking (SCC) and Galvanic Corrosion as well as Biological and Microbiologically Influenced Corrosion (MIC) but these are not studied for this research.

Uniform surface corrosion is an electrochemical process creating a voltaic cell. It is most common and easily observed when iron rusts. This can be seen schematically in Figure 1.

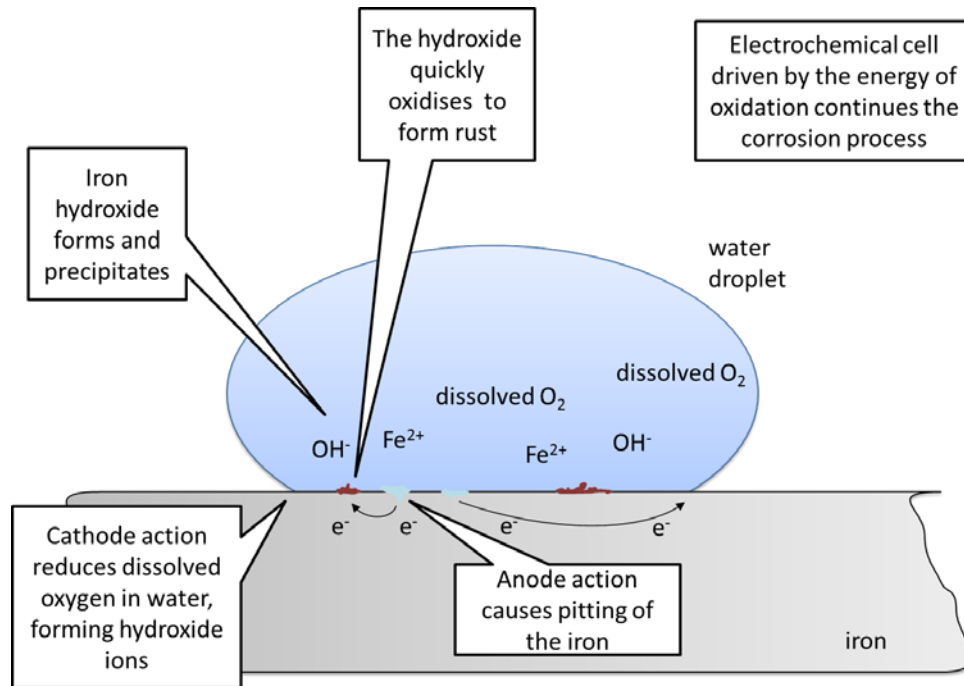


Figure 1: Corrosion taking place, rusting of a metal in atmospheric conditions, adopted from Maass (2013) and Ebbing (1990)

During corrosion, the oxidising iron supplies electrons to reduce the dissolved oxygen from the air as the cathodic reaction. The iron surface inside the droplet acts as the anode where the metallic ions dissolve to go into solution according to the following process:



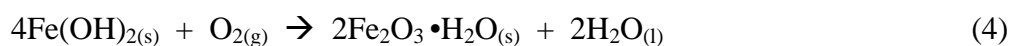
The electrolyte carries ions from the anode to the cathode. The electrons can move through the metallic iron to the outside of the droplet where dissolved oxygen is reduced:



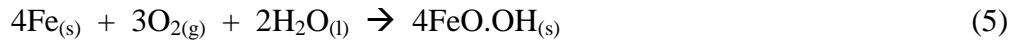
Within the droplet, the hydroxide ions can move inward to react with the Fe^{2+} ions so that iron hydroxide is precipitated:



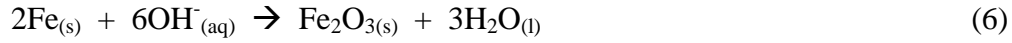
Rust is then produced by the oxidation of the precipitate:



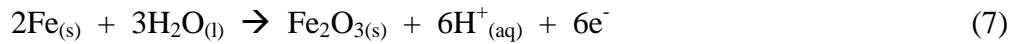
Combining reactions (1) and (2) can also produce a different form of iron hydroxide which can be oxidised to form rust:



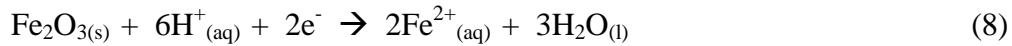
The anodic oxidation process in alkali could also occur via the following reaction:



In higher pH solutions, the anodic reaction directly produces a surface film of ferric oxide, as per Wright (2014) according to the reaction:



This surface film can be reduced cathodically in an acid environment according to:



The rusting of unprotected iron in the presence of air and water is then inevitable; driven by an electrochemical process (Kotz and Purcell, 1991). In fact, nearly all metals will corrode in an oxidising environment forming metal oxides, hydroxides or sulphides; as per Roberge (2006) and Wright (2014). They also state in their respective texts that these reactions are normally exothermic.

The reduction reaction is not necessarily the oxygen reduction reaction, especially in an environment that is not directly exposed to atmospheric conditions. Hydrogen ion reduction may also occur at the cathode especially if hydrogen ions are present in the environment such as when the steel is exposed to acidic media as per the following reaction:



The fact is, however, that all the above process steps have to occur simultaneously for electrochemical corrosion to take place. The electrons that are provided into the solution by the metal must equal the electrons that are taken up by the hydrogen to form a gas or by the oxygen to form the metal hydroxide. This forms the bases of Mixed Potential Theory as described in Jones (1996) and Fontana (1979).

As per these authors mixed potential is defined as the effective potential of the metal surface in contact with an electrolyte that is driving electrochemical corrosion, its principals are based in the fact that the total rate of oxidation must equal the total rate of reduction. This

means that “the sum of anodic oxidation currents must equal the sum of cathodic reduction currents” (Jones, 1996). Mixed potential theory explains metal corrosion as a reaction of two or more electrodes working simultaneously at the interface of the given metal surface and electrolyte. It includes both anodic and cathodic polarisation in which diffusion of species is related to the current flowing in the electrolyte. The kinetic parameters that are determined form an Evans diagram ($\log i$ vs E graph) are the corrosion potential and the corrosion current densities. Electrochemical corrosion is caused by these mixed electrodes formed on the metal surface, with oxidation directly coupled to the reduction reaction. The resulting potential of the electrodes is the mixed potential, driving corrosion. That needs to be controlled for the elimination of the corrosive reaction.

Therefore Mixed Potential Theory states that, when two half-cell reactions occur simultaneously on a metal surface, the potential will polarise to an intermediate value called the system potential (Jones, 1996 and Fontana, 1979). Further they state that when a metal dissolves in an acid, the theoretical system potential and exchange current density can be found at the intercept of the anodic reaction, of the metal going into solution (as per reaction 1), and the cathodic reaction, of the acid reducing to hydrogen gas (as per reaction 9).

This is shown in the graph below, Figure 2, at the point of E_{system} and i_{system} . At the system potential, all the rates (current densities) are equal, i.e. $i_{\text{cathodic}} = i_{\text{anodic}} = i_{\text{system}}$. These are the system details if only two reactions are taking place. If further reactions are occurring, one has to consider all of these reactions and find the total anodic and total cathodic lines. This is achieved by adding up all the anodic potentials and current densities along the anodic ‘leg’ as well as all the cathodic potentials and current densities along the cathodic ‘leg’. Where these two lines intercept, the new system potential and system current density are found and this is the point where corrosion is taking place; Jones (1996) and Fontana (1979).

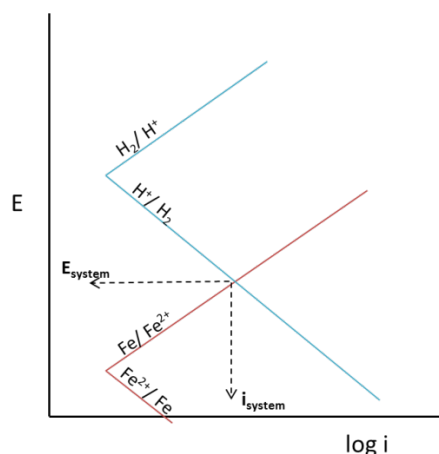


Figure 2: Log i vs E diagram showing where corrosion is taking place

The environment in which corrosion is taking place defines the type and rate of corrosion as well as the reaction products. In fact, at a specific temperature and electrolyte conditions, the electrode potential, E , defines the products of corrosion, i.e. which reactions actually do take place from the ones listed above. Normally, a thermodynamic E -pH diagram is helpful in this regard. Figure 3 is an example of such; it shows the stable forms of iron at 25°C in water; taken from Bradford (2001). The graph shows that at negative potentials, approximately -0.6 V and below, metallic iron is stable and therefore no corrosion is possible. At higher potentials and acidic pH values, ferrous ions (Fe^{2+}) will form giving rise to active corrosion while ferric ions (Fe^{3+}) are only produced at potentials above 0.7 V. Diagrams, such as the one shown in Figure 3 are widely used to predict corrosion products and are helpful in explaining corrosion activity.

In order to understand the rate of corrosion, one must examine the electrochemical polarisation curves of the electrode reactions which take place on the metal surface. Since the reaction rate is proportional to the flow of electrons (measured as current, i), the current density shows the magnitude of corrosion as a function of potential; examples of such curves are given in the results section of this report.

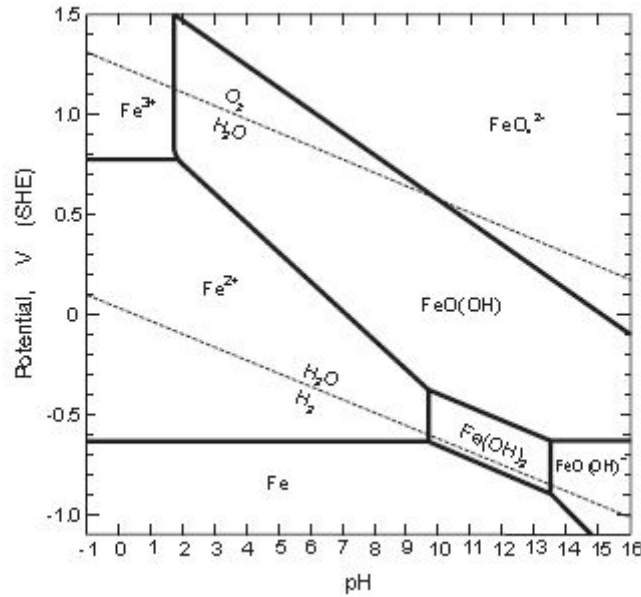


Figure 3: Iron equilibrium diagram, Bradford (2001)

Corrosion attack on a metal can only occur at the surface of the metal where it comes into contact with an electrolyte and oxygen or an oxidising agent. Any modifications to the surface or its environment can change the rate of reaction. Hence this will form the basis for designing methods to protect metals from corrosion. The aim of active corrosion protection is to influence the reactions which proceed during corrosion, i.e. it being possible to control the reactions themselves in such a manner that corrosion is avoided or drastically reduced. Examples of such an approach are the development of corrosion-resistant alloys and the addition of inhibitors to aggressive, corrosive medium.

Corrosion protection techniques include a variety of concepts (Wright, 2014):

- Removal of the oxidising agent
- Prevention of the surface reaction by cathodic or anodic protection; these will include sacrificial anodes and impressed current processes
- Inhibition of the surface reaction by chemical inhibitors and pH control
- Protective coatings which range from paint to galvanising, electroplating and anodising
- Modification of the metal which includes developing alloys
- Modification of surface conditions such as designing to avoid reactive metal combinations or maintenance to remove corrosive agents in the system

2.2 Corrosion characterisation

The equilibrium at an electrode is dynamic which means that the ionic species are produced and discharged simultaneously at the conducting surface, i.e. the metal dissolves as ions and ions deposit back on the metal surface at equal rates, Fontana (1979). This implies that the magnitude of the current leaving and entering the metal at equilibrium is the same and is called the exchange current density. Activation energy is the excess energy required to dissolve the metal atoms at the metal surface into metal ions in solution, well explained by Martinez and Stern (2001). If the equilibrium is disturbed, a net current flows across the electrode surface displacing the potential in a direction depending to an extent on the direction and magnitude of the current. This shift in potential is called polarisation and its value is the overpotential (Jones, 1996).

The model used to describe the corrosion process assumes that the rates of both the anodic and cathodic processes are controlled by the kinetics of the electron transfer reaction at the metal surface (Lorenz and Mansfeld, 1981 and Jones 1996). This is generally the case for corrosion reactions. The relationship between the rates of an electro-chemical reaction, which are directly proportional to the current density, and the driving force of such a reaction, the electrode potential, for a system undergoing activation polarisation is described by the Butler-Volmer equation (Jones, 1996 and Noren and Hoffman, 2005):

$$i = i_o \exp \left[\frac{\alpha n F (E - E_{equ})}{RT} \right] - i_o \exp \left[\frac{-(1-\alpha)n F (E - E_{equ})}{RT} \right] \quad (A)$$

Where:

- i = electrode current, i.e. the current resulting from the reaction
- i_o = a reaction dependent constant called the exchange current
- α = a symmetry factor or charge transfer coefficient; also the reaction's Tafel constant (constant for a given reaction)
- n = the number of electrons involved in the electrochemical reaction
- F = Faraday's constant, 96487 C
- E = electrode potential = E_{system}
- E_{equ} = equilibrium potential (constant for a given reaction)
- R = universal gas constant, 8.314 J/mol.K
- T = temperature of the system

And the overpotential is defined as:

$$\eta = E - E_{corr} \quad (B)$$

From the experimentally obtained polarisation diagram, a plot on linear axis results in a small region of linearity around E_{system} , i.e. at low overpotentials the Butler-Volmer equation is linear and the Stern Geary equation applies (Jones, 1996 and Pardo et al., 2010):

$$i = i_o \frac{nF}{RT} \eta \quad (C)$$

A tangent line can be constructed along this region which both the anodic and cathodic curves would generally have; the intersection of the tangent lines gives i_{system} and E_{system} . This is graphically shown in Figure 4, adopted from Stern and Geary (1957).

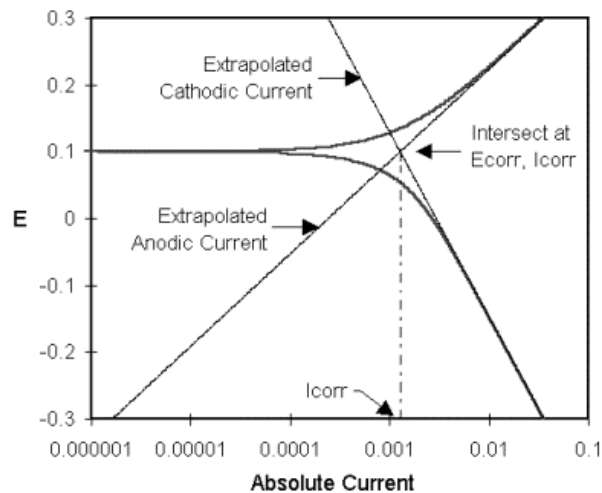


Figure 4: Corrosion process showing anodic and cathodic current components, adopted from Stern and Geary (1957)

This means that at small overpotentials, the electrochemical response is linear and the slope of this region is known as the polarisation resistance (R_p) which is inversely proportional to the corrosion current density. At slightly higher potentials and on an E vs $\log i$ graph, the linear regions are known as Tafel regions, these have a Tafel slope which is graphically represented in Figure 5. The Tafel equations therefore describe polarisation kinetics under activation control.

$$R_p = \frac{\Delta \text{overpotential}}{\Delta i_{\text{applied}}} \quad (D)$$

According to Jones (1996) and Pardo et al. (2010), as the overpotential tends to zero, the slope R_p is also inversely proportional to the corrosion rate, and equation (C) can be re-written as follows:

$$R_p = \frac{\beta_a \beta_c}{2.3 i_{corr} (\beta_a + \beta_c)} \quad (E)$$

Where: i_{corr} = corrosion current density
 β_a and β_c = Tafel constants for the anodic and cathodic reactions respectively

The requirement is that both β_a and β_c are positive in the above equations (Jones, 1996). Approximate values of the Tafel constants are suggested as $\beta_a = \beta_c = 0.1$ V (Jones, 1996) but experimentally obtained values are used for further calculations.

Rearranging the equations above gives the Tafel equations for both the anodic (subscript a) and cathodic (subscript c) reactions taking place, where they have the following equations:

$$\eta_a = b_a \log(i/i_o) \quad \text{and} \quad \eta_c = b_c \log(i/i_o) \quad (F)$$

Where b is the Tafel slope and is defined as $b = 2.3 RT/\alpha nF$

A potentiodynamic scan must be run slow enough to ensure equilibrium is reached and meaningful results are obtained. i_{corr} can be calculated from equation (E) once the Tafel constants and the polarisation resistance are obtained from experimental curves, or estimated in some cases. The corrosion rate, r, can then be calculated by applying Faraday's Law (Jones, 1996) as follows:

$$r = \frac{m}{t A} = \frac{j a}{n F} = 0.00327 \frac{j a}{n \rho} \quad \left[\frac{mm}{yr} \right] \quad (G)$$

Where: m = mass reacted [g]
 t = time [sec]
 A = exposed surface area [cm²]
 j = current density = i/A [A/cm²]
 a = atomic weight [g/mol]
 n = the number of electrons involved in the electrochemical reaction
 F = Faraday's constant, 96487 C
 ρ = density of the material [g/cm³]

The equivalent weight of an alloy, $1/N_{eq}$, must be considered, which is the ratio of a/n in the above equation, and is the weighted average for its alloying elements. They can be calculated as follows (Jones, 1996):

$$N_{eq} = 1 / \sum \left(\frac{f_i \cdot n_i}{a_i} \right) \quad (H)$$

The anodic and cathodic reactions are all part of the same system. Observing the system over a specified potential range, with the associated liberation and consumption of electrons, is graphically represented in Figure 5. The exchange current density of the system, j_o but sometimes still referred to as i_o , is affected by the nature of the surface on which the reaction(s) occur. This implies that kinetics, i.e. the rate of reaction, is strongly affected by the metal that is reacting.

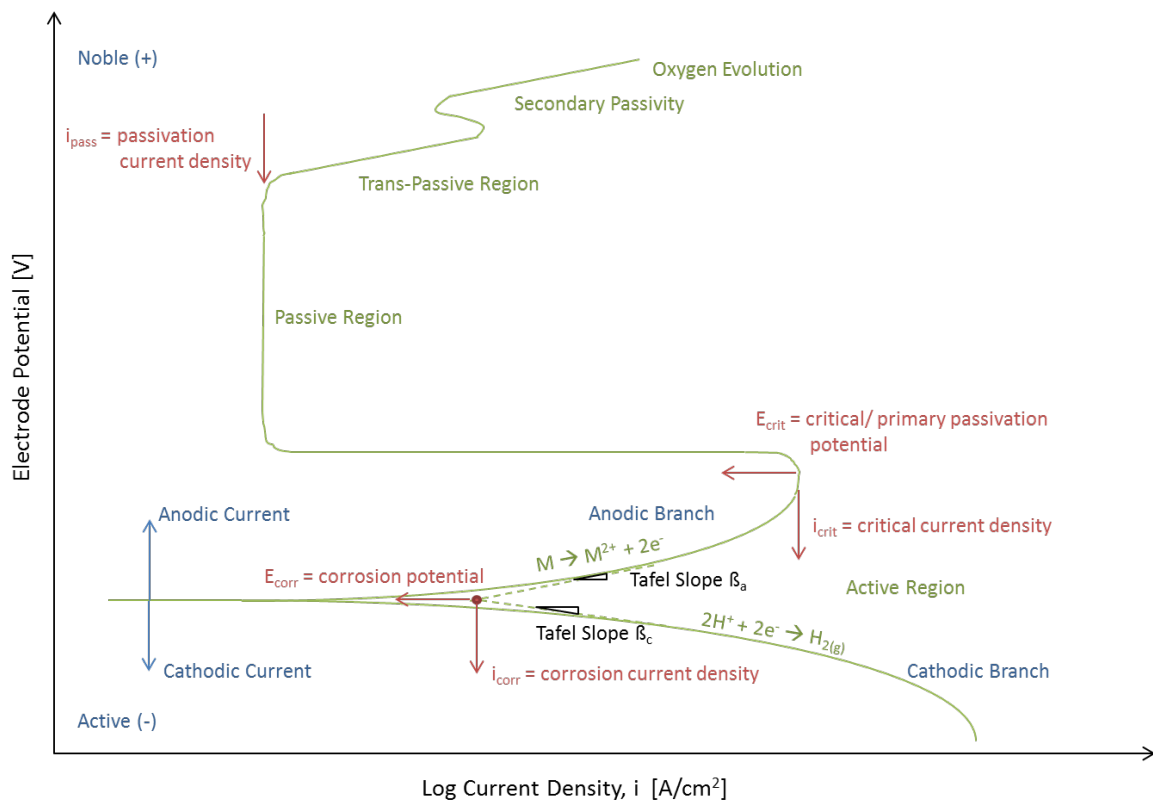


Figure 5: Typical Polarisation Diagram of a material exhibiting cathodic and anodic regions, adopted from Jones (1996) and Wright (2014)

In the active region, the metal corrodes as the applied potential is increased. As the ‘active nose’ is reached, further increase in the corrosion rate, measured by the current, ceases and that is where the onset of passivation occurs. Normally the formation of a passive film on the

metal surface causes passivation, as potential is increased further. Where that film breaks down, by further increasing the potential applied, is the start of the trans-passive region.

Passivity is the reduction in the corrosion rate that occurs due to the formation of a thin, oxidised, protective film on the metal surface. In order for the film to be protective however, it must be uniform and continuous, stable, tenacious and self-repairing (Henkel and Henkel, 2003, Higginson et al., 1989 and Van der Merwe, 2012). It is said (Jones, 1996) that as temperature increases the entire graphs shifts to the right increasing the current densities and thus increasing the overall rate of corrosion.

Some metals in specific environments can be anodically protected by increasing the potential to encourage passivity of the metal surface. However, anodic protection can also increase corrosion if passivity does not occur because the anodic dissolution is accelerated at these higher potentials. This is a direct application of the equations (A) and (F) above and can be seen in Figure 6.

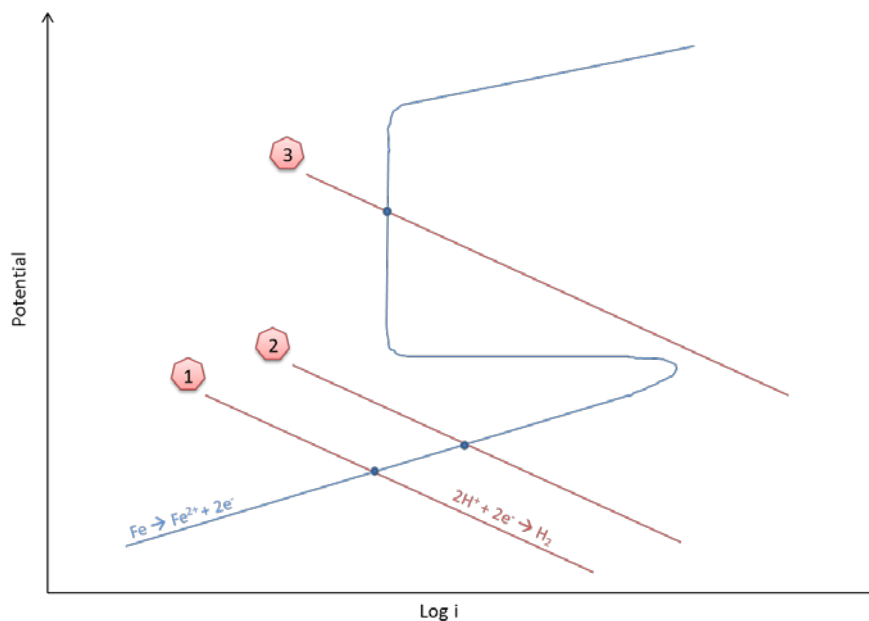


Figure 6: Polarisation Diagram illustrating change in potential

From Figure 6 it can be seen that moving from line 1 to line 2, the corrosion potential, E_{corr} , increases but so does the corrosion current density, i_{corr} and thus the corrosion rate. Moving further towards line 3, the E_{corr} increases again, but i_{corr} , and thus the corrosion rate, drop because passivity is induced. Observing higher potentials thus has the possibility of increasing or decreasing corrosion rates depending on whether passivity is reached. This can

then be seen when measuring the open circuit potential over an extended period of time, illustrated in Figure 7 below.

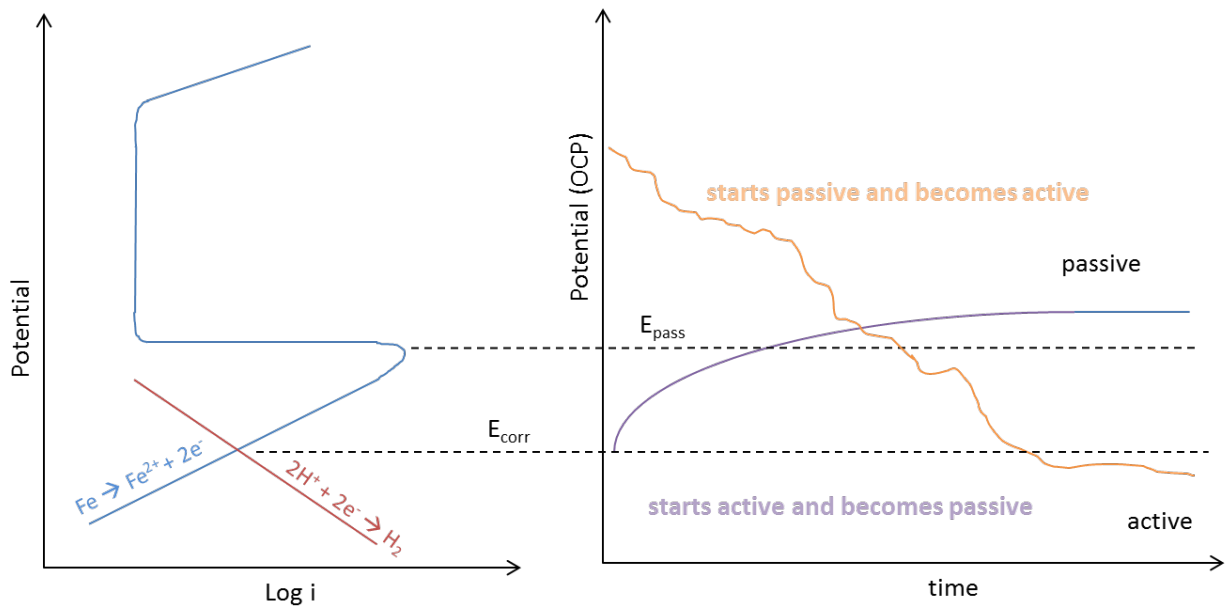


Figure 7: Log i vs E comparison with E vs time curves

The polarisation curve is experimentally determined and measures the current difference between the anodic and cathodic curves of the Evans diagram. It shows the electrode kinetic data and is sometimes referred to as Mixed Potential Diagram, Ahmad (2006). The cases that are possible for describing the behaviour of stainless steel are shown in the diagrams below (Figure 8 to Figure 13). The curves on the right hand side show the experimentally obtained polarisation diagram under various conditions while the curves on the left hand side indicate the respective equivalent Evans curves which theoretically explain how the reactions are occurring on the surface of the metal. It is critical to understand these in order to describe and explain what is happening in the system from a corrosion point of view.

If the cathodic curve intersects the anodic curve in the active region, as in Figure 8, the sample will corrode rapidly even though it may be passivated under different experimental conditions. If the cathodic curve intersects the anodic curve as in Figure 9, the sample can experience either high or low corrosion rates: it intersects in the active, partially passive and passive regions. Experimentally, cathodic current loops are observed after the ‘active nose’ transitioning from the active into the passive region. Multiple loops can be observed (Talbot and Talbot, 2007) as the anodic and cathodic lines become superimposed. They explain that throughout a certain potential range the current density is fluctuating between being positive and negative during which the sample is experiencing large fluctuations in the corrosion rate.

This is undesirable in practice as the surface thought to be passive can be rendered active by, for example, scratching the passive film. Once active, the surface may not passivate again and corrosion occurs rapidly destroying the material. If the cathodic curve intersects the anodic curve in the passive region, as in Figure 10, the material will passivate spontaneously and is therefore the most desirable. The remaining curves are deviations and specifics of the ones described already. Potentiodynamic polarisation measurements are valuable tools in order to compare sample environment conditions so that the most suitable materials and/or least destructive environments can be selected.

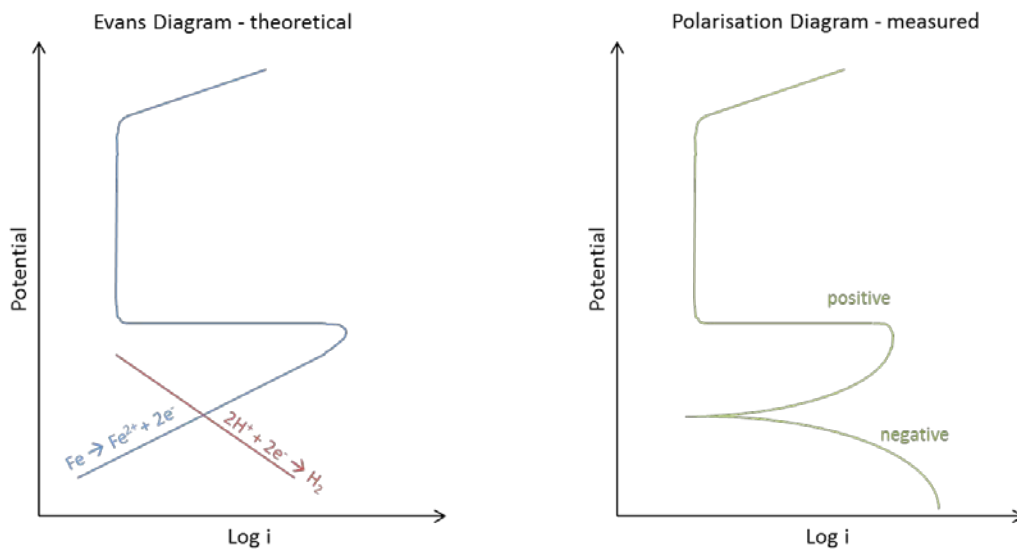


Figure 8: Schematic diagram of potential controlled polarisation curves - Case 1

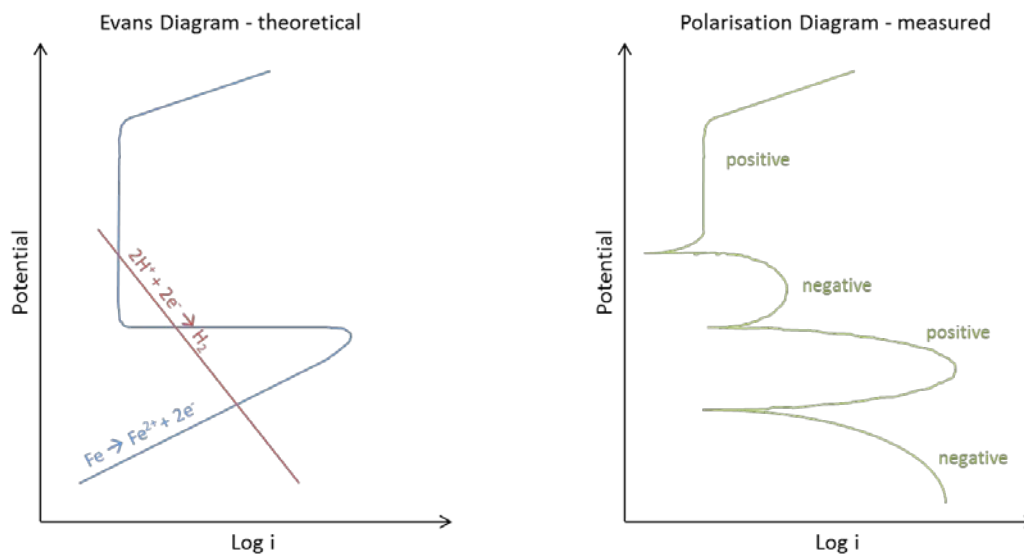


Figure 9: Schematic diagram of potential controlled polarisation curves - Case 2

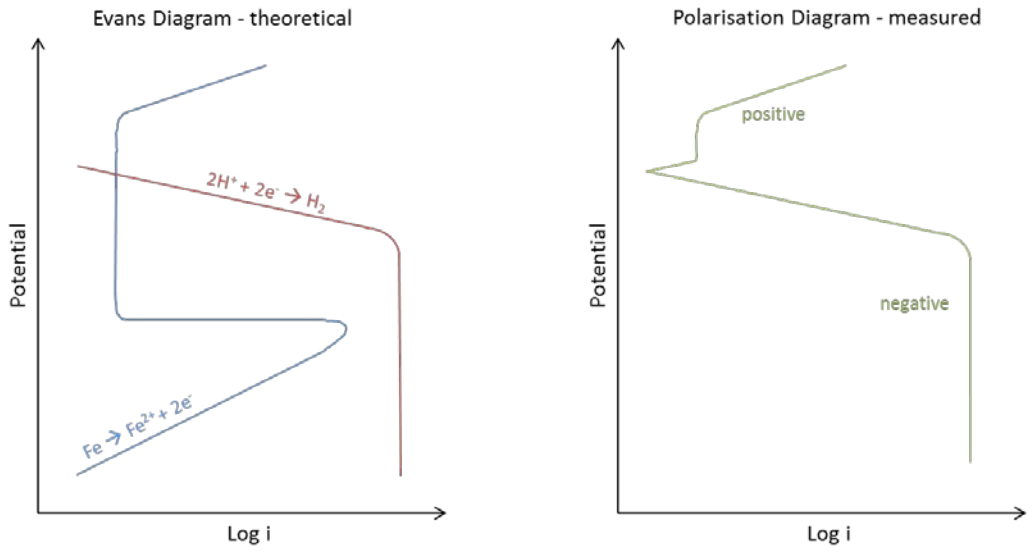


Figure 10: Schematic diagram of potential controlled polarisation curves - Case 3

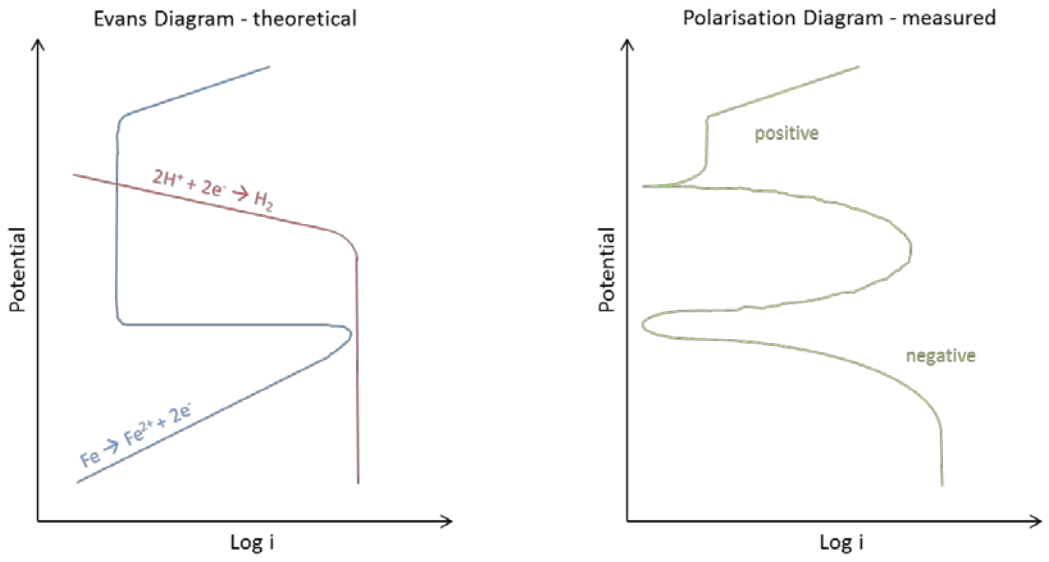


Figure 11: Schematic diagram of potential controlled polarisation curves - Case 4

All these curves are adopted from Talbot and Talbot (2007)

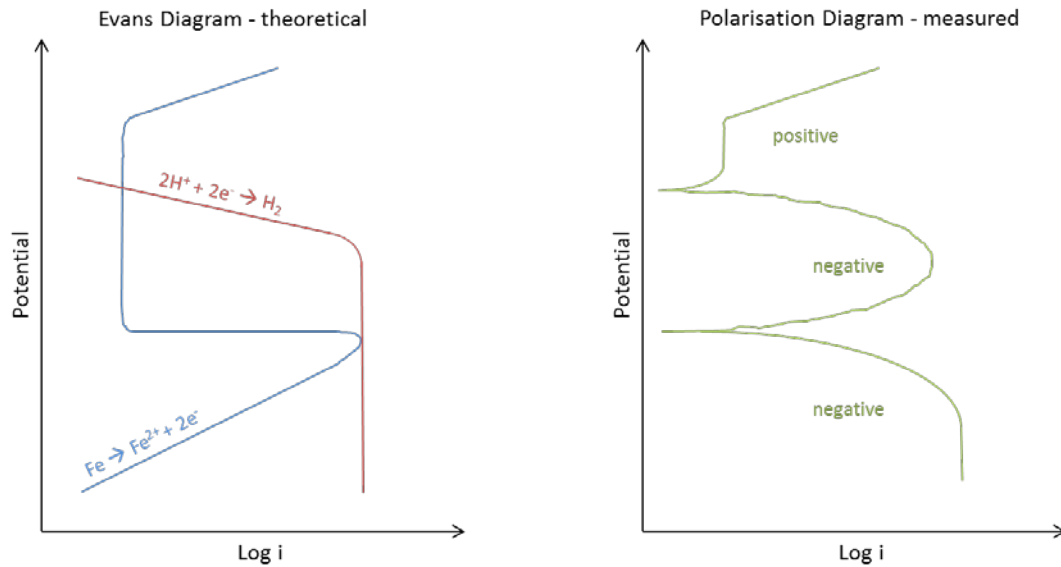


Figure 12: Schematic diagram of potential controlled polarisation curves - Case 5

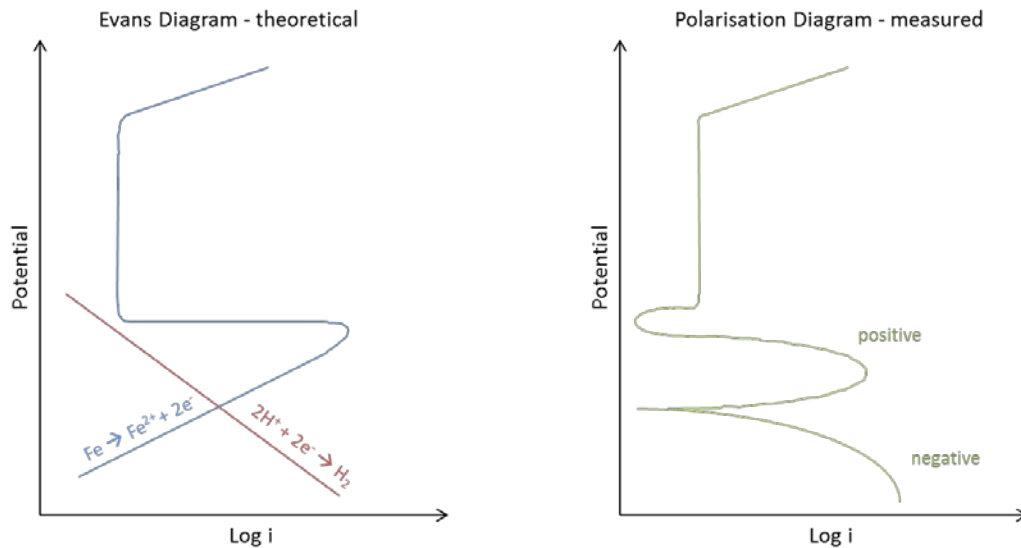


Figure 13: Schematic diagram of potential controlled polarisation curves - Case 6

During experimental testing, the electrochemical behaviour of the metal is unknown and needs to be experimentally determined. E_{system} is measured against a known reference potential by way of a voltmeter (Jones, 1996 and Talbot & Talbot, 2007). The corrosion rate is, however, still unknown and more complicated to determine because the corrosion current inside the metal cannot be measured directly. In such cases an external current is applied to the metal which can be measured and causes a “change away from the corrosion potential” (van der Merwe, 2012). This is called polarisation. It is measured using a three electrode set-up: the current applied and flowing between the working electrode and counter electrode is measured by an inbuilt ammeter while the change in potential due to this current is measured by an inbuilt voltmeter between the working electrode and the reference electrode. The

greater the current applied, the further polarisation away from E_{system} takes place (van der Merwe, 2012).

2.3 Stainless Steel

Stainless steels are typically classified by their crystalline structure into five distinct categories (Jones, 1996, Davis, 1994, ASSDA, 2014, BSSA, 2014 and Outokumpu Stainless Steel Oy, 2004). The microstructure inherent in each steel group is a function of the primary alloying elements.

Austenitic stainless steels, the 200 and 300 series, have an austenitic, i.e. a face-centered cubic, crystal structure. They contain a minimum of 16% chromium and sufficient nickel and/or manganese to retain an austenitic structure at all temperatures from the cryogenic region to the melting point of the alloy. The most widely used austenitic steel is 304 Stainless Steel, also known as *18/8* for its composition of 18% chromium and 8% nickel. Type 304 is also referred to as A2 stainless. The second most common austenite steel is the 316 grade, also called marine grade stainless, used primarily for its increased resistance to corrosion. The basic properties of austenitic stainless steel include excellent corrosion and oxidation resistance; excellent weldability (during all welding processes); excellent formability, fabricability and ductility; excellent cleanability and hygiene characteristics; good high temperature and excellent low temperature properties; is non-magnetic (if annealed) and is hardenable by cold work.

Low-carbon versions, for example 316L and 304L, are used to avoid corrosion problems caused by welding. The 'L' refers to the low carbon content of the alloy at below 0.03 wt%; which reduces the sensitisation effect (precipitation of chromium carbides at grain boundaries) caused by the high temperatures involved in welding.

Ferritic stainless steels generally have higher strengths than austenitic grades, but have reduced corrosion resistance, because of the lower chromium and nickel content.

Duplex stainless steels (DSS) have a mixed microstructure of austenite and ferrite, the aim usually being to produce a 50/50 mix, although in commercial alloys the ratio may be 40/60. Duplex stainless steels have roughly twice the strength compared to austenitic stainless steels and also improved resistance to localised corrosion, particularly pitting, crevice corrosion and stress corrosion cracking. Often in industry, duplex stainless steels are selected for the most

severe corrosion resistant applications. *Standard duplex* is 22% chromium with UNS S31803/S32205 known as SAF2205 being the most widely used.

Many nickel-based steel alloys, which are not part of the stainless steels any longer, also exhibit high resistance to corrosion and **Hastelloy** is one of the best. In addition to outstanding resistance to all manner of pitting and cracking corrosion, parts made from Hastelloy metal blends tend to find good use across a wide range of chemical applications that might otherwise oxidise the metal. Hastelloy C-276[®] is a nickel-molybdenum-chromium alloy with excellent corrosion resistance in severe environments.

The division of stainless steels based on microstructure is useful because the members within one family tend to have similar physical and mechanical properties; however the properties for one family can be very different from the properties of another. The difference between the families is fundamental to their atomic level: the ferritic stainless steel has a body centered cubic (bcc) crystal structure while the austenitic stainless steel has a face centered cubic (fcc) structure. Schaeffler and DeLong Diagrams (Davis, 1994) will be able to give specifics about the actual structure as a function of stabilising additives such as silicon, niobium, carbon and manganese. In the ferritic stainless steel, the iron and chromium atoms are arranged on the corners of a cube and in the center of that cube. In the austenitic stainless steels the iron, chromium and nickel atoms are arranged on the corners of the cube and in the center of each of the faces of the cube. This seemingly small difference significantly affects the properties of these steels. A pictorial view of these changes to the steel's microstructure can be seen in Figure 14 below ('Duplex Stainless Steels: Part One', 2007).

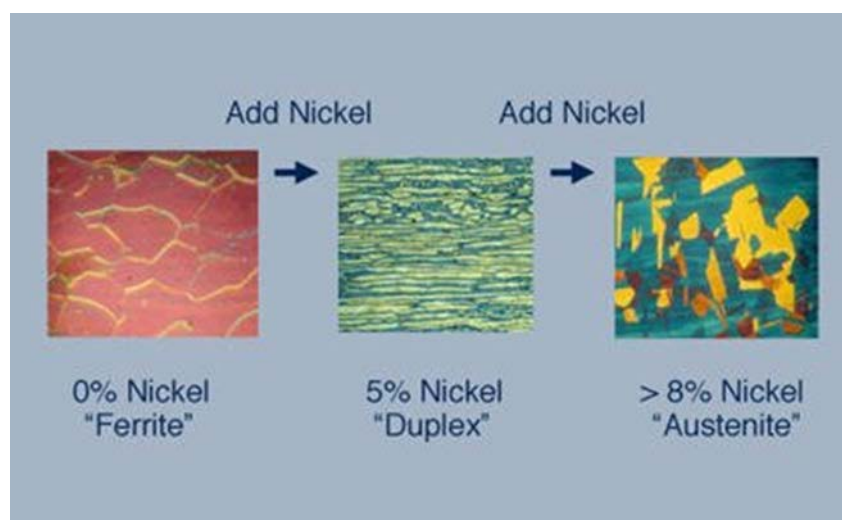


Figure 14: Microstructure changes based on the addition of nickel to the steel (DSS, 2007)

In metallurgical terms, austenitic stainless steels are made up of the matrix component iron and the alloy components chromium, nickel, molybdenum etc. Analysis of the passive surface layer shows a completely different morphological structure:

- Approximately 65 wt% is chromium and chromium oxide and
- Approximately 35 wt% is iron and iron oxide

Only small amounts of nickel and molybdenum etc. are found in the passive layer, as documented in Henkel and Henkel (2003) and also highlighted by Davis (1994). They state that under atmospheric conditions, the thickness of the passive layer is between 1.5 – 2.5 nm and shows a constant transition to the base material. Further Stefanov et al. (2000) found that the preferred formation of chromium oxide or chromium hydroxide is due to the strong affinity of chromium to oxygen and that the resulting compounds are relatively stable so that reactions with other elements are suppressed to a large extent; hence the term passive layer. The surface oxides formed under various conditions have been studied by, for example, Asteman et al. (1999) drawing the same conclusions. This passivation layer has the typical characteristic of conducting electrons and preventing the flow of ions, which usually stops corrosion circuits from being produced. However, as the passive layer is exposed to different environments and temperatures, the passive layer may change with the result that re-passivation phenomena can be observed in certain conditions. It is observed that atoms which form the passive layer are in a constant dynamic state of equilibrium. Henkel and Henkel (2003) as well as Asteman et al. (1999) explain that in principal, the formation of the passive layer on the austenitic stainless steel surface corresponds to an oxidation of the surface and is therefore not only dependent on the condition or preparedness of the surface but also on the oxidation condition surrounding the surface such as medium concentration, temperature and time. In fact, they indicate that the oxidation conditions are “of far less importance for the passivation result than the surface condition of the stainless steel surface”.

2.4 Current surface modifying trends for austenitic stainless steels

There was a drive in the 1980's to investigate improved surface hardness of austenitic stainless steels and thus increasing the possibility of wider applications. This, however, led to significant loss of corrosion resistance, mostly due to the effect of sensitisation; as per Triwiyanto et al. (2012). They explain that sensitisation is a common problem in austenitic steel where precipitation of chromium carbides (Cr_{23}C_6) occurs at the grain boundaries at higher temperatures, typically between 450°C and 850°C. The diffusional reaction in forming

the chromium carbide leads to the depletion of chromium in the steel which renders it unable to produce the Cr₂O₃ passive layer. This reduces the corrosion resistance property of the stainless steel. Much work has since been done (by Sun et al., 1995; Lu and Ives, 1995 and Banda & van der Merwe, 2014) to improve the corrosion resistance of, especially austenitic stainless steels in different media; below is a summary of some of the techniques used thus far and their shortcomings.

The main method of protecting metal components from attack by the local environment is by use of **surface coatings**. There are a number of surface coating systems available which include paint, galvanising and applying plastic liners. Some of these coatings are described below, as per Roymech (2014).

Various machines require grease and oil for lubrication. These products also provide a degree of corrosion protection of the lubricated surfaces and adjacent surfaces.

There are a number of wax based products available which can be sprayed on surfaces and provide a significant level of corrosion resistance at minimum costs. Depending on the operating conditions these products can last from one to ten years or more.

Virtually all plastics can be applied as metal surface coatings by spraying, fluidised-bed, electrostatic, rotational molding, flock or 'slush' coating or dipping. The coating system has the benefits of the strength of the base metal with the relevant properties of the plastic coating. This option has similar disadvantages as the painting option. The resulting surface must be sound and continuous and the thermal and mechanical properties of the coating are generally inferior to the base metal (Yang and Gasworth, 2000).

Enamel (Vitreous Enamel) is a thin layer of glass fused by heat onto the surface of a metal being protected. The process involves dipping or spraying the glass coatings onto metallic substrates and subsequent fusion operations. Vitreous enamelled components may have single or multiple coatings and they may be fired after each application or they may be fired as a single operation. The firing process uses a high temperature furnace to chemically bond the enamel to the metal substrate. Enamelled steel surfaces have excellent corrosion protection (Maskall and White, 1986).

Ceramic coatings are used to provide corrosion resistance against numerous chemicals as the ceramic materials are inert. They also provide erosion resistance as the ceramics are very hard and can withstand high temperature conditions. A typical coating thickness is 50 to 100 μm and can be done selectively. These coatings provide excellent finish and are deposited as slurry on metallic substrates, like cast iron, steel, stainless steel and aluminium. They are subsequently chemically treated to attain hard, impervious and corrosion resistant layers of excellent bond strength (Yu and Bennett, 2005).

Coatings based on the impact of high-velocity solid particles have, as per Kuroda et al. (2008), attracted much attention in industrial applications; these form part of thermal spraying processes. **Thermal spraying** techniques are, coating processes in which heated or melted materials are sprayed onto a surface, the heating is done by electrical (plasma or arc) or chemical means (combustion flame) (Pawlowski, 2008 and Zhu and Wang, 2009). Pawlowski (2008) describes how thermal spraying is specifically attractive in surface modification techniques because it can provide thick coatings, ranging between 20 μm to several mm, depending on the process and applied over a large area at high deposition rate as compared to other coating processes such as electroplating. Coating materials available for thermal spraying are also numerous and include metals, alloys, ceramics, plastics and composites. They are fed in powder or wire form, heated to a molten or semi-molten state and accelerated towards substrates in the form of μm -sized particles; as per Pawlowski (2008). Combustion or electrical arc discharge is usually used as the source of energy for thermal spraying. According to Pawlowski (2008), several variations of thermal spraying are distinguished such as plasma spraying, detonation spraying, wire arc spraying and High Velocity Oxy-Fuel coating spraying (HVOF). Zhu and Wang (2009) explore a variety of laser-thermal spraying hybrid cladding technologies and their application. They found that with all the processes available, the prepared surface is very coarse and porosity exists which induced mechanical failures of these coatings under low temperatures and impacted the “corrosion feature under high temperature”. Thermal spraying is in fact mostly used to produce coatings on structural materials which do not only serve as corrosion protection but more often to provide protection against high temperature erosion, wear and change the appearance of a surface for cosmetic purposes. Thermal spraying is a line-of-sight process and the bond mechanism is primarily mechanical and thus applications are not compatible with the substrate if the area to which it is applied is complex or blocked by other bodies, Pawlowski (2008).

Much work has been done on stainless steel, primarily using 316 stainless steel and titanium alloys, Kuroda et al. (2008), which shows both molten and unmolten particles in the coating indicating that large particles were not fully molten during the application. The actual process of applying a thermal spray was discussed and linked to the resulting microstructure of the surface coating. No electrochemical or other testing was performed by the authors on the samples to indicate this effect on corrosion behaviour.

Another surface treatment recently developed includes the **Laser Spray Ionisation** and it refers to one of several methods for creating ions using a laser interacting with a spray of neutral particles (Aoki et al., 2004) or ablating material to create a plume of charged particles (Trimpin, 2009). In one version of the laser spray interface, explosive vaporisation and mist formation occur when an aqueous solution effusing from the tip of the stainless steel capillary is irradiated from the opposite side of the capillary by a 10.6 μm infrared laser, Aoki et al. (2004). The ion abundances were found to be orders of magnitude greater than those obtained by conventional electrospray ionisation in the case of aqueous solutions. This approach to laser spray ionisation is a hybrid of three basic techniques for the generation of gaseous ions from the condensed phase, i.e. energy-sudden activation, nebulisation and the action of an electric field, Aoki et al. (2004). As per the authors, laser spray has better ionisation efficiency than conventional electrospray ionisation (ESI). In particular, the sensitivity became more than one order of magnitude higher in negative ion modes. They also found that this technique has a potential benefit for low concentration samples due to the condensation effect of the formed droplet by the irradiation of laser.

An alternative to traditional welding and thermal spray is **Laser Cladding**. Compared to build-up welding processes, laser cladding has a significantly lower, more localised heat input and even materials that are considered difficult to weld, can more easily be welded using laser cladding (oerlikon, 20014). In addition, the typically small melt pool formed during laser cladding allows this technique to be used for complex geometries and the repair of surfaces (Shepeleva, 2000). The technology is similar to thermal spray in that it has an energy source to melt the powder that is being applied to the substrate but where it differs is that it uses a concentrated laser beam as the heat source, the coating material in powder form is carried by an inert gas through the powder nozzle and it melts the substrate that the powdered coating is being applied to (thermalspraydepot.com and oerlikon, 2014). The laser optics and powder nozzle are moved across the substrate surface to deposit single tracks or complete

layers. This results in a metallurgical bond that has superior bond strength over thermal spray and thus the resulting coating contains minimal voids, i.e. less porosity. The basic system is made up of a laser to generate the beam, a set of optics to direct and focus the beam, a powder feeder and a part manipulator. The laser cladding systems are fully automated providing precise control of the cladding process as was observed at the National Laser Centre in Pretoria. The laser cladding technology, especially in the application of steel surface alloys, has been widely used commercially (Beyer, 2004). The main advantage of the laser cladding process is the concentrated beam of energy from the laser which can be focused and concentrated onto a very small area and keeps the heat affected zone of the substrate very shallow (Wang et al., 2004). This minimises the chance of cracking, distorting or changing the metallurgy of the substrate and the lower total heat minimises the dilution of the coating with material from the substrate. Other benefits of laser cladding include the already mentioned excellent metallurgical bond between the coating and the substrate and thus a fully dense coating, a fine homogeneous microstructure is expected to result from the rapid solidification rate and the well-controlled process ensures excellent reproducibility and minimal finishing effort (oerlikon, 2014 and Wang et al., 2004). Wang et al. (2004) add that the “hardness, toughness, and strength of the laser cladding layers are higher” when the authors compared them with other surface coating techniques such as plasma spray using austenite stainless steel base materials.

There are other surface applications that can be used to combat corrosion problems such as addition of chemical corrosion inhibitors, ion implantation, electroplating and electroless deposition but these are not relevant for the purpose of this research report.

2.5 Improvements to the corrosion resistance of stainless steel using Precious Metals

According to Jones (1996), the corrosion resistance of stainless steel depends on two factors: its chromium content, normally ranging between 10 - 30 wt%, and the level of additional elements varying the structure of the alloy. Nickel is also an important alloying element as, according to Higginson et al. (1989), it causes rapid spontaneous passivation when exposed to sulphuric acid while corroding rapidly when exposed to hydrochloric acid. Jones (1996) mentions that “Nickel in conjunction with chromium improves high-temperature oxidation resistance of the stainless steels, just as it does aqueous corrosion resistance at lower temperatures”. The text also states that “Nickel has intrinsically low corrosion rates in acid

solutions in the active state”. Selecting the most appropriate type of stainless steel for the conditions of use is critical to preventing and minimising corrosion of stainless steel surfaces. This is particularly important in strong acid, high salt and high temperature environments.

Streicher (1977) reports that initial investigations into improving the corrosion protection of stainless steels began as early as 1911 and included winding a platinum wire around specimens during testing. The effects of adding small amounts of PGMs to stainless steels have been investigated since the 1950s (McGill, 1990) and have gained recent interest for commercial use especially in aggressive chemical environments (Potgieter and Brookes, 1995). Sherif et al. (2009) state that it was known (examples are Potgieter et al., 2008 and Varga et al., 1997) that the corrosion resistance, electrochemical and pitting corrosion, of all types of stainless steels is significantly increased by alloying them with small amounts of PGMs. Govender et al. (2012) mentions that several Fe-Cr systems alloyed with PGMs have been studied at low temperatures where it has been shown that ruthenium improves the passivation in reducing acid solutions when added via bulk alloying or surface deposition. However, specifically for sulphuric acid, chloride and bromide environments, only iridium, osmium and ruthenium enhance a passive film on stainless steels (Streicher, 1977). Every metal alloy must therefore be evaluated for its application.

Corrosion occurs on the surface of metals where it interacts with its environment, altering the surface properties of that metal; therefore it can be significantly reduced by the application of a suitable surface treatment. The surface treatment would involve changing the chemical composition of the surface such as during nitriding or changing the physical structure of the surface such as is achieved by thermal spraying. In this study, the surface of 304L austenitic stainless steel was clad by a coating of ruthenium alloyed with 304L stainless steel. The concern with a metallic coating is galvanic corrosion, i.e. the preferential corrosion of the substrate if the coating is more noble than the substrate. Accelerated corrosion could occur depending on the ratio of the surface areas of the anode and cathode. Coating/cladding a more noble metal onto the surface for protection is effective providing there are no defects and therefore metallic coatings must be well understood to be effective. The loss of adhesion between the coating and the substrate, permeability of the coating layer to environmental exposure elements as well as inter-diffusion between the two must be considered.

The cladding of dissimilar metals onto one another is generally a high-temperature roll bonding or co-extrusion process. It results in “a continuous, pressure-welded, diffusion bond

between the two alloys” (Jones, 1996) retaining the advantageous properties of the outer layer. The microstructure of the coating is dependent on the coating material (e.g. chemical composition) as well as the process (and its process parameters) used for application. A number of surface modification methods have been studied to specifically improve corrosion as well as wear and hardness. According to Lekala et al. (2012) “the laser surface alloying technique is particularly applicable in cases where a change in the chemical composition and microstructure of the surface is required”. Using this technique, a number of alloying elements can be added together, heated up forming a melt pool which is then applied to the surface similar to a welded layer. Upon application, the melt pool, consisting of the alloyed materials, reacts with the molten surface of the substrate to create a new and slightly different alloyed layer exhibiting unique properties. The one of interest in this research report is the increase in corrosion resistance. Other reasons why laser processes are used is because they offer reduced “processing time, unlimited specimen size and easy control of the treated surface thickness”, as per Tjong et al. (1997). He added that the surface morphology and composition can easily be studied using Scanning Electron Microscopy (SEM) and Energy Dispersive X-ray Spectroscopy (EDS) and that the corrosion behavior can be tested by means of potentiodynamic and corrosion potential measurements. This is exactly what has been done in this research. Laurence in a discussion (2014) pointed out that the rapid cooling rates found in laser surface treatments avoid the precipitation of intermetallic and interstitial compounds which generally cause brittleness and reduce corrosion resistance of stainless steels.

Ruthenium is a noble metal known to be resistant to a wide variety of cold and hot acids and therefore should provide a resilient protective barrier between the austenitic stainless steel and an acidic environment. A surface layer or film including ruthenium, which improves the efficiency of the hydrogen evolution reaction in reducing acids, provides additional corrosion protection properties. Ruthenium is a hard metal (Perry, 1984) and thus also likely to improve the erosion corrosion resistance of its alloy with the 304L stainless steel. In order to afford adequate protection, any such surface layer should be compact, uniform and impervious to corrosive electrolytes (Strafford et al., 1993). It is also important that the electronegativity of iron and ruthenium are very close to each other to eliminate the possibility of forming intermetallic compounds at the interface or the one preferentially dissolving the other one; the electronegativities of iron and ruthenium are 1.83 and 2.20 respectively (Electronegativity using the Allen scale (Allen, 1989), values for the elements in their most common and stable

oxidation states). This difference of 0.37 cannot be considered 'very close' but certainly sufficiently close for limited solubility. Iron and ruthenium are in the same period in the Periodic Table, iron above ruthenium, and the difference in electronegativity is small. The metal of lower valence is more likely to dissolve the one of higher valence (Jones, 1996); iron has oxidation states of +2 and +3 while those of ruthenium are +3, +4, +6 and +8 (Perry, 1984). This implies that ruthenium is likely to dissolve in iron to form an inter-diffusion interface which would in this case be beneficial. The melting point of ruthenium is 2334°C (BSSA, 2014) (according to Perry (1984) the melting point of ruthenium is simply stated as >1950°C), substantially higher than the average melting point of 304 stainless steel which is between 1400 and 1450°C (BSSA, 2014). This would indicate that ruthenium is also more temperature resistant in comparison. Ruthenium however, is one of the rare transition elements and thus expensive compared to base metals due to its rareness and difficulty extracting from its ore.

2.6 Mechanisms to explain why the addition of ruthenium to stainless steels improves corrosion prevention

Parameters that are pertinent to the attainment of passivity of a given metal in a specific medium are the exchange current density, i_o , of the electrochemical reactions taking place on the surface of the metal; the limiting diffusion current density, i_L , and the values of the Tafel slopes, β_a and β_c (McGill, 1990 and Potgieter et al., 1990). They emphasised that passivity is favored by high exchange current density and limiting diffusion current density as well as low Tafel slopes. From these parameters, only the exchange current density is closely related to the type of metal exposed to the corrosive medium.

The mechanism by which noble metals such as PGMs induce passivation on a stainless steel surface is explained by McGill (1990). He states that for alloys containing noble metals the hydrogen over-potential, compared to the original surface, is reduced which actually implies enhanced corrosion. However, the less stable compounds dissolve first, in the case of stainless steel including a high nickel dissolution rates, allowing the more noble metals, in this case the PGM added, to accumulate directly on the surface where hydrogen evolution occurs. This does not seem to occur as a homogeneous layer on the surface, but rather that the noble metal atoms tend to cluster together forming separate islands, as per Potgieter et al. (1995). They also found that these microcrystals cover only a small portion of the surface. Tomashov et al. (in Tjong, 1989) reported that "the initial dissolution of Cr into electrolyte

from chromium alloys containing PGM additions resulted in the surface diffusion of PGM's into the surface defect sites of the lattice such as the edges, kinks, corners, etc." They suggest this is because the PGM atoms are not chemically or physically bonded to the adjacent chromium atoms during active dissolution of the alloy. Corrosion occurs preferentially along high energy sites/areas like grain boundaries, dislocations and similar defects (Jones, 1996). Tjong (1989) reported that there was a significant PGM redistribution associated with the surface diffusion which resulted in the accumulation of PGM's on the active sites. According to the authors (Jones, 1996 and Tjong, 1989), this resulted in the PGM physically blocking the defect points in the crystal lattice and hence reducing the rate of dissolution of chromium from the alloys. They found that this is 'because the PGM atoms lose their bonds to adjacent Cr atoms and hence become adatoms during active dissolution of the alloy' Higginson et al. (1989) confirmed that redistribution and enrichment of the PGMs occurs on the surface of the stainless steel prior to the establishment of passivity. In fact, several authors (for example: Potgieter & Brooks, 1995, Sherif et al., 2009 and Myburg et al., 1998) agree that ruthenium blocks the surface defects thereby inhibiting the dissolution of the metal at these active sites.

Corrosion proceeds by an electrochemical reaction which can be broken down into two or more cathodic and anodic reactions. In reducing acidic media, the cathodic reaction taking place is the standard hydrogen reduction reaction, evolving hydrogen gas as per equation (9).

The exchange current density of this reaction on iron alloys is low (Kelly, 1965) and low exchange current densities are not conducive to the establishment of a passive film. In fact, according to McGill (1990), a surface with a low exchange current density will experience a slow discharge of hydrogen in acidic solution and therefore a steady dissolution of the metal.

PGMs are known to have a high cathodic exchange current density with ruthenium being widely considered to be an effective cathode for the evolution of hydrogen (Potgieter et al., 1990). Ruthenium dioxide was specifically investigated as a cathode material for hydrogen evolution in acid media; in 1 M sulphuric acid (H_2SO_4) a Tafel slope of 40 mV was obtained and an exchange current density of $6 \times 10^{-5} \text{ A/cm}^2$, which is about one order of magnitude lower than that for platinum (Koetz and Stucki, 1987). This research investigated the proposal that introducing ruthenium will increase the exchange current density of the 304L stainless steel such that the equilibrium reaction (9) is shifted up, i.e. to the right as graphically represented in Figure 15 (adapted from Potgieter et al., 1990) and that this shift is sufficient in a reducing medium to take the system into the passive region and thus reduce the

actual corrosion rate of the sample. Tomashov et al. (in McGill, 1990) have also observed this effect of initial rapid corrosion of the stainless steel followed by passivation in non-oxidising acid media such as sulphuric acid. The solution concentration is critical as too high a concentration results in no passivation since the dissolution rate is too fast (McGill, 1990). Potgieter and Brookes (1995) observed that adding too small an amount of ruthenium can increase corrosion rates as it increases the efficiency of the cathodic hydrogen reaction. Therefore, passivation is induced only if the passivation potential of the PGM-metal alloy is less than the over-potential of the hydrogen evolution reaction on the alloying PGM. The same authors conclude that there is a maximum amount of ruthenium that can be added to stainless steel to improve corrosion resistance. The actual amount of ruthenium depends on the exposure media and temperature.

Working with ruthenium must be done with care as ruthenium is a suspected carcinogen and its compounds strongly stain the skin. Ruthenium tetroxide (RuO_4) is highly toxic. However, as part of the alloy with stainless steel, it is not considered harmful.

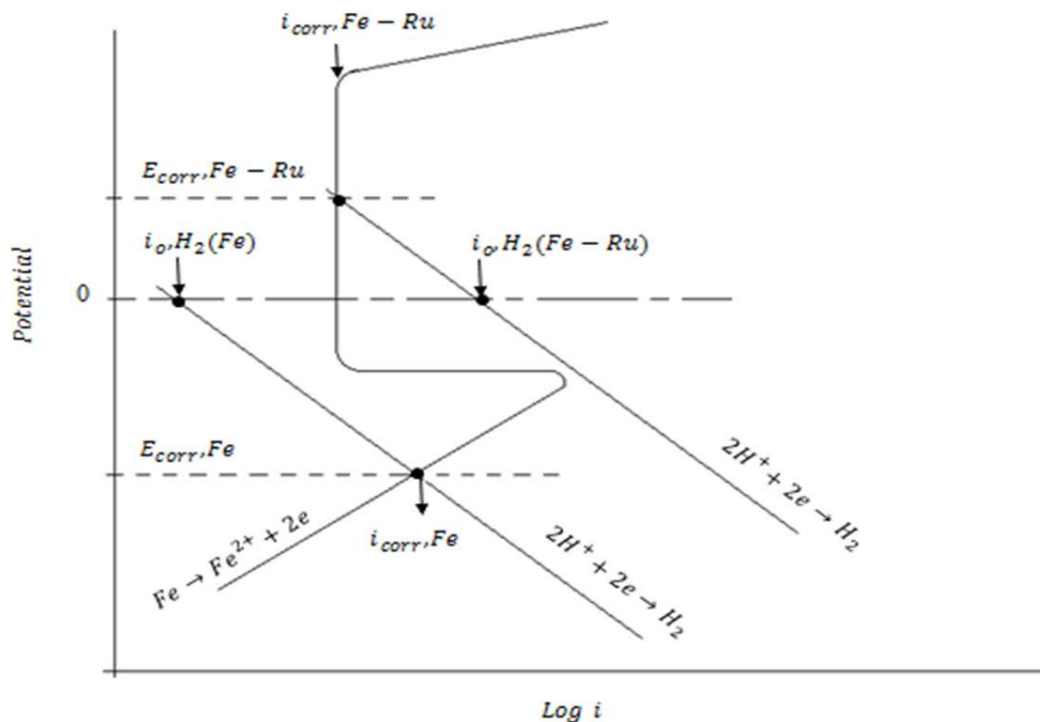


Figure 15: Effect of ruthenium on the corrosion potential of steel (adapted from Potgieter et al., 1990)

Reaction (9) occurs in acidic media, i.e. where H^+ ions are available. On the other hand, in an open to air sodium chloride (NaCl) solution, the reduction of oxygen would occur as the cathodic reaction according to equation (2) as explained by Sherif (2012).

In this case he suggests that the hydroxide groups adsorb onto the stainless steel surface reducing the corrosion rate by facilitating the formation of a passive layer of chromium and iron oxide. He also states that both of these cathodic reactions are “greatly decreased in the presence of ruthenium which is, in fact, led to decreasing the dissolution rate of the alloy”. Sherif (2012) further observed that the ruthenium did not form an independent phase but was included in the composition of hydroxide and oxide layers that form on the surface of the alloy. This increases passivation and the corrosion resistance of these layers and therefore decreases uniform corrosion and prevents pitting corrosion. He also reported that ruthenium has the ability to decrease the aggressiveness of the attack by chloride ions. Chloride ions are very aggressive due to their small size, high diffusivity and strong acidic anionic nature which are often reported to lead to pitting corrosion (Ibrahim et al., 2009). They mentioned that the pits and crevices are initiated by the adsorption of the chloride ions on certain defective sites on the passive film and grow perpendicularly to the surface being attacked rather than spreading out evenly as rust does. Once the pit is formed, its growth is autocatalytic, with chloride ions causing the hydrolysis of corrosion products in these pits and hence preventing re-passivation of the pit surface. This means that, for example, thicker tubes and pipes will not necessarily last much longer than thin ones before failing due to chloride induced corrosion. Sherif (2012) showed that the presence of ruthenium increased the passivation efficiency of duplex stainless steel and prevented pitting corrosion in 0.6 M NaCl solution. This is in agreement with previous research (Higginson et al., 1989) which suggested that the chloride ions increased the rate of surface diffusion of ruthenium during selective dissolution of the metal and therefore reduced localised corrosion. From Tjong (1989) it is known that ruthenium easily adsorbs oxygen and forms chemically stable oxides in aqueous electrolytes. He confirmed that in stainless steel containing ruthenium, the ruthenium is incorporated into the hydroxide or oxide layers formed onto the steel. Higginson et al. (1989) actually suggested the presence of an extreme outer layer of precipitated ferric hydroxide.

Tests carried out with platinum and palladium added to the stainless steel in sulphuric acid indicated that corrosion rates increase significantly with an increase of the nickel content

(McGill, 1990). In an oxidising environment, the presence of PGMs in the stainless steel may be detrimental. Potgieter et al. (in McGill, 1990) speculated that in such conditions, the corrosion potential lies in the trans-passive region leading to high rates of metal dissolution rather than passivation of the metal surface. The study also highlights that palladium additions did not alter the microstructure of the alloy and therefore the only explanation is its effect on the cathodic polarisation characteristics. McGill (1990) explained that “the lower level additions tend to flatten the Tafel portion of the curve, while the higher level additions tend to steepen and displace it, so the intersection of this and the anodic curve – that is, where the electrochemical equilibrium between the two reactions lies – is well into the region of passivity.” This means that palladium additions cause the exchange current density, i_o , to increase and the passivation current density, i_{pass} , to reduce, but not enough for spontaneous passivation to occur. Potgieter and Brookes (1995) confirmed that ruthenium containing Duplex Stainless Steel (DSS) alloys passivated under certain conditions; in fact they observed an increase in corrosion potential (E_{corr}) and a decrease in the corrosion current density (i_{corr}) and therefore lower corrosion rates, with an increase in the ruthenium content of the alloy. The reasons for this effect are the same as explained above and amount to the ruthenium atoms accumulating on the surface of the alloy during dissolution at the early stages of exposure.

Ruthenium, besides being the economically preferred PGM option, exhibits high catalytic activity and low over-voltage for oxygen evolution (Tjong, 1989). Liang et al. (2010) clearly stated that “Stainless steel alloyed with Ru actually exhibited somewhat better corrosion resistance than that of stainless steel alloyed with same amount of Pd.”

2.7 Dissolution behaviour of stainless steels

The anodic reaction in all corrosion processes is the oxidation of the metal to its ions. It is generally known that the anodic reaction of steel when exposed to an acidic media is the dissolution of iron as per equation (1).

In 304L stainless steel, the iron could also be replaced with chromium or nickel. The electrons given off by this reaction are consumed at the cathode during reactions (9) or (2). The anodic branch for stainless steel shows an active-passive region. The active region indicates the dissolution of iron as per equation (1). The passive area is likely due to the formation of oxide layers and corrosion products. In the presents of noble metals this could

also be due to the accumulation of the noble metal on the alloy surface. A rapid increase in the corrosion rate follows upon increasing the potential in the positive direction as it results in a breakdown of the passive film. It should be noted that on a polarisation diagram (indicated in Figure 5), apparent trans-passivity can also be due to anodic breakdown of water as per the equation:



Passivity and passive layer properties have been studied for over 150 years (Jones, 1996). Jones suggested that chromium forms a stable oxide (Cr_2O_3) in preference to iron (Fe_3O_4 and Fe_2O_3) when present. Higginson (1989) stated that these layers are not a stoichiometric mixture of iron and chromium oxides, but that the inner layer of the passive film is richer in chromium and, in fact, that the formation of chromium oxide is the crucial part of the passivation process. Uhlig (in Jones, 1996) stressed that chemisorbed oxygen establishes the passive film which then reduces the exchange current density, i_0 , for the dissolution reaction; the extent varies with composition, e.g. chromium content.

Potgieter et al. (1990) suggested that the presence of ruthenium in stainless steel inhibits the anodic dissolution of chromium and iron and increases the probability to form a stable passive layer. Potgieter et al. (1995) reported that during active dissolution, ruthenium causes the increase in the corrosion potential and lowers the critical as well as the passivation current densities. They stated that the ferritic phase of duplex stainless steel is preferentially dissolved in reducing acids in the region of the corrosion potential while dissolution of the austenitic phase occurs at higher potentials and when exposed to oxidising acids. Sherif et al. (2009) agreed that the presence of a small amount of ruthenium in the alloy inhibits the anodic dissolution reaction during active corrosion and added that it has been found that “the presence of Ru in the DSS alloy increases the formation of Cr_2O_3 and Fe_3O_4 in the passive film, compared to normal DSS that contained no Ru”. Graphically it was represented as in Figure 16 below. They observed that ruthenium seems to act as a ‘blocking agent’ decreasing the dissolution rates of chromium and iron and therefore increasing the probability of the stainless steel to form a stable passive layer. In the same study they suggested that the ruthenium interaction effect with the iron leads to the formation of Fe_3O_4 and allows the free diffusion of chromium to the surface to form the Cr_2O_3 which then decreases the corrosion of the DSS. The experiments carried out were at 9% nickel and used Open Circuit Potential (OCP), potentiodynamic cyclic polarisation, potentiostatic current-time, EIS and weight-loss

measurements. Some of these experimental methods were used as the basis for the experiments conducted during this investigation.

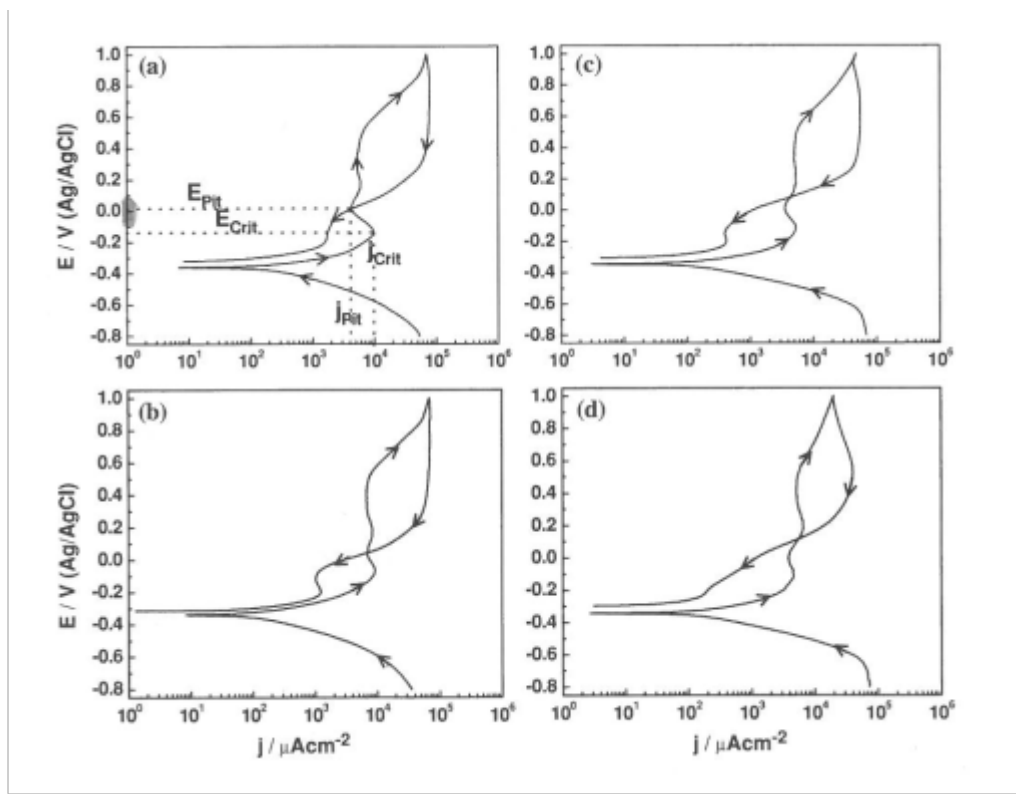


Figure 16: Potentiodynamic cyclic polarisation curves for various alloys increasing their ruthenium additions and exposure in 2 M HCl solution; taken from Sherif et al. (2009)

The Literature Review revealed the constant need for improved corrosion resistant materials in various applications. It showed that the most commonly used stainless steel, type 304, has great potential for such an enhancement by alloying the metal with ruthenium; this is explored in this report. The proposed mechanisms in which ruthenium is reducing active dissolution on the metal surface and in fact enhancing passivation shall be investigated for a variety of environments. Of great interest shall be how these alloys compare against commercially available steels at these various conditions.

3. Experimental Procedure

The high-level methodology for this project consisted of:

- sample preparation
- sample characterisation in the form of chemical and microstructural analysis
- electrochemical scans by exposure of the samples to the corrosive media at various temperatures

Experimental procedures are followed so that results from this study can be evaluated and compared effectively and that these results can be evaluated against other work performed in this field.

3.1 Sample Preparation

Sample preparation began with identifying a suitable testing plan in order to achieve the project objectives. The targeted ruthenium consisted of 0.0, 1.0, 2.0, 3.0, 4.0 and 5.0 wt%. The required quantities for each sample were prepared carefully so that the actual laser cladding could be conducted at the Council for Scientific and Industrial Research (CSIR) as per the agreed methodology which is detailed in section 3.2.

The preparation for the individual microstructure and corrosion resistance tests was carried out as per the requirements and set test procedure for each test in the corrosion laboratory of the university. The test procedures are described in the sections that follow. It was planned to expose every sample to all conditions (every acidic media and temperature) but unfortunately this was not possible as some samples, like the targeted 1 wt% Ru sample, were destroyed in the testing and no further testing could be carried out. Table 1 below provides an overview of the samples that were tested for this investigation.

S/S blank	refers to the blank 304L stainless steel sample, no additions made
0% Ru	refers to the 304L stainless steel sample cladded with 304L powder only
1 – 5 % Ru	refers to the 304L stainless steel sample cladded with a mixture of 304L and ruthenium powder prepared in the stated ruthenium concentration
316 S/S	refers to the 316 stainless steel sample
SAF2205	refers to the duplex stainless steel grade SAF2205 sample
HC276	refers to the Hastelloy C-276® sample

The purpose of including commercially available steels, such as the last three steels in Table 1, was such that a comparison could be made between them and the 304L stainless steels including ruthenium. This was to investigate the possibility of being able to offer a commercially viable solution if the corrosion tests indicated similar or superior performance.

Table 1: Samples tested for this research report

Sample	25°C			45°C	
	1 M H ₂ SO ₄	1 M H ₂ SO ₄ + 1% NaCl	1 M HCl	1 M H ₂ SO ₄	1 M H ₂ SO ₄ + 1% NaCl
S/S blank	Yes	Yes	Yes	Yes	Yes
0 % Ru	Yes	Yes	Yes	Yes	Yes
1 % Ru	Yes	No	No	No	Yes
2 % Ru	Yes	Yes	Yes	Yes	Yes
3 % Ru	Yes	Yes	Yes	Yes	Yes
4 % Ru	Yes	Yes	Yes	Yes	Yes
5% Ru	Yes	Yes	Yes	Yes	Yes
S/S 316	Yes	Yes	Yes	No	Yes
SAF2205	Yes	Yes	Yes	No	Yes
HC276	Yes	Yes	Yes	No	Yes

3.2 Laser Surface Alloying Technique

Stainless Steel 304L base plate was used for all the test samples. A mixture of 304L stainless steel powder and ruthenium sponge of 99.8% purity was used to clad the base plate using a laser surface cladding technique. Strictly speaking, the resultant clad product is no longer a 304L stainless steel but an austenitic stainless steel containing ruthenium, in this text it is however referred to as ruthenium containing 304L stainless steel. The ruthenium powder was added to the stainless steel powder in varying ratios to obtain the target ruthenium contents in the coating of: 1 wt%, 2 wt%, 3 wt%, 4 wt% and 5 wt%. Melting both powders together and cladding it onto the base plate ensured good adhesion between the cladding and the stainless steel base plate. The cladding is thus isolating the underlying stainless steel from the environment. The minimum thickness that can be achieved with this technique is 500 µm; it can of course be applied as a thicker cladding.

A set of 5 mm thick 304L stainless steel plates were used as substrates for cladding the ruthenium and stainless steel powder onto one side of the plates; the resultant sample is called a coupon. The plates were de-burred and wiped with acetone before the cladding process started. The plates were plasma cut into approximately 40 x 60 mm sections and the cladded portion was 20 x 30 mm providing approximately 600 mm² of cladding onto the base plate. The cladding was applied in beads or strips along the surface as can be visually seen in Figure 17 and Figure 19.

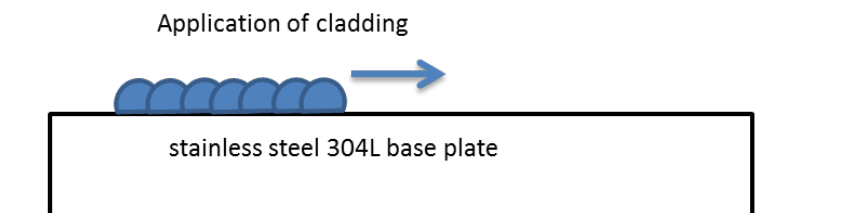


Figure 17: Graphical application of the laser cladding onto a base plate

All the coupons were cleaned with a water wash, air dried and again cleaned with acetone before cladding; this was to ensure the surface was free from any contaminants or prior oxidation of the steel. Figure 18A shows the completed coupons.

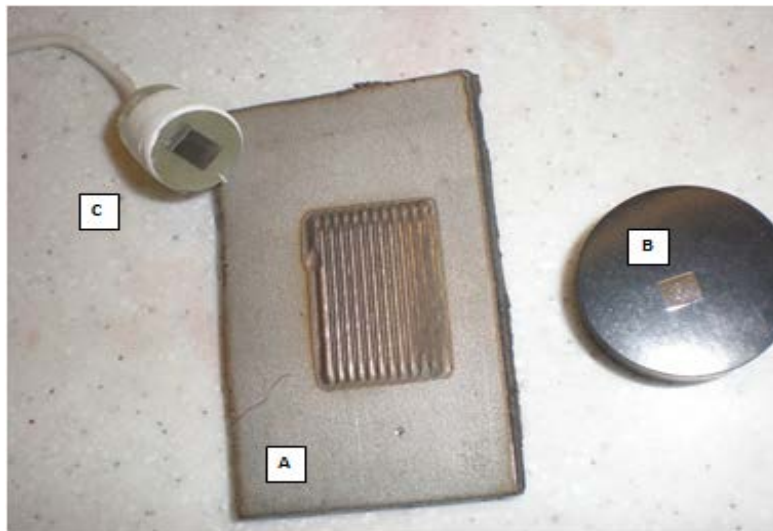


Figure 18: Samples used for the experimentation where A is the cladded coupon, B is the hot mounted sample for SEM analysis and C is the cold mounted sample for electrochemical testing

The laser cladding was performed using a 4.4 kW Rofin Sinar diode pumped Nd:Y AG laser. The 1.064 μm radiation was delivered via a 400 μm core diameter step index optical fiber to a 200 mm focal length collimator. The collimated beam was focused with a 300 mm focal

length lens. The optical assembly was mounted on a KIKA KR60L30HA 6 axis articulated arm robot to control the cladding process. The laser spot size was 2 mm diameter. The step over for all the samples; i.e. the center-to-center distance of successive weld beads, was 0.8 mm. The powder consumable was delivered from a GTV Verschleiss-Schutz GmbH powder feeder to an ILT (Institut für Lasertechnik, Aachen, Germany) supplied co-axial powder nozzle with a powder focus of 1.5 mm at 12 mm stand-off from the nozzle tip. The laser power used was 1200 W and the scan speed was 2 m/min bi-directional. The carrier shield gas used during the welding and subsequent cooling was argon at a flowrate of 3 Std L/min to create an inert atmosphere for the cladding.

It was noticed that the base plates deformed slightly during the cladding process, this is believed to be the result of the high temperatures that only one side of the plate was exposed to. The base plate turned into a slightly concave shape on the cladded side, this would be unacceptable when applying such a surface cladding to a mechanical piece of equipment. For these samples however, it was not considered a problem but will have to be addressed for actual industrial applications.

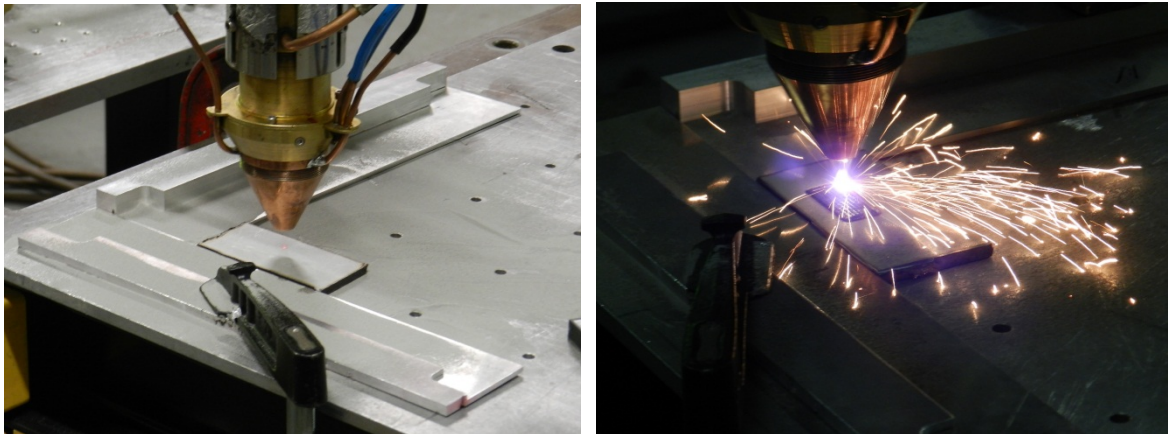


Figure 19: Laser Surface cladding performed at the National Laser Centre

3.3 Sample Characterisation

The laser cladded samples were characterised in terms of their microstructure and elemental composition in the cladded region. This analysis was performed on the surface and on the approximately 800 μm through-thickness cross section of the cladding. For that, the coupons were cut into approximately 5 x 5 mm rectangles with one surface of the cladding available for analysis. The approximately 0.25 cm^2 test samples required for observation under the microscopes were mounted separately in Bakelite® powder using an Advanced Laboratory

Solutions (ALS) OPAL 410 mounting press. One sample per composition was mounted such that the alloyed surface could be examined and the second sample was mounted such that the cross-section of the cladding could be examined. The samples were wet ground in stages from 240, followed by 600 and down to 1200 grit size using silicon carbide paper as were the samples for electrochemical testing. The samples were then polished up to 3 μm surface finish using fine powder on a Rockwell automated powder grinding machine. The samples were cleaned with ethanol and dried with compressed air. The samples were then removed from the resin so that they could be analysed under the optical microscope and in the Scanning Electron Microscope. The clean and dry samples were electrolytically etched in 10% oxalic acid solution as recommended in the literature, by Small, Engelhart and Christman (2008) at approximately 5 V for 30 seconds to be able to expose the details of the ruthenium doped 304L microstructure and grain boundaries better. The samples were carefully cleaned and preserved for analysis.

3.3.1 Optical Microscopy

Optical Microscopy uses visible light and a system of lenses to magnify images of small samples as well as help to enhance resolution and sample contrast. Microstructural characterisation of the samples was conducted so that the structure could be evaluated and images taken using a Leica DM 6000M optical microscope. The thickness and grain structure of the cladded surface coating was analysed in order to identify the influence of the ruthenium alloyed with the stainless steel on the phase and grain size of the austenitic stainless steel.

3.3.2 Scanning Electron Microscopy

Scanning Electron Microscopy (SEM) produces scanned images at high spatial resolution scanning it with a focused electron beam which interacts with atoms in the sample, producing various signals that can be detected and to provide information about the surface topography and composition of the sample. The chemical composition as well as the ruthenium distribution within the coating of the samples produced was obtained from such an SEM scan. The samples were scanned until a clear image was obtained, as large as possible an area was selected for the chemical analysis via Energy Dispersive Spectroscopy (EDS). Figure 20 shows this more clearly.

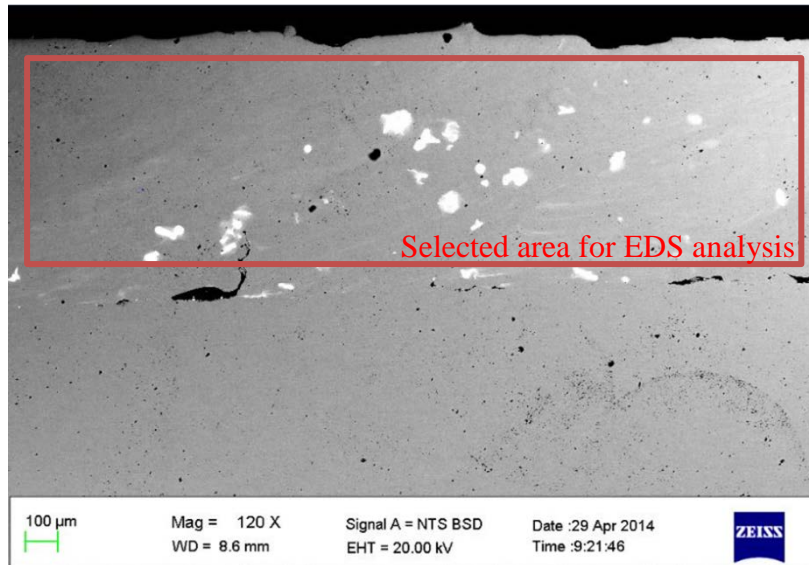


Figure 20: Selection of a suitable area for EDS analysis

In this study the microstructures were evaluated using a Carl Zeiss Sigma Field Emission (FE) SEM equipped with an Oxford x-act Energy Dispersive Spectroscopy EDS detector.

Figure 18B shows such a mounted sample that was used. The SEM was conducted to attain a guideline of the composition of the alloyed surface. The elemental composition of the alloyed surface was analysed by scanning its surface area using the EDS of the Zeiss Sigma FESEM. The EDS was conducted at approximately 8.5 mm working distance and at an acceleration voltage of 20.0 kV. The overall composition was determined by obtaining an average of the measured compositions.

3.4 Corrosion Characterisation

Corrosion occurs via electrochemical reactions and therefore electrochemical techniques are ideal for the study of the corrosion processes. In electrochemical studies, a metal sample with a surface area of a fraction of a square centimeter is used to model the metal in a corroding system. The metal sample is immersed in a solution typical of the environment which the metal is expected to be encountering, i.e. in the system being studied (Basics of Corrosion Measurements, 2014). The measurements were carried out using a PGSTAT 302Metrohm Autolab potentiostat with Nova software.

The samples prepared for electrochemical tests were cut from the coupon to a size so that an approximate surface area of 0.25 cm² was exposed to the corrosive environment. The exact surface areas per sample were measured using a Vernier as this was required in subsequent calculations. The sample was connected with an otherwise insulated copper wire before it

was cold mounted in epoxy resin such that the alloyed surface would be exposed. The samples were ground down in stages to 1200 grit size as explained in section 3.3 to ensure a smooth surface during the testing. The surface was washed, dried and inspected for any abnormalities and to ensure good adhesion between the metal and the resin; if any problem was suspected, the sample was remounted. An example of such a sample used is shown in Figure 18C.

One sample was taken per composition and set in resin for testing in the different media. Each sample could be used a few times, after each test the surface was reground with 1200 grit silicon carbide paper to ensure a fresh surface was exposed for the next test. The penetration depth of the corrosive media was not measured, the surface was reground until any markings or indents had been removed and thereafter polished. The 'fresh' surface was not checked again under a microscope between tests. Once the cladded layer was completely removed, a new piece was set in resin for electrochemical testing.

The electrochemical tests were conducted in an electrochemical cell consisting of the working electrode, i.e. the cold mounted sample, a counter electrode made of platinum (tests using the hydrochloric acid, used a graphite counter electrode) and a silver-silver chloride in 3 molar potassium chloride (Ag/AgCl, 3 M KCl) reference electrode in a Luggin tube to ensure it being as close as possible to the working electrode. All potentials were specified or reported as the potential of the working electrode with respect to the Ag/AgCl reference electrode.

The electrochemical polarisation measurements were carried out with an Autolab potentiostat, the PGSTAT302 with a differential electrometer amplifier controlled by a computer. Nova software was used to simulate the test procedures as well as to analyse the resultant potentiodynamic polarisation curves for each alloy tested under the varying conditions. Each sample was tested separately in the environment. Figure 21 shows the set-up of the electrochemical cell and Figure 22 shows the experimental set-up used. The cell is open to the atmosphere but no additional aeration was taking place.

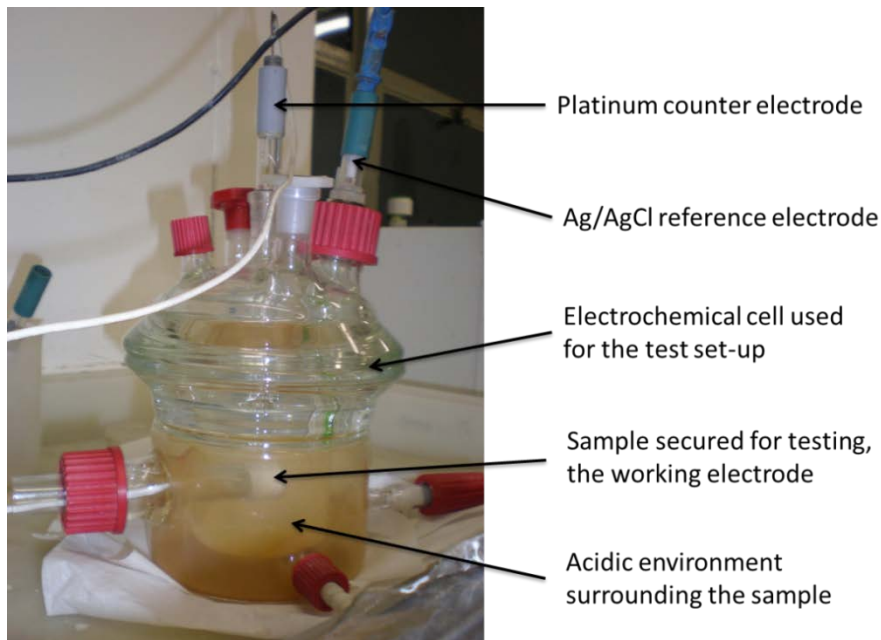


Figure 21: Electrochemical Cell used for all electrochemical experimentation

The potentiodynamic polarisation procedure consisted of the following consecutive steps:

1. Open Circuit Potential for 12 hours
2. Anodic scan from -500 mV to +1100 mV at a scan rate of 1 mV/sec
3. Polarisation at -500 mV for 5 min
4. Anodic scan from -500 mV to +1100 mV at a scan rate of 1 mV/sec

The tests were conducted according to the ASTM G5 standard. These two measurements, i.e. the OCP and polarisation scans, are typically used to determine corrosion characteristics of metal specimens in aqueous solutions.

The open circuit potential, OCP, also referred to as equilibrium potential or corrosion potential, E_{corr} , is the potential at which there is no current flowing; i.e. the experiment is based on the measurement of the open circuit potential for a 12 hour period to ensure that equilibrium is reached. This experiment was conducted first so that the sample could reach equilibrium within the 12 hour period and to allow time for passivation to occur before the first potentiodynamic/anodic scan was run.

Potentiodynamic anodic polarisation characterises the sample by its current-potential relationship. The potential of the sample was scanned at a rate of 1 mV/sec going in the positive direction so that it acts as the corroding electrode. Throughout the whole scan the sample would function as both the anode and the cathode, but at a particular moment the

sample would be the anode and the counter electrode the cathode, so that the net current, i.e. the difference between the anodic and cathode currents, can be measured on the surface. Experimentally only the net current can be measured. The first anodic or exposed surface scan therefore runs immediately after the sample has been exposed to the environment for 12 hours and was able to form a passive layer (if possible) and thus 'steady state' was reached. This is referred to as 'exposed scan' or 'exposed surface scan' when reporting results.

Polarising the sample at -500 mV for 5 minutes in between the two anodic scans is a definite disruption and is referred to as 'electrochemical cleaning' whereby the applied potential is so low that hydrogen evolution is occurring rapidly on the surface. This ensures that any air-formed oxide film or passive layer that had formed during the OCP scan is stripped and a 'clean' or fresh surface area is exposed for the second anodic scan. This is referred to as 'fresh scan' or 'fresh surface scan' when reporting results. It is therefore expected that the graphs from the first and second anodic scan provide a clear contrast between the passivated and non-passivated surfaces.

Potentiodynamic anodic polarisation diagrams yield important information such as:

- The corrosion rate of that sample under the tested conditions
- The ability of the material to spontaneously passivate in the particular environment
- The potential region over which the sample remains passive

The corrosive environment the samples were exposed to during the testing, was altered by varying the media, the temperature and of course using the different alloy composition samples. The three solutions used were 1 M sulphuric acid and 1 M sulphuric acid with 1 wt% sodium chloride salt as well as 1 M hydrochloric acid. The temperatures the samples were exposed to were 25°C and 45°C; the temperatures were kept constant by a thermostat controlled water bath. One factor was varied at a time and its effect on corrosion resistance of the sample evaluated. For each condition a number of tests were conducted to obtain a statistically relevant result.

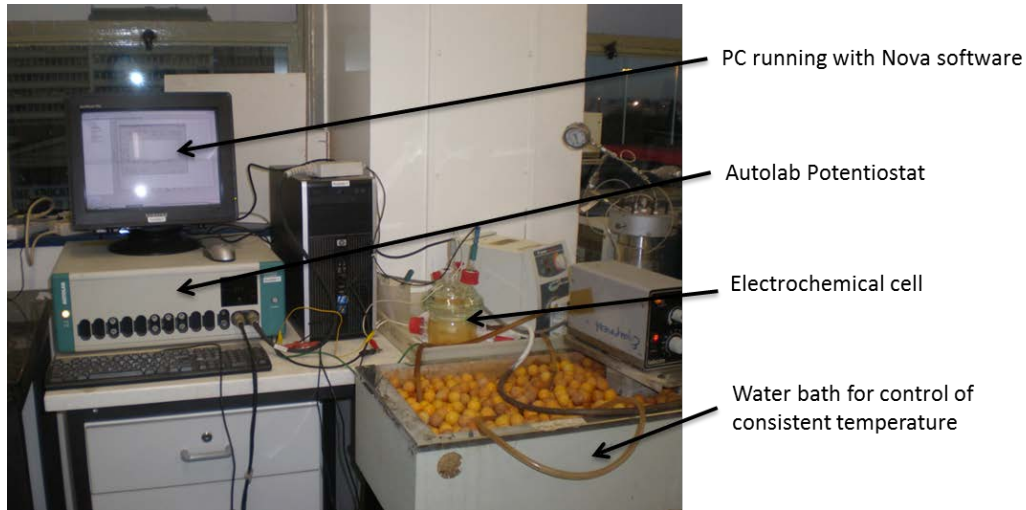


Figure 22: Experimental set-up in the university's Corrosion Laboratory

Potentiodynamic polarisation measurements serve to predict how a material will behave when exposed to a particular environment. This technique is of particular interest for this report as the scans are relatively quick and can give a good indication of the ability of the sample to form a protective layer in the selected environments. It must be remembered that this is an artificial method for corroding the samples and finally, long term exposure tests might be necessary in order to finalise the results.

Table 2: Equivalent weight and current density values

Metal/ alloy	Equivalent weight	Density [g/cm³]
Stainless steel 304L	25.12*	7.90*
Stainless steel 304L with 1% Ru	22.23 ^{calc}	7.90
Stainless steel 304L with 2% Ru	22.33 ^{calc}	7.90
Stainless steel 304L with 3% Ru	22.43 ^{calc}	7.90
Stainless steel 304L with 4% Ru	22.54 ^{calc}	7.90
Stainless steel 304L with 5% Ru	22.64 ^{calc}	7.90
Stainless steel 316	25.50*	8.00*
SAF2205	24.67 ^{calc}	7.85 ^(MacSteel, 2014)
Hastelloy C276	27.09*	8.89*

* Represents values obtained from Jones (1996)

The equations presented in section 2.2 and constants shown in Table 2 are used with the NOVA software for the calculations of the presented values. The calculations can be found in Appendix B.

Approximate values of the Tafel constants are suggested as $\beta_a = \beta_c = 0.1$ V (Jones, 1996) but for the NOVA software used for these experiments, actual Tafel constants were calculated by selecting two points along the anodic and cathodic experimental curves in this region. These are then used for further calculations.

4. Results

4.1 Microstructural Characterisation

The SEM used allowed the selection of a few areas for chemical analysis using Energy Dispersive Spectroscopy, in this case 2 – 3 areas were selected and 4 – 6 spots/points selected for analysis. The samples were analysed in order to investigate the chemical composition, i.e. an elemental analysis, in particular to determine the ruthenium level in the laser cladded surface. The ruthenium concentrations of the laser cladded surface, as obtained using EDS, are shown in Table 3.

Table 3: Composition of the laser alloyed surface of the stainless steel

Expected Ru Conc. [wt%]	Sample Area 1 Ru Conc. [wt%]	Sample Area 2 Ru Conc. [wt%]	Sample Area 3 Ru Conc. [wt%]	Average Ru Conc. [wt%]	% off target	Variance
1.0	0.72	0.16	-	0.44	56.0	0.0784
2.0	0.84	0.79	-	0.82	59.3	0.0006
3.0	2.90	3.22	2.65	2.92	2.6	0.0544
4.0	1.81	1.80	3.70	2.44	39.1	0.7980
5.0	5.24	4.19	4.57	4.67	6.7	0.1884

It can be seen that the ruthenium varied significantly from its targeted value in the laser cladded layer on the samples; sample area 2, for example, only indicated 0.16 wt% Ru when targeting 1 wt%. Relatively large areas were selected for the analysis to ensure as best a representation as possible. Ideally, the entire surface area should be selected for analysis but that was not possible. To provide an indication of the error and spread of results, the % off target and variances (the square root of the standard deviation) were calculated and included in Table 3. This indicated that the most off target results were achieved with the two lowest ruthenium containing samples but the largest differences from the targeted values were seen on the two highest ruthenium containing samples. All the average measured ruthenium concentrations are below the targeted value, notably the 1 and 2 wt% were furthest off target while 3 and 5 wt% were relatively close to the expected values. The points analysed were mostly to identify the ruthenium islands which showed between 27 and 100% ruthenium, details can be found in Table 22 in Appendix C.

The following SEM images show the morphology of the ruthenium and 304L stainless steel clad layer which highlights the variability introduced by the ruthenium and the cladding process in a graphical manner.

Figure 23 shows the 304L stainless steel base plate highlighting the consistency of the structure. The image does, however, show dark grey and white ‘spots’ but these must be viewed in comparison the following figures. The shading from light to dark occurred only due to the position of the light source when taking the image and does not indicate a change in the structure. The analysis of the stainless steel base plate indicated very consistent results were obtained with EDS as can be seen in Table 4.

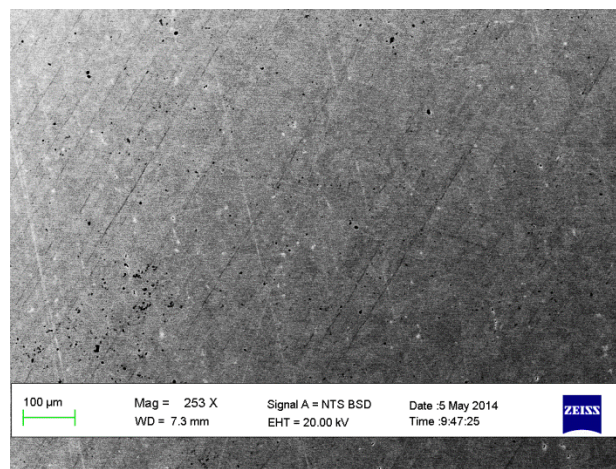


Figure 23: Surface view of the blank stainless steel sample

Table 4: Chemical Analysis of the stainless steel base plate

	Fe wt%	Ni wt%	Cr wt%	Si wt%	Mn wt%
S/S plate 1	70.97	7.99	19.11	0.50	1.42
S/S plate 2	71.03	8.02	19.13	0.47	1.36
Average	71.00	8.01	19.12	0.49	1.39

The image magnification was selected in order to obtain a clear visual that was meaningful for the sample, as sample sizes differed slightly and quite a large range in ruthenium concentrations was tested, it was not possible to select the same magnification for all the samples. This would have been ideal for comparison but all details regarding the magnification are given on the Figures. Due to the cladding process, where the powder to be clad onto the base plate is melted to very high temperatures and then applied/‘welded’ onto the cold substrate, porosity (or a lack of adhesion between the clad and the substrate) is

introduced as shown in Figure 24. In this sample, only 304L stainless steel was cladded onto the 304L stainless steel substrate without any ruthenium added at this stage.

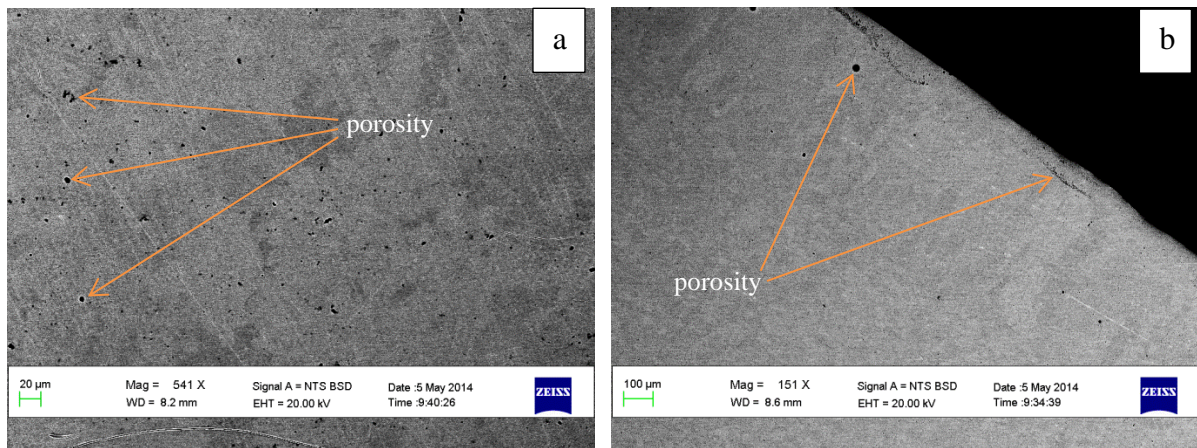


Figure 24: 0 wt% Ru laser cladded sample, (a) surface view (b) a cross sectional view

Porosity is introduced in all the cladded samples which was due to the application process. The ruthenium is clearly visible as the almost white inclusions in the cladded layer, it is either as stringers or island like clusters; seen in Figure 25, Figure 26 and Figure 27. This is as expected from the literature, Potgieter et al. (1995).

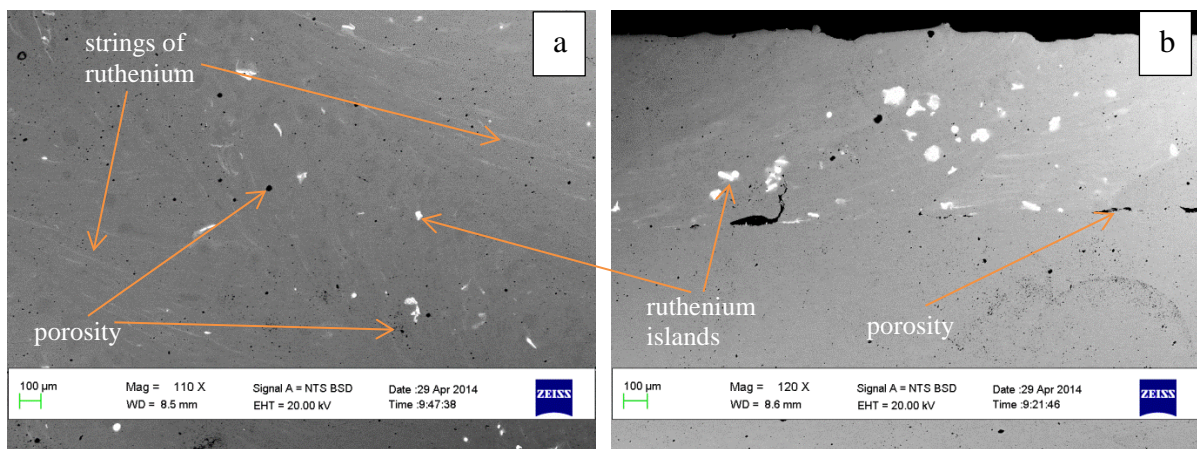


Figure 25: 2.92 wt% Ru laser cladded sample, (a) surface view and (b) cross-sectional view

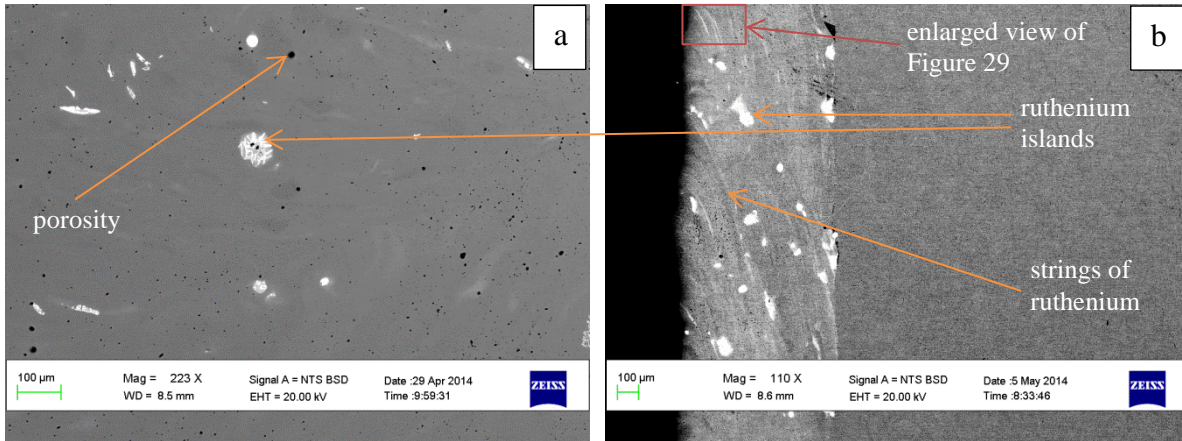


Figure 26: 2.44 wt% Ru laser cladded sample, (a) surface view and (b) cross-sectional view

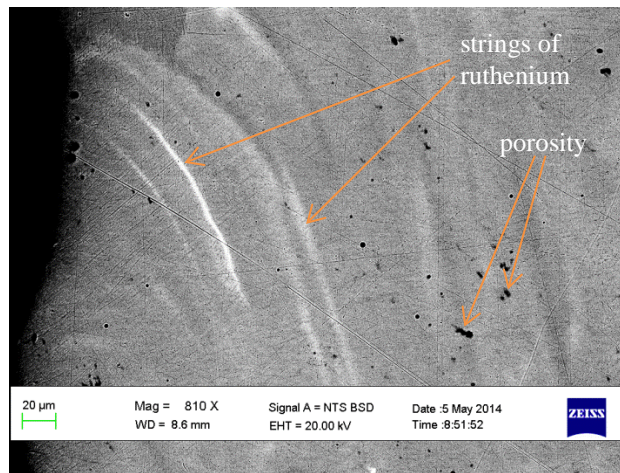


Figure 27: Higher magnification cross-sectional view of the 2.44 wt% Ru laser cladded sample

As the ruthenium concentration increased, more ruthenium was distributed among the stainless steel cladded layer increasing the amount and size of the ruthenium clusters. This is clearly visible by directly comparing Figure 25 with Figure 28. This was, however, not verified by a quantitative analysis and only visually observed. It also looks like, as the ruthenium concentration increased, the porosity increased along the boundary between the base plate and cladded zone. The beads cladded by the laser, as shown in Figure 17, are clearly visible on the right hand side image in Figure 28. Figure 29 shows an enlarged view of one ruthenium ‘cluster’ indicating how randomly arranged it can be.

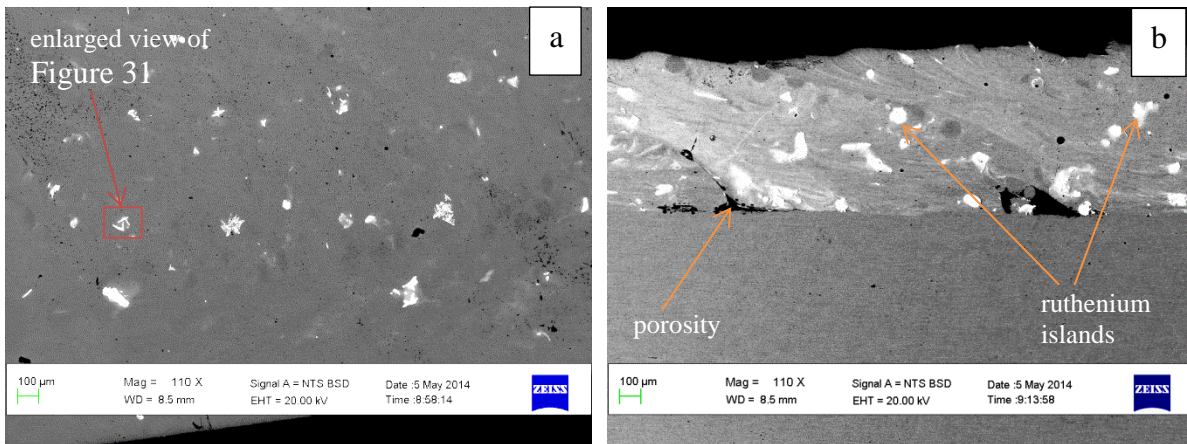


Figure 28: 4.67 wt% Ru laser cladded sample, (a) surface view and (b) cross-sectional view

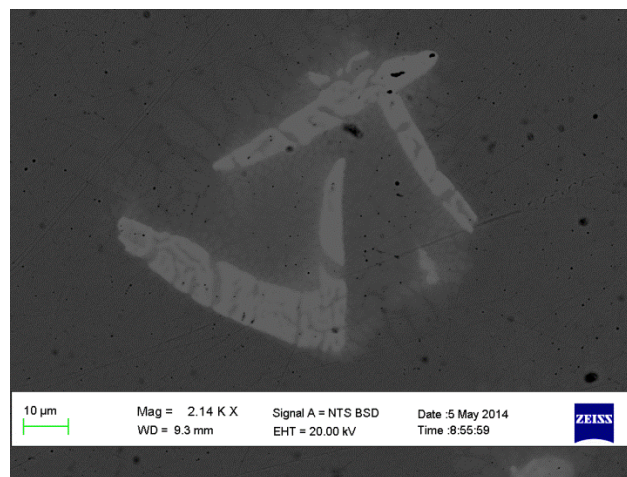


Figure 29: Higher magnification surface view of the 4.67 wt% Ru laser cladded sample

The thickness of the cladded layer was measured at a few points in each of the samples and an average thickness of 770 μm was obtained. The range was between 700.0 μm and 809.1 μm giving a spread of 14.2% which is reasonably consistent especially bearing in mind the application methods being beads along the surface.

The actual composition of the surface layers for the samples shown in the SEM figures above were obtained and are given in Table 5; these clearly show the variability introduced by the application of the surface cladding esp. for the ruthenium. For the 2.92 wt% Ru sample, for example, iron was reduced by 4.9 wt%, nickel proportionally increased by 1.8% and chromium remained relatively stable dropping by only 0.2 wt% while the added ruthenium took up the remaining weight percentage. For the 2.44 wt% Ru sample, iron was reduced by 5.3 wt%, nickel proportionally increased by 1.4% and chromium increased slightly by 0.3 wt% while again the added ruthenium took up the remaining weight percentage. For the 4.67 wt% Ru sample iron was reduced by 6.2 wt%, nickel increased by 1.6% and chromium

dropped by 0.7 wt% while the added ruthenium took up the remaining weight percentage. It is again observed that the ruthenium variability is largest in the 2.44 wt% sample. The alloy generated can no longer be considered a 304L stainless steel especially as the ruthenium content increases but for the purpose of this report it is referred to as ruthenium containing 304L stainless steel to remind the reader of its origin.

Table 5: Chemical Analysis of the laser cladding section of the samples

	Fe wt%	Ni wt%	Cr wt%	Si wt%	Mn wt%	Ru wt%
Surface 2.92 wt% Ru	66.26	9.81	18.91	0.79	1.6	2.65
Cross section 2.92 wt% Ru	65.91	9.76	18.84	0.74	1.5	3.22
Surface 2.44 wt% Ru	66.06	9.20	20.06	1.28	1.6	1.81
Cross section 2.44 wt% Ru	65.44	9.68	18.85	0.77	1.6	3.70
Surface 4.67 wt% Ru	65.29	9.75	18.46	0.73	1.6	4.19
Cross section 4.67 wt% Ru	64.41	9.53	18.39	0.83	1.6	5.24

4.2 Microstructure Analysis

From Wang et al. (2004) it is expected that the laser cladding method of application produces an extremely fine microstructure and small grain size. The samples tested were observed under a Leica optical type microscope and the following images obtained, these represent typical views of the samples as they were observed. In Figure 30 the stainless steel base plate is shown on the left hand side and the alloyed material on the right hand side. Structural changes introduced by the cladding application (similar to a welding application) are observed even though the austenitic nature of the steel is visible. The interface observed for the 0.44 wt% Ru sample is well adhered to the base plate as there are no visible detachments or porosity between the two. The ruthenium seems well distributed throughout the alloyed layer, it is assumed that the ruthenium is present as a solid solution or as pure ruthenium particles which disseminated into the stainless steel matrix, and has not formed other phases. For this research however, no elemental distribution was provided to confirm this statement.

It must also be noted that the laser clad sample was exposed to rapid cooling and therefore is not expected to form all the phases that one would normally observe during slow cooling.

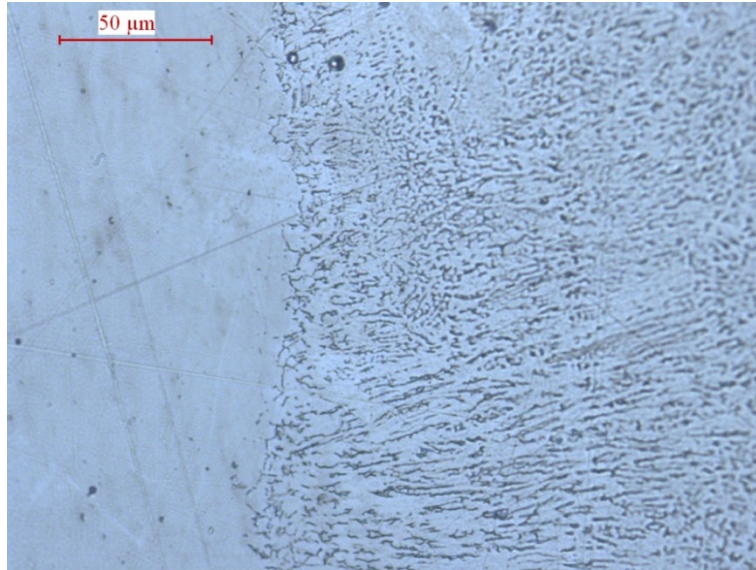


Figure 30: Microstructural view of the interface of the 0.44 wt% Ru sample

Observing the interface at a higher ruthenium content and at a higher magnification in Figure 31, the same is observed as in Figure 30. Many thin parallel lamellae shaped structures are observed with alternating light and dark contrast which are assumed to have formed along certain crystallographic habit planes. The actual surface of the cladded layer would have been interesting to look at and it is suggested that in future experiments this is done. Important to corrosion is the ability of the surface layer to permit the acidic environment, in this case the sulphuric and hydrochloric acid, to penetrate into the substrate, i.e. the stainless steel base plate. The photographs would suggest that there is no such route for the media to get to the substrate. Observed porosity and grain boundaries might be able to provide a possible access route but the images do not indicate a clear straight through passage from the surface to the underlying base plate. The cladding is in this way protecting the underlying, from a corrosion point of view 'weaker', material. The interface of the allowed cladding looks well adhered to the stainless steel base plate and structurally the alloy appears reasonably uniform with a good distribution of the ruthenium in the cladded layer.

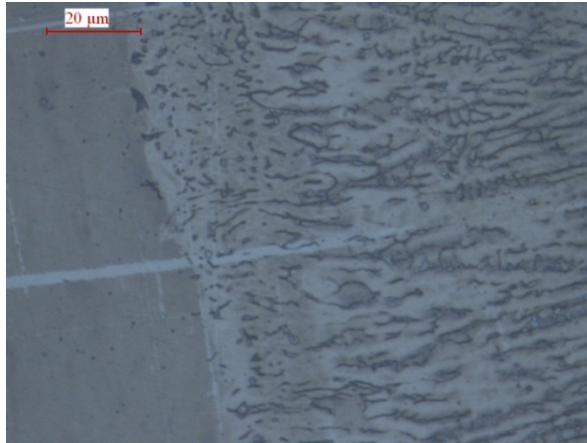


Figure 31: Microstructural view of the interface of the 0.82 wt% Ru sample

In Figure 32 the stainless steel base plate is on the right hand side while the cladded layer is on the left hand side of each image. At these higher ruthenium compositions, it is observed that the larger element ruthenium is not greatly distributed but started forming relatively large islands of pure ruthenium in the cladded layer. The typical austenitic structure is observed in the 304L base plate. In the treated phase, i.e. the cladded layer, equilibrium was not reached during the rapid cooling. Alloying higher concentrations of ruthenium did not change the phase, but the ruthenium would have altered the properties of the alloy slightly. The adhesion between the base plate and the cladded layer visually looks good as no gaps are observed and there is no obvious diffusion of the alloy into the parent material/ base plate.

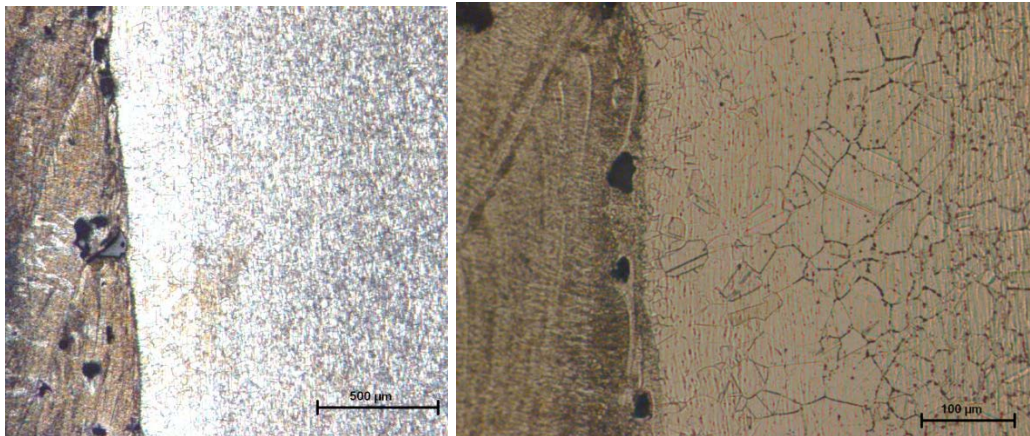


Figure 32: Microstructural view of the interface of the 2.44 wt% Ru sample, both images show the samples at different magnifications and different sections of the sample

Observing the structure of the 2.44 wt% Ru sample in Figure 33 more closely, it seems to follow a branch like network which is probably due to the application of the alloyed material by the cladding process and subsequent rapid cooling or it might be a superimposed etchant effect. Branching had not specifically been observed with other ruthenium compositions but it cannot be said that it is specific to the 2.44 wt% Ru as no other such structures were

observed. Reasonably uniform distribution of the ruthenium within the stainless steel is observed, however.

It is important to note that this uniform distribution is only based on the images observed and no XRD analysis has been conducted to confirm this statement. This is suggested to be conducted for any further research in this field.

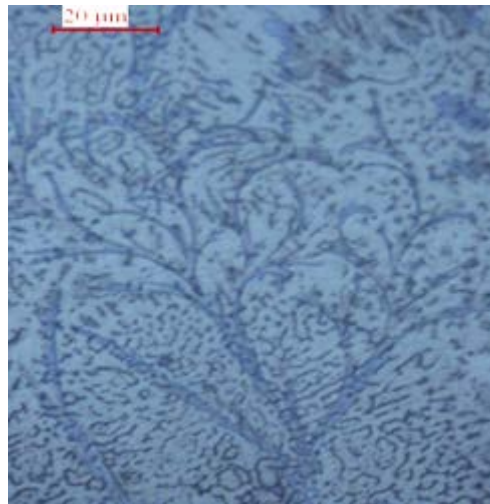


Figure 33: Microstructural view of the alloyed section of the 2.44 wt% Ru sample

Looking at the highest amount of ruthenium added, i.e. 4.67 wt% Ru, the ruthenium stringers observed with the SEM as well as porosity are also visible in these images. In Figure 34, the 304L stainless steel base plate is observed on the right hand side and the applied cladding on the left hand side. The interface is clearly identifiable and looks adherent but not as good as at lower ruthenium concentrations. Variability is becoming more evident it seems as the amount of ruthenium increases. The fine structure of the cladding application is again observed in the elongated crystal structure. A dark line was found parallel to the interface.

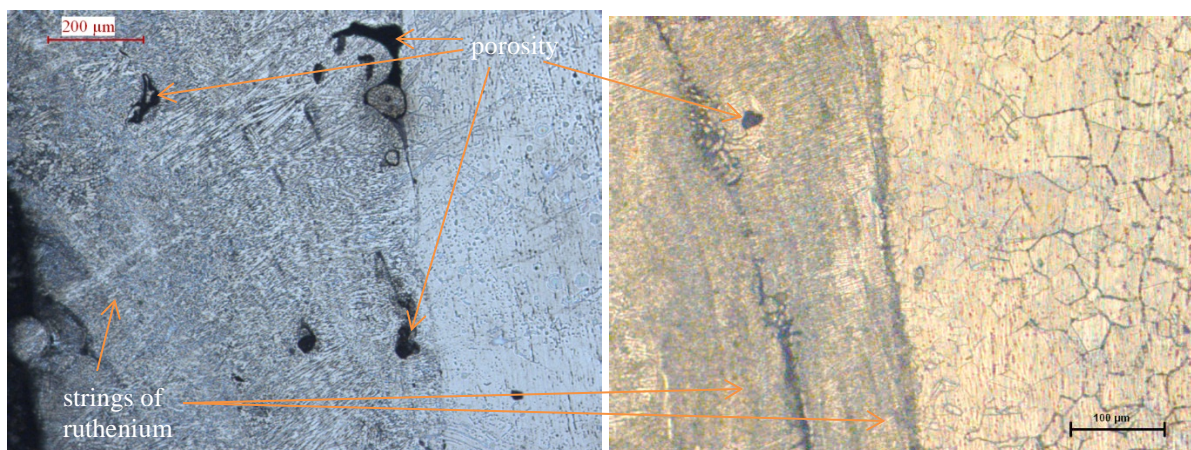


Figure 34: Microstructural view of the interface of the 4.67 wt% Ru sample, both images show the samples at different magnifications and different sections of the sample

Directly comparing Figure 35 with Figure 30, the difference the additional ruthenium is making becomes more obvious mainly in the loss of consistency of the cladded layer. The formation of the lamellae grains is still prominent and there is no notable change in lamellae grain size with an increase in ruthenium composition. The interface appears adherent as described before.

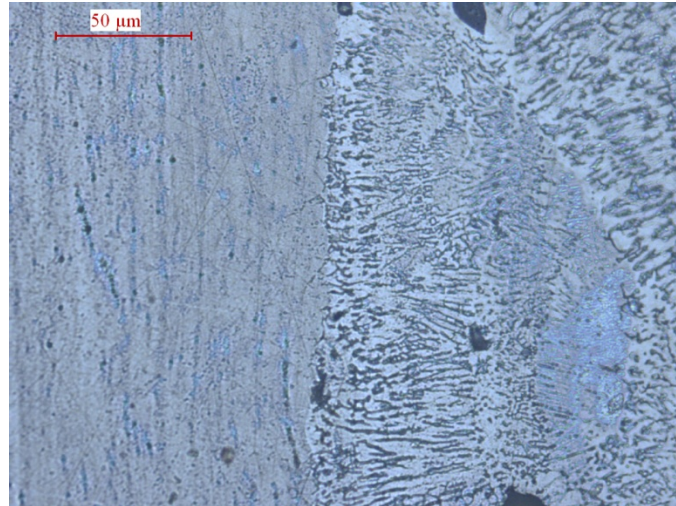


Figure 35: Microstructural view of the interface of the 4.76 wt% Ru sample at higher magnification

4.3 Electrochemical Testing

A number of parameters were used to give an indication of corrosion resistance; these included the corrosion rate [mm/year], the measured corrosion potential, E_{corr} [V], the Open Circuit Potential (OCP) [V] over time, the passivation exchange current density, i_{pass} [A/cm^2] and the critical exchange current, i_{crit} [A/cm^2].

The experimental set-up and procedure is explained in section 3.4 above.

4.3.1 1 M H_2SO_4 solution at 25°C

The repeatability of the results had to be gauged to determine the validity of the results. The graphs below are examples of the testwork carried out as per the test procedure described in section 3.4 and show the results of the repeatability of the various ruthenium containing samples as well as the stainless steel blank sample. The only difference was that after each test the surface was reground with 1200 grit paper to ensure a fresh surface of the same sample was exposed for the next test. All the tests conducted for this section were tested in

1 M sulphuric acid at a temperature of 25°C. The remainder of the results showing repeatability can be found in Appendix D.

The three curves for each condition in Figure 36 show results for the first anodic scan, i.e. after the 12 hours exposure and before polarisation, are reasonably consistent, the biggest difference was seen in the critical current density, i_{crit} , between test 1 ($1.48 \times 10^{-5} \text{ A/cm}^2$) and tests 2 and 3 (both close to $7.42 \times 10^{-6} \text{ A/cm}^2$). The Tafel slopes for the cathodic reaction were almost the same, the E_{corr} was similar around -0.25 V, the potential range over which passivation occurred is the same for the three tests at 1.04 V and so was the trend going from the passive to the trans-passive region. For the fresh surface scan the consistency was also reasonable but it can be seen that the i_{crit} was at a much higher value (above $2.0 \times 10^{-4} \text{ A/cm}^2$) while the passive region was almost identical with the samples from the exposed surface scan in terms of current density but at a slightly reduced potential range stretching just over 1.0 V. The i_{crit} for tests 1 and 2 were closer to each other compared to test 3 from the fresh surface scan which is lower. The E_{corr} was lower for the fresh surface scan, dropping by approximately 0.1 V.

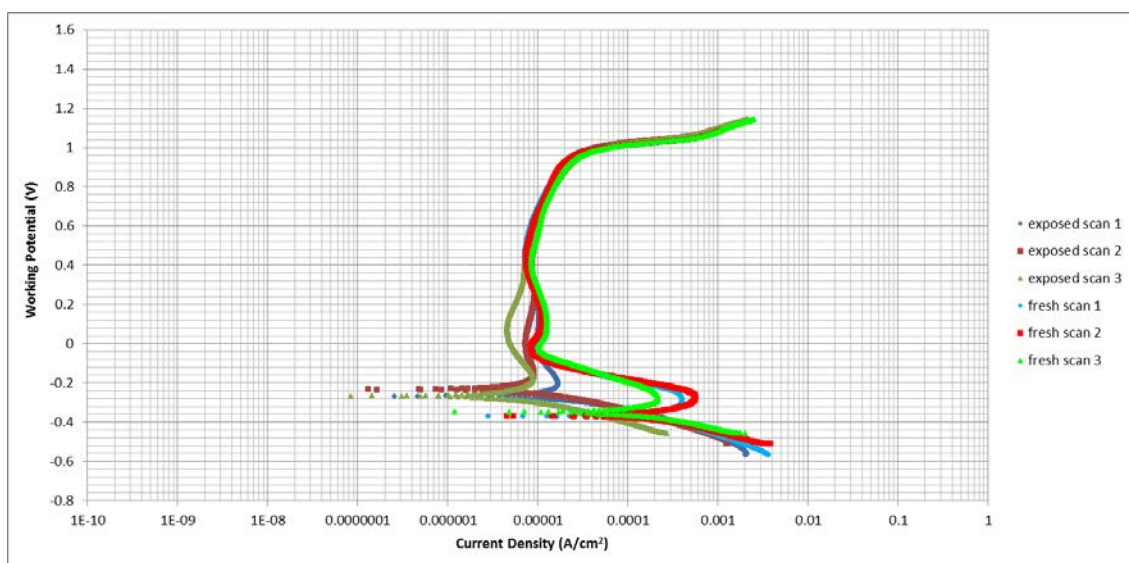


Figure 36: Log i vs E graphs for the Stainless Steel blank sample in 1 M H_2SO_4 at 25°C

As seen in Figure 37 there was reasonable consistency in the start of the test but the OCP quickly separated slightly and finally a difference of 0.1 V (ranging between 0.04 V and -0.06 V) between the three tests was observed after 12 hours. The final OCP value was around 0 V and the graph very flat throughout the 12 hour period indicating stable results were achieved.

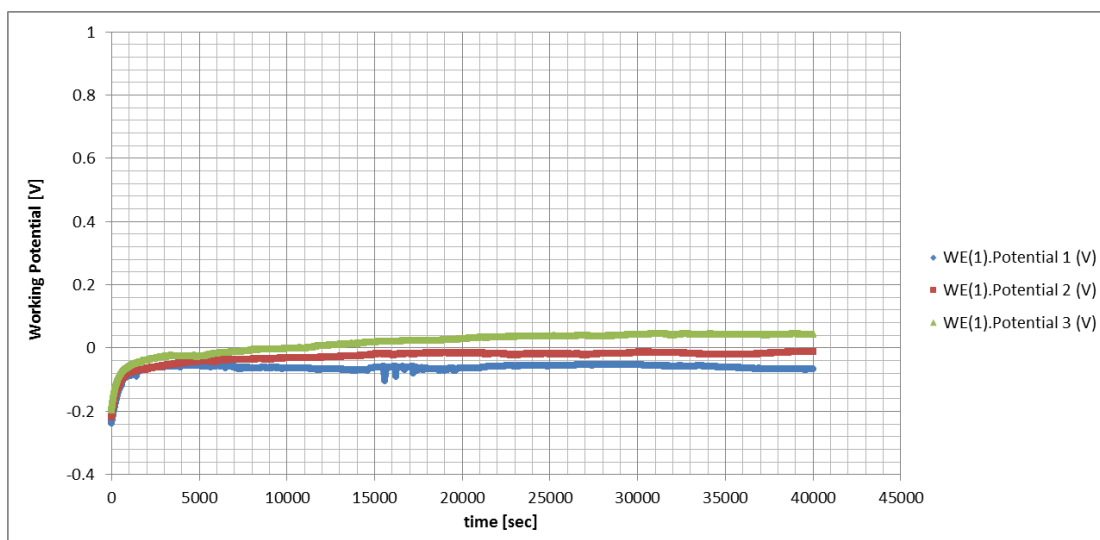


Figure 37: E vs time graphs for the Stainless Steel blank sample in 1 M H₂SO₄ at 25°C

For the samples containing 0.82 wt% Ru, the graphs actually took on a different shape which will be explained in the next section. The current density increased with an increase in working potential in the passive region and displayed the traditional transitional shape. The repeatability of the results, however, was reasonable. For the samples from the exposed surface scan, the corrosion potential, E_{corr} , showed a slight spread of values between the samples ranging almost 0.2 V (between 0 and 0.2 V) and they were all positive potentials in this environment. This reduced the passive range to less than 1 V before all the curves coincide into the trans-passive region at the same potential and current density. The samples from the fresh surface scan showed a stable passive current density with increasing potential but at an order of magnitude larger current density than the samples from the exposed surface scan before they combined going into the trans-passive region which was the same as that observed for the exposed surface scan. The variability within E_{corr} values was approximately the same as that from the exposed surface scan but at a lower, negative value.

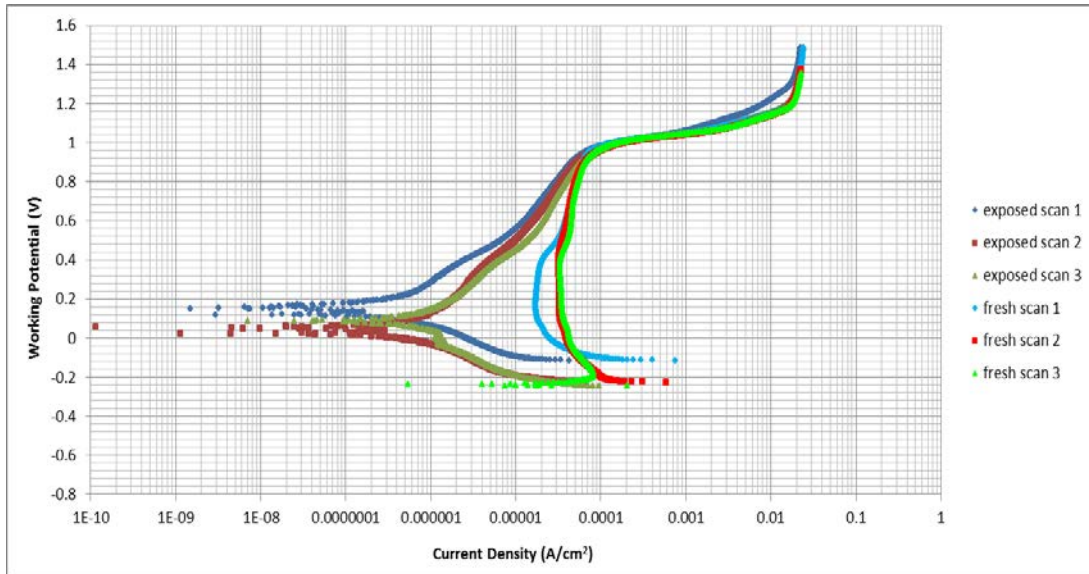


Figure 38: Log i vs E graphs for the 0.82 wt% Ru sample in 1 M H_2SO_4 at 25°C

The OCP determination in this case showed repeatability between tests 2 and 3 while the first test was different in that it started at a lower value, exhibiting a dip at the start and a more gradual increase over time and stabilised after 12 hours at over 0.1 V higher value than the results for tests 2 and 3. The OCP had certainly reached a stable value after the 12 hour period at almost 0.3 V. Looking at both Figure 38 and Figure 39, test 1 should perhaps be disregarded.

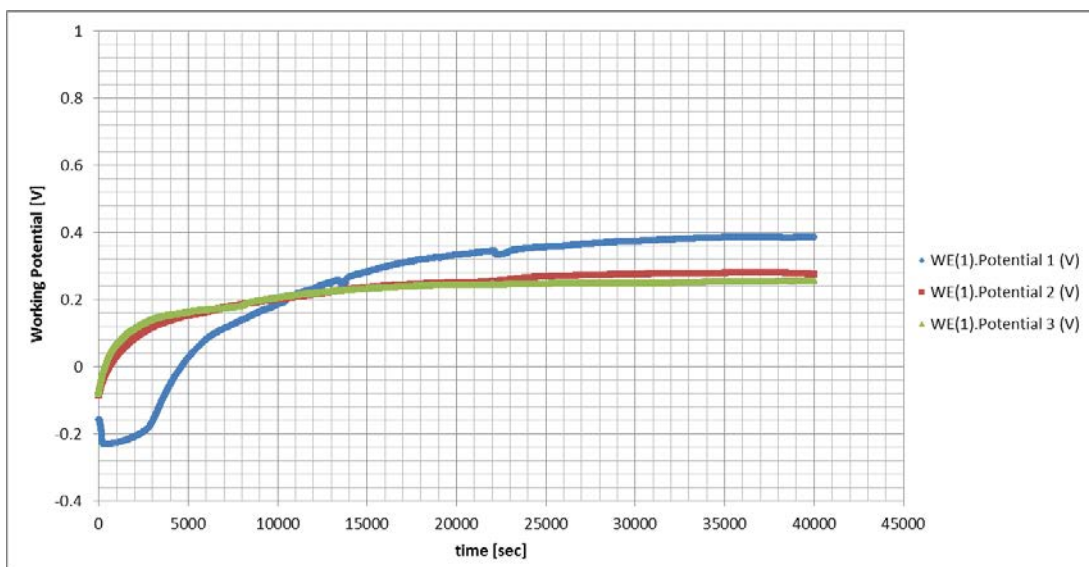


Figure 39: E vs time graphs for the 0.82 wt% Ru sample in 1 M H_2SO_4 at 25°C

The samples containing the highest amount of ruthenium, i.e. 4.67 wt% Ru, showed repeatability between tests 1, 2 and 3 from the exposed surface scan as these almost coincided; see Figure 40. The results from the fresh surface scan however, showed variability especially with regards to their passive region behaviour. The first anodic scan, i.e. after the

12 hours of exposure to the acid, showed the typical transition shape with an E_{corr} of around 0.1 V and a passive region of approximately 0.9 V. The results for the second scan, i.e. with the freshly exposed surface area, were similar to that shown in Figure 9 indicating cathodic loops and on average lower, negative E_{corr} values as well as a reduced passive region as small as 0.6 V. For the samples with 4.67 wt% Ru, it can be noticed that the differences in current density between the exposed and fresh surface scans were reduced compared to the scans with the 0.82 wt% Ru sample.

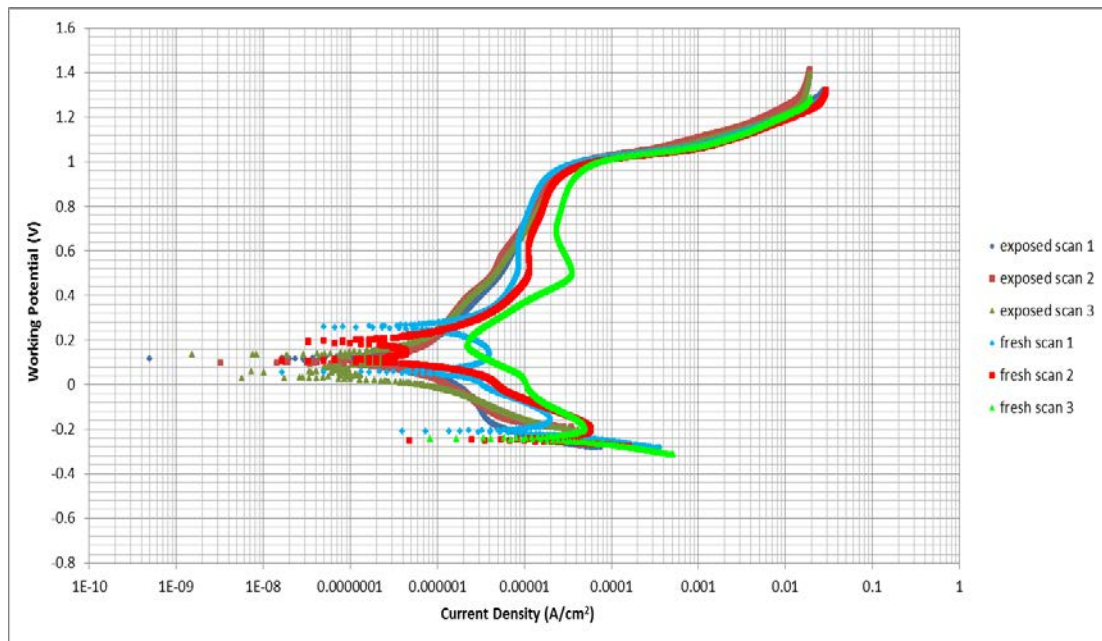


Figure 40: Log i vs E graphs for the 4.67 wt% Ru sample in 1 M H_2SO_4 at 25°C

It seems that as the ruthenium concentration increased so did the inconsistency, as can be seen in Figure 41, the OCP curves over a 12 hour period showed inconsistencies throughout that time period mostly for test 3. After 8 hours the curves do coincide more closely and with a final spread of less than 0.01 V and final stable values achieved at around 0.2 V.

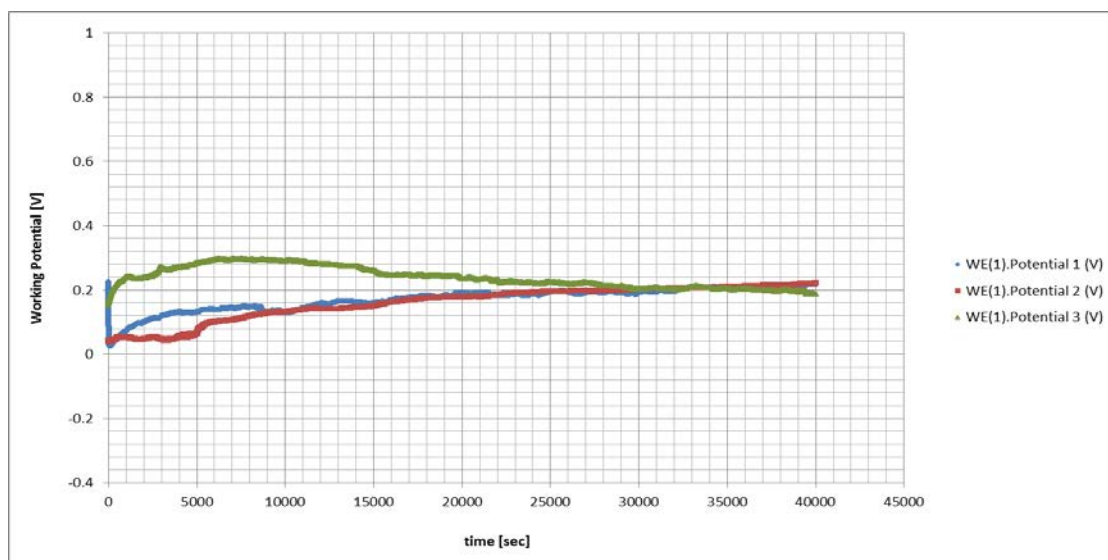


Figure 41: E vs time graphs for the 4.67 wt% Ru sample in 1 M H₂SO₄ at 25°C

Taking a representative curve from each of the samples tested in 1 M sulphuric acid at ambient temperature, they are compared in Figure 42 and Figure 43 below. This was also done for Open Circuit Potentials and is graphically represented in Figure 44. The stainless steel blank sample result was used as a reference with which to compare the other results, as well as the cladded sample with only the stainless powder and no ruthenium.

For the exposed samples (Figure 42), the passivation current density for the samples containing ruthenium was orders of magnitude smaller than when no ruthenium was added; except for the 0.44 wt% Ru sample which was closer to the stainless steel blank sample. The stainless steel blank sample displayed the traditional curve as per Figure 5 with an E_{corr} at -0.24 V, a small active nose, i_{pass} around 1.0×10^{-5} A/cm² and a passive potential range of 1.2 V. The cladded sample without ruthenium had the lowest E_{corr} with -0.36 V, a much more prominent active nose, i_{pass} slightly higher at 2.0×10^{-5} A/cm² and a passive potential range of 1.2 V too. The 0.44 wt% Ru sample had an E_{corr} value the same as that of the stainless steel blank sample but a much reduced active nose before passivation over a potential range of just over 1.0 V and a corresponding curve going into the trans-passive region. The 0.82 wt% Ru curve and, in fact all the curves with a higher ruthenium content, exhibit the transition shape implying the formation of a stable passive film. E_{corr} was in the positive potential range reducing the passive range to approximately 1.0 V. The 2.92 wt% Ru curve had the highest E_{corr} value at almost 0.2 V and thus the shortest passive potential range with 0.8 V. The 2.4 wt% Ru E_{corr} was only marginally lower than that of the 2.92 wt% Ru sample and the curves coincided with each other. The 4.67 wt% Ru sample had an E_{corr} value similar to the

0.82 wt% Ru sample and followed that curve going into the passive region. The trans-passive behaviour was the same for all the samples.

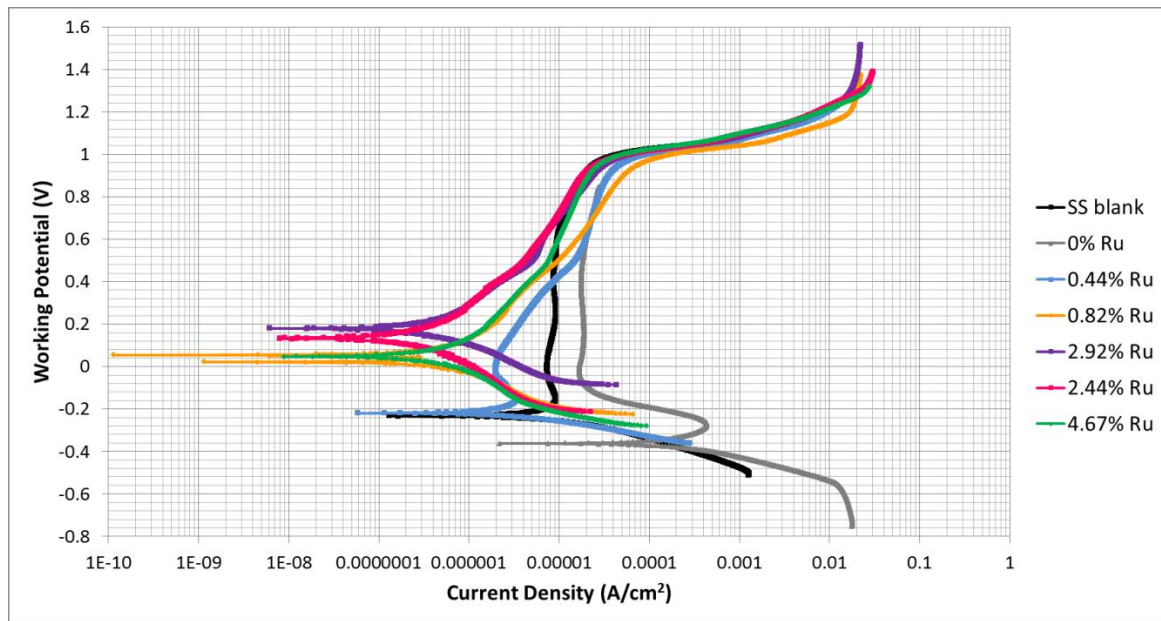


Figure 42: Log i vs E graphs from the exposed surface scan comparing all samples in 1 M H_2SO_4 at 25°C

This spread in results was not observed for the samples from the second anodic scan, i.e. the electrochemically cleaned sample after the over 12 hour exposure time, all the results were within one order of magnitude. The E_{corr} values for the stainless steel blank and the clad sample without ruthenium were identical at -0.36 V while all the samples containing ruthenium had very similar E_{corr} values, higher and around -0.24 V. The active noses were prominent for the samples without ruthenium but small for all the samples with ruthenium. The passive region extended over a similar potential range of 1.0 V before the trans-passive behaviour which was the same for all the samples. The i_{pass} values are highest for the 0.82 wt% Ru sample and decreased with the 2.92 wt% Ru, the 0.44 wt% Ru, 0 wt% Ru, 4.67 wt% Ru, 2.44 wt% Ru and were the lowest for the stainless steel blank.

The i_{pass} for the stainless steel blank sample had very similar values for the exposed and fresh surface scans but the ruthenium containing samples showed much lower current densities during the exposed surface scan compared to the fresh surface scan.

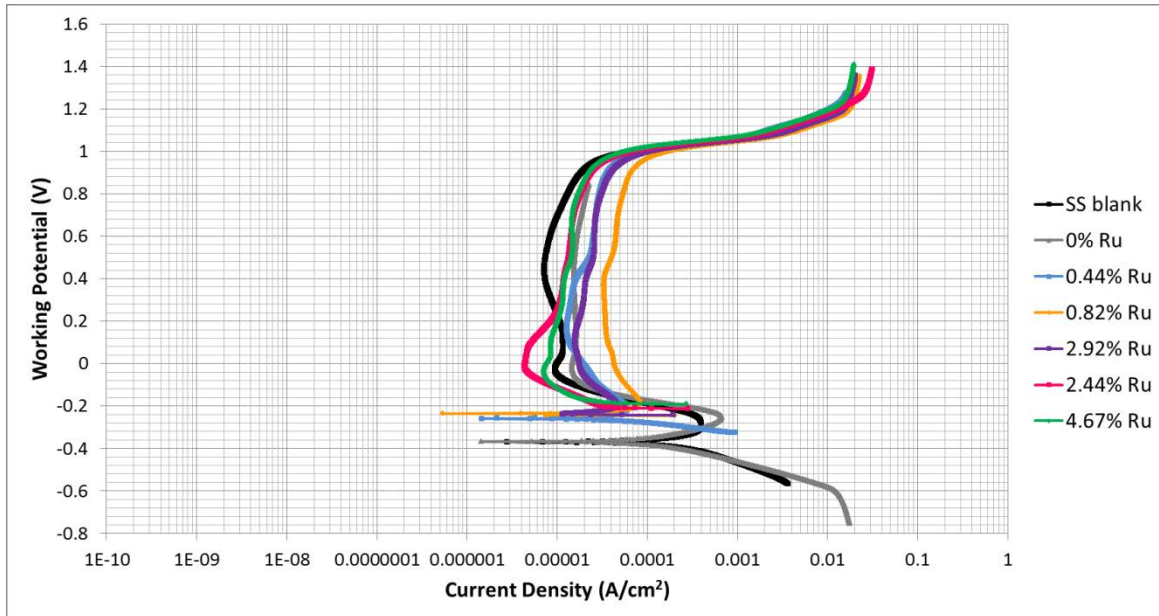


Figure 43: Log i vs E graphs from the fresh surface scan comparing all samples in 1 M H₂SO₄ at 25°C

Observing the potential over time, as in Figure 44, the curve for the stainless steel blank sample increased rapidly initially and then gently leveled off at 0 V. The potential of the clad sample without ruthenium was decreasing over time until leveling off only after 9 hours to a stable value which was the lowest OCP value under these conditions with -0.23 V. All the ruthenium containing samples increased initially but very quickly leveled off to a stable value except the 4.67 wt% Ru sample which seemed to still follow on a slight upwards trend after the 12 hours of exposure. The 0.82 wt% Ru sample exhibited the highest OCP value at 0.28 V, closely followed by the 2.92 wt% Ru sample, the 4.67 wt% Ru sample while the 0.44 wt% Ru and 2.44 wt% Ru samples had the same OCP value of 0.12 V but that being the lowest number of the ruthenium containing alloys.

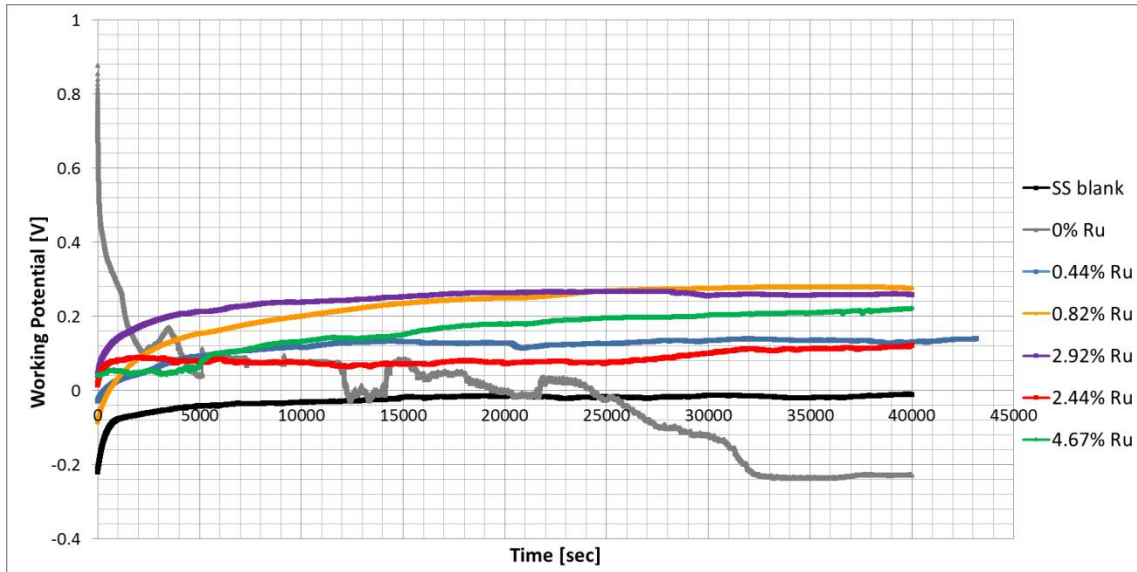


Figure 44: E vs time graphs comparing all samples in 1 M H₂SO₄ at 25°C

Noticing indicators for determining and comparing corrosion activity, it is best to compare them as in Table 6 where the average E_{corr} , i_{corr} , current density at 0.2 V, the corrosion rate, polarisation resistance and OCP values of the valid tests were calculated to give a good representation as comparison. The full results are available in Appendix D. A graphical representation of the values in the table is given below the table in Figure 45 to Figure 49 so that trends could be identified better.

Table 6: Indicators of corrosion rate using average sample measurements from the exposed surface scan in 1 M H₂SO₄ at 25°C

	E_{corr} [mV]	i_{corr} [A/cm ²]	i at 0.2 V [A/cm ²]	Corrosion rate [mm/year]	Polarisation resistance [Ω]	OCP after 12 hours [mV]
S/S blank	-257	8.43×10^{-6}	8.26×10^{-6}	0.088	17 161	-12
0.0% Ru	-358	1.66×10^{-4}	1.65×10^{-5}	1.722	407	-242
0.44% Ru	-222	8.99×10^{-6}	3.74×10^{-6}	0.083	31 331	134
0.82% Ru	76	5.06×10^{-7}	1.43×10^{-6}	0.005	417 007	305
2.92% Ru	121	4.43×10^{-7}	8.40×10^{-7}	0.004	384 535	336
2.44% Ru	134	3.35×10^{-7}	1.80×10^{-6}	0.003	1 040 400	204
4.67% Ru	88	6.54×10^{-7}	1.11×10^{-6}	0.006	543 803	233

Generally, the higher the corrosion potential, the more corrosion protection a sample is offering and therefore looking at this value and comparing it graphically for the various

ruthenium compositions yields Figure 45. In the 1 M sulphuric acid environment, the highest corrosion potentials were obtained in the range of 0.82 wt% to 2.92 wt% Ru whereas the 4.67 wt% Ru sample had a slightly lower OCP values. The remaining samples had lower results by over 300 mV difference.

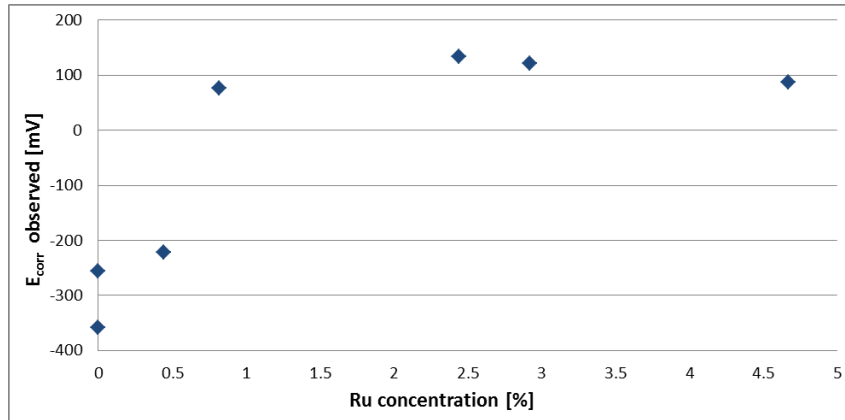


Figure 45: E_{corr} comparison at various ruthenium compositions for the exposed surface scan in 1 M H_2SO_4 at 25°C

The lower the corrosion current density, the slower the rate of corrosion and looking at this value graphically results in Figure 46. It is seen that in this medium the lowest values were observed in the range of 0.82 wt% to 2.92 wt% Ru with the 4.67 wt% Ru sample only being marginally higher while the other samples were much higher. Table 6 gives the exact values.

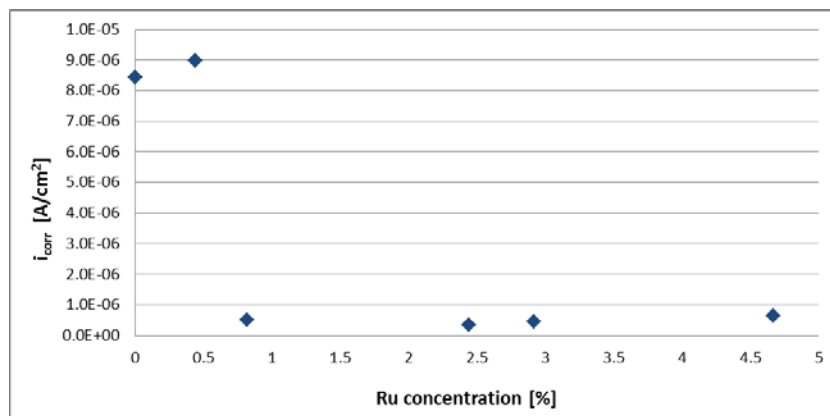


Figure 46: i_{corr} comparison at various ruthenium compositions for the exposed surface scan in 1 M H_2SO_4 at 25°C

Monitoring the current density at a particular potential, such as 0.2 V which was at the start of the passive region for most samples, gave a good indication of the corrosion activity at that potential; presented in Figure 47. In this case, all the ruthenium containing samples showed improved corrosion resistance as the current densities were significantly lower; the lowest results are obtained from 0.82 wt% Ru onwards.

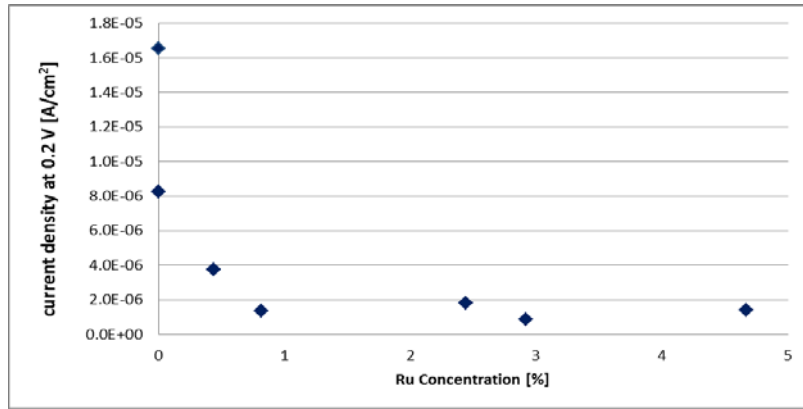


Figure 47: i at 0.2V comparison at various ruthenium compositions for the exposed surface scan in 1 M H_2SO_4 at 25°C

The actual corrosion rate is calculated as explained in the literature review section 2.2 and since rates varied significantly, they were plotted on a log scale to be able to show the trend. Significantly reduced corrosion rates were observed for the ruthenium containing samples as soon as 0.82 wt% Ru had been added and the two lowest rates were observed for the 2.44 wt% and 2.92 wt% Ru samples.

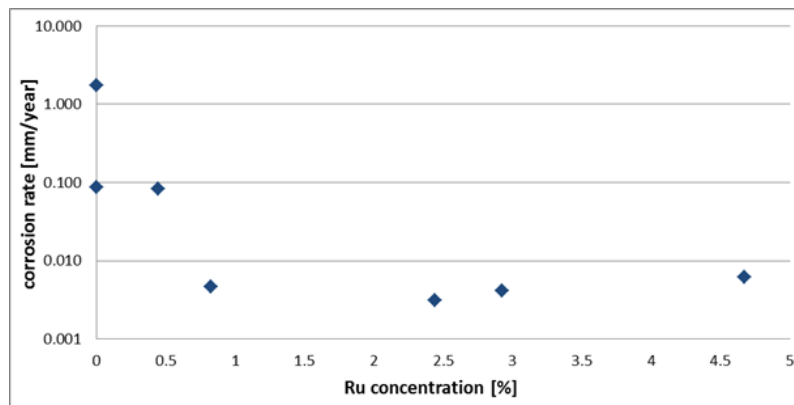


Figure 48: Corrosion rate at various ruthenium compositions for the exposed surface scan in 1 M H_2SO_4 at 25°C

For polarisation resistance, as per equations D and E (section 2.2), a high value is desired suggesting good corrosion resistance and thus protection against corrosion. The highest value obtained was for the 2.44 wt% Ru sample but in fact all samples containing ruthenium had an increased polarisation resistance and therefore improved corrosion protection in this environment; this was most evident for an addition of at least 0.82 wt% Ru.

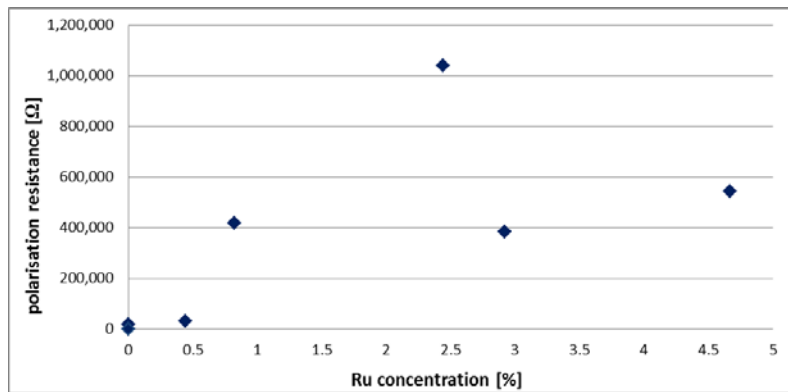


Figure 49: Polarisation resistance at various ruthenium compositions for the exposed surface scan in 1 M H₂SO₄ at 25°C

Large positive OCP values are desired for maximum corrosion protection, provided that the OCP value is greater than the E_{pass} value to ensure passivity and lower than E_{trans} to avoid dissolution in the transpassive region. All additions of ruthenium tested in this experiment shift the OCP into the positive region, i.e. brought the OCP values to the more noble region; presented in Figure 50. The highest result was obtained for the 2.92 wt% Ru sample while the range of 0.82 wt% Ru to 4.67 wt% Ru showed the highest results.

In theory, the OCP values should be the same as the E_{corr} values which was not the case with any of these results; they did follow the same trend however but the OCP values were always higher than the corrosion potential.

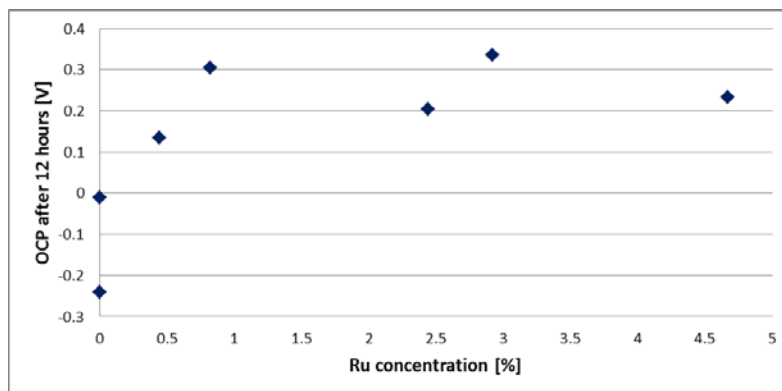


Figure 50: OCP comparison at various ruthenium compositions from the exposed surface scan in 1 M H₂SO₄ at 25°C

During the second anodic scan a fresh surface area of the sample was exposed and the results obtained from such a scan also need to be investigated and compared so that the behaviour of the samples in this condition can be obtained. Table 7 and Figure 51 to Figure 54 give the average results of E_{corr} and i_{corr} values as well as the corrosion rate and polarisation resistance from the valid tests carried out; the remaining results can be found in Appendix D. No current

density values were obtained at a specific potential as the results were very close to each other and did not give more meaningful results than the values already looked at.

Table 7: Indicators of corrosion rate using average sample measurements from the fresh surface scan in 1 M H₂SO₄ at 25°C

	E _{corr} [mV]	i _{corr} [A/cm ²]	Corrosion rate [mm/year]	Polarisation resistance [Ω]
S/S blank	-363	4.81x10 ⁻⁴	5.0068	169
0.0% Ru	-369	3.75x10 ⁻⁴	3.8994	199
0.44% Ru	-265	5.64x10 ⁻⁵	0.5188	1 097
0.82% Ru	-274	3.74x10 ⁻⁶	0.0432	N/A*
2.92% Ru	-303	1.13x10 ⁻⁴	1.0537	582
2.44% Ru	-256	2.64x10 ⁻⁴	2.4598	396
4.67% Ru	-236	8.17x10 ⁻⁵	0.7657	763

The N/A* implies that no suitable measurements were obtained during that scan to be able to calculate the parameters.

Much lower E_{corr} values were observed than during the exposed surface scan, all of them were negative numbers which implies less corrosion protection during the fresh surface scan. The highest number was obtained for the 4.67 wt% Ru sample, closely followed by the 2.44 wt% Ru and in general, all the ruthenium containing samples exhibited higher E_{corr} values than the 304L stainless samples alone.

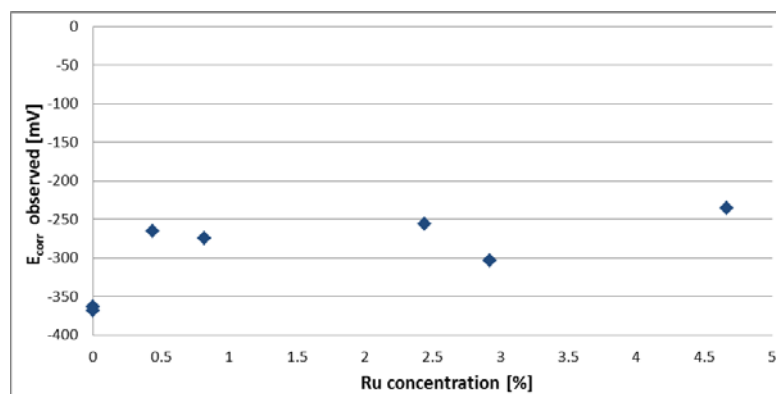


Figure 51: E_{corr} comparison at various ruthenium compositions from the fresh surface scan in 1 M H₂SO₄ at 25°C

Since the current density is a direct indication of corrosion rate, these values should be as low as possible and again it was observed that all the ruthenium containing samples had the lowest current densities compared the samples without the precious metal. The prominent gap

between them, as observed during the exposed surface scan, had however been reduced during the fresh surface scan. The lowest value was obtained for the 0.82 wt% Ru sample followed by the 0.44 wt% Ru sample with the next lowest being the 4.67 wt% Ru sample and then the 2.92 wt% Ru sample.

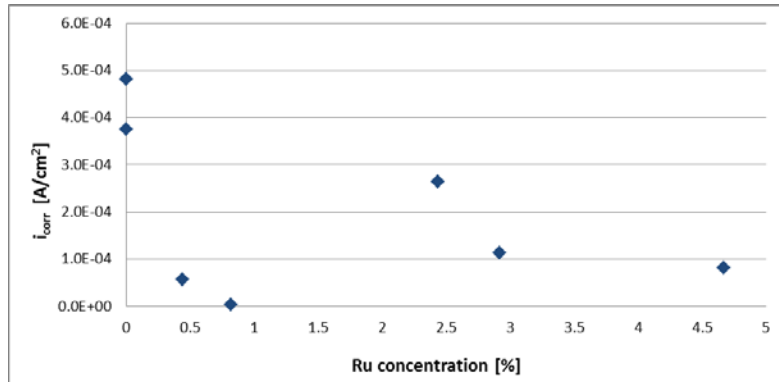


Figure 52: i_{corr} comparison at various ruthenium compositions from the fresh surface scan in 1 M H₂SO₄ at 25°C

As suspected, the corrosion rate follows exactly the same trend as the current density showing lower values with the addition of ruthenium in this environment but larger numbers than obtained during the exposed surface scan. The lowest value was obtained for the 0.82 wt% Ru sample followed by the 0.44 wt% Ru sample with the next lowest being the 4.67 wt% Ru sample and then the 2.92 wt% Ru sample which follows the same ranking order as the current densities.

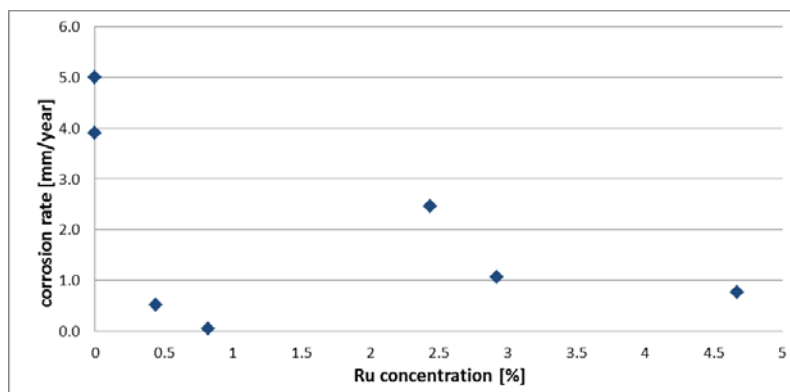


Figure 53: Corrosion rate comparison at various ruthenium compositions from the fresh surface scan in 1 M H₂SO₄ at 25°C

Polarisation resistance values are desired to be as large as possible for good corrosion protection and as can be seen below, all the ruthenium containing samples show significantly elevated polarisation resistance more than five times that of the stainless steel blank sample. The highest value was obtained for the 0.44 wt% Ru sample followed by the 4.67 wt% and

then 2.92 wt% Ru samples even though none of them come close to the values obtained during the exposed surface scan.

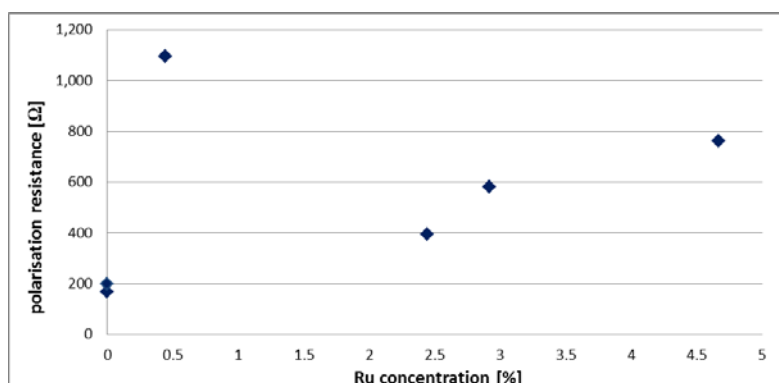


Figure 54: Polarisation resistance comparison at various ruthenium compositions from the fresh surface scan in 1 M H₂SO₄ at 25°C

In order to assess true passivity, one needs to compare the OCP values to the E_{pass} values: if $\text{OCP} < E_{\text{pass}}$ then the sample in this condition is active but if $\text{OCP} > E_{\text{pass}}$ then the surface is passive. For all samples the average OCP values after 12 hours were higher than the average E_{pass} values for the two scans indicating passivity which is what is desired. This difference was especially prominent for the ruthenium containing samples. All potentials are negative for the stainless steel blank and 0 wt% Ru sample as well as all the E_{pass} values from the fresh surface scan. Looking at Table 8, it was observed that the cladded sample with no ruthenium had the lowest passivation potentials and values were increasing with the addition of ruthenium but not directly. The highest values were seen for the 0.82 wt% Ru sample and upwards.

Table 8: Passivation potential comparison to OCP values at 1 M H₂SO₄ at 25°C

	E_{pass} from exposed surface scan [mV]	OCP after 12 hours [mV]	E_{pass} from fresh surface scan [mV]
S/S blank	-233	-12	-367
0.0% Ru	-362	-242	-368
0.44% Ru	-220	134	-260
0.82% Ru	55	305	-236
2.92% Ru	178	336	-235
2.44% Ru	138	204	-311
4.67% Ru	49	233	-243

In order to assess the real benefit of the ruthenium containing samples in a specific media, it is best to compare them with stainless steels that are commercially available and would be suitable in the media tested. This was done and the results can be observed in Figure 55 and Figure 56 below. Variability of the 316 stainless steel, the SAF2205 duplex stainless steel and the Hastelloy C276 samples was excellent and most of them were only repeated once, the results of these repeat experiments are not given in this report however.

The stainless steel 304L blank serves as a reference for comparison and two ruthenium containing samples were selected for the comparison which has been described above. Figure 55 shows the results after the exposure for 12 hours in 1 M sulphuric acid at 25°C. The 316 stainless steel behaved very similarly to the ruthenium alloys in that it displayed the transition shape but with a higher E_{corr} of 0.23 V and thus a slightly reduced passive range and higher current densities throughout that range compared to the 2.92 wt% Ru sample, as an example. The SAF2205 duplex stainless steel displayed the lowest E_{corr} at -0.36 V, a significant active nose and the highest but stable i_{pass} which was almost an order of magnitude larger than that of the 304L stainless steel. The Hastelloy C276 had a flatter cathodic Tafel slope than the 304L stainless steel but an identical E_{corr} value, small active nose but then slightly higher current densities in the passive region before a shallower and earlier trans-passive region. From that point of view it indicates that the SAF and Hastelloy materials did not indicate as good a corrosion resistance as the ruthenium containing 304L stainless steels. However, their passive regions are stable, they have a significantly lower passivation potential and certainly spread over a wider potential range compared to the ruthenium containing samples which certainly implies a stable passive film is formed on the surface of the material.

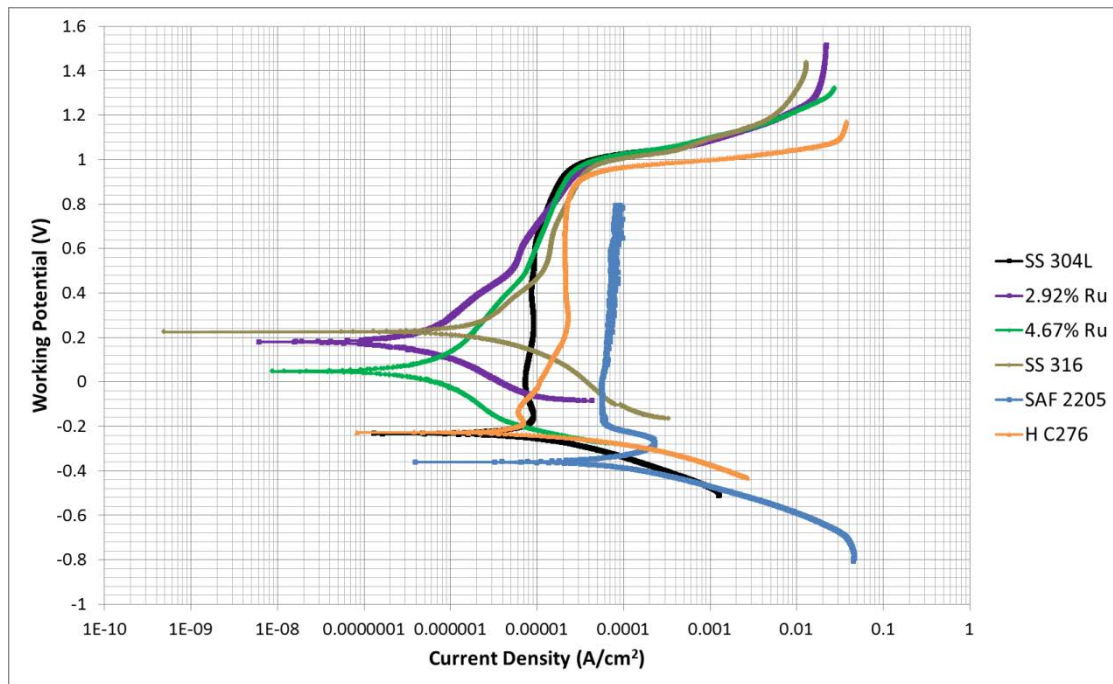


Figure 55: Log I vs E graphs from the exposed surface scan comparing ruthenium samples to other steels in 1 M H_2SO_4 at $25^\circ C$

On a fresh surface area, the various types of steel behave similarly. The 316 stainless and SAF2205 had similar E_{corr} values just below those of the ruthenium containing alloys but higher than the blank 304L stainless steel while the Hastelloy material had the highest E_{corr} value at -0.16 V. All indicated small active noses, or small levels of activity, before a stable passive region was observed in a very similar range as the ruthenium containing alloys, the SAF material in fact almost the same as the 304L stainless steel blank sample. They also all displayed similar results going into the trans-passive region. The passive region was shortest for the Hastelloy being 0.9 V and slightly higher, just above 1 V, for the 316 stainless steel and SAF2205.

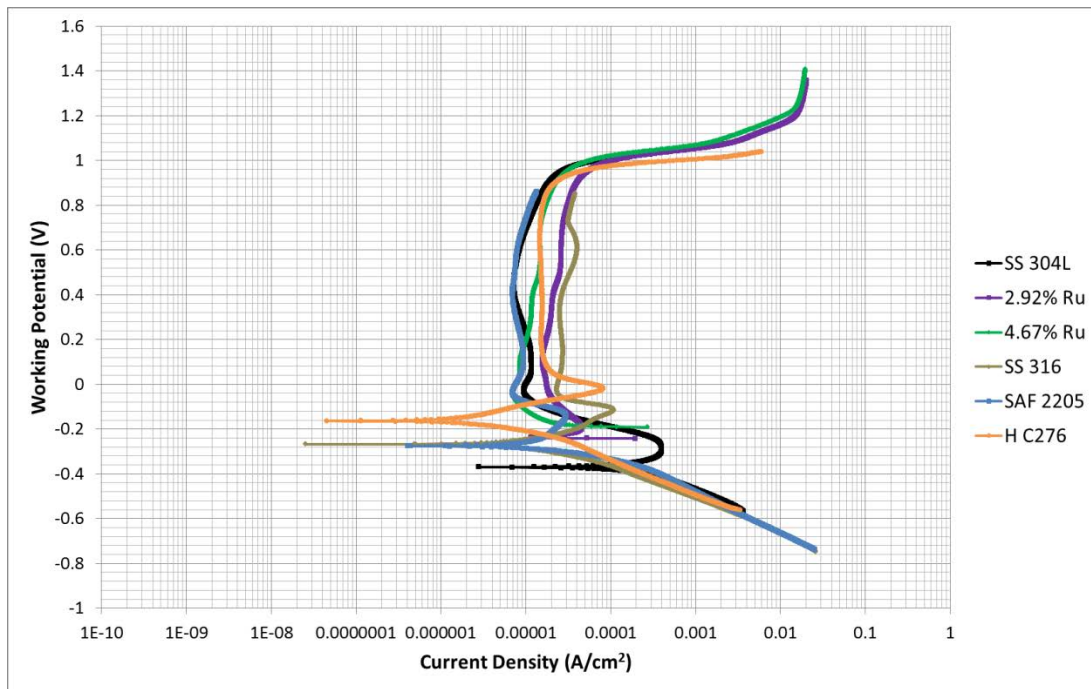


Figure 56: Log i vs E graphs from the fresh surface scan comparing ruthenium samples to other steels in 1 M H_2SO_4 at 25°C

4.3.2 1 M H_2SO_4 + 1% NaCl solution at 25°C

As with the tests in 1 M sulphuric acid, the repeatability of results had to be investigated to ensure the validity in the comparison that follows. The graphs below are again examples from the testwork carried out and show the results after repeating the same experiment, in the same environment with the same sample. The remaining repeatability results can be found in Appendix E.

The three test results from the exposed surface scan coincided as can be seen in Figure 57 and so are the results from the fresh surface scan even though test 1 did deviate slightly having a higher i_{crit} . The active region for the exposed tests was consistent, the E_{corr} was also identical for the three tests at -0.34 V and they have a prominent nose before gently moving into the passive region at i_{pass} values of less than $1.0 \times 10^{-4} A/cm^2$. The test results for the fresh surface showed steeper Tafel slopes, marginally lower E_{corr} values at -0.38 V, a shorter active nose and a gentle slope going into the passive region which was just less than that after exposure. The first test from the fresh surface scan showed a significantly increased i_{crit} when compared to the other tests from the fresh surface scan. It was observed this time that the average i_{crit} and i_{pass} for the test results from the exposed surface scan had a higher value than from the fresh surface scan which is opposite to what was observed without the sodium chloride. The

passivation potential range tested had however not changed when comparing the exposed and fresh surface scan results. The trans-passive region was not obtained during these tests.

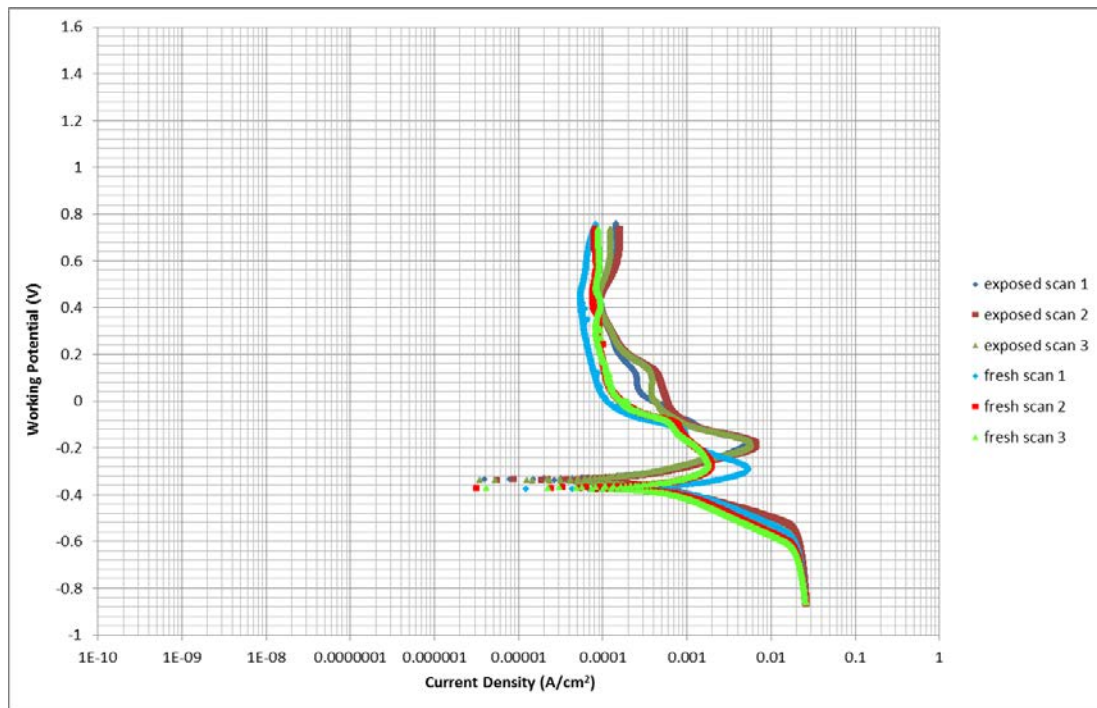


Figure 57: Log i vs E graphs for the Stainless Steel blank sample in 1 M H₂SO₄ + 1% NaCl at 25°C

The inconsistency, when observing the potential over a 12 hour period, is slight and appears significant in Figure 58 only because of the selected scale. The overall trend of the graphs is similar in that the potential increased over time and seemed not to have stabilised at the end of the 12 hours but the scale had been much increased to show this. The obtained OCP values from these experiments differed by only 0.02 V where tests 2 and 3 were almost identical reaching a value of -0.364 V.

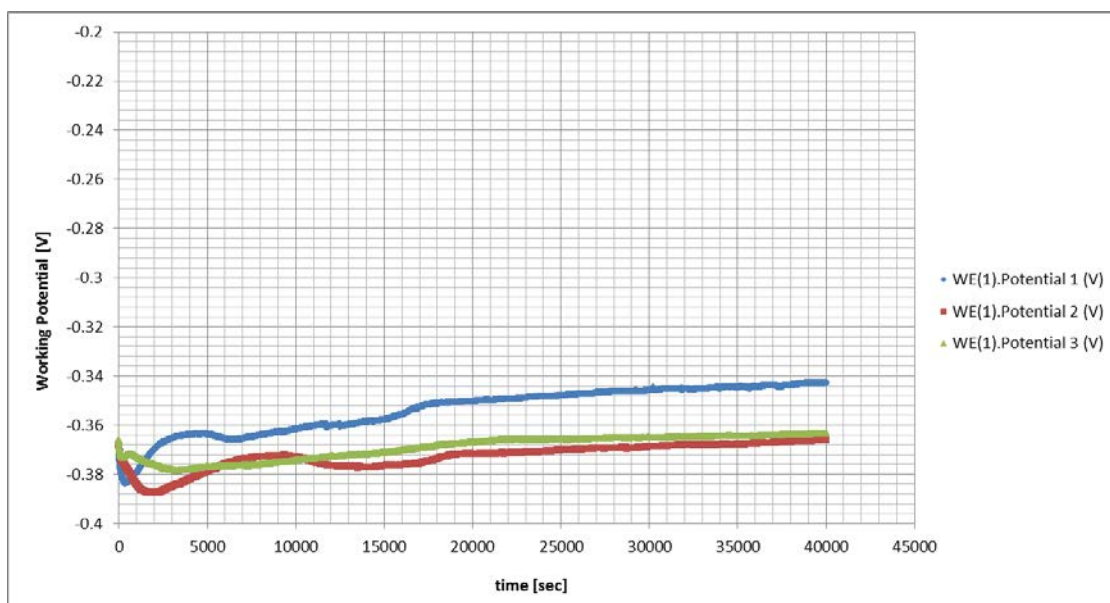


Figure 58: E vs time graphs for the Stainless Steel blank sample in 1 M H₂SO₄ + 1% NaCl at 25°C

Tests for the 0.44 wt% Ru sample could not be conducted in this environment; the sample was destroyed during the previous testwork. It was therefore decided to take two samples of the next ruthenium composition and perform all the tests on both samples so that again, repeatability could be observed.

The microscopic analysis showed that as ruthenium was added to the stainless steel, some variability must be expected and this was observed in the electrochemical test results. The Tafel slopes of the graphs from the exposed surface scans were similar even though test 1 from the exposed surface scan did not show the traditional transition curve but showed cathodic loops forming and the active region from the 3rd experiment was at a significantly higher potential. The E_{corr} values had a reasonable spread, tests 2 and 3 in the region of 0.2 V, but E_{corr} from test 1 was closer to 0 V. All three curves entered the trans-passive region at 1 V potential implying that the passive range extends over a maximum of 0.8 V. For the fresh surface scan, the curves showed significantly increased corrosion densities which implies less corrosion protection; the opposite to what was observed on the stainless steel blank sample in this environment but similar to what was observed for this sample in the 1 M sulphuric acid at ambient conditions. Repeatability for the fresh surface scan improved especially for tests 1 and 2. They showed passivity between 3×10^{-5} and 6×10^{-5} A/cm², and the passive region of the curves extended over a potential range of 1.2 V ending in the same trans-passive region at 1.0 V as the scan after exposure. The 3rd test exhibited a cathodic loop before passivation which significantly shortened its passive range.

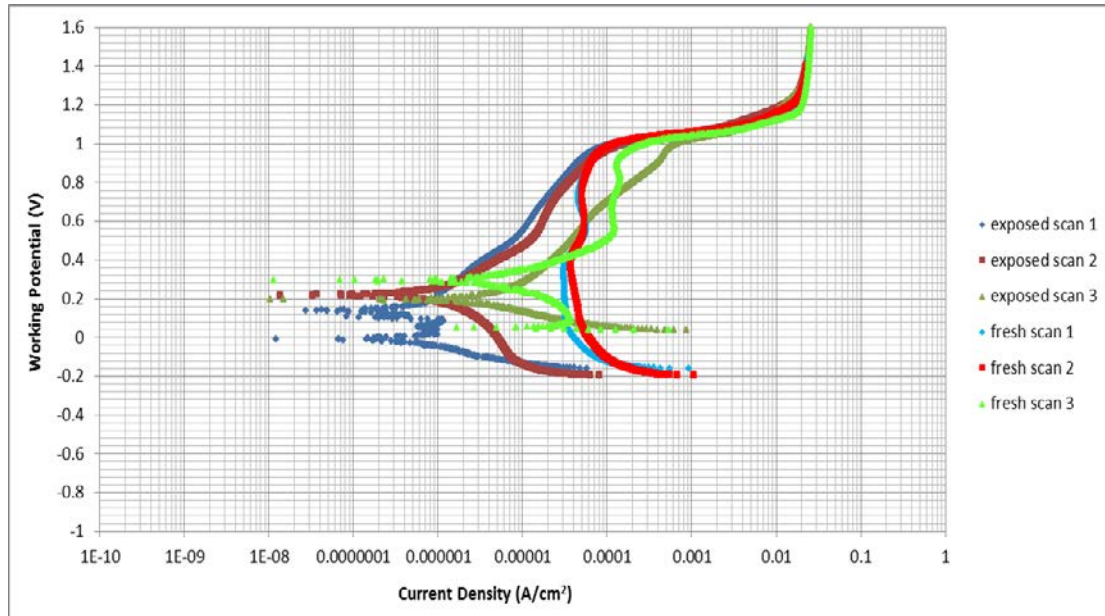


Figure 59: Log i vs E graphs for the 0.82 wt% Ru sample #1 in 1 M H_2SO_4 + 1% NaCl at 25°C

Observing the potential over time, variability was observed as can be seen in Figure 60, the shapes of all three tests were different: test 1 slowly increasing with time and then starting to level-off, test 2 steeply increasing potential at first but then slowly dropping over time and test 3 dipping down first, then rising gently and then slowly levelling off. None of the tests seem to have obtained a stable value after the 12 hour test. The OCP values for tests 1 and 2 were close to each other at approximately 0.32 V, while test 3 was 0.15 V higher; significant variability which must be kept in mind when analysing these results.

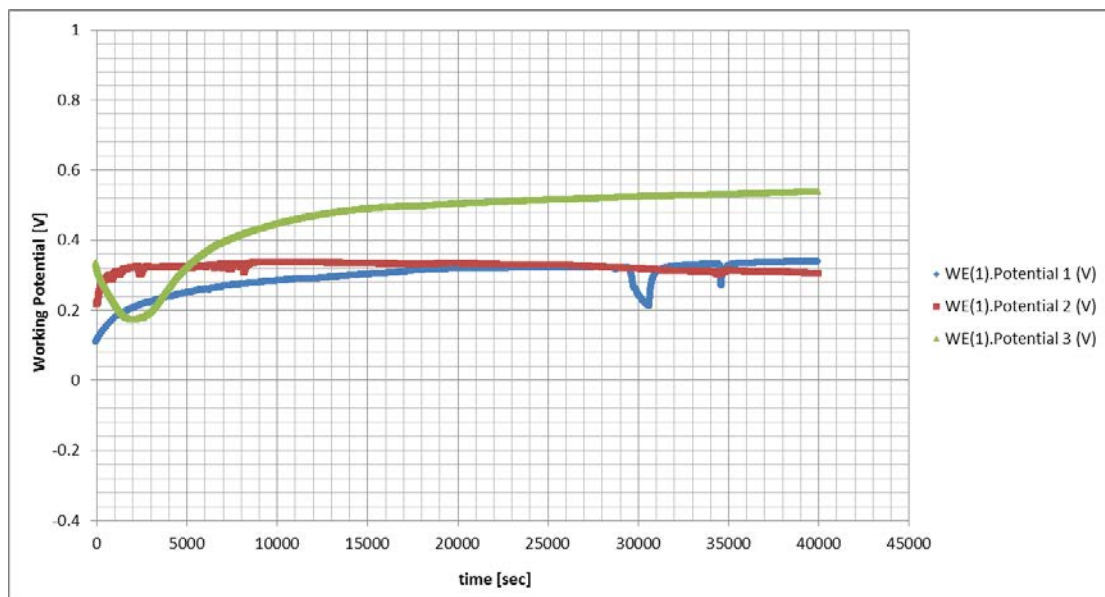


Figure 60: Log E vs time graphs for the 0.82 wt% Ru sample #1 in 1 M H_2SO_4 + 1% NaCl at 25°C

For the second sample with the 0.82 wt% Ru composition, see Figure 61, reasonable repeatability was observed. For the tests from the exposed surface scan, a significant

difference in i_{crit} was observed, i.e. over two orders of magnitude ranging from, approximately 2×10^{-5} A/cm² for the 1st test to 2×10^{-3} A/cm² for the 3rd test. The E_{corr} values for these three tests were however reasonably close to each other at -0.26 V. The curves for test 1 and 2 did, thereafter, almost merge again in the passive and trans-passive regions showing good repeatability. The passivation potential range was consistent at over 1.0 V which was longer than observed for sample #1 with the 0.82 wt% Ru composition. Repeatability from the fresh surface scan was improved significantly and, in fact, the curves are very similar to tests 1 and 2 from the exposed surface scan. The E_{corr} was slightly reduced to approximately -0.35 V. Test 3 behaved differently in that it showed reduced corrosion protection during the exposed surface scan, i.e. higher current densities throughout the test, but better corrosion protection during the cleaned surface scan.

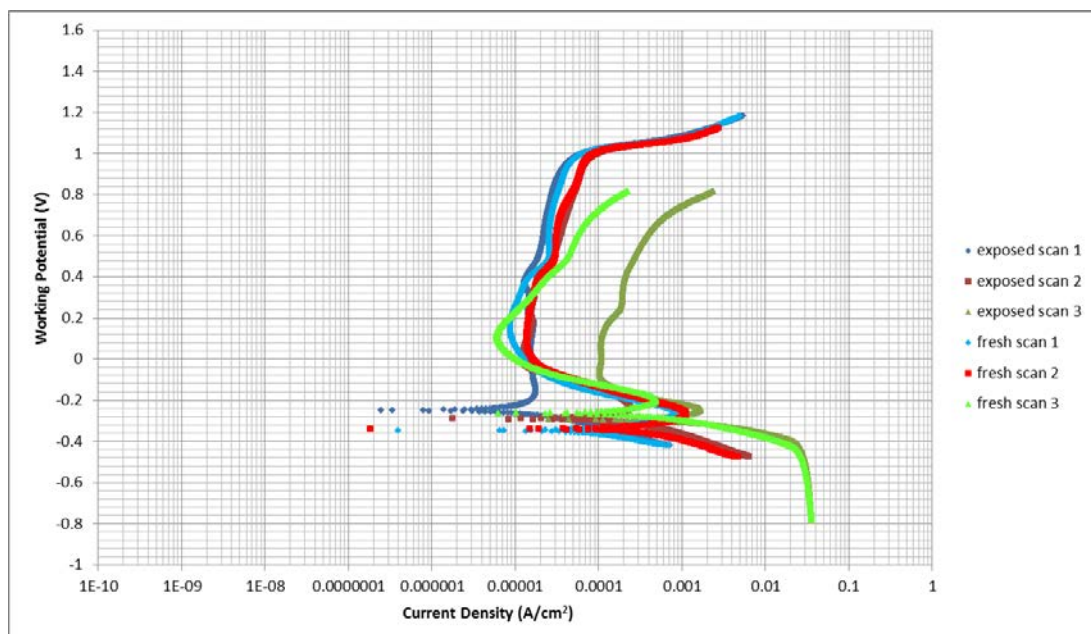


Figure 61: Log i vs E graphs for the 0.82 wt% Ru sample #2 in 1 M H₂SO₄ + 1% NaCl at 25°C

For the potential over time graphs, as can be seen in Figure 62, tests 1 and 2 showed repeatability, in fact a potential close to the starting potential of 0.05 V which is significantly lower than what was obtained for the 1st sample, but test 3 being quite different. Relatively stable values were obtained quickly but the values vary significantly between the tests with an overall OCP range of 0.35 V. It indicates that test 3 should not be used for comparisons in further analysis.

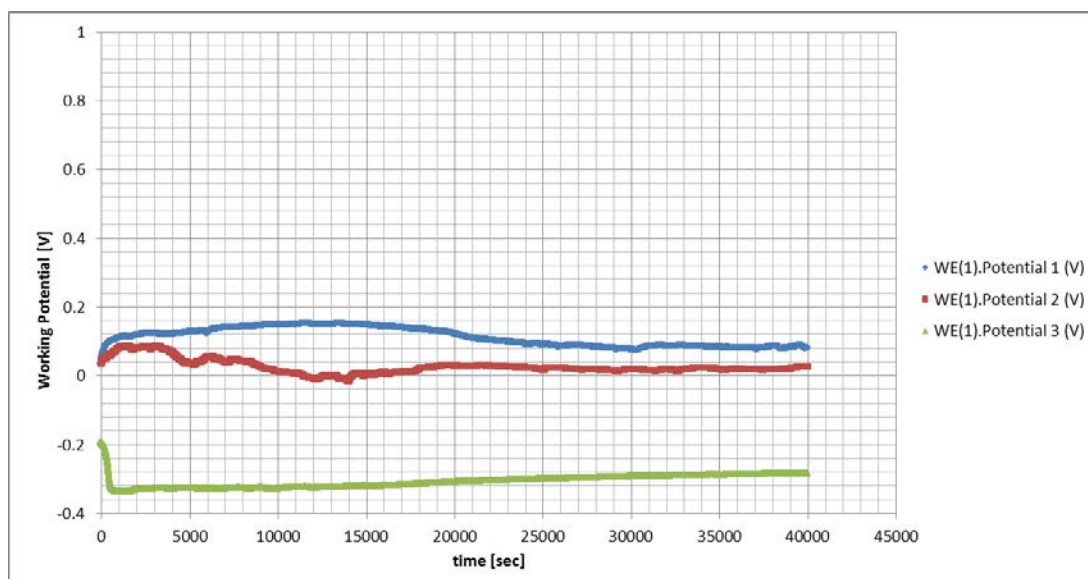


Figure 62: E vs time graphs for the 0.82 wt% Ru sample #2 in 1 M H₂SO₄ + 1% NaCl at 25°C

For the highest amount of ruthenium added, the 4.67 wt% Ru samples, consistency was reasonable especially for the fresh surface scans. During the exposed surface scan, the cathodic Tafel slopes appeared very similar, the E_{corr} values were close to each other around -0.2 V and a small nose was observed before passivity. Test 4 results showed cathodic loops forming as observed in Figure 65 suggesting unstable behavior but besides that, passivity was observed over approximately 1.0 V before all curves coincide in the trans-passive region. Test 3 of the exposed surface scans showed an order of magnitude higher i_{crit} compared to the other tests but that difference slowly reduced until the trans-passive region was reached. Thus passivation was observed over a similar potential range compared with other tests. Repeatability was improved during the fresh surface scans: all having a much larger active nose with higher maximum densities around 1×10^{-3} A/cm² and less steep curves going into the passive region with a slightly reduced passive potential range of 0.8 V. The trans-passive behavior is the same as that for the exposed surface scans. From the fresh surface scan, only test 1 results were slightly lower in current density than the other results from the fresh surface scan. They were at higher values than the ones from the exposed surface scan, indicating higher corrosion rates on a fresh surface area which is what was observed in the sulphuric acid only.

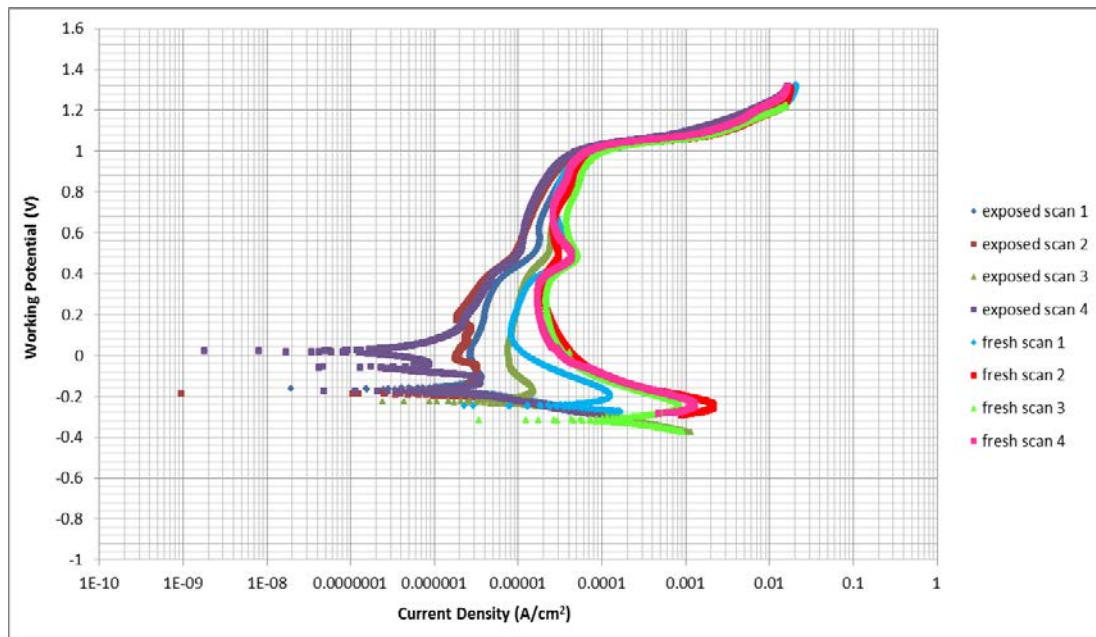


Figure 63: Log i vs E graphs for the 4.67 wt% Ru sample in 1 M H_2SO_4 + 1% NaCl at 25°C

The potential observed over time showed some variability during the 12 hour time period but all curves showed the same trend of an initial steep increase in potential and then a leveling off towards the OCP value. Only tests 2 and 4 reached a stable OCP value but since the OCP range was just about 0.1 V, it can be assumed that for all tests the values are close to the OCP values. The results were in the region of 0.2 V.

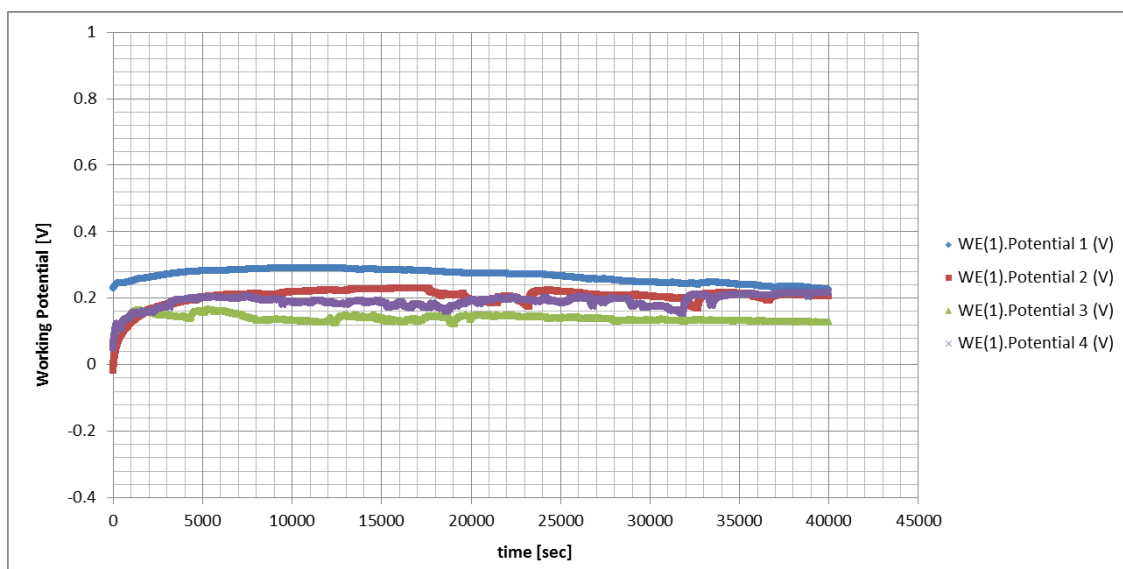


Figure 64: E vs time graphs for the 4.67 wt% Ru sample in 1 M H_2SO_4 + 1% NaCl at 25°C

Taking a representative curve from each of the samples tested in a solution of 1 M sulphuric acid with 1% sodium chloride at ambient temperature, one can compare them and thus the typical behavior of a sample with a specific composition, as in Figure 65 and Figure 66 below. This can also be done for Open Circuit Potentials and graphically that is represented

in Figure 67. The 304L stainless steel blank sample result was used as a reference to compare the other results to, as well as the cladded sample with only the stainless powder and no ruthenium.

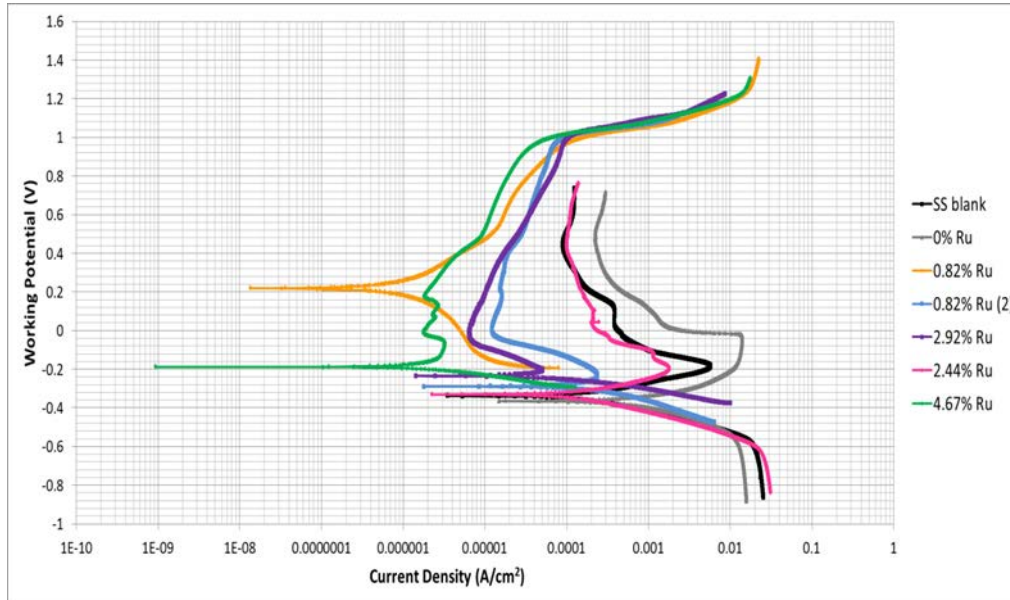


Figure 65: Log i vs E graphs from the exposed surface scan comparing all samples in 1 M H_2SO_4 + 1% NaCl at 25°C

The two curves without ruthenium behaved as expected having much worse corrosion protection in comparison to the ruthenium containing samples. The stainless steel blank had an E_{corr} of -0.35 V, a long but small nose before passivity was reached slowly at i_{pass} at approximately 1×10^{-4} A/cm². The cladded sample without ruthenium performed worse from a corrosion point of view; that is, it had the lowest E_{corr} at -0.37 V, a large nose with current densities exceeding those of the stainless steel blank throughout the entire scan, i.e. the i_{crit} and i_{pass} values were significantly higher. The two 0.82 wt% Ru samples showed very different results and were almost contradictory to each other in terms of shape and actual critical parameters; this can be seen from the orange and blue lines in Figure 65. It is very clear, however, that the added ruthenium dramatically improved that performance by orders of magnitude really showing the benefit of the precious metal. A clearer trend regarding the benefit of additional ruthenium was observed with the blue, purple and green lines in Figure 65. As the ruthenium content increased so did the E_{corr} values, the noses were getting smaller indicating reduced dissolution and the i_{pass} values decreased significantly and stable passivity was reached for all of them over a range of over 1.0 V. The passive region occurred over the same potential range in all samples except slightly reduced for the cladded sample only. One of the 0.82 wt% Ru samples exhibited the transition shape with a much larger E_{corr} value of

above 0.2 V which was over 0.5 V above the other 0.82 wt% Ru sample. This of course reduced the passive potential range by that amount as all the curves followed the same trans-passive behaviour. The clear outlier was the behaviour of the 2.44 wt% Ru sample which seemed to represent more of the stainless steel blank sample behaviour; it is suspected that the ruthenium layer has been ground off by that time.

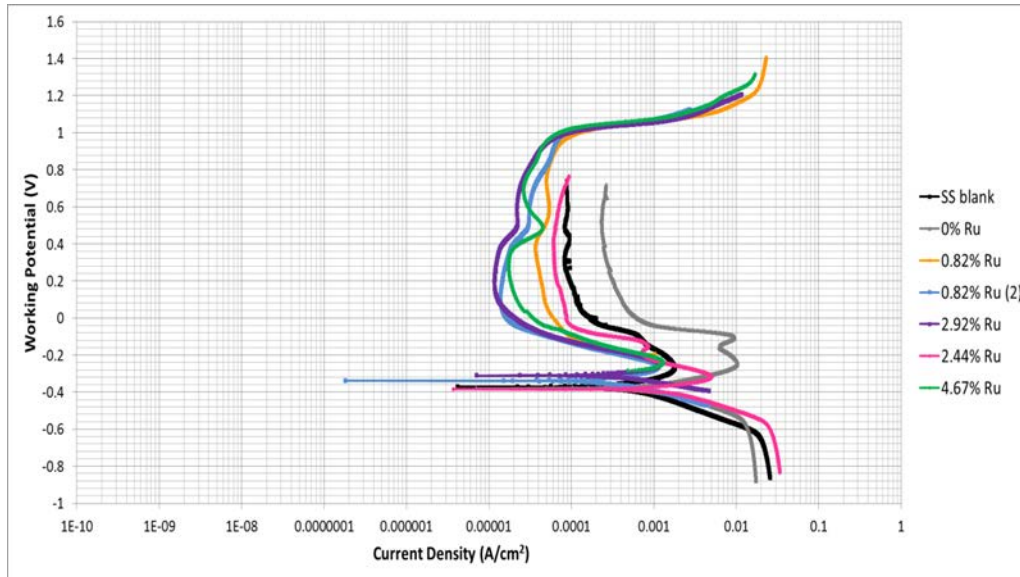


Figure 66: Log i vs E graphs from the fresh surface scan comparing all samples in 1 M H_2SO_4 + 1% NaCl at 25°C

For the test results from the fresh surface scans, as per Figure 66, it was still observed that the cladded sample without ruthenium addition was performing much worse than the stainless steel sample, having much larger current densities, and those are more prone to corrosion than the samples with added ruthenium. All the results this time correspond closely to each other and the clear trend with regards to increasing ruthenium concentration was not observed any more, the 2.92 wt% Ru had the lowest current densities but not by a significant amount. In fact, all E_{corr} values were close to each other between -0.38 V and -0.40 V, the i_{crit} values for all the samples containing some ruthenium were similar at just below $1 \times 10^{-3} A/cm^2$, the i_{pass} values were close and the values going into the trans-passive region were almost identical. Again the outlier was the 2.44 wt% Ru sample showing the lowest corrosion protection, in fact, again closer to the stainless steel blank sample result and thus it was suspected that the alloy layer had been ground off before the testing but that was not confirmed.

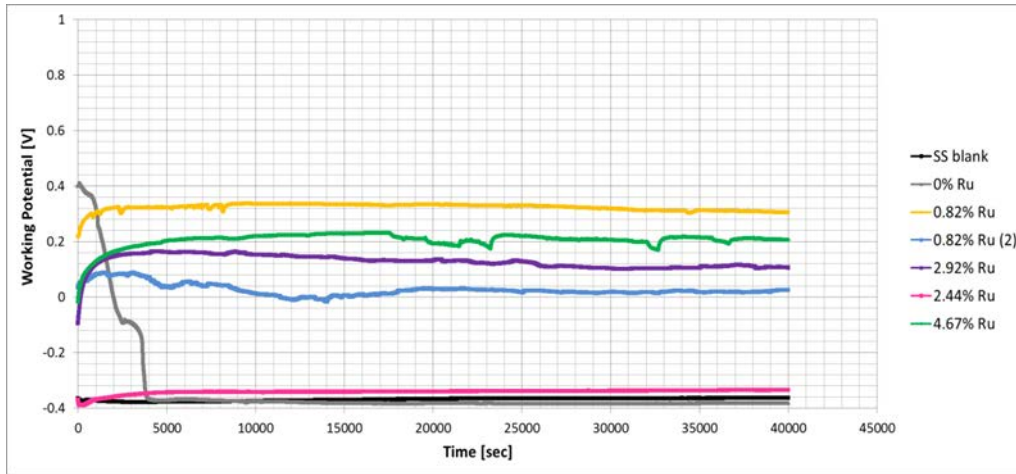


Figure 67: E vs time graphs comparing all samples in 1 M H₂SO₄ + 1% NaCl at 25°C

Observing the potential over time, it was again noticed that the two 0.82 wt% Ru samples were not consequential to the other ruthenium compositions and seem contradictory. It was observed however, that in this regard the stainless steel blank and cladded sample without ruthenium behaved very similarly and had almost identical OCPs which were the only negative numbers at just above -0.4 V. If one ignores the first 0.82 wt% Ru sample (orange line in Figure 67), the trend was confirmed which showed that the OCP values increase, i.e. become more noble and less active, with an increase in ruthenium. The 2.44 wt% Ru sample did not follow this trend and was suspected of containing no more ruthenium.

Table 9 provides a few indicators for comparing corrosion activity during the exposed surface scan such as the average E_{corr} , i_{corr} , current density at 0.1 V, the corrosion rate, polarisation resistance and OCP values of the valid tests which give a good representation for a comparison; these are graphically represented in Figure 68 to Figure 73. The full results are available in Appendix E. The results showed only one corrosion potential measured that was positive which was for the 0.82 wt% Ru sample while all others showed an increasing trend with increasing ruthenium composition. In general, it was observed that the 0.82 wt% Ru sample had the most desirable corrosion protection parameters and for almost all the parameters corrosion activity was reduced with an increase in ruthenium content with the exception of the additional 0.82 wt% Ru sample. The 2.44 wt% Ru sample behaved almost the same as the stainless steel blank sample and it was suspected that the cladded layer was actually ground off before these tests were conducted; this was already observed in the previous graphs.

Table 9: Indicators of corrosion rate using average sample measurements from the exposed surface scan in 1 M H₂SO₄ + 1% NaCl at 25°C

	E _{corr} [mV]	i _{corr} [A/cm ²]	i at 0.1 V [A/cm ²]	Corrosion rate [mm/year]	Polarisation resistance [Ω]	OCP after 12 hours [mV]
S/S blank	-336	2.19x10 ⁻⁴	3.70x10 ⁻⁴	2.28	374	-357
0.0% Ru	-352	6.15x10 ⁻⁴	6.54x10 ⁻⁴	6.40	189	-365
0.82% Ru	208	3.39x10 ⁻⁶	1.26x10 ⁻⁵	0.03	102 256	394
0.82% Ru (2)	-278	3.23x10 ⁻⁴	1.51x10 ⁻⁵	2.98	4 965	54
2.92% Ru	-239	2.81x10 ⁻⁵	5.48x10 ⁻⁶	0.26	5 686	114
2.44% Ru	-330	1.79x10 ⁻⁴	2.92x10 ⁻⁴	1.67	653	-336
4.67% Ru	-189	3.48x10 ⁻⁶	3.81x10 ⁻⁶	0.03	29 576	192

Generally, the more noble the corrosion potential, the greater is the tendency not to corrode. In the 1 M sulphuric acid environment with added 1% sodium chloride, the highest corrosion potential obtained was for the 0.82 wt% Ru sample which was in fact the only positive value obtained. The trend that could be seen from Figure 68 was that the values did increase with an increase in ruthenium composition, therefore the next highest value being observed for the 4.67 wt% Ru sample and then the 2.92 wt% Ru sample. The sample that did not correspond was the 2.44 wt% Ru sample which had a value closer to that of the stainless steel blank sample, thought to have had its surface cladding ground off before testing. The two 0.82 wt% Ru samples behaved very differently showing the inconsistency between samples.

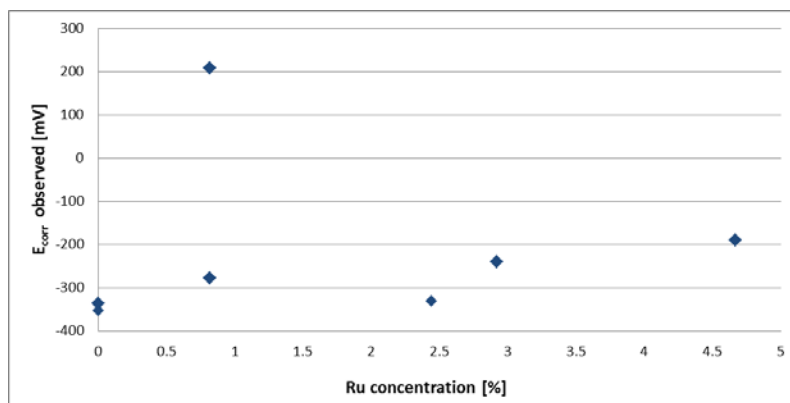


Figure 68: E_{corr} comparison at various ruthenium compositions from the exposed surface scan in 1 M H₂SO₄ + 1% NaCl at 25°C

The corrosion current density is directly proportional to the corrosion rate and therefore low values for i_{corr} imply that corrosion is taking place slowly and looking at these values graphically results in Figure 69. It is seen that in this medium the lowest values were

observed with an increase in ruthenium concentration, lowest value being at 4.67 wt% Ru and also one of the 0.82 wt% Ru samples being at a very low value. In fact the two 0.82 wt% Ru samples behaved very differently which was emphasised by these comparisons. The 2.44 wt% Ru sample, as previously observed, had a number closer to that of the stainless steel blank sample.

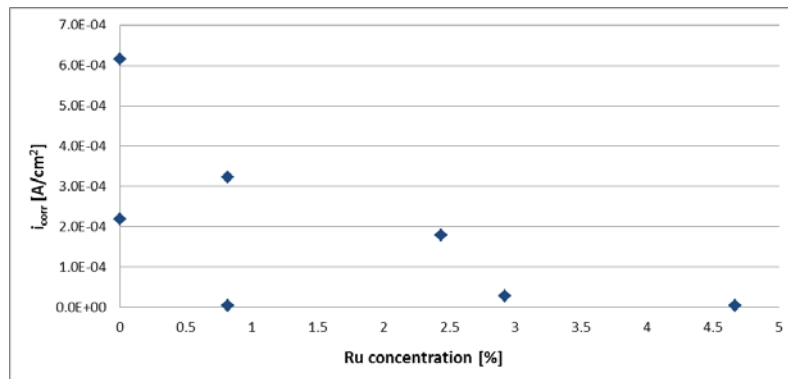


Figure 69: i_{corr} comparison at various ruthenium compositions from the exposed surface scan in 1 M H₂SO₄ + 1% NaCl at 25°C

Considering the current density at a particular potential, such as 0.1 V selected in this case, which is graphically presented in Figure 70, gives a good indication of the corrosion activity at that potential especially since it is plotted on a log scale. The start of the passive region is represented from 0.1 V upwards for the samples and the trend observed here is continuous through that region, thus giving a good indication of ranking the samples in terms of their corrosion protection during passivity. The graph shows very clearly that in this case, all the ruthenium containing samples (with the exception of the 2.44 wt% Ru sample which behaved very similarly to that of the stainless steel blank sample) showed improved corrosion resistance, the lowest results were at 4.67 wt% Ru followed by the 2.92 wt% Ru sample. The two 0.82 wt% Ru samples were distinctly different but this time followed the trend.

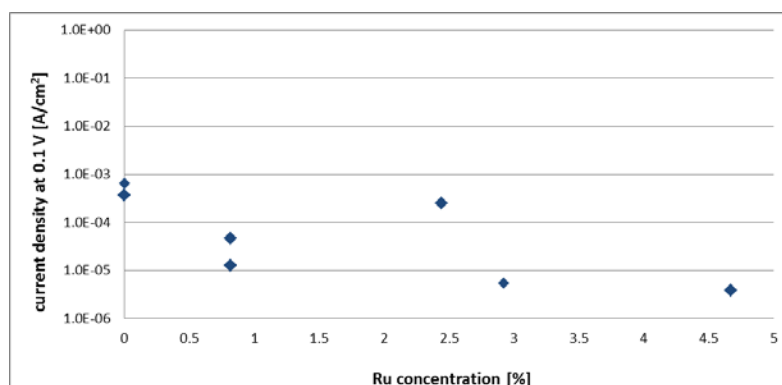


Figure 70: j at 0.1V comparison at various ruthenium compositions from the exposed surface scan in 1 M H₂SO₄ + 1% NaCl at 25°C

Figure 71 shows corrosion rates which confirmed the general observed trend from above that the corrosion rate is indeed decreasing with an increasing amount of ruthenium but not all the individual points confirm this statement such as the two 0.82 wt% Ru samples. For the ruthenium containing samples, the two 0.82 wt% Ru samples had the highest and lowest corrosion rate observed with the next lowest rate being at 4.67 wt% Ru and the 2.44 wt% Ru sample was again the outlier from that trend.

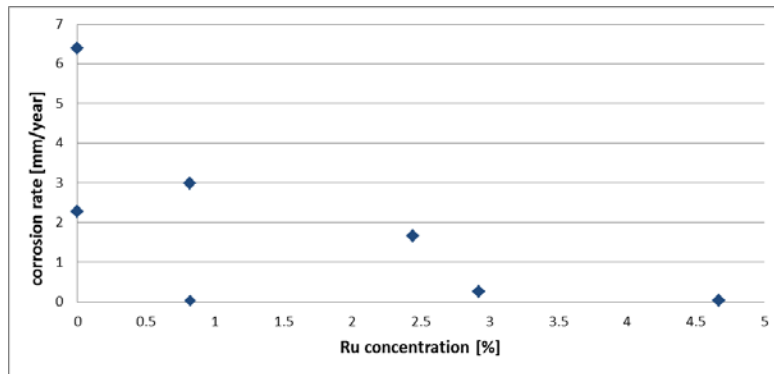


Figure 71: Corrosion rate comparison at various ruthenium compositions from the exposed surface scan in 1 M H₂SO₄ + 1% NaCl at 25°C

The polarisation resistance should ideally be as high as possible and one of the 0.82 wt% Ru samples showed the highest value from all the samples. The rest of the samples followed the trend of increasing polarisation resistance with increasing ruthenium content, which confirms other test results already showed under these conditions. Due to the log scale, it might not be immediately obvious, but the 2.44 wt% Ru sample was again significantly lower than the other ruthenium containing samples.

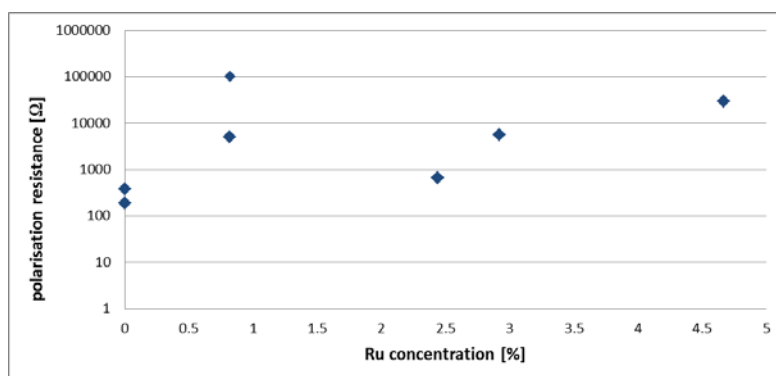


Figure 72: Polarisation resistance comparison at various ruthenium compositions from the exposed surface scan in 1 M H₂SO₄ + 1% NaCl at 25°C

The OCP values followed exactly the same trend as the E_{corr} values, as theoretically these should be the same value. Values that quickly go to more noble values are desired for maximum corrosion protection and all samples containing ruthenium tested in this

experiment shifted the OCP into the more noble region, presented in Figure 73. The two samples without ruthenium had almost reached the same values and appear as one data point, from there onwards the highest values were observed with an increase in ruthenium concentration, the highest value being one of the 0.82 wt% Ru samples and the next highest at 4.67 wt% Ru. In fact the two 0.82 wt% Ru samples behaved very differently again. It does look like the OCP values would level off after the 4.67 wt% Ru data point as the imaginary curve one can draw in Figure 73 starting from 0% Ru to the first 0.82% point, the 2.92% and finally the 4.67% Ru, do tend to flatten out. The exception was the 2.44 wt% Ru sample which behaved almost the same as the stainless steel blank sample and it was suspected that the cladded layer was ground off before these tests were conducted.

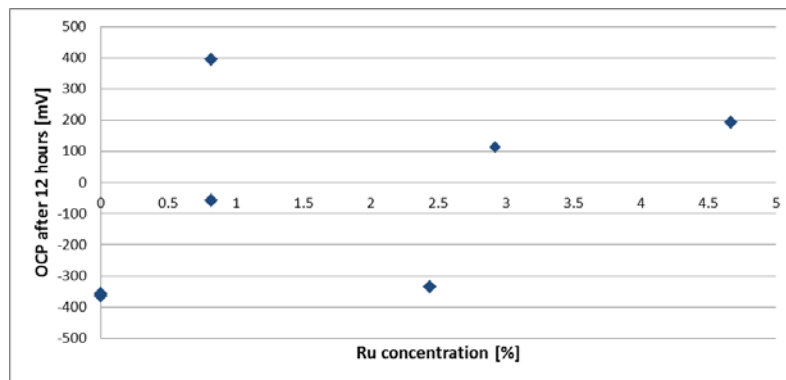


Figure 73: OCP comparison at various ruthenium compositions from the exposed surface scan in 1 M H₂SO₄ + 1% NaCl at 25°C

During the second anodic scan a fresh surface area of the sample is exposed and the results obtained can be seen in Table 10 which gives the average results of E_{corr} and i_{corr} values as well as the corrosion rate and polarisation resistance from the valid rests carried out; the remaining results can be found in Appendix E. All the E_{corr} values were negative with the ruthenium containing samples having lower values. The other parameters did follow a similar trend that the indication was that corrosion resistance increases with an increase in ruthenium composition.

Table 10: Indicators of corrosion rate using average sample measurements from the fresh surface scan in 1M H₂SO₄ + 1% NaCl at 25°C

	E _{corr} [mV]	i _{corr} [A/cm ²]	Corrosion rate [mm/year]	Polarisation resistance [Ω]
S/S blank	- 373	1.70x10 ⁻³	17.66	67
0.0% Ru	- 380	1.65x10 ⁻³	17.21	47
0.82% Ru	N/A*	N/A*	N/A*	N/A*
0.82% Ru (2)	- 317	1.12x10 ⁻³	10.35	114
2.92% Ru	- 318	5.36x10 ⁻⁴	4.98	119
2.44% Ru	- 387	5.36x10 ⁻³	50.01	47
4.67% Ru	- 283	1.55x10 ⁻⁴	1.46	314

The N/A* implies that no suitable measurements were obtained during that scan to be able to calculate the parameters.

There is an observable trend looking at the E_{corr} comparison in Figure 74 where the values definitely increased with an increase in ruthenium composition, the 2.44 wt% Ru sample was still not corresponding as it was suspected the cladded layer was ground off and in fact, the 0.82 wt% Ru had the second highest value so a definite improvement was observed on this fresh surface when exposed to sulphuric acid and chloride ions.

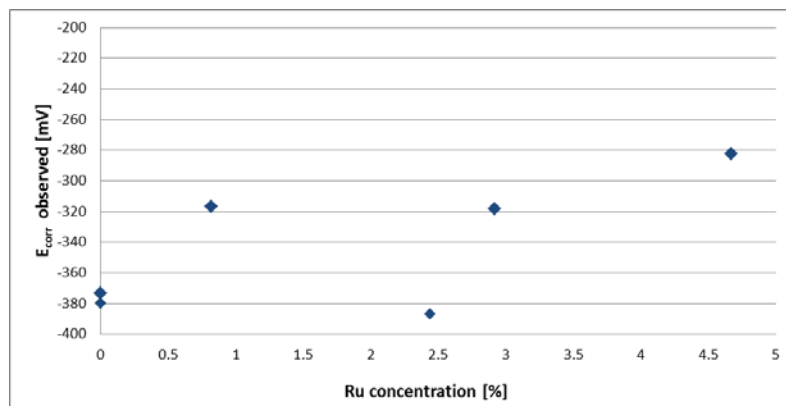


Figure 74: E_{corr} comparison at various ruthenium compositions from the fresh surface scan in 1 M H₂SO₄ + 1% NaCl at 25°C

Much lower i_{corr} values were observed than for the exposed surface scan, as per Figure 75, but a similar trend in that the values decreased with increasing ruthenium content indicating better corrosion protection. Again, the two samples without ruthenium had similar values and the 2.44 wt% Ru sample showed the highest values by far suggesting that no ruthenium was

left on that surface before the test (and should be disregarded) while the lowest value was obtained from the 4.67 wt% Ru sample.

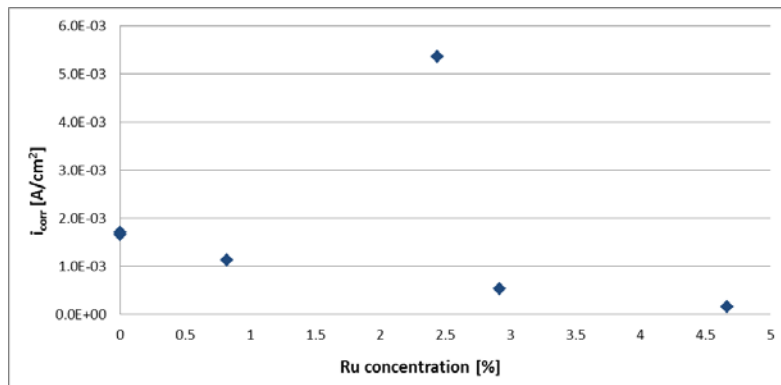


Figure 75: i_{corr} comparison at various ruthenium compositions from the fresh surface scan in 1M H₂SO₄ + 1% NaCl at 25°C

The corrosion rates of course show the same trend, Figure 76 shows that the corrosion rates were higher than for the exposed surface scan, the lowest value was obtained from the 4.67 wt% Ru sample and by far the highest value was observed from the 2.44 wt% Ru sample and the overall trend was definitely decreasing corrosion rates with an increase in ruthenium content.

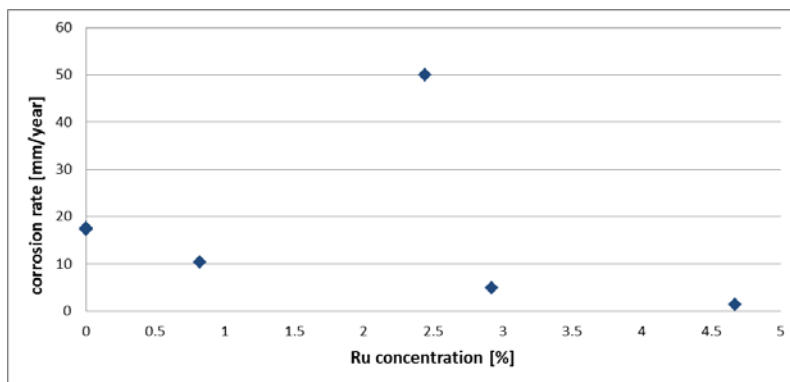


Figure 76: Corrosion rate comparison at various ruthenium compositions from the fresh surface scan in 1 M H₂SO₄ + 1% NaCl at 25°C

The highest value for the polarisation resistance was obtained for the 4.67 wt% Ru sample followed by the 2.92 wt% Ru sample and then the 0.82 wt% Ru sample; thus a trend is confirmed that the polarisation resistance increases with increasing ruthenium content. The 2.44 wt% Ru sample was again coinciding with the stainless steel blank sample and should not be considered in the evaluation. The values were significantly lower during the fresh surface scan compared to the exposed surface scan which implies that a fresh surface is much more vulnerable to corrosion attack than one that had the opportunity to build up a passive film.

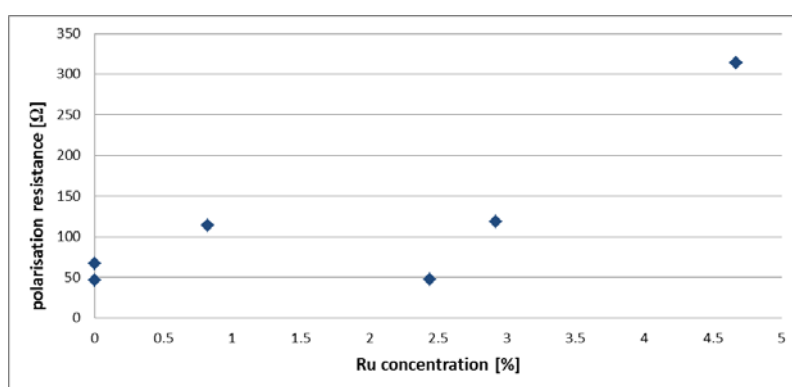


Figure 77: Polarisation resistance comparison at various ruthenium compositions from the fresh surface scan in 1 M H_2SO_4 + 1% NaCl at 25°C

From Table 11, it is observed that the OCP values for all the ruthenium containing samples were higher than the corresponding E_{pass} values indicating passivity, except the 2.92 wt% Ru sample from the fresh surface scan. Only the samples containing no ruthenium showed negative OCP values and a trend was observed in terms of increasing OCP values with an increase in ruthenium composition (except the 0.82 wt% Ru repeat sample). In most of the samples, the E_{pass} values from the fresh surface scan were higher than the values from the exposed surface scan, the exception was the second 0.82 wt% Ru sample. The 2.44 wt% Ru sample was not taken into consideration this time as it was suspected to contain no more ruthenium.

Table 11: Passivation potentials comparison to OCP values in 1 M H₂SO₄ + 1% NaCl at 25°C

	E _{pass} from the exposed surface scan [mV]	OCP after 12 hours [mV]	E _{pass} from the fresh surface scan [mV]
S/S blank	5.3	-357	52
0.0% Ru	17	-365	221
0.82% Ru	215	394	60
0.82% Ru (2)	-15	54	34
2.92% Ru	-47	114	131
4.67% Ru	-125	192	26

Often in chloride contaminated environments, exotic steels are selected to ensure protection from the chloride ion attack, a small comparison of well-known steels is performed here, Figure 78 and Figure 79. As mentioned before, the variability of the 316 stainless steel, the SAF2205 duplex stainless steel and the Hastelloy C276 samples was excellent.

After exposure to 12 hours in the solution, the 304L stainless steel performed worse which is indicated by E_{corr} as low as -0.33 V, a large active nose until passivity was reached only at E_{pass} close to 0.4 V and i_{pass} approximately 1.0x10⁻⁴ A/cm². The ruthenium containing samples performed well in this environment. The 316 stainless steel had the same E_{corr} as the 304L stainless steel blank sample but a reduced nose and reaching passivity, i_{pass} at 1.0x10⁻⁵ A/cm²; i.e. an order of magnitude better than the 304L stainless steel. The SAF2205 showed excellent corrosion resistant properties having an E_{corr} value of -0.216 V and lowest current densities throughout the passive region of the scan. The Hastelloy performed well having slightly higher E_{corr} of -0.2 V and achieving passivity quickly around values between the 2.92 wt% Ru and 4.67 wt% Ru samples. The passive region was very similar for all the tested materials except the 304L stainless steel where it was reduced substantially. The transpassive region was the same for all of the samples except the Hastelloy reached it seemingly marginally earlier, i.e. at slightly lower potentials.

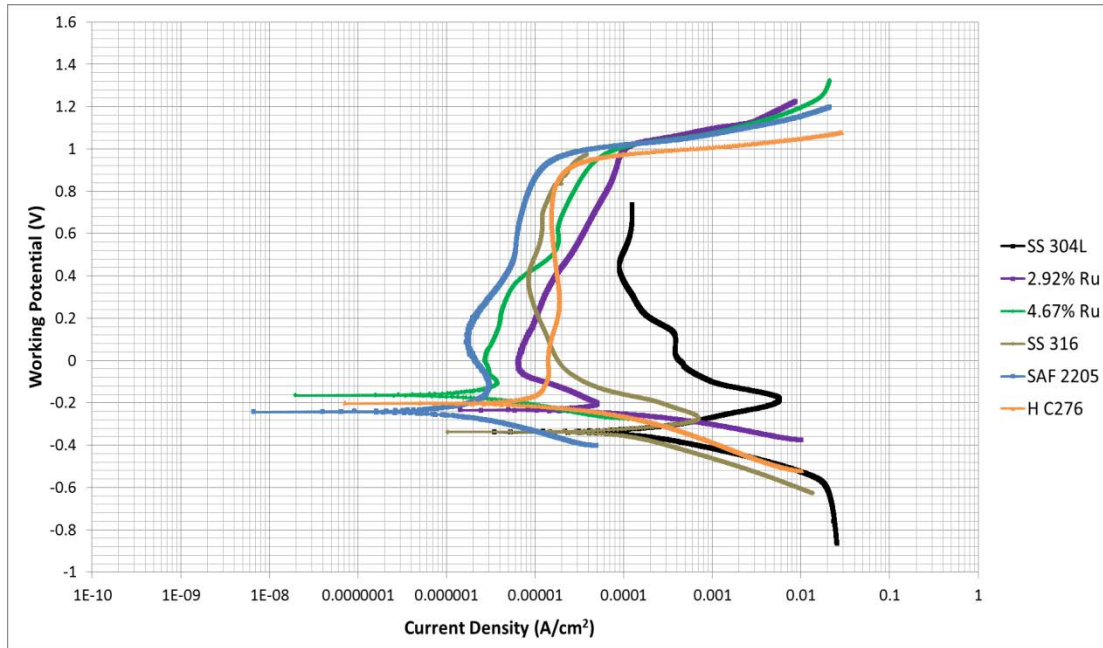


Figure 78: Log I vs E graphs from the exposed surface scan comparing ruthenium samples to other steels in 1 M $H_2SO_4 + 1\% NaCl$ at $25^\circ C$

On a fresh metal surface the trend was similar with the 304 L stainless steel blank being the most prone to corrosion attack in this environment as it had the lowest E_{corr} of -0.37 V, a large active nose and passivity reached at the highest current density, around 1×10^{-4} A/cm^2 . The ruthenium containing alloy with 304L stainless steel behaved much better having larger corrosion potentials and passivity reached at lower current densities. The 316 stainless steel is often used when chlorides are present and it behaved well in this condition having much higher E_{corr} values at -0.25 V, a small nose and passivity was reached at lower current densities than the 304 stainless steel even though the values increased with increasing potential crossing the 304 stainless steel passive region at just above 0.4 V. The SAF2205 had an E_{corr} value of -0.32 V which was slightly below that of 316 stainless but it then had a smaller nose and reached passivity at the lowest current densities of all the steels compared in this section. The Hastelloy material had the highest E_{corr} value at just below -0.2 V but then had a long nose so that initially its passive region was situated between that of the two ruthenium containing alloys but after 0.4 V exhibited lower current densities then them before reaching the trans-passive region at a slightly lower potential.

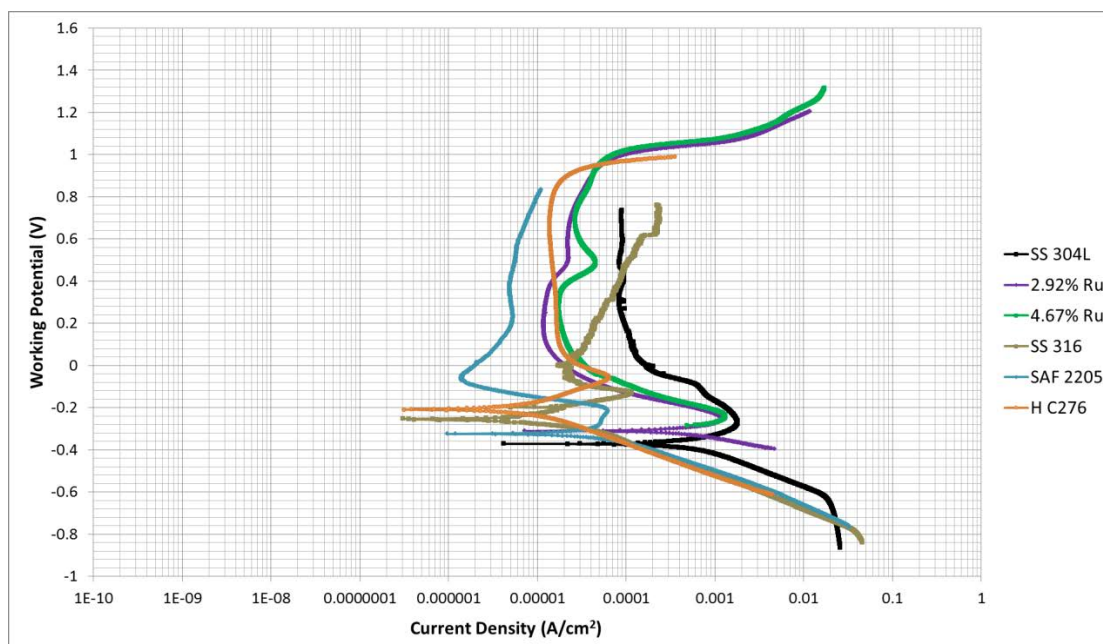


Figure 79: Log i vs E graphs from the fresh surface scan comparing ruthenium samples to other steels in 1 M H_2SO_4 + 1% NaCl at 25°C

4.3.3 1 M H_2SO_4 solution at 45°C

Considering the variability of the results is the first step in any analysis so that the usefulness and validity in subsequent comparisons can be assessed. The samples were exposed to the same test procedure as explained in section 3.4 in an environment of 1 M sulphuric acid keeping the temperature constant at 45°C using a temperature bath. The graphs that follow show repeat results of the same test sample, the remaining graphs to show repeatability of all the samples can be found in Appendix F.

The inconsistency of the stainless steel blank sample under this condition was more than expected, see Figure 80, compared to the same media at 25°C. Test 1 results indicated higher current densities and thus more corrosion activity than the test results 2 and 3 which are fairly close to each other. The curves are almost an order of magnitude apart with regards to their current density at passivation and the E_{pass} also showed variability especially for the fresh surface scans. The E_{corr} values for the three test runs, however, are close to each other at approximately -0.33 V. The curve of the 1st test scan does not display stable passivation until 0.2 V and above as it was observed during the 2nd test scan and when tested at ambient temperatures. All three curves for the exposed scans showed a prominent ‘double nose’ shape which is, to a lesser degree, also represented during the scan of the cleaned surface. It can,

however, be observed that the results from the exposed and fresh surface scan are similar to each other.

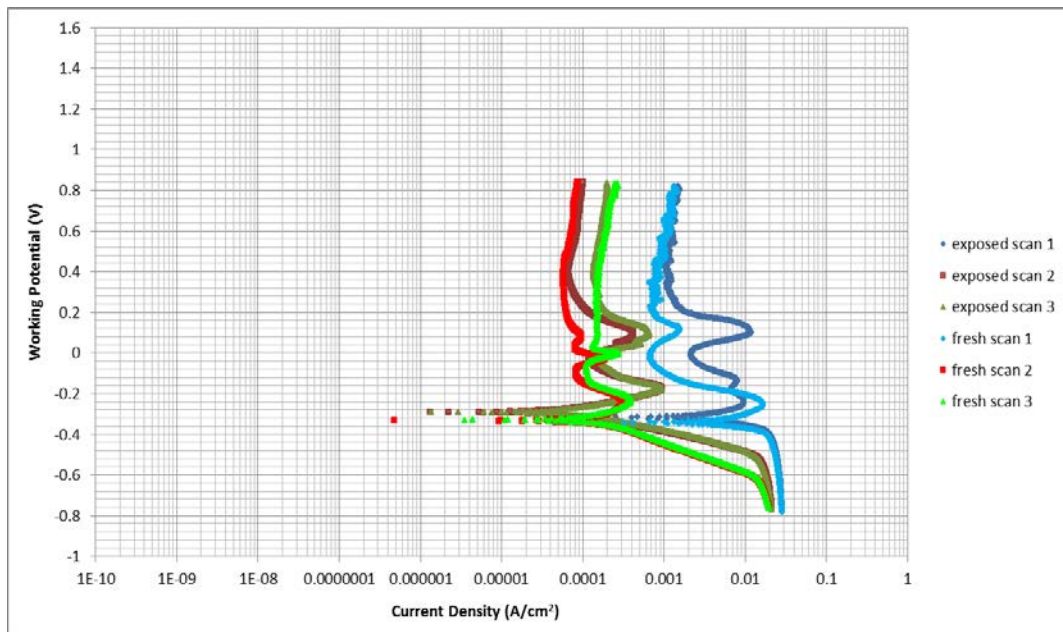


Figure 80: Log i vs E graphs for the Stainless Steel blank sample in 1 M H₂SO₄ at 45°C

The variation between the tests had much improved for the OCP test runs as can be seen in Figure 81; the curves literally coincide. Observing the potential over the 12 hour period, the graphs indicate stable values throughout after an initial short drop in potentials. The final OCP values were almost identical at a value of -0.26 V.

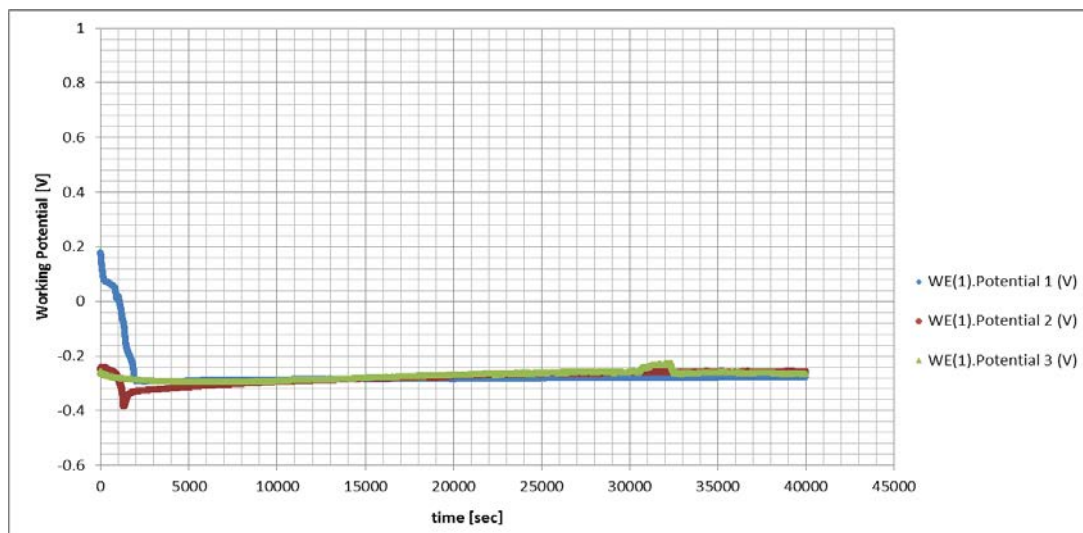


Figure 81: E vs time graphs for the Stainless Steel blank sample in 1 M H₂SO₄ at 45°C

The test results for the 0.82 wt% Ru sample from the exposed surface scan showed significant variability due to the fact that test 2 showed much reduced current densities compared to tests 1 and 3, Figure 82. It will not be used in further comparisons. The Tafel

slopes were consistent, the E_{corr} values showed a variance of 0.05 V averaging at about -0.26 V after which a small active nose was observed. Tests 1 and 3 showed a second nose before passivity is reached over an order of magnitude range of current densities while test 2 showed the lowest i_{pass} down to 2×10^{-5} A/cm². The range over which passivity is observed is thus highly variable. This variance, however, was not observed in the three test results from the fresh surface scans. The variability in the Tafel slopes was present but narrows already as the E_{corr} values are approached which were around the -0.26 V value, they displayed active noses and achieved passivity before 0 V which was reasonably stable until the trans-passive region was reached which meant that the passive potential range under these conditions was at least 0.8 V.

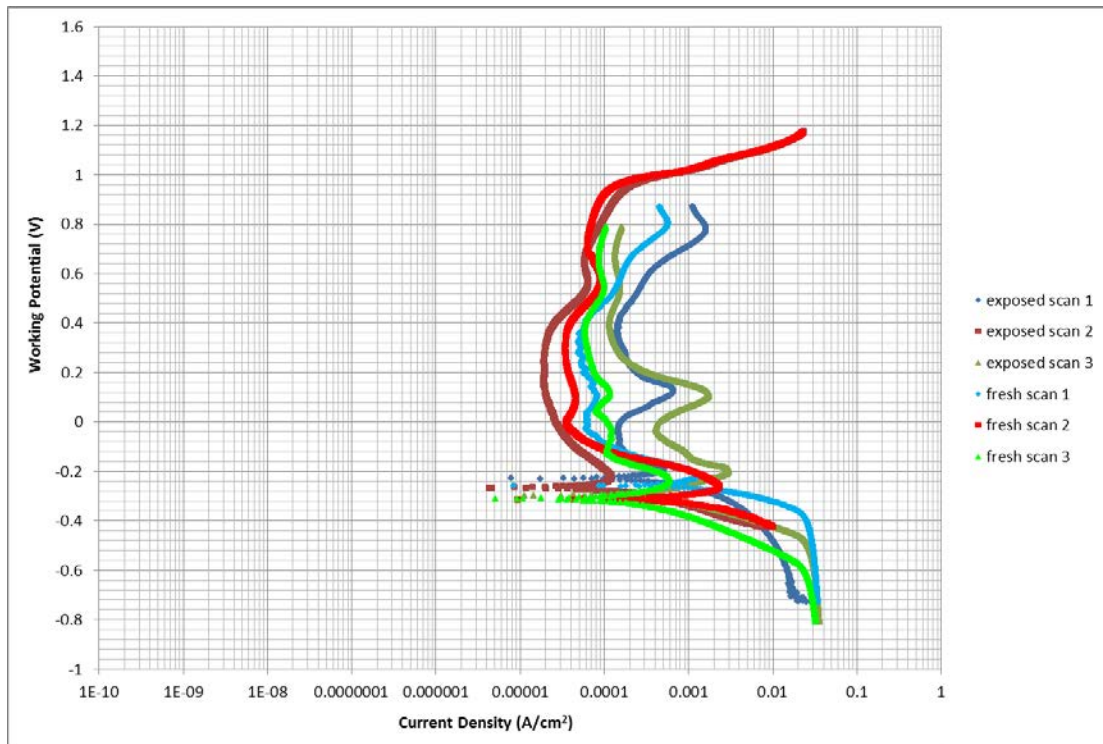


Figure 82: Log i vs E graphs for the 0.82 wt% Ru sample in 1 M H₂SO₄ at 45°C

The potential over time measured and shown in Figure 83 confirmed this variability as the shape and final OCP values after 12 hours were very different for test 2 compared to tests 1 and 3; it does look like tests 1 and 3 have reached stable OCP values at just below -0.2 V.

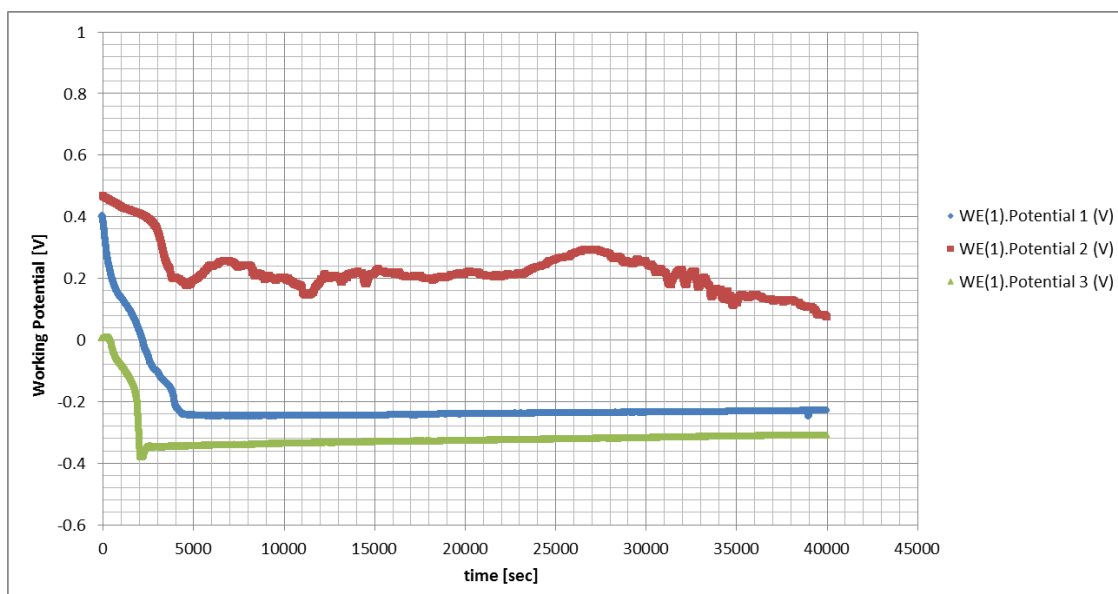


Figure 83: E vs time graphs for the 0.82 wt% Ru sample in 1 M H₂SO₄ at 45°C

For the highest ruthenium concentration tested, i.e. 4.67 wt% Ru as shown in Figure 84, repeatability was reasonable; test 1 showed slightly higher current densities throughout the test while test results 2 and 3 were very close. It was observed that in this environment the corrosion resistance of the results from the exposed surface scan is better than for the fresh surface scan, i.e. observing the order of magnitude lower i_{pass} , but the curves merged in the passive region and going into the trans-passive region. E_{corr} values for the exposed surface scan were all around -0.2 V, they all had short active noses after which tests 2 and 3 exhibited cathodic loops before going into the passive region at about 0.2 V while still experiencing increasing current densities with increasing potential until the trans-passive region was reached at 1.0 V which implies that the passive region extends over a range of 0.8 V. Test 1 had a longer active nose, displayed no cathodic loops but reached the passive region at about the same potential but showing higher current density values suggesting reduced corrosion resistance. For the fresh surface scan very similar trends were observed, i.e. the E_{corr} values were around -0.2 V but the active noses were larger for tests 2 and 3 before they displayed erratic passivity and non-passivity until a stable passive layer is formed at 0.5 V and above. The trans-passive region was reached at 1.0 V. Test 1 from the cleaned surface scan followed closely the curve for test 1 from the exposed surface scan throughout the entire scan.

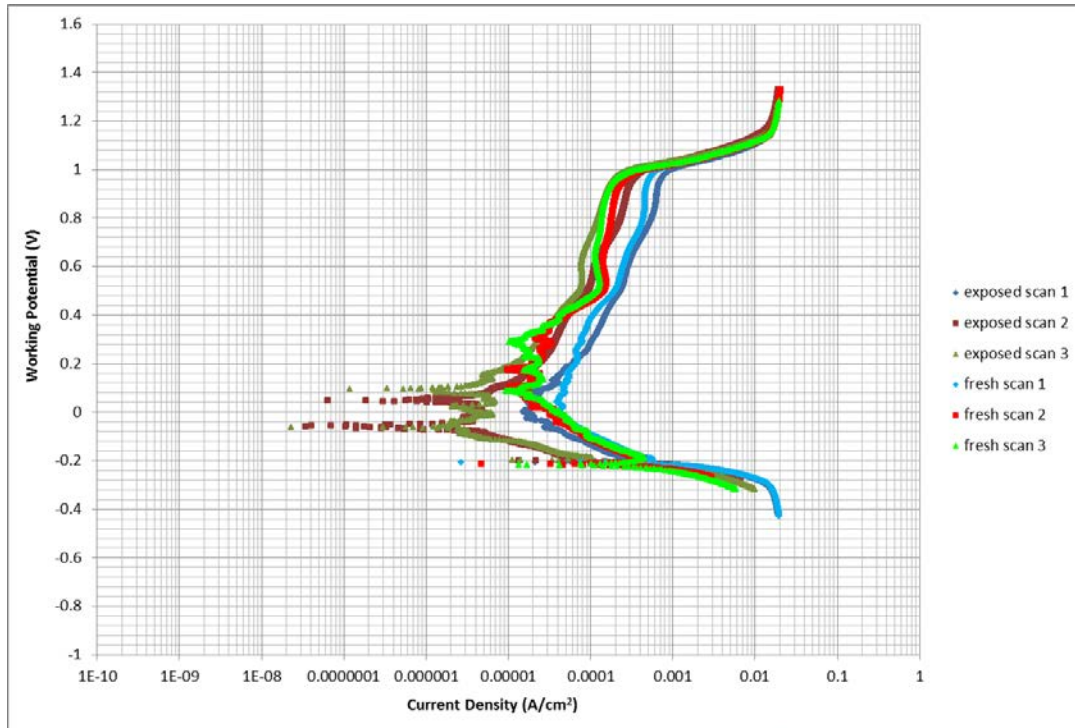


Figure 84: Log i vs E graphs for the 4.67 wt% sample in 1 M H_2SO_4 at 45°C

The potential measured over a 12 hour period gave some variation (just over 0.15 V spread of values) but stable values were obtained after equilibrium was allowed to be reached. The trend is that the potential reduces reasonably quickly to level out at the OCP value but there were minor fluctuations throughout the testing period for this high ruthenium composition as is observed in Figure 85.

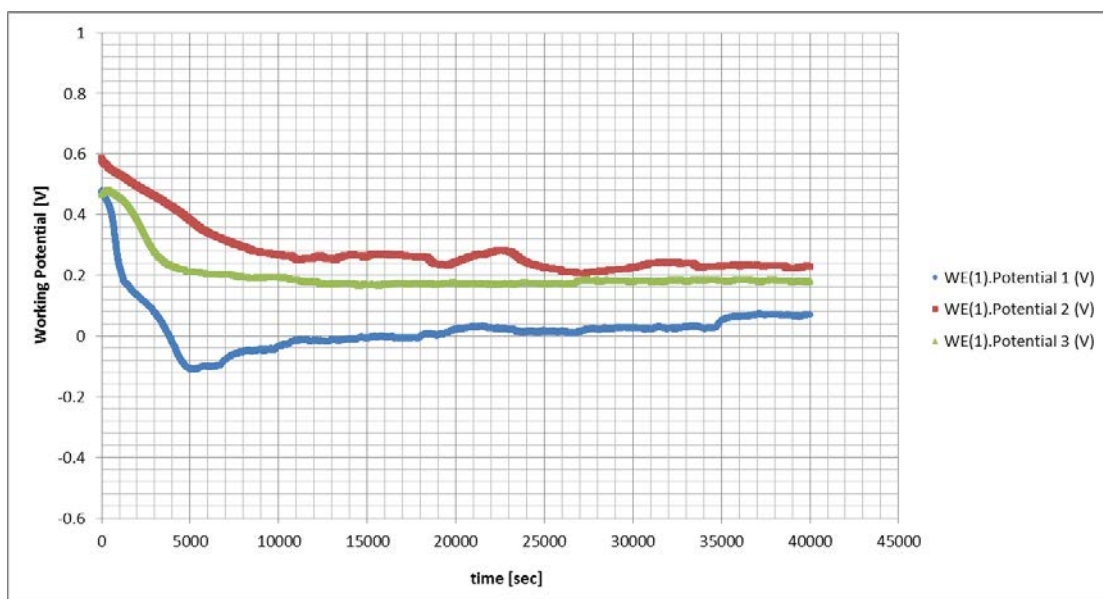


Figure 85: E vs time graphs for the 4.67 wt% Ru sample in 1 M H_2SO_4 at 45°C

A representative curve for each of the samples tested during the exposed surface scan was taken for comparison in Figure 86.

In this set of experiments where the samples were exposed to a higher temperature as well as an acidic medium, the curves of the stainless steel blank sample, the cladded sample without ruthenium and the 0.82 wt% Ru behaved very similarly. After low E_{corr} values around -0.32 V they had small active noses but thereafter still displayed wavy behaviour indicating that, at high temperatures, they struggled to reach passivity which is only observed from 0.2 V upwards. The 0.82 wt% Ru sample showed only slightly better corrosion resistance than the samples without ruthenium as it had lower current densities below 0.6 V but as the potential was increased the curve turned and the sample behaved similarly to the stainless steel blank sample. In this case the stainless steel blank sample coincided very well with the 0.82 wt% Ru sample both exhibiting lower current densities than the cladded sample without ruthenium even though the shapes were similar. However, it is very clear that the two samples with a higher concentration of the added metal, i.e. the 2.92 wt% and 4.67 wt% Ru, showed a significantly improved corrosion resistance. This is indicated by the lowest E_{corr} values at -0.2 V, lower E_{pass} values of approximately 0.1 V, a much reduced i_{pass} value of 1×10^{-5} A/cm² reduced from 1×10^{-3} A/cm² and in fact, the entire passive region was at significantly lower current densities which also showed that the passive region had a slightly extended range from 0.8 V to 0.9 V. The 2.44 wt% Ru sample shows very odd results in that it seems to behave only slightly better than the stainless steel blank sample in the active region and worse than even the cladded sample without ruthenium in the passive region.

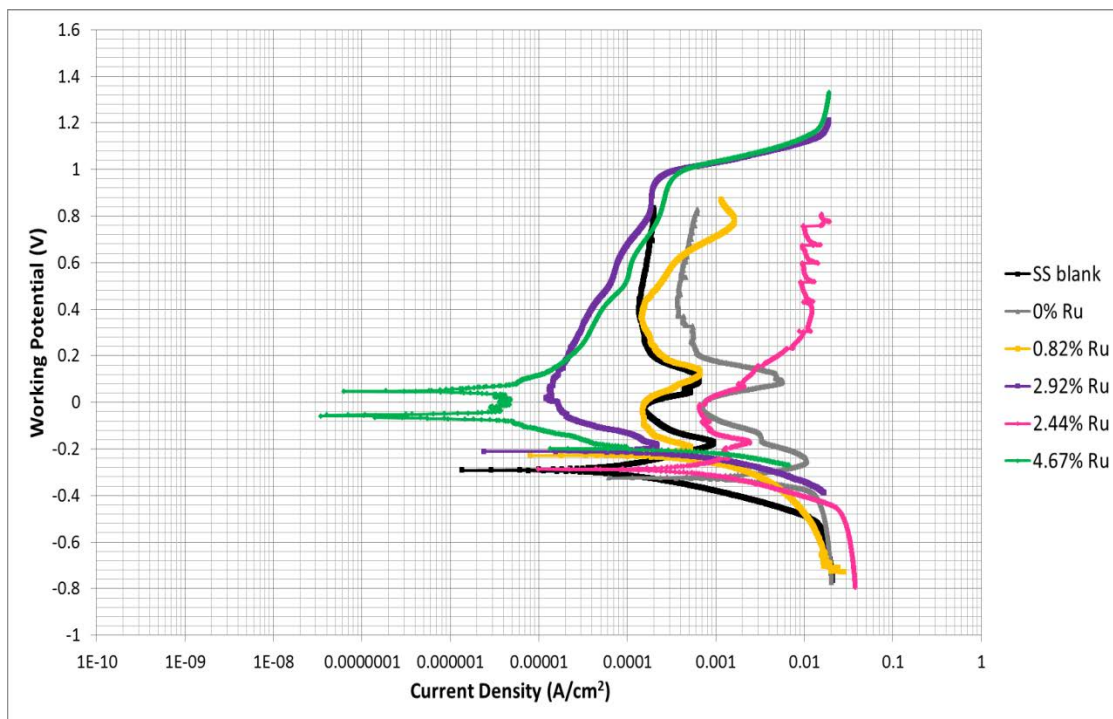


Figure 86: Log i vs E graphs from the exposed surface scan comparing all samples in 1 M H_2SO_4 at 45°C

The specific results from the fresh surface scan looked different but the general trend was the same as those from the exposed surface scan except that all the curves were lying in a narrower current density range. The cladded sample without ruthenium behaved similarly to the stainless steel blank sample with a much larger active nose though and slightly less stable passivation as the current densities throughout the potential range were higher. The passive region of the 2.44 wt% Ru sample was again higher than the stainless steel blank or cladded sample without ruthenium suggesting more corrosion activity on the sample surface. In the active region it behaves similar to the other ruthenium containing samples even though it had the lowest E_{corr} value from all the ruthenium containing samples. This is contrary to what one would expect but the results were confirmed as can be seen in Figure 168 which can be found in Appendix F. The 0.82 wt% Ru sample on the other hand showed better corrosion protection on the fresh surface and so do the 2.92 and 4.67 wt% Ru samples, as observed by increased E_{corr} , reduced i_{pass} values and passivation starting at lower potentials indicating that the general trend is still an improvement in corrosion protection with the addition of ruthenium. The 2.92 wt% and 4.67 wt% Ru curves were very similar suggesting that perhaps the corrosion protection cannot be improved from this point onwards with further additions of ruthenium.

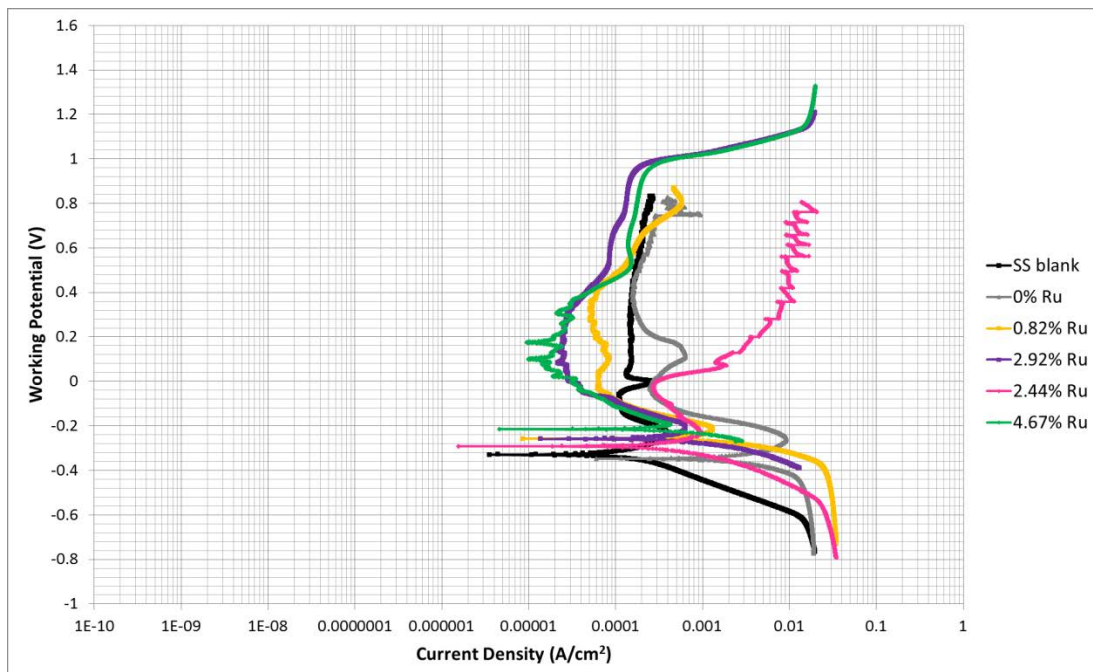


Figure 87: Log i vs E graphs from the fresh surface scan comparing all samples in 1 M H_2SO_4 at 45°C

Observing the potential vs time graphs in Figure 88, it indicated that the stainless steel blank sample, the cladded stainless sample without ruthenium addition, the 0.82 wt% and 2.44 wt% Ru samples behaved very similarly resulting in negative OCP values after 12 hours

which were between -0.23 V and -0.30 V. The curves suggest that smaller addition of ruthenium add no value to the corrosion protection at 1 M sulphuric acid at elevated temperatures. Only at higher values of ruthenium addition, i.e. 2.92 wt% and 4.67 wt% Ru, the potentials shifted into the positive, more noble region stabilising at 0.12 V for the 2.92 wt% Ru sample and at 0.23 V for the 4.67 wt% Ru sample.

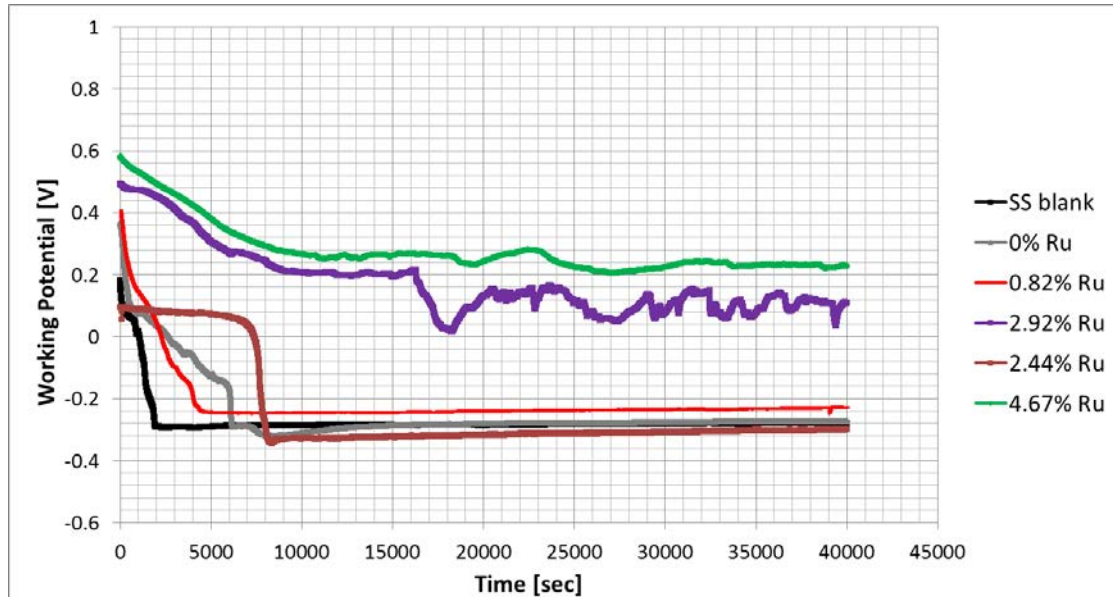


Figure 88: E vs time graphs comparing all samples in 1 M H₂SO₄ at 45°C

Comparing indicators of corrosion activity can be done as in Table 12 where the average E_{corr} , i_{corr} , current density at 0.1 V, the corrosion rate, polarisation resistance and OCP values of the valid tests were calculated to give a good representation for a comparison. This serves to establish the sample with the best corrosion resistance and is thus useful in order to rank the various samples. In general corrosion rates were very high compared to the tests in sulphuric acid at 25°C indicating more active corrosion with the increase in temperature. The benefits that the ruthenium additions provide are also very obvious especially in the 4.67 wt% Ru sample having very low corrosion rates, current densities and a high polarisation resistance. The full results are available in Appendix F. A graphical representation of the values in the table is given in Figure 89 to Figure 94 so that trends could be identified better.

Table 12: Indicators of corrosion rate using average sample measurements from the exposed surface scan in 1 M H₂SO₄ at 45°C

	E _{corr} [mV]	i _{corr} [A/cm ²]	i at 0.1 V [A/cm ²]	Corrosion rate [mm/year]	Polarisation resistance [Ω]	OCP after 12 hours [mV]
S/S blank	-301	9.09x10 ⁻⁴	4.27x10 ⁻³	9.46	526	-268
0.0% Ru	-315	1.27x10 ⁻³	3.69x10 ⁻³	13.17	48	-289
0.82% Ru	-265	2.66x10 ⁻⁴	7.75x10 ⁻⁴	2.46	525	-155
2.92% Ru	-238	1.77x10 ⁻⁴	1.91x10 ⁻⁵	1.65	316	29
2.44% Ru	-293	5.79x10 ⁻⁴	2.18x10 ⁻³	5.41	208	-297
4.67% Ru	-299	9.83x10 ⁻⁷	7.50x10 ⁻⁴	0.01	353 620	-25

The corrosion potential was following a general trend of initially increasing with the addition of ruthenium but, as additions get larger, to decrease again, the highest value being the 2.92 wt% Ru sample but the 4.67 wt% Ru sample (suggesting that further additions of ruthenium might not be of further benefit) being slightly lower than the 0.82 wt% Ru sample. The two samples without ruthenium behaved very similarly with the cladded sample having a lower E_{corr} than the blank as per Figure 89 but all the ruthenium containing samples showed higher E_{corr} values (even though the 4.67 wt% Ru sample only marginally) and therefore implying that the addition of ruthenium to the stainless steel is of benefit from a corrosion point of view.

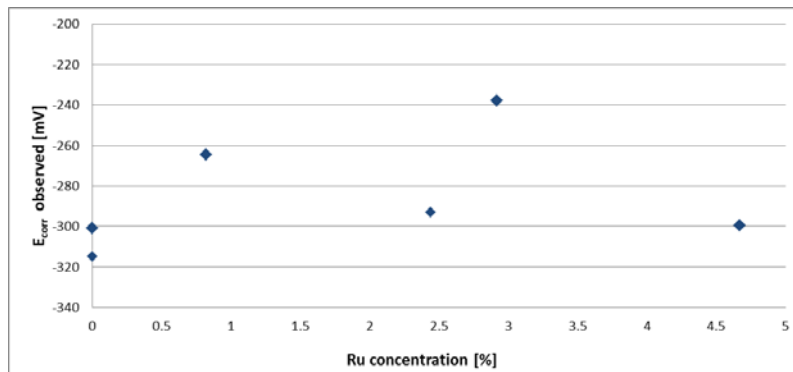


Figure 89: E_{corr} comparison at various ruthenium compositions from the exposed surface scan in 1 M H₂SO₄ at 45°C

Observing corrosion current density values in Figure 90, the results clearly show that the addition of ruthenium reduced the current densities significantly and that in this case the general trend is a decreasing i_{corr} value with an increase in ruthenium concentration. The lowest value was observed for the 4.67 wt% Ru sample followed by the 2.92 wt% Ru sample and then the 0.82 wt% Ru sample with the 2.44 wt% Ru sample being slightly higher again

but the cladded sample without ruthenium and the stainless steel blank samples indicated higher results. The cladded sample does show the highest results implying the highest corrosion activity occurs in that sample surface.

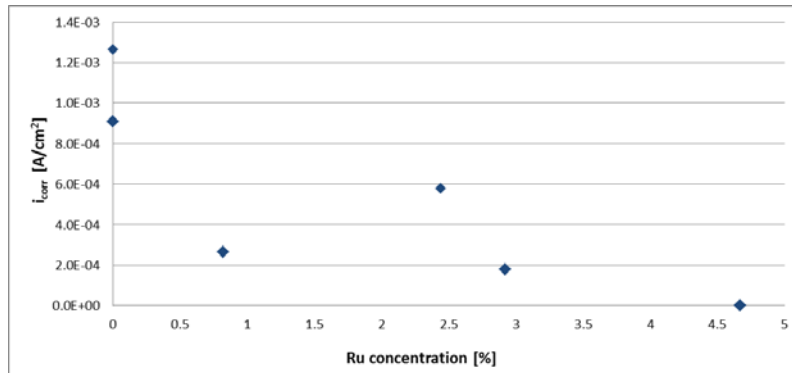


Figure 90: i_{corr} comparison at various ruthenium compositions from the exposed surface scan in 1 M H₂SO₄ at 45°C

The current density at a specific value was selected, in this case 0.1 V was chosen, to give an idea about the corrosion activity at that potential, i.e. the ranking order of the samples in terms of corrosion passivity at the onset of passivation. From Figure 91 it is again very clear that the ruthenium addition was of great benefit for the corrosion protection of the sample, current densities immediately dropped and are lowest at 2.92 wt% Ru with the 4.67 wt% and 0.82 wt% Ru samples following closely. The difference between the ruthenium containing samples and the samples without ruthenium was very noticeable but not as evident as in the tests with 1 M sulphuric acid at 25°C, all the values were approximately two to three orders of magnitude smaller in this case, indicating much more corrosion activity when the temperature was increased by 20°C.

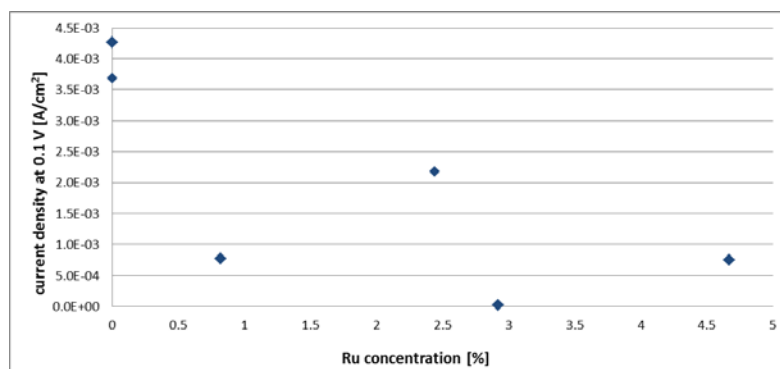


Figure 91: Current density at 0.1 V comparison at various ruthenium compositions from the exposed surface scan in 1 M H₂SO₄ at 45°C

Figure 92 shows the highest corrosion rates are observed in the cladded sample without the PGM addition as one would observe in industrial applications followed by the stainless steel blank sample; the ruthenium containing samples showed a significantly reduced corrosion

rate. A reasonably clear trend established itself that corrosion rates are decreasing with an increase in ruthenium content, the 4.67 wt% Ru sample having the lowest corrosion rate but the 2.44 wt% Ru sample having the highest corrosion rate from the ruthenium containing samples. Again, these were significantly higher than what was observed at ambient conditions.

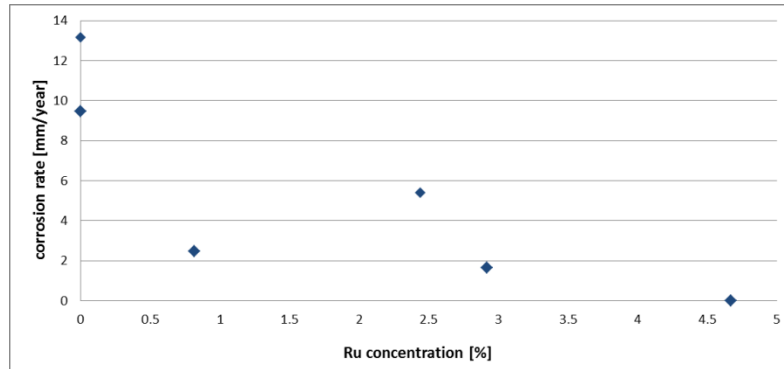


Figure 92: Corrosion rate comparison at various ruthenium compositions from the exposed surface scan in 1 M H_2SO_4 at $45^\circ C$

The polarisation resistance is in slight contradiction to the trend the other graphs have hinted at; in this case the resistance was stable with increasing ruthenium composition suggesting that the added ruthenium was having no effect on the corrosion protection of the material except that the 4.67 wt% Ru sample has a dramatically increased polarisation resistance. The cladded sample without ruthenium had the lowest value as expected.

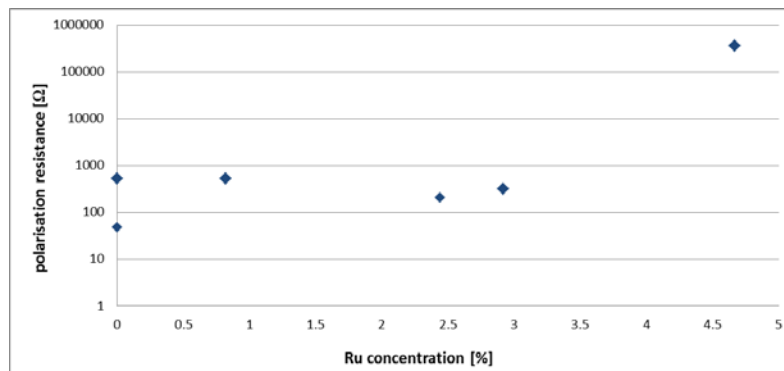


Figure 93: Polarisation resistance at various ruthenium compositions from the exposed surface scan in 1 M H_2SO_4 at $45^\circ C$

The OCP values follow the same trend as the E_{corr} values, as previously mentioned that the values should be the same; in this case the OCP values were higher than the E_{corr} values and in some cases substantially higher. In Figure 94 it can be seen that the OCP values for the higher ruthenium containing samples (2.92 wt% and 4.67 wt% Ru) are higher than the samples without ruthenium but the lower ruthenium containing samples (0.82 wt% and

2.44 wt% Ru) exhibit values that are in between the two samples without ruthenium. The highest and only positive result is observed for the 2.92 wt% Ru sample.

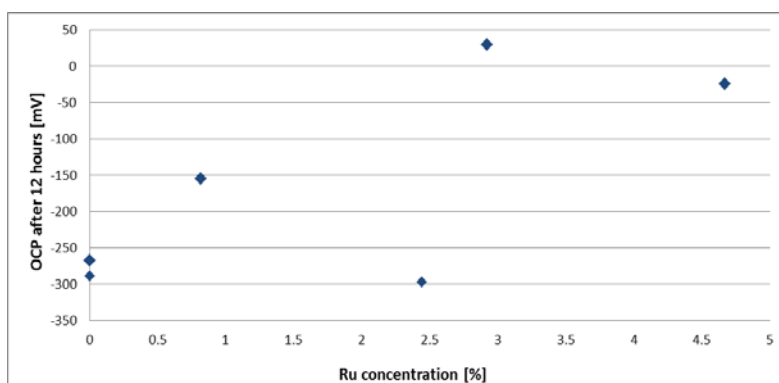


Figure 94: OCP comparison at various ruthenium compositions from the exposed surface scan in 1 M H₂SO₄ at 45°C

The results obtained from both the exposed and cleaned surface scans need to be investigated and compared so that the behaviour of the samples in both conditions, i.e. after equilibrium has been reached and on a fresh surface, can be obtained. Table 13 and Figure 95 to Figure 98 give the average results of E_{corr} and i_{corr} values as well as the corrosion rate and polarisation resistance from the fresh surface scan from the valid tests carried out; the remaining results can be found in Appendix F. The table highlights the beneficial effects of the ruthenium addition on a fresh surface area at higher temperatures where corrosion rates are much higher. The trend is, however, not uniform with an increase in ruthenium concentration where the best results had been achieved for the 2.92 wt% Ru sample.

Table 13: Indicators of corrosion rate using average sample measurements from the fresh surface scan in 1 M H₂SO₄ at 45°C

	E_{corr} [mV]	i_{corr} [A/cm ²]	Corrosion rate [mm/year]	Polarisation resistance [Ω]
S/S blank	-336	5.77×10^{-3}	60.05	160
0.0% Ru	-338	4.63×10^{-3}	48.12	41
0.82% Ru	-294	3.08×10^{-3}	30.63	50
2.92% Ru	-256	9.27×10^{-4}	8.61	117
2.44% Ru	-305	2.60×10^{-3}	24.23	57
4.67% Ru	-276	2.09×10^{-3}	19.55	89

The lowest E_{corr} values obtained were for the two samples without ruthenium, as soon as even a small amount of ruthenium is introduced, the corrosion potentials increased with the highest

value been obtained from the 2.92 wt% Ru sample and the trend seemed to either be levelling off after that or, in fact, decrease slightly as the 4.67 wt% Ru sample is slightly lower. The 2.44 wt% Ru sample is also reduced, the lowest of the ruthenium containing samples, but still higher than the samples without ruthenium. All samples are negative and in the same range as the E_{corr} values obtained from the fresh surface scan in 1 M sulphuric acid at 25°C.

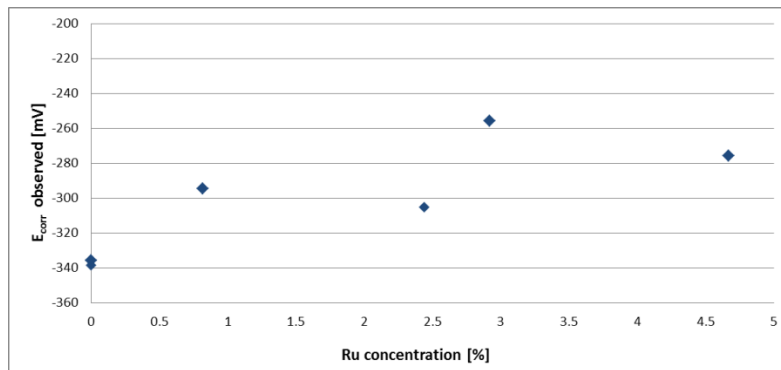


Figure 95: E_{corr} comparison at various ruthenium compositions from the fresh surface scan in 1 M H_2SO_4 at 45°C

The corrosion current density values obtained are the highest, indicating the most active corrosion behavior, for the samples without ruthenium (with the cladded sample having the highest value); with the addition of ruthenium these values drop even if not by a large amount. The trend was, as with the E_{corr} values, a levelling off or slight turn seems to be observed towards the 4.56 wt% Ru sample with the lowest number being achieved by the 2.92 wt% Ru sample. The values obtained here were higher than for this sulphuric acid solution at ambient temperature and only slightly higher than the values obtained from the exposed surface scan.

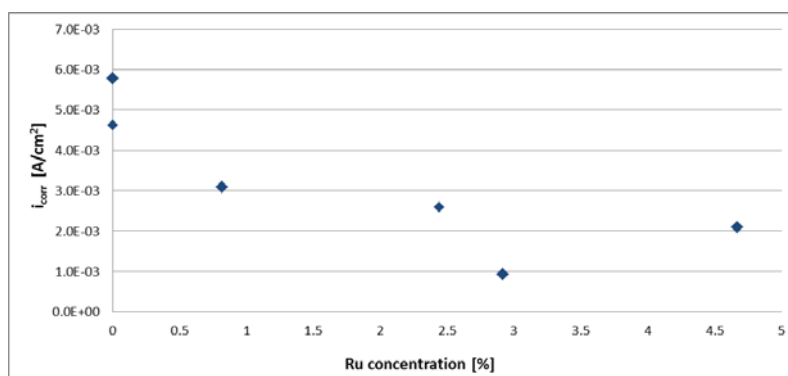


Figure 96: i_{corr} comparison at various ruthenium compositions from the fresh surface scan in 1 M H_2SO_4 at 45°C

Looking at Figure 97 the trend observed above was again noted, the samples without ruthenium have significantly higher corrosion rates than the samples with ruthenium (this time the blank sample showing higher corrosion rates), the lowest value being obtained by

the 2.92 wt% Ru sample followed by the 4.67 wt% Ru sample, the 2.44 wt% Ru and then the 0.82 wt% Ru sample. Corrosion rates were extremely high, much higher than during the exposed surface scan and also much higher than during the scan at 25°C.

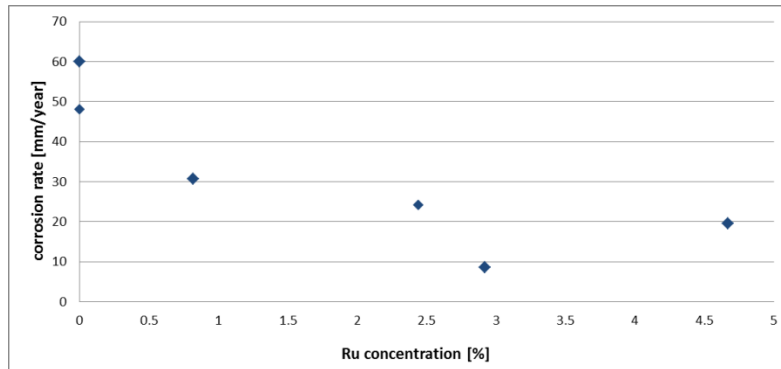


Figure 97: Corrosion rate comparison at various ruthenium compositions from the fresh surface scan in 1 M H₂SO₄ at 45°C

The largest value for the polarisation resistance was obtained for the stainless steel blank sample which was not as expected and the lowest value was for the cladded sample without ruthenium as expected. For the ruthenium containing samples a trend was observed as before that the highest value, implying most corrosion protection for the sample, was obtained for the 2.92 wt% Ru sample followed by the 4.67 wt% Ru sample, the 2.44 wt% Ru and then the 0.82 wt% Ru sample. The values were lower here than for the exposed surface scan and they were also significantly lower than for the testing at ambient conditions where the trend was different as well.

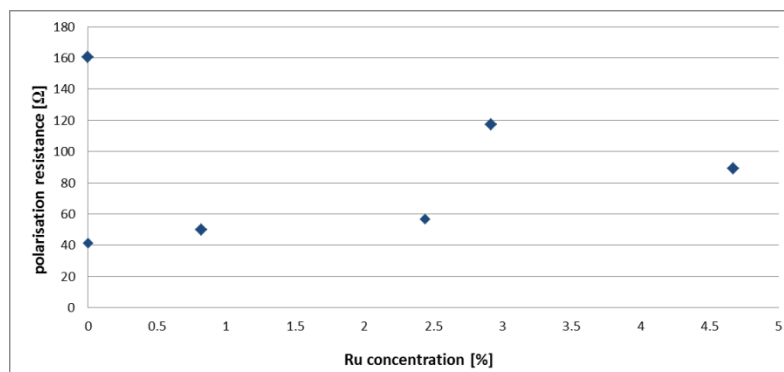


Figure 98: Polarisation resistance comparison at various ruthenium compositions from the fresh surface scan in 1 M H₂SO₄ at 45°C

OCP values need to be above the E_{pass} in order to give good corrosion protection, indicating a less active/ more noble surface and thus passivation. Higher OCP values only give reduced corrosion rates if it means passivity has been reached; without passivity at higher OCP value actually gives increased corrosion. The very general trend observed for the 1 M sulphuric

acid test at 45°C was one of increasing OCP after 12 hours with an increase in ruthenium composition but there was a large amount of variability. In this case the OCP values were all much lower than the E_{pass} values for the exposed and fresh surface scans, except for the 2.92 wt% Ru sample from the exposed surface scan where it is slightly higher. This suggests active corrosion in those cases. The only sample that had a negative E_{pass} value was the 2.44 wt% Ru sample (which incidentally had the most negative OCP value) while the only positive OCP value was that for the 2.92 wt% Ru sample showing passivity during the exposed surface scan conditions.

Table 14: Passivation potentials comparison to OCP values in 1 M H₂SO₄ at 45°C

	E_{pass} from the exposed surface scan [mV]	OCP after 12 hours [mV]	E_{pass} from the fresh surface scan [mV]
S/S blank	299	-268	232
0.0% Ru	366	-289	373
0.82% Ru	353	-155	398
2.92% Ru	24	29	154
2.44% Ru	-59	-297	-40
4.67% Ru	12	-25	333

No tests were carried out comparing the various different steels to the ruthenium containing 304L stainless steel under these conditions.

4.3.4 1 M H₂SO₄ + 1% NaCl solution at 45°C

As with previous results, variability was considered before the results were compared. The same methodology was followed when conducting these experiments as was described in section 3.4 above. The samples were all exposed to the same test procedure in an environment of 1 M sulphuric acid with the addition of 1% sodium chloride keeping the temperature constant at 45°C using a temperature bath. These are extremely harsh conditions for a 304L stainless steel. The graphs that follow show repeat results using the same test sample. The remaining graphs to show repeatability of all the samples can be found in Appendix G.

The repeatability of the stainless steel blank samples exposed to the 1 M sulphuric acid with the addition of 1% sodium chloride at 45°C was very good. From Figure 99 it is seen that all

curves almost coincide in the active region except that the corrosion potential was at a slightly higher value for the experiments conducted during the exposed surface scan, they were at $E_{\text{corr}} = -0.32 \text{ V}$ compared to the values during the fresh surface scan where $E_{\text{corr}} = -0.37 \text{ V}$. The i_{crit} was almost identical for all, i.e. for both anodic scans, but the E_{crit} was again higher for the experiments conducted during the exposed scan but prominent active noses were observed for all the scans. The curves then varied slightly in the passive region but did all follow the same trend. Acceptable variability is observed and results are comparable. The graphs did show that the results from the exposed and fresh surface scans were only slightly different with the trend being that the corrosion protection was improved for the fresh surface scan which showed the same trend as the experiments conducted in 1 M sulphuric acid with 1% sodium chloride at ambient temperature.

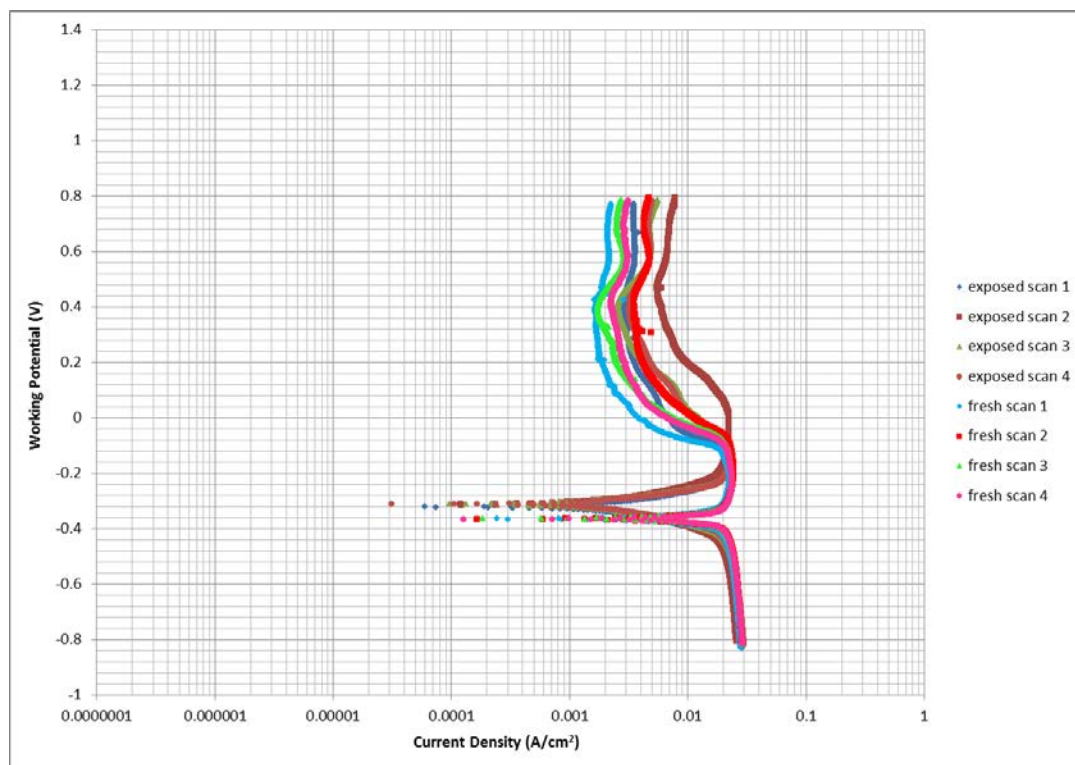


Figure 99: Log i vs E graphs for the Stainless Steel blank sample in 1 M H_2SO_4 + 1% NaCl at 45°C

Acceptable repeatability for the stainless steel blank sample was confirmed by the potential measured over time, in Figure 100, the curves follow the same trend: indicating a sharp drop in potential and levelling off to the OCP values observed after 12 hours. The range of OCP values was minimal averaging around -0.32 V which emphasised the repeatability of the results.

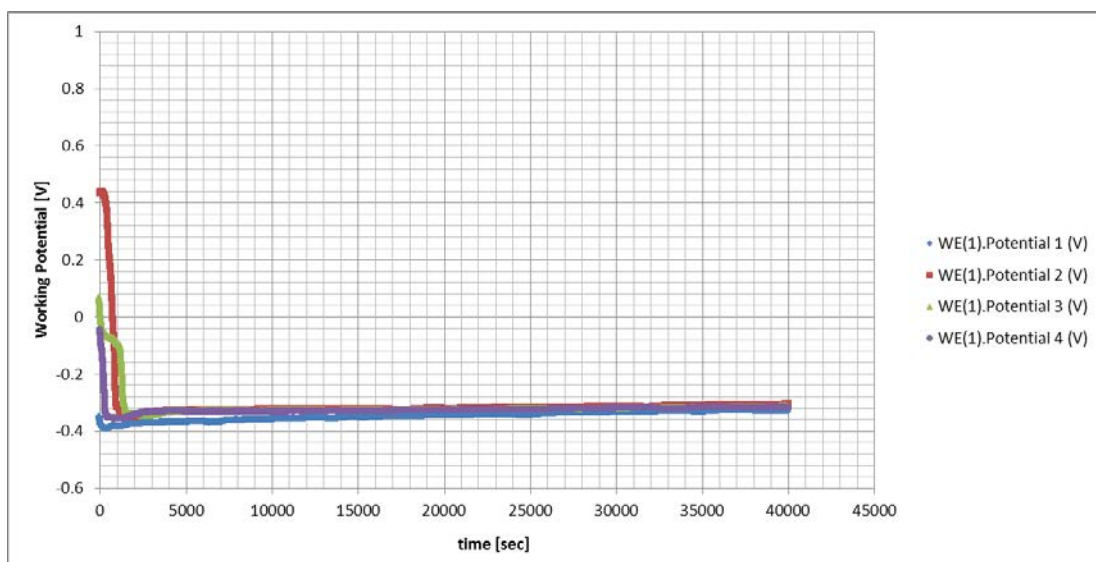


Figure 100: E vs time graphs for the Stainless Steel blank sample in 1 M H₂SO₄ + 1% NaCl at 45°C

With the addition of a small amount of ruthenium, shown in Figure 101 with the 0.82 wt% Ru content, it did not seem to have introduced any additional variability as all three scans follow the same curve. During the exposed surface scans, the tests showed steep Tafel slopes, E_{corr} values at just below -0.2 V, small noses and a passive region where the current densities increase with an increase in potential indicating a stable passive layer formed on the surface. The samples exhibit the same behavior during the fresh surface scan as during the exposed surface scan having as low potentials but the nose was larger and thus lower current densities were observed throughout the passive region but for none of the tests has a trans-passive region been observed. However, it is obvious that in all cases the corrosion protection was improved during the fresh surface scan, i.e. lower current densities in the passivation region. Repeatability is very reasonable for this sample in this environment.

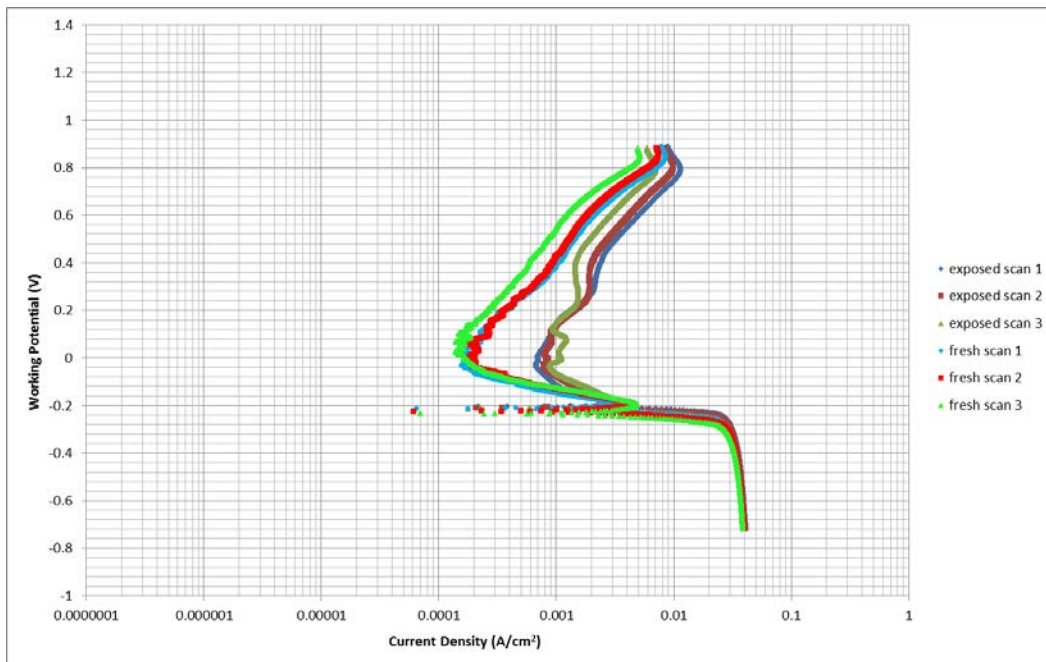


Figure 101: Log i vs E graphs for the 0.82 wt% Ru sample in 1 M H_2SO_4 + 1% NaCl at $45^\circ C$

As the potential is observed over time in Figure 102, it confirmed that repeatability is observed throughout the 12 hours. The OCP values have definitely reached a stable value after the 12 hours; the final value was just below -0.2 V for all three tests.

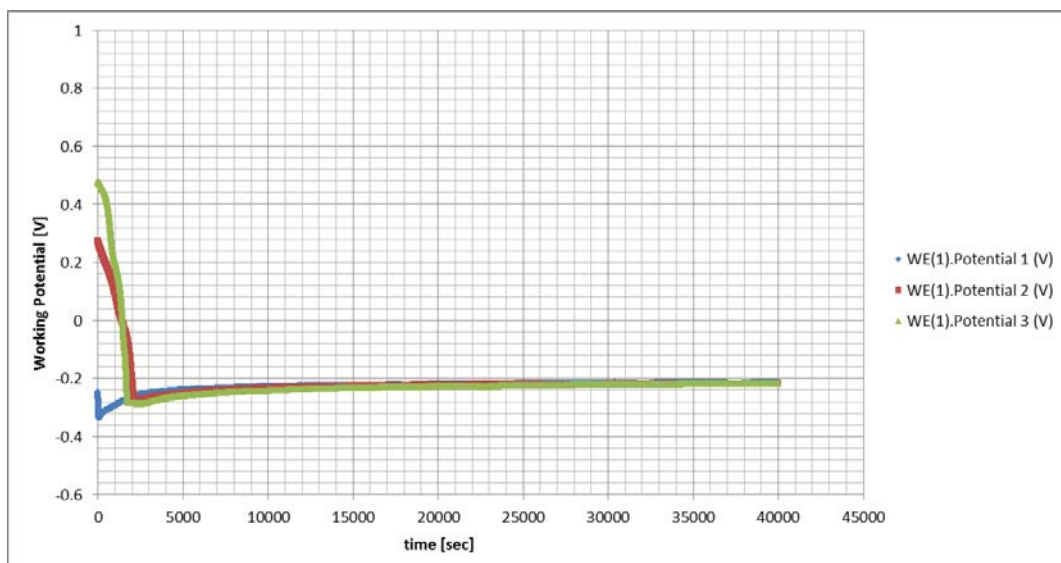


Figure 102: E vs time graphs for the 0.82 wt% Ru sample in 1 M H_2SO_4 + 1% NaCl at $45^\circ C$

For the sample with the 4.67 wt% Ru concentration, the variability was not great and that was one of the reasons why it was repeated three times. Tests 1, 3 and 4 were reasonably consistent with test 2 being not confirming the same trend. During the exposed surface scan the E_{CORR} values were all just below -0.2 V, they had small active noses reaching the passive region before 0 V while passivity was still characterised by an increase in current densities as the potential was increased. The E_{CORR} values for the fresh surface scan were also just below

the -0.2 V, they had reduced noses and reached passivity only above 0.1 V with generally lower current densities but also increasing in current densities with an increase in potentials. Exposed surface scan test results have Tafel slopes that were less steep than test results from the cleaned surface scan; they had lower current densities in the active region but higher current densities in the passive region. The trans-passive region had not been reached for these tests. Test 2 results were very similar for the exposed and fresh surface scans with lower E_{corr} values or around -0.315 V, broader noses but a very stable passive region starting at below 0 V; initially not as stable but after 0.5 V with a consistent i_{pass} of 1×10^{-4} A/cm² which was lower than the other three tests.

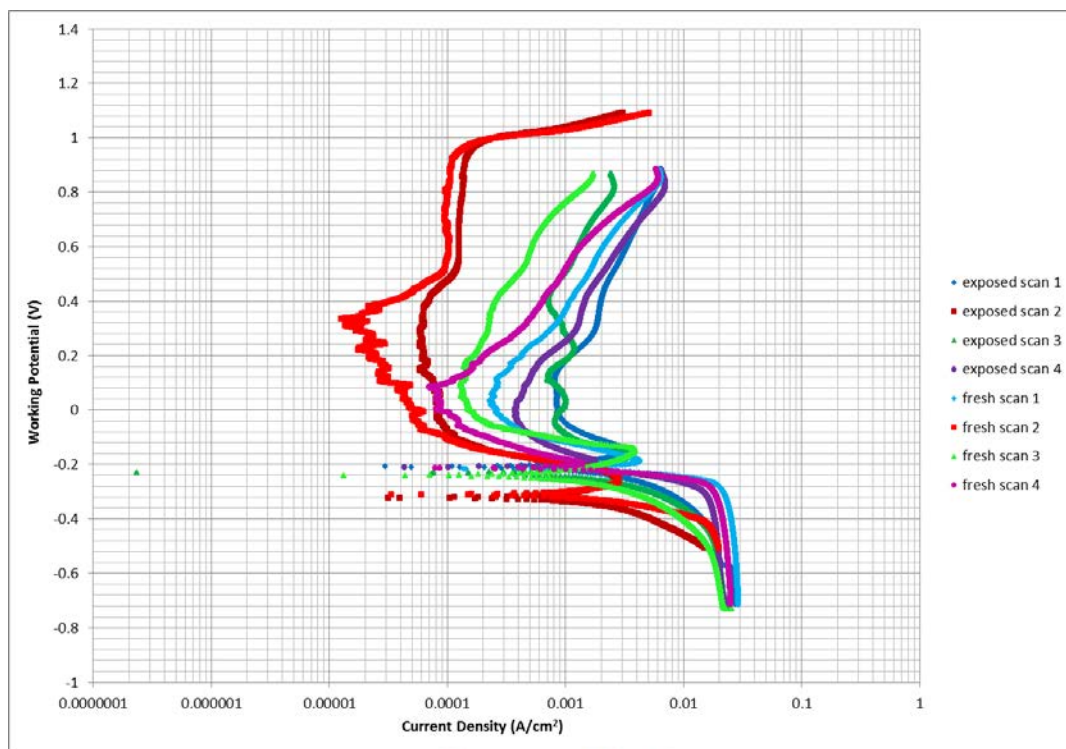


Figure 103: Log i vs E graphs for the 4.67 wt% Ru sample in 1 M H₂SO₄ + 1% NaCl at 45°C

The potential over time graphs in Figure 104 confirmed that test 2 was behaving differently to the other three tests but those remaining three tests showed acceptable consistency and the final OCP value was almost identical for these tests at just below -0.2 V. The potential dropped quickly initially and then stabilised at the OCP value after 4 hours.

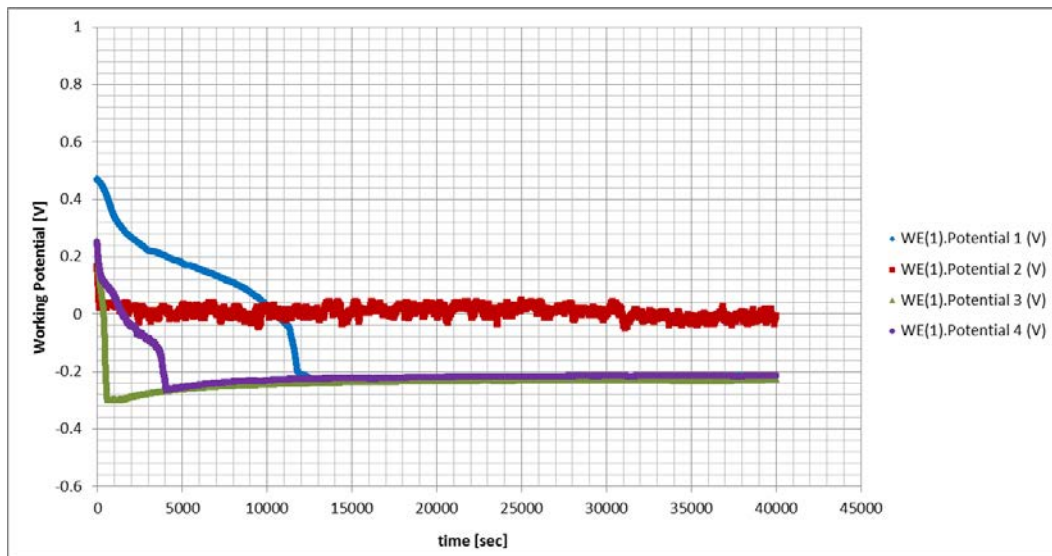


Figure 104: E vs time graph for the 4.67 wt% Ru sample in 1 M H₂SO₄ + 1% NaCl at 45°C

Selecting a representative curve per sample and then combining them provides an indication as to which sample gives more or less corrosion protection and the most suitable amount of ruthenium can be found in this harsh environment.

The curves for the stainless steel blank and cladded sample without any ruthenium behave in a very similar way: their active region was at a slightly lower potential, the E_{corr} was at a lower potential at -0.31 V, the i_{crit} was at a much higher current density to display a large active nose until the passive region was reached at approximately 0.4 V. All the curves seem to come together at a potential of 0.5 V and above. The samples containing ruthenium also behaved similarly, they had the same shape and in fact, all had almost identical E_{corr} values at just below -0.2 V. The graphs obtained from the samples with 0.82 and 2.92 wt% Ru were similar and the samples with 2.44 and 4.67 wt% Ru had similar values throughout the potential scan. The latter having lower current densities throughout the passive region, indicating more corrosion protection while still increasing current densities with an increasing potential.

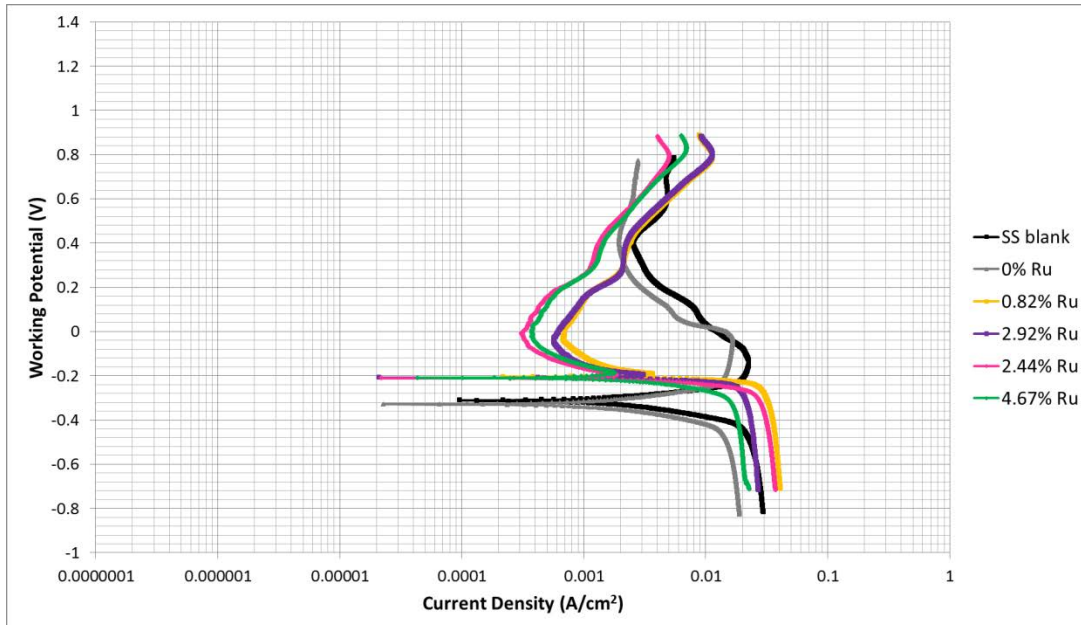


Figure 105: Log i vs E graphs from the exposed surface scan comparing all samples in 1 M H_2SO_4 + 1% NaCl at 45°C

The trend observed during the anodic scan on a fresh surface area was similar to that observed during the exposed surface scan in that the stainless steel without ruthenium behaved very differently compared to the samples containing ruthenium. The curves for the stainless steel blank and clad sample without any ruthenium had their active region at a lower potential, the E_{corr} value was at a lower potential at -0.36 V, the i_{crit} was at a much higher current density exhibiting a large active nose which only gently moved into the passive region which starts at approximately 0.4 V. All the curves seem to coincide, just like during the exposed surface scan, but at values above 0.7 V. The samples containing ruthenium also behaved similarly, they had the same shape and in fact, all had almost identical E_{corr} values at -0.18 V and E_{pass} values of 0.1 V. There was a trend of decreasing current density with increasing ruthenium content but it was neither clear nor prominent on the fresh surface area while still increasing current densities with an increasing potential.

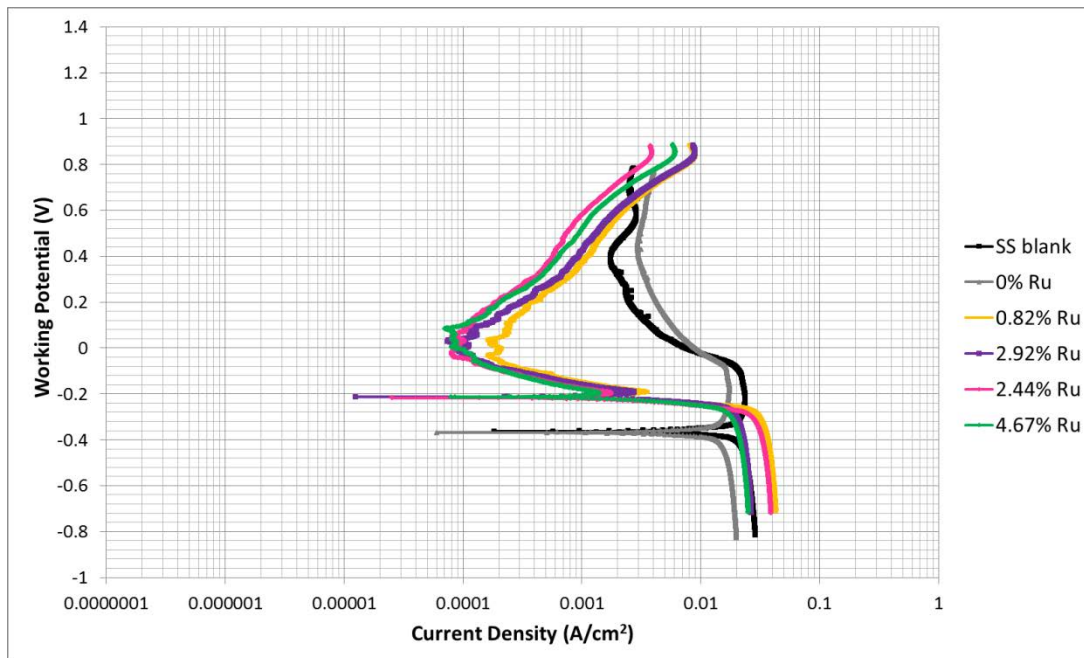


Figure 106: Log i vs E graphs from the fresh surface scan comparing all samples in 1 M H_2SO_4 + 1% NaCl at 45°C

The potential vs time curves shown in Figure 107 indicate that lower potentials were obtained without the ruthenium present at around -0.32 V and almost identical values were obtained with the ruthenium present at -0.2 V which is slightly higher and thus more noble.

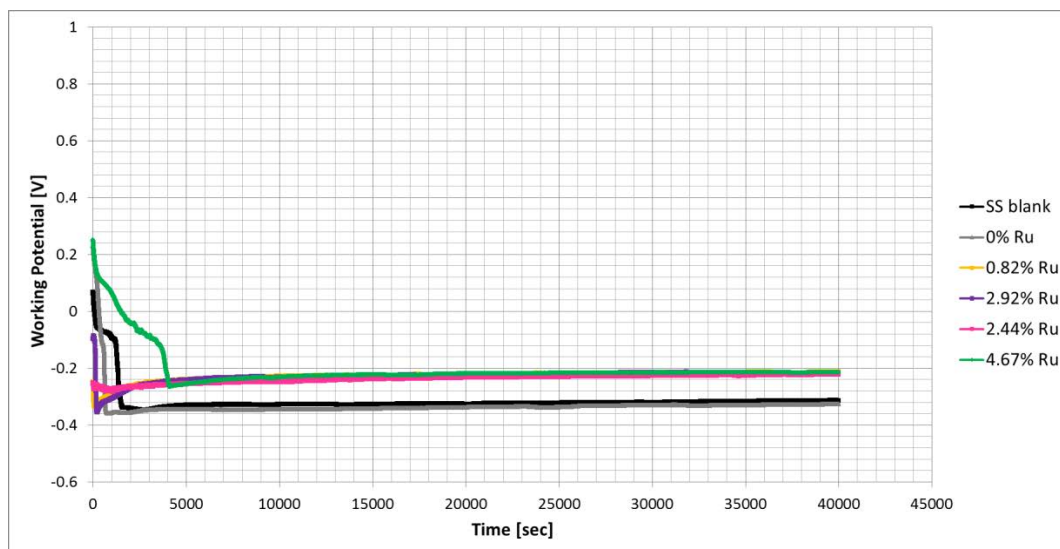


Figure 107: E vs time graphs comparing all samples in 1 M H_2SO_4 + 1% NaCl at 45°C

Table 15 lists some of the indicators for comparing corrosion activity during the exposed surface scan such as the average E_{CORR} , i_{CORR} , current density at 0.1 V, the corrosion rate, polarisation resistance as far as these were able to be calculated and OCP values of the valid tests which give a representation for a comparison. These are graphically represented in Figure 108 until Figure 112 so that trends can be observed more easily and a ranking order can be established. The full results are available in Appendix G. It showed that all the

observed corrosion potentials are negative implying harsh conditions which the samples were exposed to and thus high corrosion rates were observed. The E_{corr} values were reasonably close to the OCP values except for the 4.67 wt% Ru sample where the OCP value was significantly higher. In general, it was observed that the range from 0.82 wt% to 2.92 wt% Ru had the most desirable corrosion protection parameters and for all the parameters investigated, corrosion activity was reduced with the addition of ruthenium; the PGM is making a significant improvement in the corrosion protection. The corrosion resistance showed an increase between the samples without ruthenium and the 4.67 wt% Ru sample which indicates improved corrosion protection with the additional ruthenium.

Table 15: Indicators of corrosion rate using average sample measurements from the exposed surface scan in 1 M H_2SO_4 + 1% NaCl at 45°C

	E_{corr} [mV]	i_{corr} [A/cm ²]	i at 0.1 V [A/cm ²]	Corrosion rate [mm/year]	Polarisation resistance [Ω]	OCP after 12 hours [mV]
S/S blank	-315	1.76×10^{-3}	9.44×10^{-3}	20.11	39.0	-317
0.0% Ru	-322	1.34×10^{-3}	5.82×10^{-3}	15.37	34.3	-322
0.82% Ru	-210	2.63×10^{-4}	9.58×10^{-4}	3.04	N/A*	-250
2.92% Ru	-214	2.60×10^{-4}	8.81×10^{-4}	3.02	N/A*	-218
2.44% Ru	-214	1.12×10^{-4}	1.05×10^{-3}	1.30	N/A*	-220
4.67% Ru	-265	9.27×10^{-4}	4.92×10^{-4}	10.85	133.6	-160

The N/A indicates that these values could not be calculated or obtained from the software*

The E_{corr} was negative for all the samples in this harsh environment with the highest values being obtained between 0.82 and 2.92 wt% Ru. The highest number observed was for the 0.82 wt% Ru sample. The 4.67 wt% Ru sample was at a slightly more negative number suggesting that further additions of ruthenium add no benefit to the sample and in fact deteriorate its performance. The two samples without ruthenium were behaving the worst from a corrosion point of view with the most negative potentials. The E_{corr} values were in the same range as the ones in 1 M sulphuric acid with 1% sodium chloride at 25°C suggesting that in this case, the temperature did not add significantly to the harshness of the environment but that was not confirmed by the graphs in section 4.3.6, it must be noticed though, that the 4.67 wt% Ru sample still showed an improvement at the lower temperature.

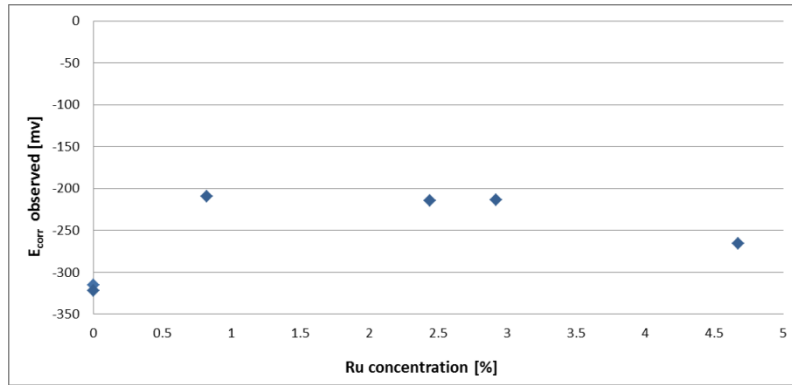


Figure 108: E_{corr} comparison at various ruthenium compositions from the exposed surface scan in 1 M H_2SO_4 + 1% NaCl at 45°C

The i_{corr} values are confirming this trend that the two samples containing no ruthenium have significantly larger numbers, the 0.82 wt%, 2.92 wt% and 2.44 wt% Ru samples had the lowest numbers as is desirable while the 4.67 wt% Ru i_{corr} value increased again. The lowest number was observed for the 2.44 wt% Ru sample. Thereafter, however, the trend showed a decrease in i_{corr} with increasing ruthenium which implies increased corrosion protection with increasing amounts of ruthenium. The values obtained during this testing were significantly higher than those obtained at ambient conditions for the same solution confirming that corrosion increases with an increase in temperature.

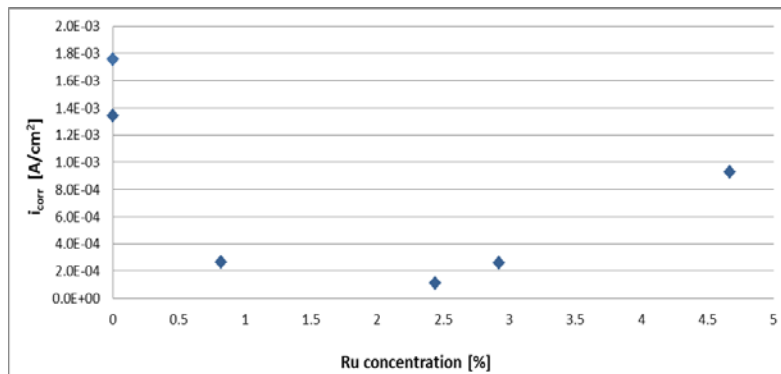


Figure 109: i_{corr} comparison at various ruthenium compositions from the exposed surface scan in 1 M H_2SO_4 + 1% NaCl at 45°C

Observing the current density at a selected potential such as 0.1 V as in Figure 110, it was observed that samples containing ruthenium had a significantly lower current density implying better corrosion protection and the lowest value was obtained for the 4.67 wt% Ru sample. The onset of passivation occurs at approximately 0.1 V and the ranking order of the samples in that region did not vary throughout and thus almost any potential could be selected to show the same trend. All ruthenium containing samples showing improved corrosion protection with values that were very similar. Again, the actual values were higher than for the tests conducted at ambient conditions showing the harshness of the environment

and thus the strength of the ruthenium to provide significant corrosion protection at elevated temperatures.

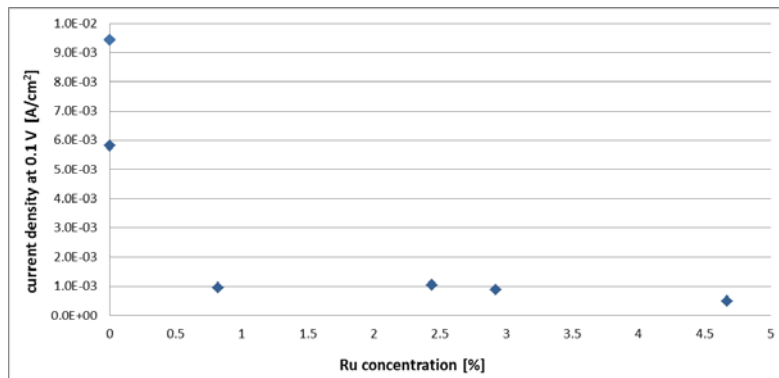


Figure 110: Current density at 0.1 V comparison at various ruthenium compositions from the exposed surface scan in 1 M H₂SO₄ + 1% NaCl at 45°C

As with i_{corr} , the corrosion rate was highest for the two samples without ruthenium but with the ruthenium containing samples, there is a downward step indicating immediately improved corrosion protection with the addition of the ruthenium to the stainless steel. The trend indicates that the lowest corrosion rates were obtained in the 0.82 wt% to 2.92 wt% Ru range with the lowest result being for the 2.44 wt% Ru sample, seen in Figure 111. The corrosion rate increased for the 4.67 wt% Ru sample suggesting that this was beyond the optimal range under these conditions.

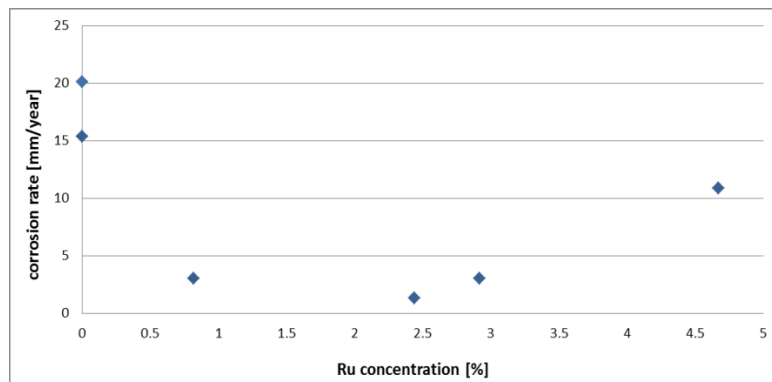


Figure 111: Corrosion rate comparison at various ruthenium compositions from the exposed surface scan in 1 M H₂SO₄ + 1% NaCl at 45°C

As per Figure 112, the most negative OCP value was obtained for the cladded sample without ruthenium which was very similar to the stainless steel blank sample. The values showed an increasing trend in OCP values as ruthenium composition increased implying less activity striving towards the passive region and therefore reduced corrosion rates. The highest value obtained was from the 4.67 wt% Ru sample, the 2.92 wt% and 2.44 wt% Ru samples showed very close results slightly less than that of the highest ruthenium composition.

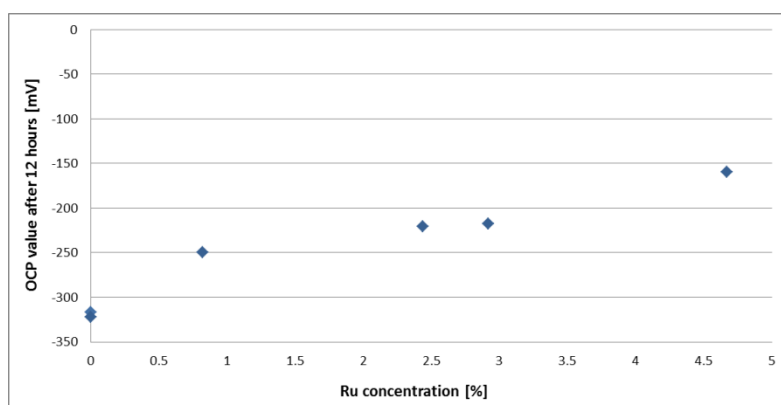


Figure 112: OCP value comparison at various ruthenium compositions from the exposed surface scan in 1 M H₂SO₄ + 1% NaCl at 45°C

During the second anodic scan a fresh surface area of the sample was exposed and the results obtained can be seen in Table 16 which gives the average results of E_{corr} and i_{corr} values as well as the corrosion rate and polarisation resistance from the valid rests carried out; the remaining results can be found in Appendix G. As observed during the exposed anodic scan, all the E_{corr} values were negative with the ruthenium containing samples having lower values. The other parameters followed a similar trend where the indication was that corrosion resistance increased with an increase in ruthenium composition but variability was larger for this scan. The numbers in general show improved corrosion protection compared to the values in 1 M sulphuric acid with 1% sodium chloride at 25°C.

Table 16: Indicators of corrosion rate using average sample measurements from the fresh surface scan in 1 M H₂SO₄ + 1% NaCl at 45°C

	E_{corr} [mV]	i_{corr} [A/cm ²]	Corrosion rate [mm/year]	Polarisation resistance [Ω]
S/S blank	-365	1.80×10^{-4}	2.06	N/A*
0.0% Ru	-358	1.94×10^{-4}	2.23	N/A*
0.82% Ru	-224	1.61×10^{-4}	1.86	N/A*
2.92% Ru	-243	2.50×10^{-4}	2.90	N/A*
2.44% Ru	-223	7.64×10^{-5}	0.89	N/A*
4.67% Ru	-274	6.73×10^{-5}	0.79	85.5

The N/A* indicates that these values could not be calculated or obtained from the software

The E_{corr} values obtained follow the same trend as the values during the exposed surface scan: the two samples without ruthenium had much lower, more negative, numbers compared to the ruthenium containing samples, Figure 113. The highest numbers were obtained for the

0.82 wt% Ru and 2.92 wt% Ru range and the 4.67 wt% Ru sample showed a slight drop in results again. The gap between the ruthenium and non-ruthenium containing samples had widened because the samples without ruthenium had lower values for the fresh surface scan.

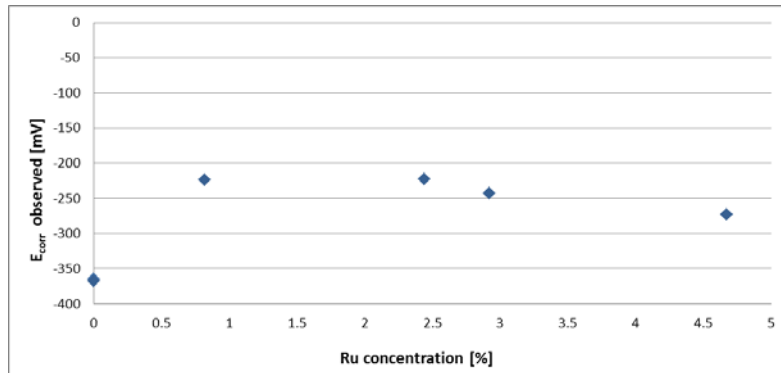


Figure 113: E_{corr} comparison at various ruthenium compositions from the fresh surface scan in 1 M H_2SO_4 + 1% NaCl at 45°C

The i_{corr} values follow a general downward trend to lower values with an increase in ruthenium concentration, as can be observed in Figure 114. The highest value however was obtained for the 2.92 wt% Ru sample which would thus not follow that trend while the lowest value was observed for the 4.67 wt% Ru sample. The two samples without ruthenium had very similar values. It is again noticed that individual values were lower than for the tests carried out in the same solution at 25°C indicating better corrosion protection at 45°C.

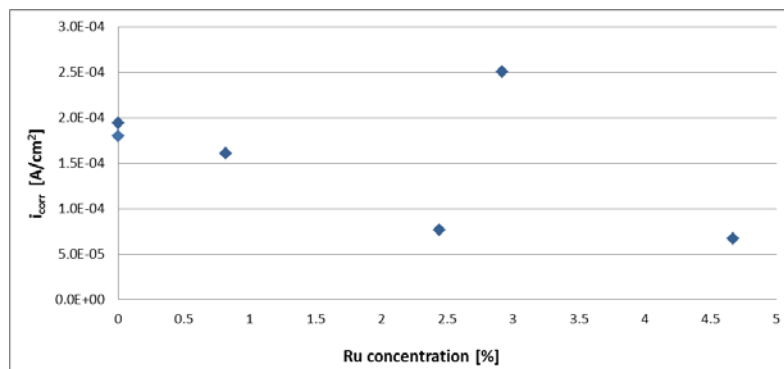


Figure 114: i_{corr} comparison at various ruthenium compositions from the fresh surface scan in 1 M H_2SO_4 + 1% NaCl at 45°C

The corrosion rate followed exactly the same trend as these values were calculated from the current density values. The two samples without ruthenium have very similar values. The general trend was for lower corrosion rates with an increase in ruthenium concentration, as per Figure 115. The highest value was again obtained for the 2.92 wt% Ru sample while the lowest value was observed for the 4.67 wt% Ru sample. Rates were lower in this case than for the test in 1 M sulphuric acid and 1% sodium chloride at 25°C as well as during the

exposed surface scan and even the results for the sulphuric acid at high temperatures without the added salt.

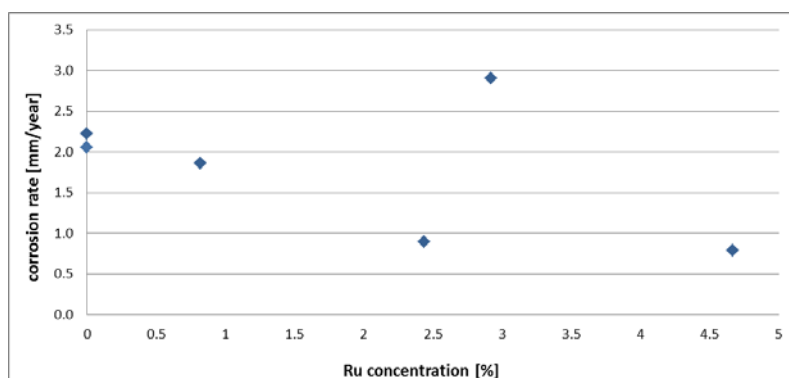


Figure 115: Corrosion rate comparison at various ruthenium compositions from the fresh surface scan in 1 M H₂SO₄ + 1% NaCl at 45°C

The passivation potentials from the exposed and fresh surface scans were similar in this environment, high positive numbers for the stainless steel blank and clad sample without ruthenium while all other results, i.e. the samples containing ruthenium, were negative but small and in fact mostly decreasing negative numbers with an increase in ruthenium. The OCP values in this case were all much smaller than the E_{pass} values for the two scans indicating active corrosion, as per Table 17. The difference between the E_{pass} values and the OCP values after the 12 hours was reasonably large, in the order of approximately 700 mV for the stainless steel blank sample and close to 200 mV for the ruthenium containing samples. For the tests in the same solution at 25°C, only the samples containing no ruthenium showed active corrosion behaviour, all ruthenium containing samples were passive.

Table 17: Passivation potentials comparison to OCP values in 1 M H₂SO₄ + 1% NaCl at 45°C

	E_{pass} from the exposed surface scan [mV]	OCP after 12 hours [mV]	E_{pass} from the fresh surface scan [mV]
S/S blank	437	-317	382
0.0% Ru	390	-322	439
0.82% Ru	-41	-250	-25
2.92% Ru	-38	-218	-17
2.44% Ru	-29	-220	-3
4.67% Ru	-21	-160	-4

As suggested before, any new alloy must be tested against already available materials to verify how it compares and to test if it is better suited for the environment than potentially competitive products. As mentioned before, the consistency of the 316 stainless steel, the SAF2205 duplex stainless steel and the Hastelloy C276 samples was excellent.

After exposure to such harsh conditions for over 12 hours, equilibrium was assumed to have been reached and a passive layer formed if possible. The 304L stainless steel sample had the lowest E_{corr} value, the largest nose and reaching the passive region slowly and at the highest current densities. The ruthenium containing samples behaved well under these conditions, much better than the 304L stainless steel blank until above 0.7 V have been reached, as can be seen in Figure 116. The 316 stainless steel sample had a lower E_{corr} value than the ruthenium containing 304L stainless steel with a similar nose but it reached a stable passive region at much lower current densities. The SAF2205 duplex stainless steel had an E_{corr} value only slightly above that of the 304L stainless steel but a much shorter and flatter nose so that it reached a stable passive region at approximately the same potential and current densities as the 316 stainless steel. The Hastelloy C276 had a large active region attaining E_{corr} at the highest potential of -0.14 V after which it had a short nose to reach the passive region at the lowest current densities, a stable $3 \times 10^{-5} \text{ A/cm}^2$ was ensured over a range of over 0.8 V. It performed the best in 1 M sulphuric acid with the addition of 1% sodium chloride at 45°C. The Tafel slopes of the 316 stainless, the SAF2205 and the Hastelloy C276 were similar and not as steep as the 304 stainless and its alloys.

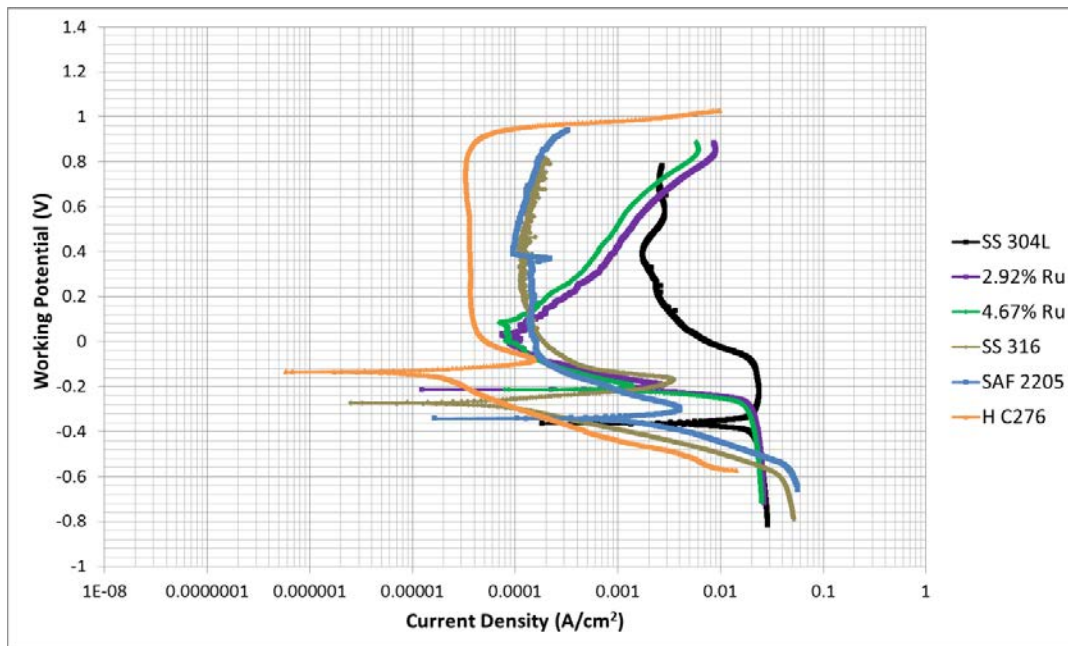


Figure 116: Log i vs E graphs from the exposed surface scan comparing ruthenium samples to other steels in 1 M $H_2SO_4 + 1\% NaCl$ at $45^\circ C$

On a fresh surface area, expressed in Figure 117, the 304L stainless steel sample still showed the lowest E_{corr} , had the largest nose and reached the passive region only after 0.4 V and above exhibiting the worst corrosion protection in this environment. The two samples containing ruthenium initially showed good resistance with higher E_{corr} values and a smaller nose but as the potential increased and with the current densities in the passive region, their curves crossed over that for the 304L stainless sample indicating worse corrosion protection from 0.7 V upwards. The 316 stainless steel indicated lower E_{corr} values than the ruthenium containing samples, a small active nose and then an unstable region is reached until 0.6 V where the sample appears to form cathodic loops and passivity is not guaranteed until it seemed to stabilise after that. The SAF2205 duplex steel had an E_{corr} value the same as the ruthenium containing samples, displayed a small cathodic loop immediately after which was followed by a seemingly stable region at i_{pass} values around $1 \times 10^{-5} A/cm^2$ before another cathodic loop at 0.47 V and thereafter only really reaching a passive region. The Hastelloy had the highest E_{corr} values at -0.12 V with a small nose but then seemed to also form cathodic loops or at least a very unstable passive region at the lowest current densities even though these also were increasing with an increase in potential before becoming stable at 0.7 V and a i_{pass} the same as that of the 316 stainless before going into the trans-passive region at 0.9 V. Again, the Tafel slopes of the 316 stainless, the SAF2205 and the Hastelloy C276 are similar and much gentler than the 304 stainless samples. It seemed that in this

environment neither the 304 samples nor its alloys with ruthenium behave as well as the other types of stainless steel.

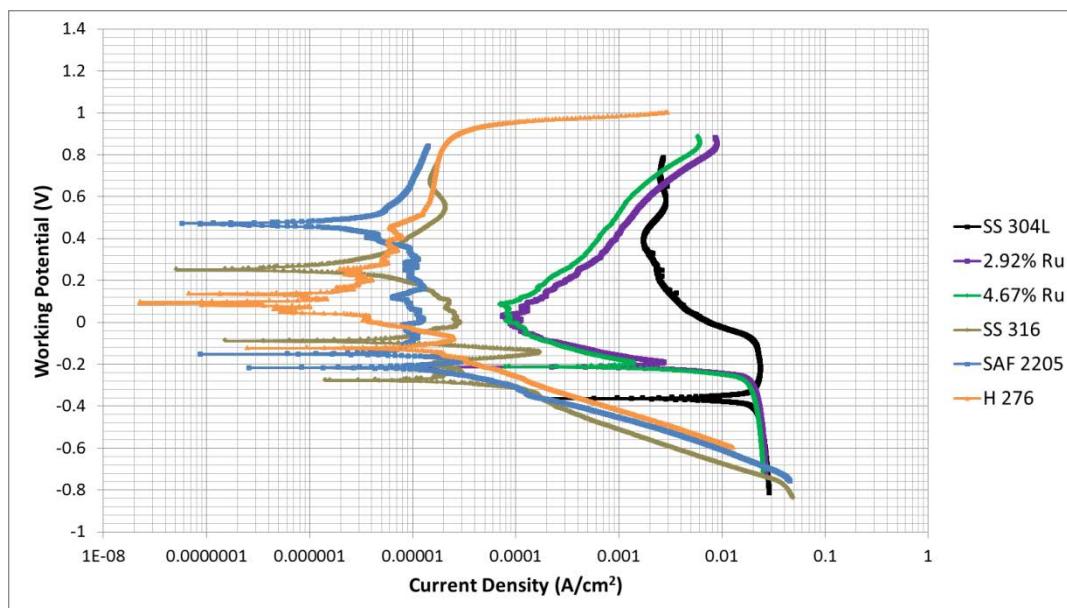


Figure 117: Log i vs E graphs from the fresh surface scan comparing ruthenium samples to other steels in 1 M H_2SO_4 + 1% NaCl at 45°C

4.3.5 1 M HCl solution at 25°C

Validity of the results must be established by testing each sample a few times in the same environment and under the same condition to show that consistent results can be observed which can be compared to each other. The same methodology was followed when conducting these experiments as was described in section 3.4 above but all samples were tested in 1 M hydrochloric acid at a temperature of 25°C. The remaining graphs to show repeatability of all the samples can be found in Appendix H.

The graphs for tests 1 and 2 were very inconsistent which was not observed before for the stainless steel blank sample but tests 3 and 4 were consistent and those will be used for further comparisons. Those results for the exposed and fresh surface scans were consistent with each other in this environment. During the exposed surface scans the two curves from tests 3 and 4 almost corresponded, both having gentle Tafel slopes, an E_{corr} value of -0.31 V, a long nose after which another kink followed before an active region began at just higher than 0.1 V and between 1×10^{-2} and 2×10^{-2} A/cm² but for these tests no trans-passive region was reached. These tests behaved similarly during the fresh surface scans with the same Tafel slopes, E_{corr} values slightly lower and not as consistent as well as some inconsistency around

the active nose and the kink but then reaching the same passive region as during the exposed surface scan. Test 1 during the exposed surface scan had gentler Tafel slopes, a reduced E_{corr} value of -0.52 V after where there was a hint of a nose before the current densities further increase with potential to display the commonly observed transition but at much smaller current densities than what was observed for tests 3 and 4. The fresh surface scan for test 1 showed a similar transition at approximately two orders of magnitude higher than the exposed surface scan, a higher E_{corr} value of -0.46 V and some variability from 0.2 V upwards but suggesting passivation as that variability occurred in a specific current density range of between 2×10^{-5} and 9×10^{-5} A/cm². The 2nd test, after the exposed surface scan, displayed values in the same low current density range as test 1 but with a lower E_{corr} value of -0.69 V and a steep transition at potentials above -0.6 V which then coincided with those of the 1st test. During the fresh surface scan, test 2 also exhibited a transition with an E_{corr} of -0.27 V after which it headed towards, and eventually joined, the curve for this test during the exposed surface scan. No trans-passive region was reached with these tests.

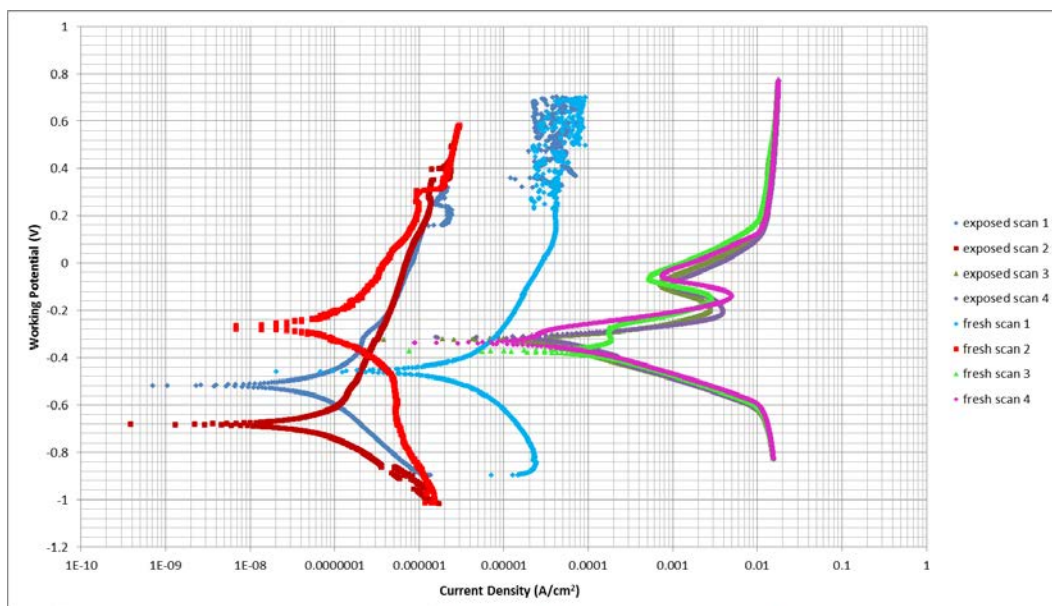


Figure 118: Log i vs E graphs for the Stainless Steel blank sample in 1 M HCl at 25°C

The potential measurements over time confirmed the inconsistencies of tests 1 and 2 compared to tests 3 and 4 which coincided with one another and with a final OCP value of -0.35 V. Results for the other two tests were significantly lower, below -0.5 V for test 2. Stable results were obtained each time with the starting potential being very close to the final OCP value after 12 hours.

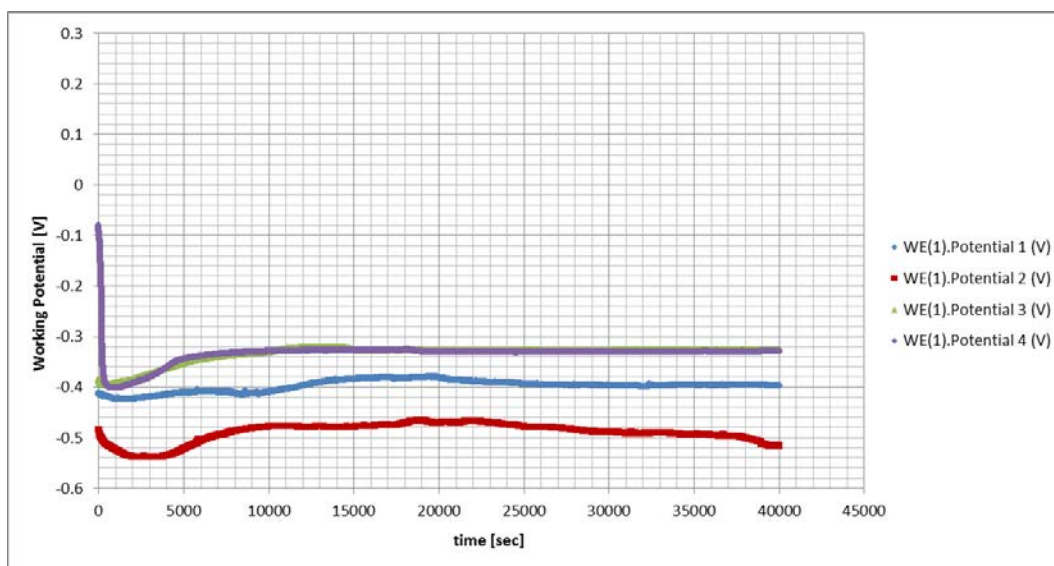


Figure 119: E vs time graphs for the Stainless Steel blank sample in 1 M HCl at 25°C

There was a significant variability observed with the samples containing 0.82 wt% Ru in hydrochloric acid as per Figure 120 with the consistency being better between the exposed and fresh surface scans than between the three tests carried out. All of them did, however, follow similar shapes and seem to reach a passive region, even though the results stretched over a large current density range. During the exposed surface scan the Tafel slopes were gentle for tests 1 and 2 while rather steep for test 3, the E_{corr} values were at -0.34 V for tests 1 and 2 while slightly higher at -0.27 V for test 3; tests 1 and 2 then followed the transition up into a passive region from 0.2 V upwards ranging around $5 \times 10^{-5} \text{ A/cm}^2$ for test 1 and $4 \times 10^{-6} \text{ A/cm}^2$ for test 2 while test 3 had a small nose after which the curve kinked back towards higher current densities until stabilising in the passive region from just above 0.2 V upwards at much higher corrosion rates at $2 \times 10^{-2} \text{ A/cm}^2$. During the cleaned surface scan, the curves followed their exposed surface scan curves reasonably closely which was especially true for tests 1 and 3 while for test 2, the E_{corr} value increased to -0.18 V before it joined again in the passive region. The variability in hydrochloric acid seems much worse than in the sulphuric acid, there were great inconsistencies observed even when tests were repeated a number of times under the same conditions.

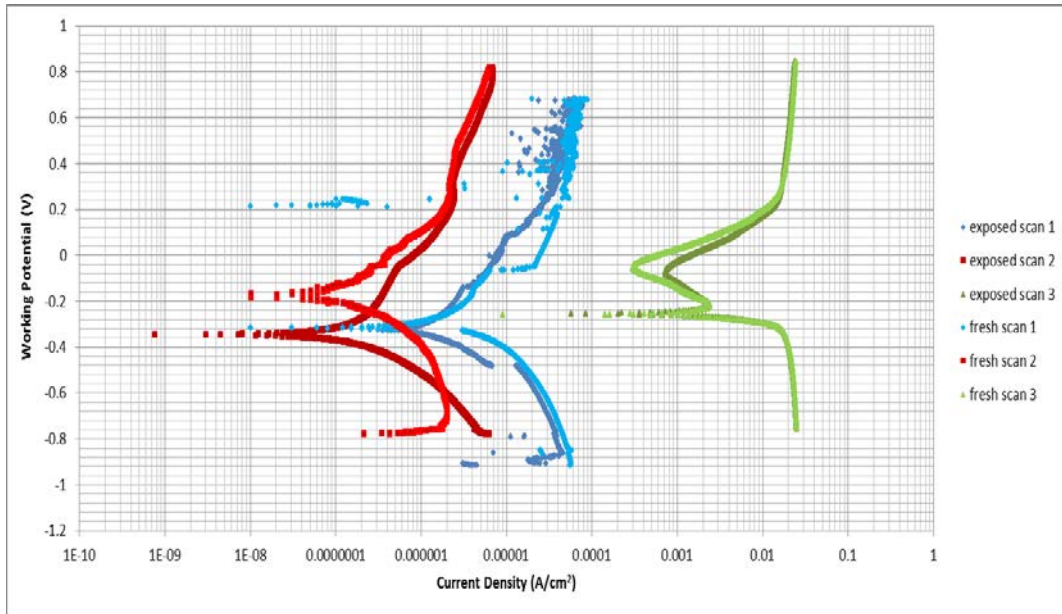


Figure 120: Log i vs E graphs for the 0.82 wt% Ru sample in 1 M HCl at 25°C

The potential over time graphs verified the variability mentioned, as in Figure 121, in this case test 1 seemed to not correspond with tests 2 and 3 which followed the same curve to reach a final OCP value of around -0.27 V. For all tests the initial values dropped sharply to then stabilise during the 12 hours of exposure but it did seem as if totally stable values are not reached but would be very close to the ones obtained at this stage.

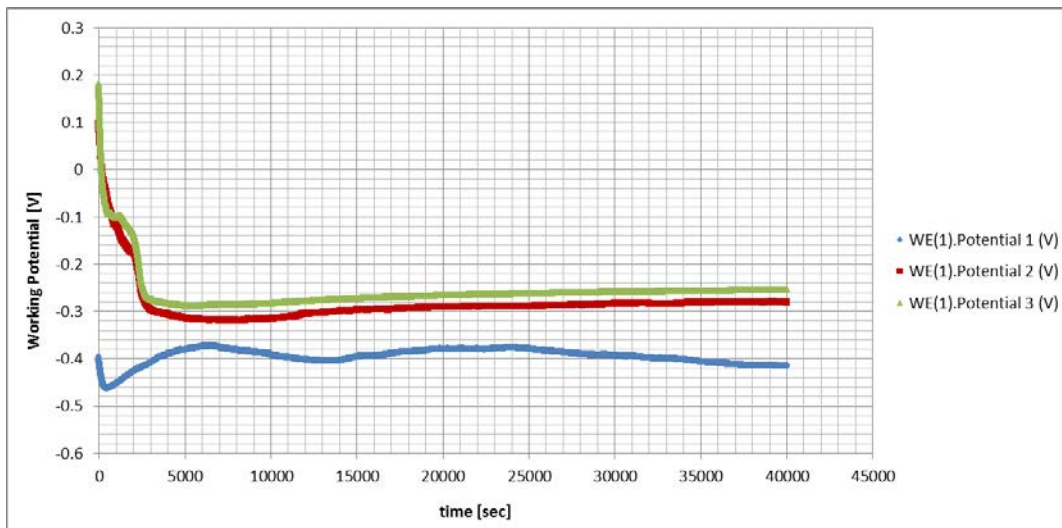


Figure 121: E vs time graphs for the 0.82 wt% Ru sample in 1 M HCl at 25°C

Looking at the 4.67 wt% Ru samples in Figure 122, large variability was observed as with previous test results and as observed before, the consistency was better between the exposed and fresh surface scans than between the three tests carried out. The general trend was that they followed a transition and all three curves did seem to reach a passive region where the current densities varied only slightly with an increase in potential, even though the results

stretched over a large current density range. During the exposed surface scan the E_{corr} values obtained were close to each other at -0.31 V (for the tests 2 and 3) and -0.52 V (for test 1) but then the shapes did change: tests 1 and 2 increased sharply in current density with the increase in potential while test 1 displayed a break of the curve after 0.5 V where the current density values decreased with a step by almost an order of magnitude but test 3 current density values increased more slowly with potential, had a slight kink in the curve and from 0.3 V upwards, increase sharply. The current density ranges over more than four orders of magnitude at, say, 0.7 V from 7.0×10^{-7} to 2.5×10^{-2} A/cm². The results for the fresh surface scan were equally variable with E_{corr} values being closer to each other at just slightly less than the previous values at -0.37 V (for tests 1 and 3) even though test 2 was just a straight vertical line and therefore meaningless for further analysis. Test 1 followed the transition with steeper Tafel slopes and higher current densities than its exposed surface scan to end up in the same passive region from 0.5 V onwards and test 3 also displayed slightly higher current densities throughout the fresh surface scan than during the exposed surface scan following it more closely and the curves corresponding well with one another from 0.3 V upwards. No transpassive region is reached with these tests. This variability made any of these tests difficult to use during a comparison with any other samples.

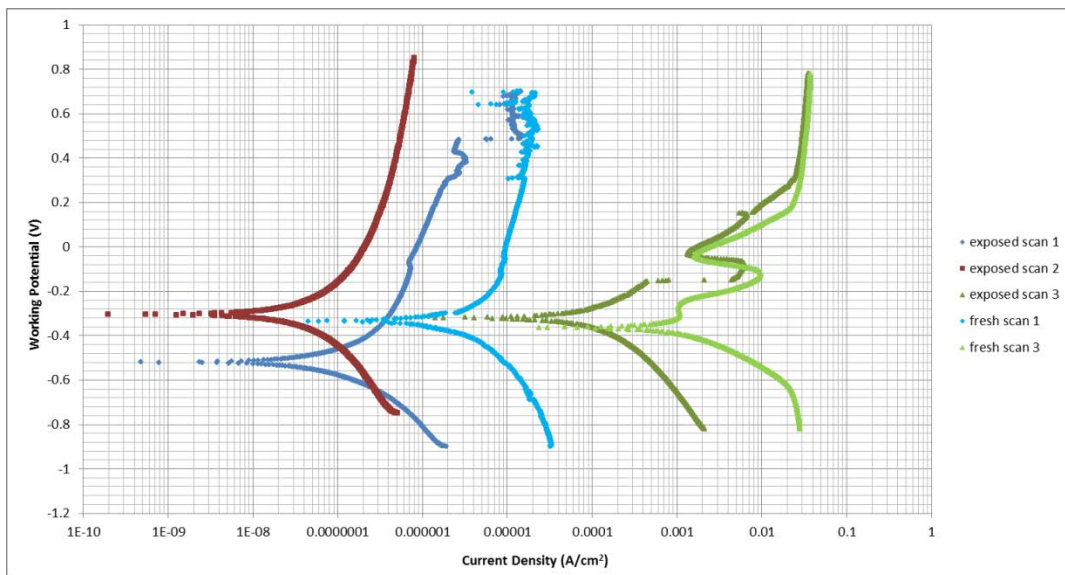


Figure 122: Log i vs E graphs for the 4.67 wt% sample in 1 M HCl at 25°C

The potential measurements over time also indicate variability. Figure 123 shows that tests 1 and 3 were close to each other for the first eight hours after which they split with test 1 values dropping to a lower number and it cannot be said with certainty that a stable value had been reached after the 12 hours. The test 3 values showed the most consistency throughout the testing time with a final OCP value of -0.32 V. Test 2 showed higher values during the test

dropping slightly as the 12 hours approached making the final variability between all three results 0.15 V.

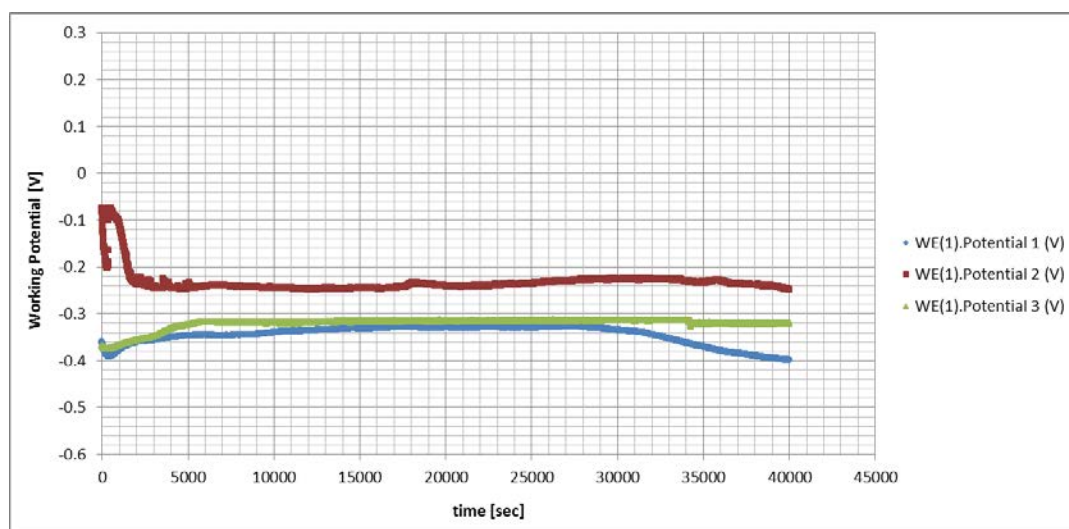


Figure 123: E vs time graphs for the 4.67 wt% Ru sample in 1 M HCl at 25°C

A representative sample was taken, as best as possible, from the results produced during the testing at 1 M hydrochloric acid so that they could be compared which gives guidance as to which alloy performs best in these conditions. This can be seen in Figure 124 for the exposed surface scan, Figure 125 comparing results during the fresh surface scan and Figure 126 comparing the potential values over time.

The stainless steel curve in Figure 124 had a steep Tafel slope, the highest E_{corr} value at -0.31 V, a small active nose and a very gentle slope to reach the passive region at 0.2 V and a high current density of approximately $1.5 \times 10^{-2} \text{ A/cm}^2$. The clad sample without any ruthenium behaved worse in this condition even though it followed the stainless steel blank sample closely, it does so always at higher current densities, it displayed the transition so that no nose was observed, has an E_{corr} slightly below that of the stainless steel blank at -0.35 V and the passive region was obtained earlier at just below 0 V and at the highest value of all these samples at $3 \times 10^{-2} \text{ A/cm}^2$. All the samples containing ruthenium seem to be performing much better in this environment as the scans showed orders of magnitude smaller current densities, all the same Tafel slopes in the active region and a transition is observed compared to the two samples without ruthenium. The sample with just a small amount of ruthenium included, at 0.82 wt%, had the highest E_{corr} value of the ruthenium containing samples at -0.32 V and also had the highest current density values of all the ruthenium containing samples being at approximately $6 \times 10^{-5} \text{ A/cm}^2$ at a potential of 0.6 V. The 2.92 wt% Ru sample had the next lowest E_{corr} value of -0.36 V but reaching passivity reasonably close to

the values obtained from the 0.82 wt% Ru sample but all of them being lower where i_{pass} was $2.5 \times 10^{-5} \text{ A/cm}^2$ at 0.6 V. The 2.44 wt% Ru sample had the next lowest E_{corr} value at -0.41 V, an initially steeper Tafel slope as potentials increase and reached a passive region of $5.5 \times 10^{-6} \text{ A/cm}^2$ at 0.6 V. The sample with the 4.67 wt% Ru had the lowest E_{corr} value at -0.52 V and then a relatively steep slope as potentials increase with a small break in the curve so that the current density at 0.6 V was actually higher than that for the 2.44 wt% Ru sample at $1 \times 10^{-5} \text{ A/cm}^2$ even though it had the lowest current density values throughout most of the scan. This definitely indicates a general trend that lower current densities are observed as the amount of ruthenium increases and thus better corrosion protection is afforded after exposure in 1 M hydrochloric acid at ambient conditions. No trans-passive region is obtained during this test.

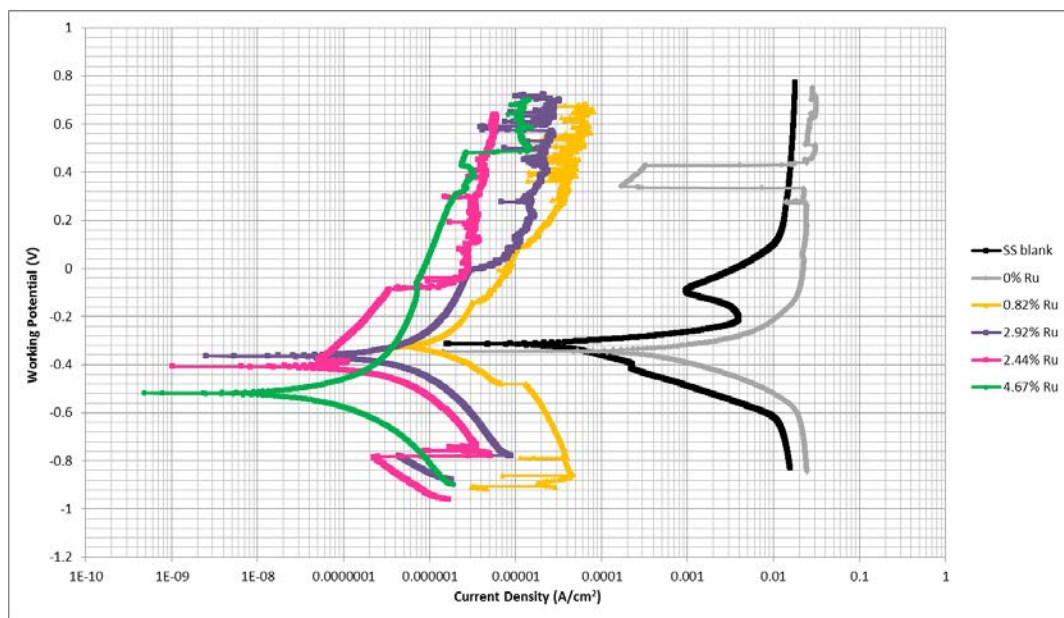


Figure 124: Log i vs E graphs from the exposed surface scan comparing all samples in 1 M HCl at 25°C

On a fresh surface area, Figure 125, it is observed that all the ruthenium containing samples show orders of magnitude lower current densities than the samples without ruthenium but the actual values were in a much narrower current density range than the samples from the first anodic scan, i.e. after exposure to the environment for over 12 hours. The stainless steel blank sample had a gentle Tafel slope, an E_{corr} value of -0.33 V which was almost the lowest for this scan, a prominent active nose which kinked back slightly to reach the passive region at just above 0.1 V and an i_{pass} value of around $1.5 \times 10^{-2} \text{ A/cm}^2$. The cladded sample without any ruthenium had the lowest E_{corr} value this time at -0.38 V, two steep Tafel slopes and seemed to reach passivity at -0.1 V already after which a slight kink back was observed which corresponded to that of the stainless steel blank sample but the entire curve ran at

slightly higher current density values compared to the blank sample so that i_{pass} was around $3 \times 10^{-2} \text{ A/cm}^2$. The 0.82 wt% Ru sample had an E_{corr} value of -0.32 V, a steep transition which then exhibited a step increase at the same potential as the kink occurred in the stainless steel blank sample, before reaching a much lower current density value of $7 \times 10^{-5} \text{ A/cm}^2$ at 0.6 V. More variability was observed during this test as potentials increased above 0.2 V which made identifying correct actual points more difficult but a trend can be observed for comparison to other samples. The 2.92 wt% Ru sample had a higher E_{corr} value at -0.24 V but displayed a uniformly shaped funnel or transition with some variability and had an i_{pass} value of $3 \times 10^{-5} \text{ A/cm}^2$ at 0.6 V. The 2.44 wt% Ru sample seemed to be behaving the best in this environment having the highest E_{corr} value at -0.19 V with a very open transition curve, the lowest current density values throughout the entire scan which was seen at 0.6 V with a current density value of $1 \times 10^{-5} \text{ A/cm}^2$. The sample with the highest amount of ruthenium included at 4.67 wt% had an E_{corr} value which was the same as that of the stainless steel blank sample, the Tafel slopes closest to the 0.82 wt% Ru sample but then going into an almost vertical passive region starting at -0.1 V and a current density around $1 \times 10^{-5} \text{ A/cm}^2$ which was the second lowest throughout the higher potential portion of the scan. No trans-passive region was obtained during this test.

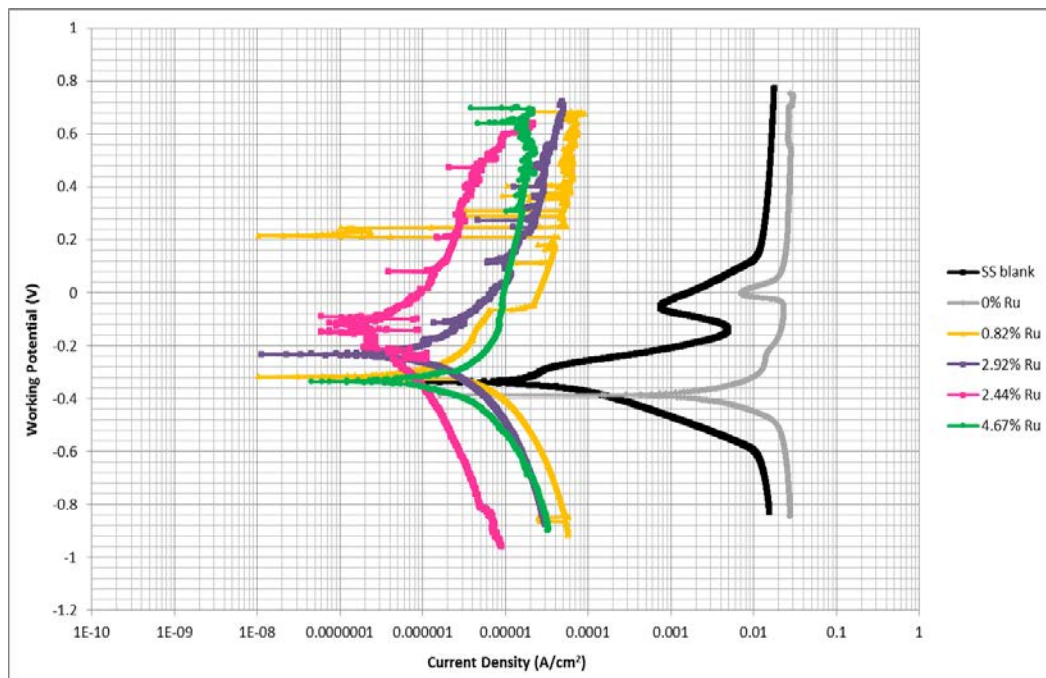


Figure 125: Log i vs E graphs from the fresh surface scan comparing all samples in 1 M HCl at 25°C

The OCP values were all very close for the tests with the hydrochloric acid and an overall range of less than 0.1 V was observed and all the curves had stabilised so that equilibrium was reached, as observed in Figure 126. The final values after the 12 hour period seem to

have been grouped into three: the clad sample without ruthenium had the lowest OCP value, the stainless steel blank sample together with the 2.44 wt% Ru and 4.67 wt% Ru samples showed values just slightly higher than that and the highest OCP values of -0.34 V were obtained for the 0.82 wt% Ru and 2.92 wt% Ru samples.

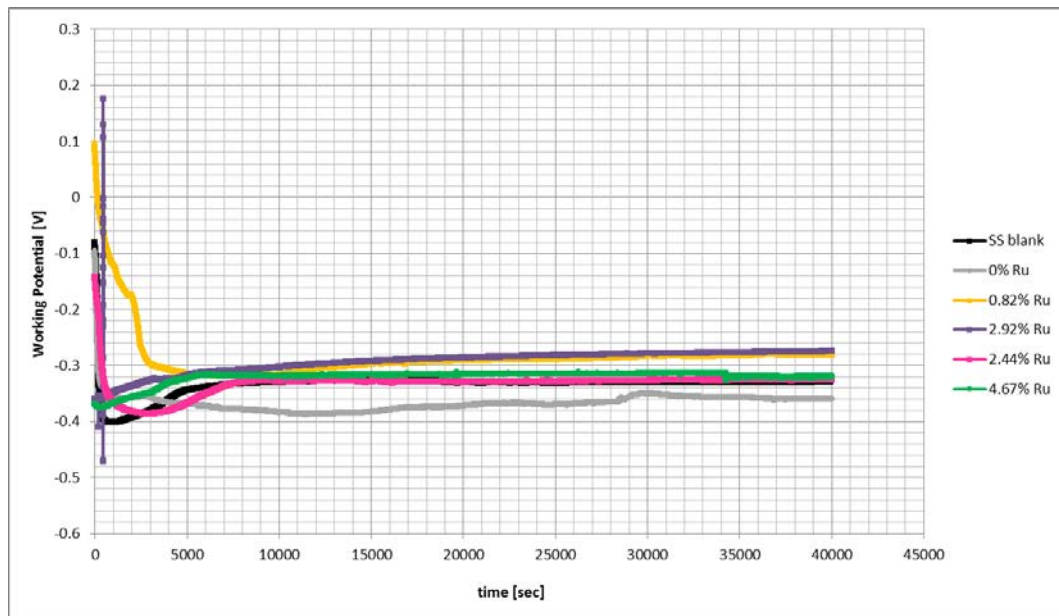


Figure 126: E vs time graphs comparing all samples in 1 M HCl at 25°C

Observing indicators for determining and comparing corrosion activity, it is best to compare them as in Table 18 where the average E_{corr} , i_{corr} , current density at 0.2 V, the corrosion rate, polarisation resistance and OCP values of the valid tests were calculated to give a good representation for a comparison. These are for the first anodic scan, i.e. after the potential has been measured for 12 hours and thus the sample has been exposed to the environment for that duration of time before the scan was conducted. The full results are available in Appendix H, the variability was significant from test to test and thus simply taking averages might not always give a clear indication to establish which alloy is stronger from a corrosion point of view but it will serve as an initial indication. A graphical representation of the values in the table is given in Figure 127 to Figure 131 so that trends could be identified better. It can already be noticed that all the E_{corr} or OCP values were large negative numbers; corrosion rates were high especially for the ruthenium containing samples while the polarisation resistance figures were also high.

Table 18: Indicators of corrosion rate using average sample measurements from the exposed surface scan in 1 M HCl at 25°C

	E_{corr} [mV]	i_{corr} [A/cm ²]	i at 0.2 V [A/cm ²]	Corrosion rate [mm/year]	Polarisation resistance [Ω]	OCP after 12 hours [mV]
S/S blank	-460	1.61×10^{-5}	6.33×10^{-3}	0.17	985 881	-393
0.0% Ru	-432	1.47×10^{-4}	8.08×10^{-3}	1.53	590 356	-368
0.82% Ru	-310	5.10×10^{-4}	4.30×10^{-3}	4.71	479 286	-317
2.92% Ru	-300	1.03×10^{-3}	9.06×10^{-3}	9.54	171 298	-305
2.44% Ru	-385	1.31×10^{-5}	8.47×10^{-3}	0.18	7 688 871	-371
4.67% Ru	-381	2.38×10^{-5}	3.60×10^{-3}	0.22	4 522 487	-322

The E_{corr} values were large negative numbers with the largest values obtained belonging to the two samples without ruthenium, the stainless steel blank sample being more negative than the cladded sample without ruthenium. The addition of ruthenium distinctly increased the E_{corr} values with the highest value being attained by the 2.92 wt% Ru sample followed by the 0.82 wt% Ru sample. The 4.67 wt% and 2.44 wt% Ru samples had values close to each other and lower than the other two ruthenium containing samples, suggesting that a limit in terms of increasing the E_{corr} values is achieved by the addition of ruthenium.

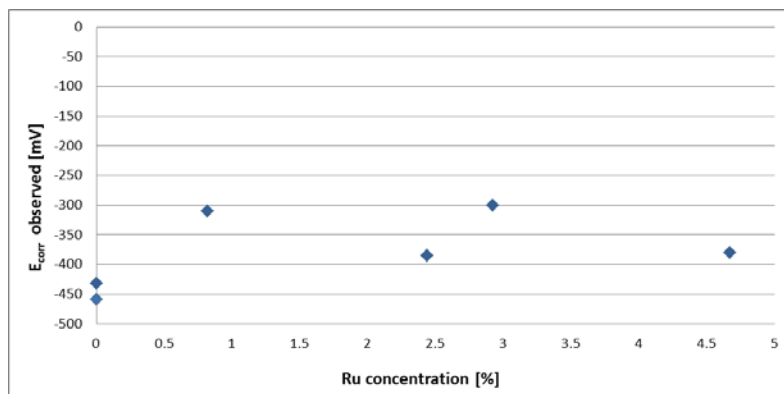


Figure 127: E_{corr} comparison at various ruthenium compositions from the exposed surface scan in 1 M HCl at 25°C

The i_{corr} values as per Figure 128 were reasonably low in comparison, for example, with the samples being tested in 1 M sulphuric acid. The lowest value was obtained for the 2.44 wt% Ru sample while the highest values were obtained by the 2.92 and 0.82 wt% Ru samples which gave therefore no clear results about corrosion improvement with ruthenium addition. The 4.67 wt% Ru sample had a result higher than the stainless steel blank sample but lower than the cladded sample without ruthenium.

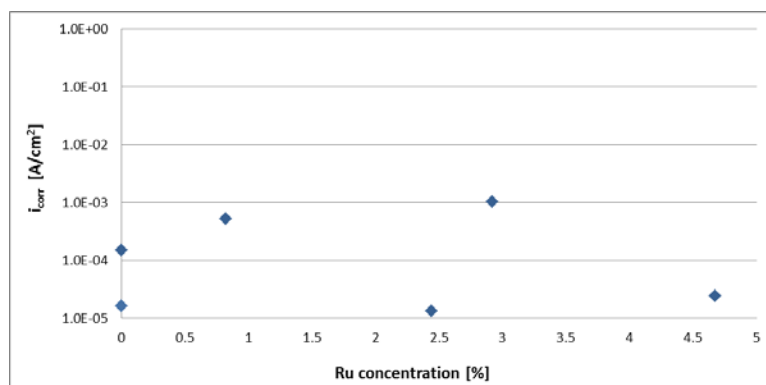


Figure 128: i_{corr} comparison at various ruthenium compositions from the exposed surface scan in 1M HCl at 25°C

Selecting a current density at a specific potential during the scan generally gives a good indication of a ranking order at that particular point which is especially interesting as the passive region is obtained. The selected value for such a comparison was 0.1 V as it gave clear results of such a ranking order at passivity, which did not change throughout the passive region. In this case it was observed that the 2.44 and 2.92 wt% Ru samples obtained current densities slightly higher than the two samples without ruthenium while the 0.82 and 4.67 wt% Ru samples attained lower values with the 4.67 wt% Ru sample achieving the lowest value which indicated the least amount of corrosion activity at that potential. Again, the trend was not clear regarding current density as ruthenium is added to the 304L stainless steel.

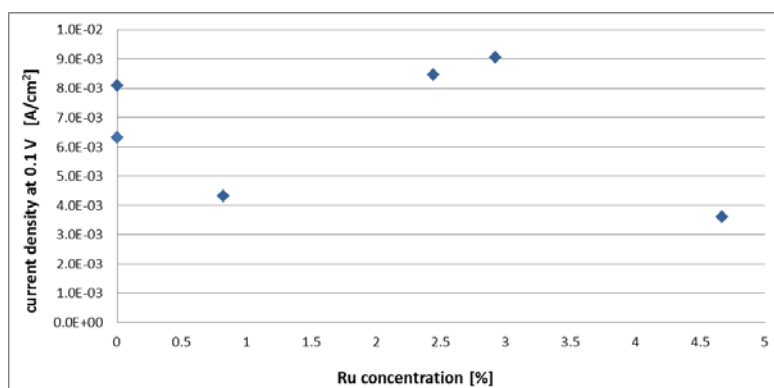


Figure 129: Current density at 0.1 V comparison at various ruthenium compositions from the exposed surface scan in 1 M HCl at 25°C

The corrosion rate calculated is not showing a trend either, in this environment the stainless steel blank sample had, on average, the lowest rate followed by the 2.44 wt% Ru sample while the highest rate was obtained by the 2.92 wt% Ru sample followed by the 0.82 wt% Ru sample. The cladded sample had a higher corrosion rate than the stainless steel blank sample but still lower than two of the ruthenium samples. There is a significant range observed in corrosion rate which stems from the large inconsistencies obtained between testing the

samples, this might be a more ‘unpredictable’ environment and perhaps a few more tests should be conducted.

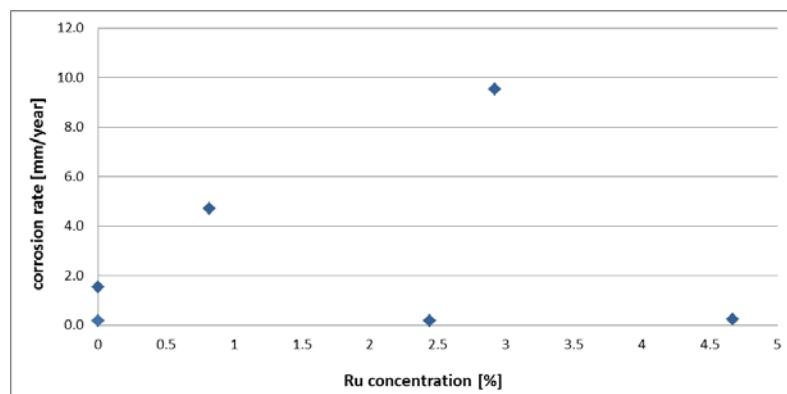


Figure 130: Corrosion rate comparison at various ruthenium compositions from the exposed surface scan in 1 M HCl at 25°C

The polarisation resistance data was of course almost a mirror image of the corrosion rate data; it shows no clear trend with regards to increasing ruthenium content in the stainless steel sample. The log scale emphasises the great range in results between the averages but that variation also exists from test to test when testing the same sample. The lowest value was obtained for the 2.92 wt% Ru sample while the highest results were obtained for the 2.44 and 4.67 wt% Ru samples.

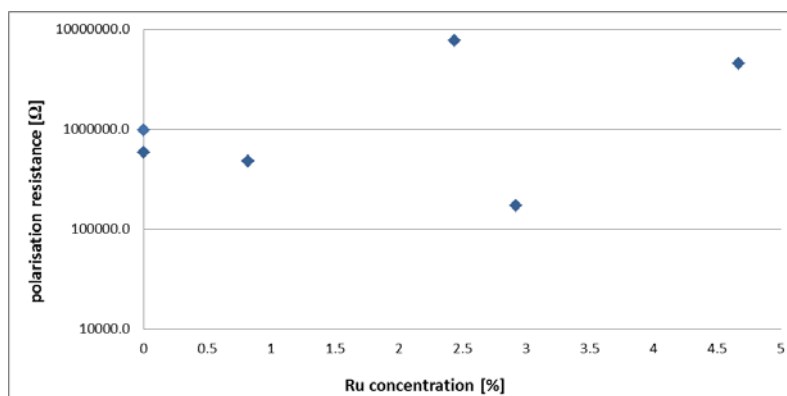


Figure 131: Polarisation resistance comparison at various ruthenium compositions from the exposed surface scan in 1 M HCl at 25°C

The results obtained from the fresh surface scan can be found in Table 19 and Figure 132 to Figure 135 give the average results of E_{corr} and i_{corr} values as well as the corrosion rate and polarisation resistance from the valid tests carried out; the remaining results can be found in Appendix H. Variability was largest with the tests conducted in the 1 M solution of hydrochloric acid which needs to be kept in mind when observing trends. All the E_{corr} values were large negative numbers and not the same as the OCP values. General corrosion rates

were higher during the fresh surface scan compared to the values obtained during the exposed surface scan indicating that a fresh surface area is more vulnerable to corrosion attack in hydrochloric acid.

Table 19: Indicators of corrosion rate using average sample measurements from the fresh surface scan in 1 M HCl at 25°C

	E_{corr} [mV]	i_{corr} [A/cm ²]	Corrosion rate [mm/year]	Polarisation resistance [Ω]
S/S blank	-362	2.93×10^{-5}	0.31	464 398
0.0% Ru	-357	6.09×10^{-4}	6.34	149 044
0.82% Ru	-452	1.44×10^{-3}	13.32	228 110
2.92% Ru	-250	2.69×10^{-3}	25.00	14 640
2.44% Ru	-238	5.01×10^{-4}	4.68	99
4.67% Ru	-350	1.51×10^{-3}	14.16	67 521

The E_{corr} values were all negative with the two samples containing no ruthenium having similar results which were lower than the results from the 2.44 wt% Ru sample (highest result obtained), the 2.99 wt% Ru sample and the 4.67 wt% Ru sample. In general, these results were higher than the ones obtained from the exposed surface scan except for the 0.82 wt% Ru sample.

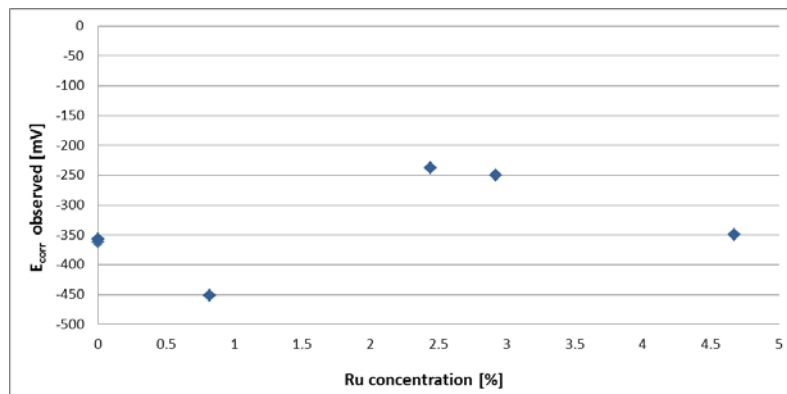


Figure 132: E_{corr} comparison at various ruthenium compositions from the fresh surface scan in 1 M HCl at 25°C

The smallest i_{corr} value was obtained for the stainless steel blank sample suggesting the least corrosion activity for that sample. The clad sample without ruthenium was significantly larger and the other values for the ruthenium containing samples were in the same range with the 2.92 wt% Ru sample having the highest value but marginally. There is no trend that an increasing amount of ruthenium is beneficial in this environment.

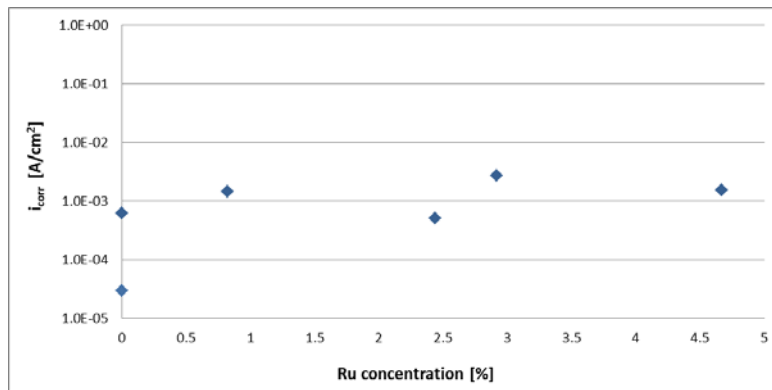


Figure 133: i_{corr} comparison at various ruthenium compositions from the fresh surface scan in 1 M HCl at 25°C

The corrosion rate emphasises again that the lowest rate obtained, by a reasonable amount, was from the stainless steel sample; the clad sample without ruthenium had a higher rate as expected but the ruthenium containing samples had even higher rates. The 2.92 wt% Ru sample had the highest corrosion rate with the 0.82 and 4.67 wt% Ru samples being close together having the next highest rates. The values were larger than during the exposed surface scan. It indicated that the ruthenium is actually harmful to the stainless steel under these conditions from a corrosion point of view.

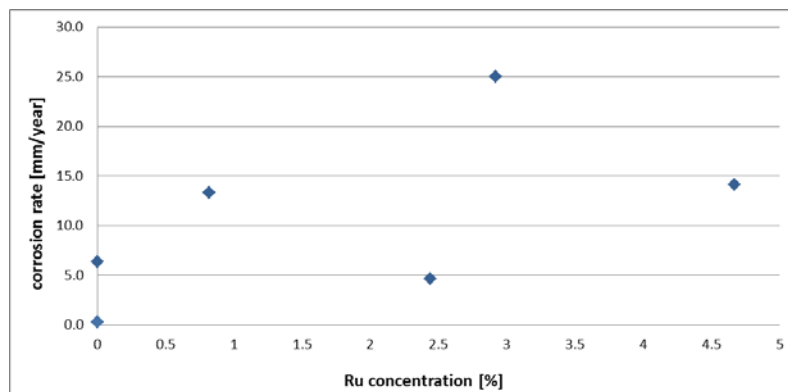


Figure 134: Corrosion rate comparison at various ruthenium compositions from the fresh surface scan in 1 M HCl at 25°C

The variability obtained in the polarisation resistance values was significant and a log scale had to be used to show all the results. The stainless steel sample had the highest value and the 2.44 wt% Ru sample had the lowest value by over 4500 times. There seems to be a slight downwards trend of polarisation resistance with ruthenium composition which was what the corrosion rates already suggested.

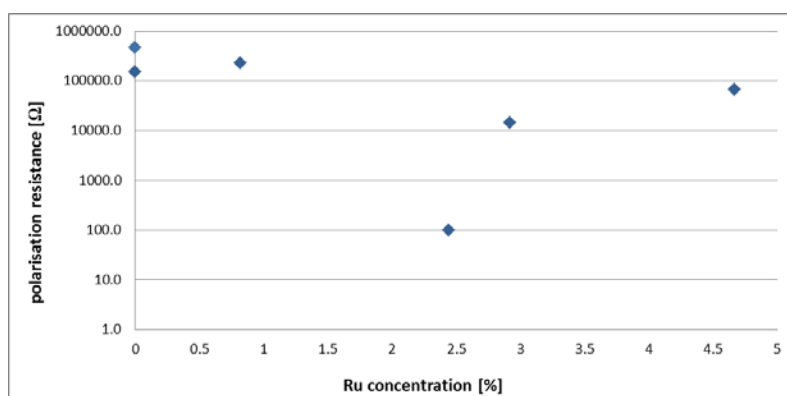


Figure 135: Polarisation resistance comparison at various ruthenium compositions from the fresh surface scan in 1 M HCl at 25°C

In order to assess true passivity, one needs to compare the OCP values to the E_{pass} values: if $\text{OCP} < E_{\text{pass}}$ then the sample in this condition is active but if $\text{OCP} > E_{\text{pass}}$ then the surface is passive. For all samples the average OCP values after 12 hours were smaller than the average E_{pass} values for the two scans indicating active behaviour on the surface exposed to the media. It is expected for corrosion of 304L in HCl to be in the active potential range, the results confirm this. All potentials were negative, the cladded sample without ruthenium always had a higher value (less negative number) than the stainless steel blank sample and thus a larger gap to the OCP value. For the ruthenium containing samples there was a trend that the E_{pass} values were increasing with an increase in ruthenium content and thus also extending the gap to its OCP value.

Table 20: Passivation potentials comparison to OCP values in 1 M HCl at 25°C

	E_{pass} from exposed surface scan [mV]	OCP after 12 hours [mV]	E_{pass} from fresh surface scan [mV]
S/S blank	-230	-393	-164
0.0% Ru	-99	-368	-74
0.82% Ru	-237	-317	-235
2.92% Ru	-232	-305	-168
2.44% Ru	-189	-371	-167
4.67% Ru	-91	-322	-150

As mentioned before, in order to assess the real benefit of the ruthenium containing samples in a specific media, it is best to compare them with stainless steels that are commercially available and would be suitable in the media tested. This was done and the results can be

observed in Figure 136 and Figure 137. Variability of the 316 stainless steel, the SAF2205 duplex stainless steel and the Hastelloy C276 samples was excellent and most of them were only repeated once.

Figure 136 shows that samples after exposure to the media for 12 hours; the 304L and 316 stainless steels were performing worse with the highest current densities, a very similar active region and corrosion potential, the nose of the 304L stainless was longer and had higher current densities until just above 0.4 V when the 316 stainless crossed as the current densities of that sample increased more quickly as the potential increased. The ruthenium containing samples performed very well in comparison, having the lowest E_{corr} values but remaining at lower current densities throughout the scan by close to three orders of magnitude in comparison to the 304L and 316 stainless. The SAF2205 sample initially had a very similar active region as the 304L stainless steel, a slightly lower E_{corr} value but very close to that of the 2.92 wt% Ru sample, a small active nose which kinked slightly before following a vertical line into the passive region at values close to the ones of the ruthenium containing samples. The Hastelloy material had the largest active region with the highest E_{corr} value of all the samples compared but then also followed a vertical line into the passive region at similar values as the SAF2205 material before it went into the trans-passive region. In this case the ruthenium containing samples were definitely better for corrosion protection in comparison to the other steels as they indicated the lowest current density values throughout most of the scan.

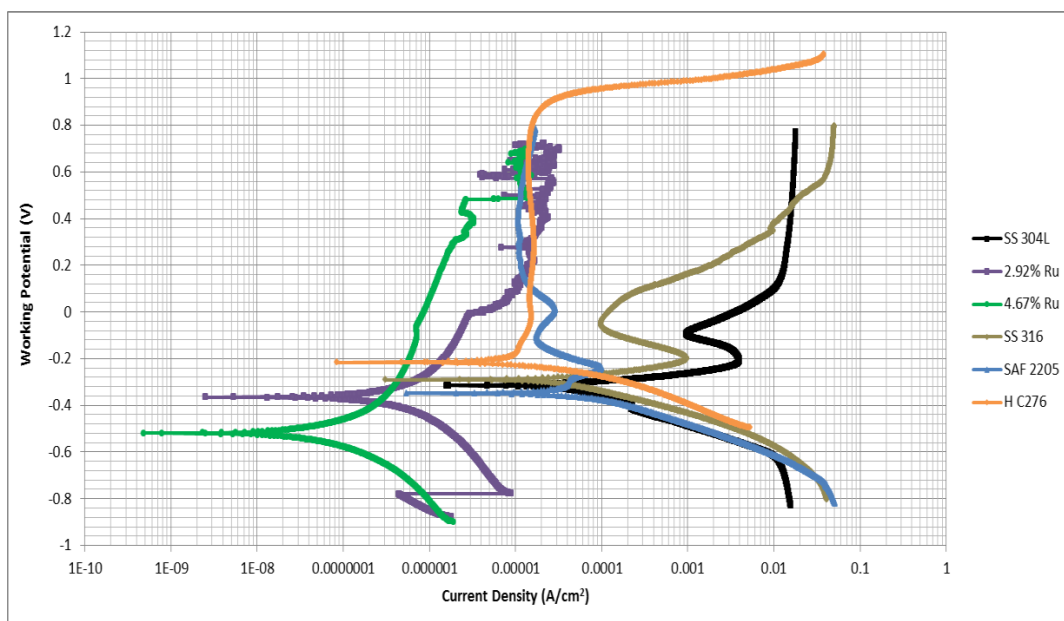


Figure 136: Log i vs E graphs from the exposed surface scan comparing ruthenium samples to other steels in 1 M HCl at 25°C

On a fresh surface, i.e. after polarisation at -0.5 V, the general trend still remained as with the exposed results except that the results were in a narrower current density range, see Figure 137. The 304L stainless steel sample had the lowest E_{corr} value, longest nose and consistently the highest current densities until 0.4 V and upwards when the 316 stainless steel line crossed it and has marginally lower values from then onwards. The 316 stainless results were again close to the ones of the 304L with higher E_{corr} values and following the curve as the nose kinked back but as with the exposed surface scan, the current densities increased slightly with potential until the curves crossed. It was very obvious again that those two types of steel (the 304L and 316 stainless) perform the worst in the 1 M hydrochloric acid environment as all other samples had orders of magnitude lower current densities. The ruthenium containing samples performed very well displaying the transition as before and in the passive region, having almost three orders of magnitude smaller current densities. The SAF2205 sample had a similar E_{corr} value as the 304L stainless steel and also the 4.67 wt% Ru sample and as the potential was increased, the curve followed in between the two ruthenium containing samples showing excellent corrosion protection. The Hastelloy C276 showed a similar behaviour as the 316 stainless steel in the active region, had a similar E_{corr} value as that and the 2.92 wt% Ru sample but then displayed a small active nose which was followed by a vertical passive region at lower current densities compared to any of the other samples tested before it turned into the trans-passive region. In this environment, the fresh surface scan indicated that the ruthenium containing samples were similar in performance to the SAF2205 material and only slightly inferior to the Hastelloy.

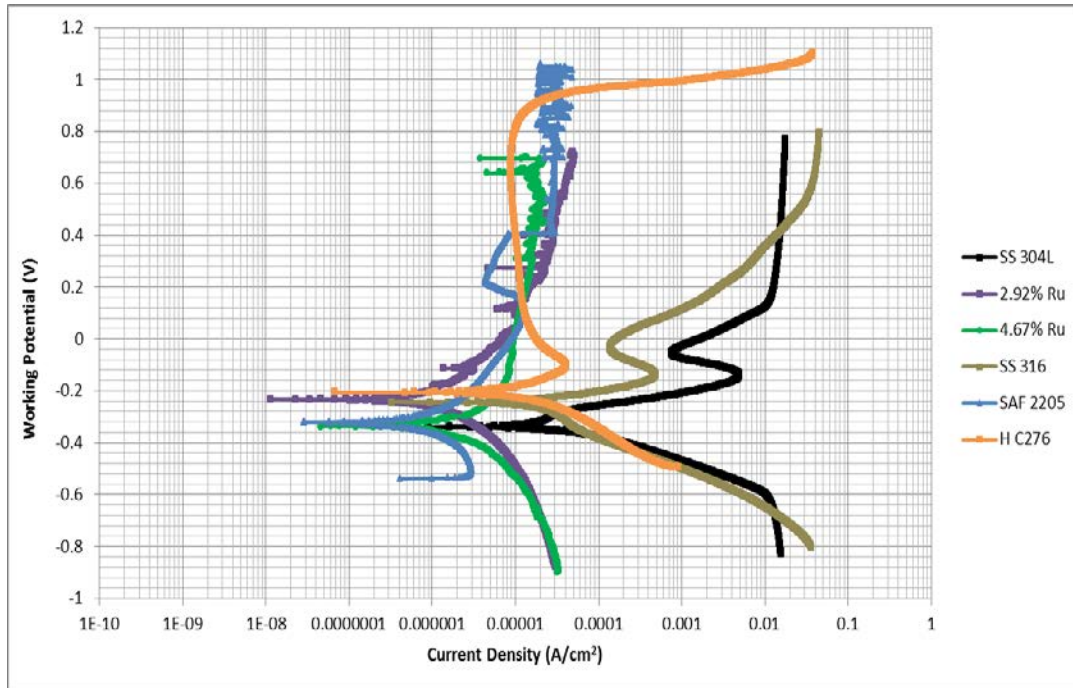


Figure 137: Log i vs E graphs from the fresh surface scan comparing ruthenium samples to other steels in 1 M HCl at 25°C

The potential over time from Figure 138 indicated that all the materials performed similarly with OCP values of just below -0.3 V after the 12 hours of exposure with the 2.92 wt% Ru sample being the only one slightly above the rest. The exception is the Hastelloy C276 which behaved slightly more erratic during the 12 hours but at consistently much higher potentials around the 0 V range, the final results however seem not to have stabilised within the 12 hours.

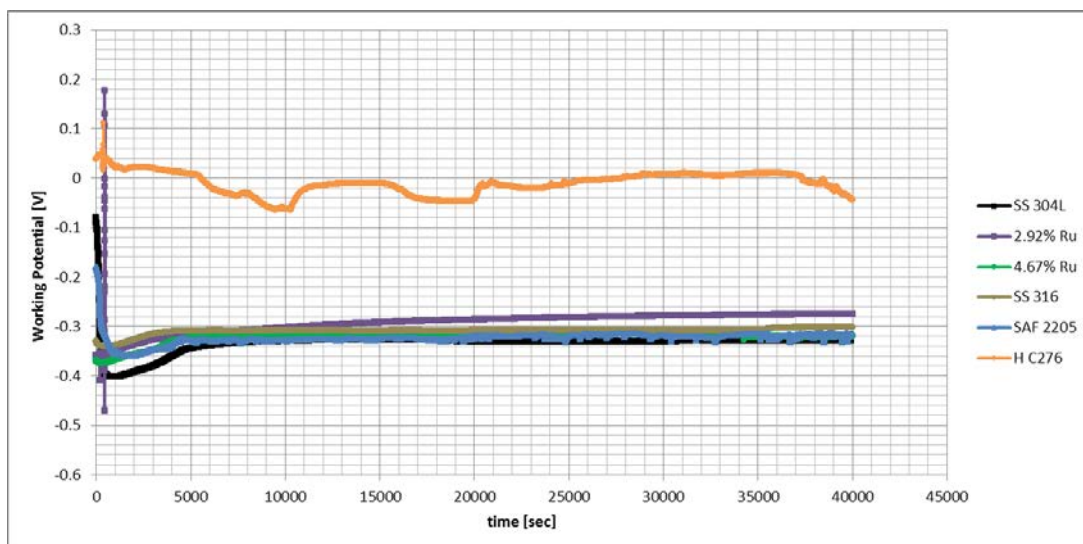


Figure 138: E vs time graphs comparing ruthenium samples to other steels in 1 M HCl at 25°C

4.3.6 Comparisons of the different environments

A way to assess how harsh the environments are that the samples are exposed to, is to compare the samples to each other in each of the environments, the results of this are presented below. The environments selected are very common industrial environments that a 304 type stainless steel could be exposed to. As before, the exposed and fresh surface scans are looked at and the 304L stainless steel blank as well as two ruthenium compositions, 0.82 wt% and 4.67 wt%. This served to understand the behaviour of the steels in the various environments. These two represented a 'low' and a 'high' ruthenium composition sample so that the effect of the different environments on the steel surface could be observed.

Observing the stainless steel blank as in Figure 139 is a good comparison for the ruthenium containing samples. After exposure to the different environments for over 12 hours, it can be assumed that equilibrium has been established and a passive film would have been formed if that was possible in the environment. Figure 139 shows clearly that the 1 M sulphuric acid at ambient conditions represent conditions in which the 304L stainless steel holds up well from a corrosion point of view: an E_{corr} value of -0.23 V was obtained, a passive region extending almost 1.2 V at an i_{pass} of around 1×10^{-5} A/cm². As sodium chloride was added, the E_{corr} dropped by about 0.1 V, a long nose was observed and a gentle slope to reach the passive region at 0.4 V which reduced the passive range by at least 0.5 V while i_{pass} was an order of magnitude higher than when no chlorides were present. The 1 M hydrochloric acid solution behaves similarly in the active region, only had a slightly higher E_{corr} value and a similarly large active nose compared to the solution of 1 M sulphuric acid with the 1% sodium chloride added but exhibited a kink afterwards to have the highest i_{pass} value of around 1.5×10^{-2} A/cm² indicating how much less suitable the 304L stainless steel is for a chloride environment and especially hydrochloric acid. As the temperature of the 1 M sulphuric acid solution was increased by 20°C, the corrosion resistance is reduced significantly which was observed by reduced E_{corr} values, a large active nose, a second nose shape formed as potentials increased until the passive region was reached only after 0.2 V reducing its range and that at two orders of magnitude higher than when at 25°C. Reduced corrosion protection was also observed when increasing the temperature of the 1 M sulphuric acid with the 1% sodium chloride from 25°C to 45°C where the E_{corr} remained almost the same but the nose was longer and extended over a larger potential range, at which point the highest current densities were obtained compared to all the other environments, with a gentle slope to the passive region which was perhaps reached at a potential slightly lower but at a i_{pass} value much higher than was

obtained at 25°C. This clearly shows that increasing the temperature of the acidic environment is detrimental to the corrosion protection of the steel.

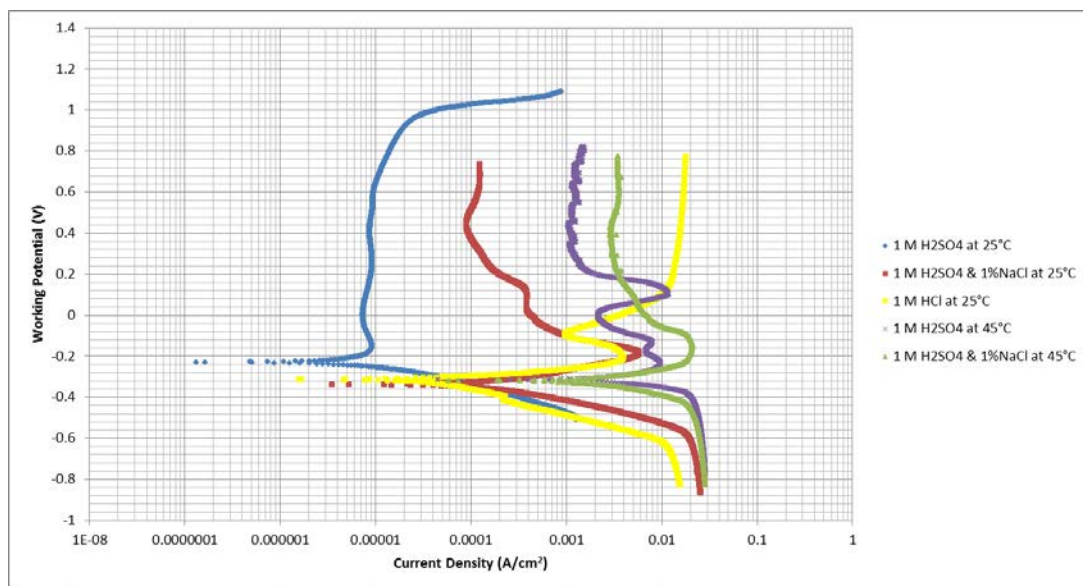


Figure 139: Log i vs E graphs from the exposed surface scan comparing the stainless steel blank sample in different environments

On a fresh surface area, the same trends were observed for the 304L stainless steel blank sample, as shown in Figure 140. In 1 M sulphuric acid the E_{corr} value was, however, more similar to the other E_{corr} values, an active nose was observed and passivity extended only over a potential range of 1 V at an i_{pass} value of around 1×10^{-5} A/cm². With the addition of the salt, the E_{corr} value did not change but a much larger nose was observed and the active region was reached at the same potential but at an order of magnitude higher value. In the 1 M solution of hydrochloric acid, the largest E_{corr} value was observed but only marginally larger, a very extended nose which kinked so that the passive region was only obtained 0.2 V above that for the sulphuric acid and at more than three orders of magnitude larger current densities achieving the highest current densities from all the samples. When the sulphuric acid is tested at elevated temperatures of 45°C it showed slightly higher E_{corr} values, a large nose with a second small nose shape at higher potentials so that the stable passive range was only obtained over 0.2 V above that at ambient conditions and two orders of magnitude higher current densities. This reduction in corrosion protection at elevated temperatures was also observed when testing the 1 M sulphuric acid with the 1% sodium chloride added at the higher temperature, a slightly higher E_{corr} value was obtained and a larger nose with a gentle slope to the passive region as the potential was increased which was over an order of magnitude larger than at 25°C. This really demonstrates the harshness of the environments as the behaviour of the steel in the different environments was observed.

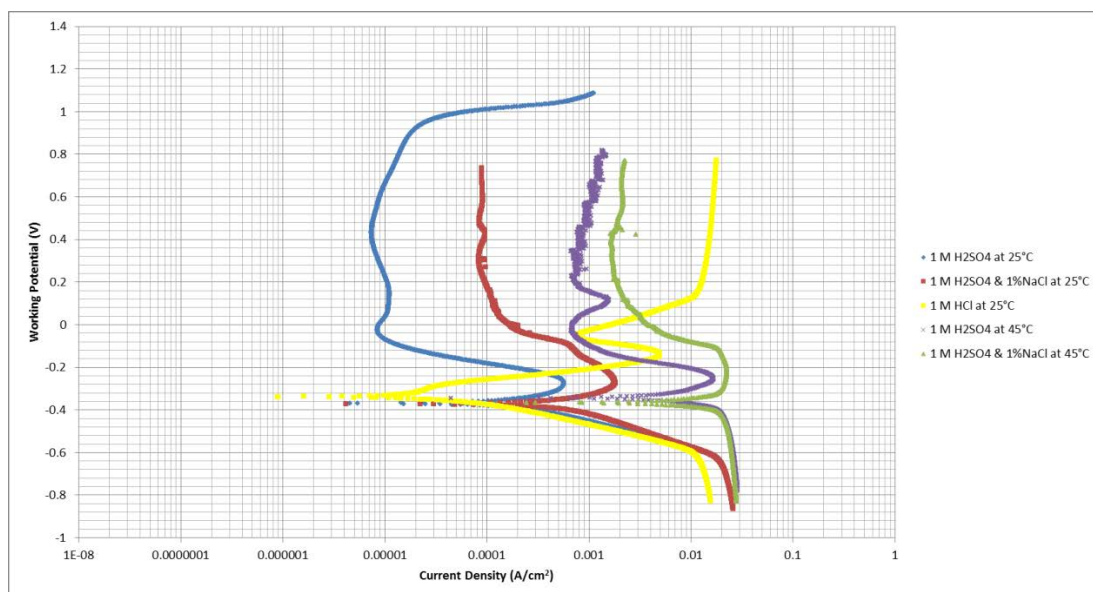


Figure 140: Log i vs E graphs from the fresh surface scan comparing the stainless steel blank sample in different environments

The ruthenium cladded sample, even at only 0.82 wt% Ru, behaves quite differently in the various environments as can be seen in Figure 141. After exposure for 12 hours, the sample performed well in the 1 M sulphuric acid with an E_{corr} value similar to the others, a small nose and a passive region where the current densities increased slightly as the potential was increased but over a range of 1 V and at the lowest current densities in comparison. This indicates that this environment was the least corrosive for the alloyed steel. When sodium chloride was added the E_{corr} dropped slightly but a much larger nose was observed and the passive region extended over the same potential range and at current density values only marginally above those obtained in the sulphuric acid alone. The material also performed well in the hydrochloric acid environment where the E_{corr} value was the lowest and a transition was observed instead of an active nose but current densities were increasing approximately at the same rate as the potentials increased compared to the sulphuric acid and having values also only marginally higher than the 1 M sulphuric acid with the 1% sodium chloride added. As the temperature of the 1 M sulphuric acid is increased to 45°C, the E_{corr} value remained unchanged but the double nose shape was observed again to barely get to a passive region while even the lowest numbers along the curve were an order of magnitude higher than those observed at ambient conditions. The 1 M sulphuric acid with the 1% sodium chloride added at 45°C was the worst condition for the 0.82 wt% Ru sample as it had the highest current density values throughout the entire scan, an E_{corr} value the same as that of the sulphuric acid at 45°C, a small flat nose and a passive region which increased slightly in

current density as the potential was increased, as was observed for most of the curves of this sample.

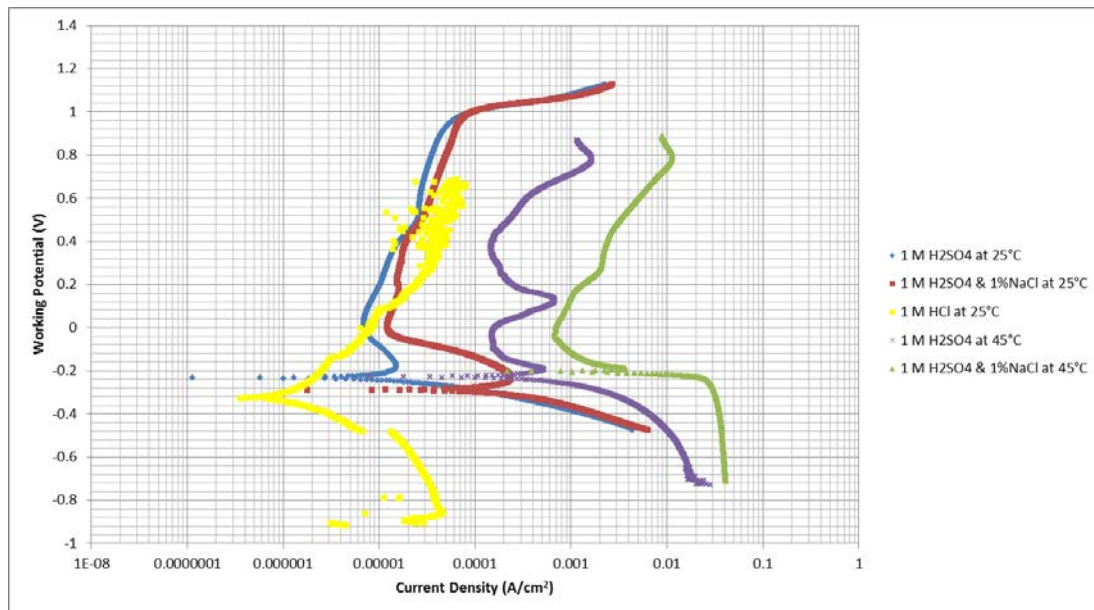


Figure 141: Log i vs E graphs from the exposed surface scan comparing the 0.82 wt% Ru sample in different environments

Again, the trends observed during the fresh surface scan are very similar to those observed during the exposed surface scan for the sample, seen in Figure 142. In sulphuric acid at 25°C, the sample performed well having the lowest current density values of this comparison but still displaying a reasonably large active nose. The sample showed the worse corrosion protection characteristics when 1% sodium chloride was added: the E_{corr} value had dropped slightly, a longer nose was observed but a stable passive region was reached at current densities only slightly larger than those for the acid only. As during the exposed surface scan, the behaviour in the hydrochloric acid was quite different compared to the others following the transitional shape, at initially the lowest current densities until -0.17 V when there was a step in the curve, and current densities were slightly above those of the sulphuric acid with the chloride addition. When the sulphuric acid was tested at a temperature of 45°C, the curve shifted again to higher current density values indicating more corrosion taking place, a similar E_{corr} value though and, in fact, a passive region which was reached earlier than when the solution was at ambient conditions but at significantly higher current densities. The worst environment is still the 1 M sulphuric acid with the 1% sodium chloride added at 45°C having the highest current densities throughout the potential range scanned, steep Tafel slopes, the highest E_{corr} value, a small active nose and a passive region where the current densities increased as the potential was increased. In general it can be noticed that the sample with

0.82 wt% Ru showed improved protection in all the environments for both the exposed and fresh surface scans compared to the blank stainless steel sample.

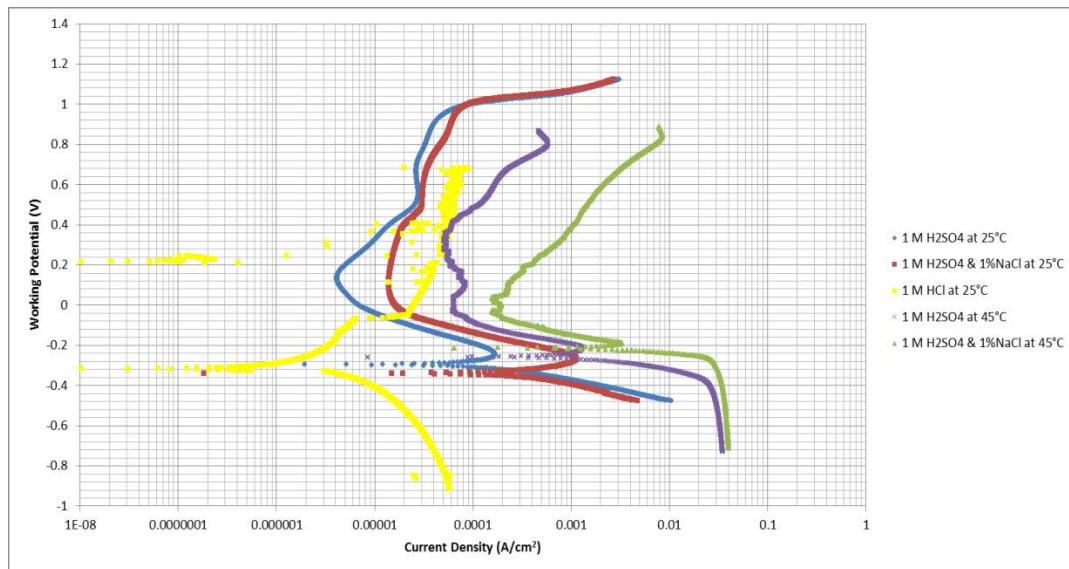


Figure 142: Log i vs E graphs from the fresh surface scan comparing the 0.82 wt% Ru sample in different environments

For the sample with the highest amount of ruthenium added to the 304L stainless steel, i.e. 4.67 wt% Ru as per Figure 143, reasonable corrosion protection was observed in the media studied. For the exposed sample in the 1 M sulphuric acid solution a transition was observed with the highest E_{corr} value and a passive range of 0.8 V and low current densities. When sodium chloride was added, the E_{corr} value dropped significantly, a small nose was observed with a reasonably well established passive region which followed the curve for the sulphuric acid at 0.2 V and above at just slightly higher current densities. The sample behaved very differently in the 1 M hydrochloric acid as was observed before; with the smaller amount of ruthenium added E_{corr} had the lowest value, they followed the typical transitional shape and had the lowest current densities. The material really behaved well in this condition compared to the sample without ruthenium. When the temperature of the sulphuric acid was increased to 45°C, it lowered the E_{corr} but displayed a cathodic loop before the curve followed the same trend as the sulphuric acid at 25°C but consistently at an order of magnitude higher current densities indicating worse corrosion protection at the elevated temperature. How much worse the condition was of the 1 M sulphuric acid with the 1% sodium chloride added at 45°C was emphasised with the 4.67 wt% Ru sample where the current densities throughout the scan were significantly higher than for any other environments looked at, having an E_{corr} the same value as the solution at 25°C, a small nose and a passive region with slightly increasing current densities as the potential was increased.

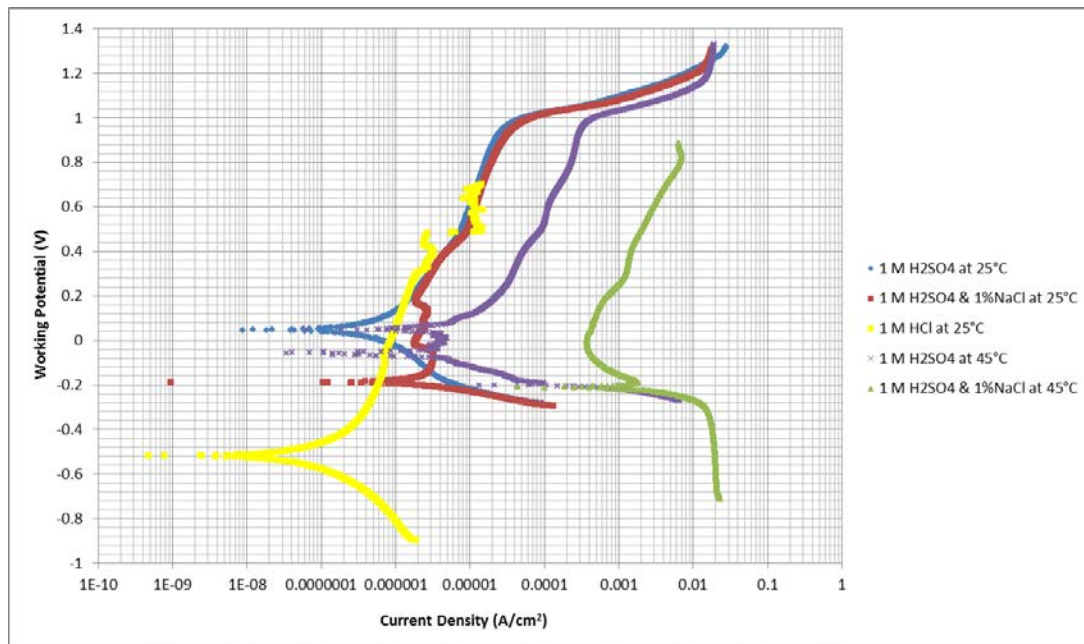


Figure 143: Log i vs E graphs from the exposed surface scan comparing the 4.67 wt% Ru sample in different environments

For the freshly cleaned surface scan, the trend was again similar to that observed during the exposed surface scan with some variations as can be seen in Figure 144. The 4.67 wt% Ru sample behaved best in the 1 M sulphuric acid with a low E_{corr} , a small active nose followed by some large cathodic loops at very small current densities before going into a stable passive region for approximately 0.5 V but at the lowest current densities for this comparison at between 1×10^{-5} and 2×10^{-5} A/cm². As soon as sodium chloride was added the E_{corr} value dropped, i_{crit} values reduced, again a small nose was observed but long so that the passive region was only reached at 0.2 V and at slightly higher current densities compared to the solution without the salt. As expected the sample behaved differently in the 1 M hydrochloric acid having the lowest E_{corr} value and a transition shape but at current densities in the range between those of the sulphuric acid and the sulphuric acid with the sodium chloride added indicating the great application of the sample in that medium. Increasing the temperature of the sulphuric acid provided a similar shape of the curve but at higher current densities than when at 25°C, no cathodic loops were observed but also only a short passive range of 0.5 V. The worst environment was again observed when testing in the 1 M sulphuric acid with the 1% sodium chloride added at 45°C having the highest current densities throughout the potential range scanned, even though the E_{corr} value was the same as the sulphuric acid at 45°C, a long active nose was observed and a passive region where the current densities increase significantly as the potential was increased. In general it can be noticed that the sample with 4.67 wt% Ru shows improved protection in all the environments for both the

exposed and fresh surface scans compared to the blank stainless steel and the 0.82 wt% Ru sample.

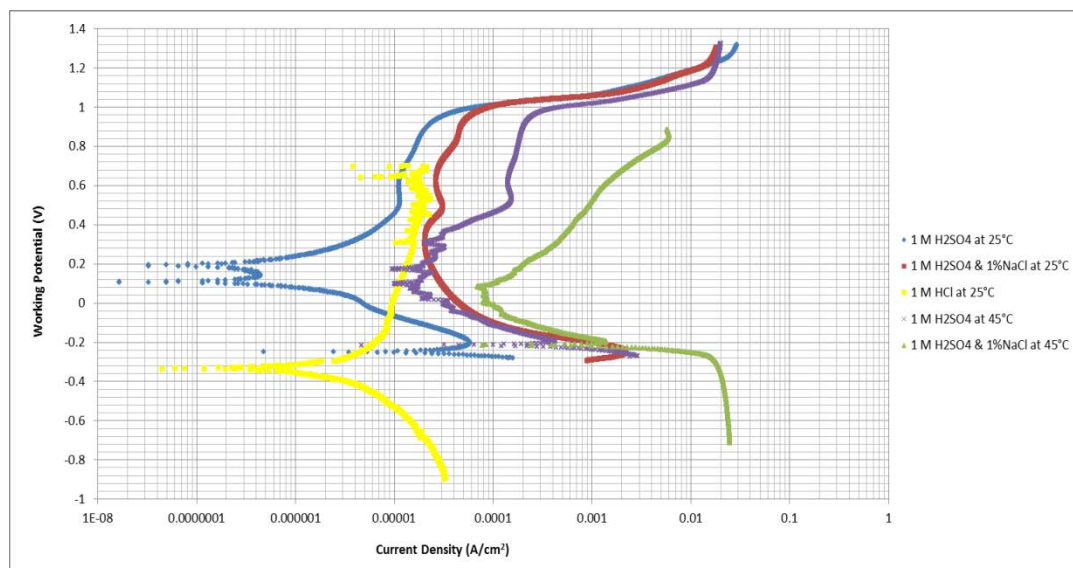


Figure 144: Log i vs E graphs from the fresh surface scan comparing the 4.67 wt% Ru sample in different environments

5. Discussion

5.1 Energy Dispersive Spectroscopy

Laser cladding is to date one of the most precise ways of applying a relatively thin metal coating containing a small amount of an alloying material onto a metal surface (Laurence, 2014). Woollin (1994) confirmed that laser surface treatment has been “demonstrated as a means of reducing compositional variation and increasing the corrosion resistance of autogenous welds to levels comparable with parent material”. It is these reasons why this particular technique was selected to prepare the samples tested. Laser cladding is used to apply a variety of metal coatings of consistent thickness, low porosity and exceptional adhesion. The low heat input ensures a fine microstructure with little distortion and therefore a relatively precise application of the alloyed layer. Laser cladding is commonly used to improve corrosion and wear properties of the surface of metals. It was therefore expected that the target ruthenium compositions be achieved with a reasonable homogeneous ruthenium composition in the cladded layer.

The EDS results showed that the expected ruthenium compositions were not attained on all samples and the variation in composition of the same sample, analysing different areas, was significant. The variance of the sample population was calculated and is given in Table 3. The cladding procedure and powder composition has caused this variation since the baseplate had a homogeneous composition. For all the samples, the laser cladding method produced lower ruthenium compositions in the cladding than the powder used to make the samples. Clustering of high concentrations of ruthenium into ‘islands’ was observed in Figure 25, Figure 26 and especially at the higher ruthenium concentrations shown in Figure 28. Therefore the bulk material will be lower in ruthenium when analysed.

The contrast of an SEM picture is normally based on three main effects: mainly elemental mass, topography and grain orientation. The sample surfaces were all polished as described in section 3.3 and therefore topography should play no or only a minor role. Ruthenium atoms are much heavier than iron, nickel or chromium atoms and should therefore appear brighter as can be seen on the images as very light or white areas. The dark areas are most likely pores of gas entrapped during the application of the cladded layers and form porosity within the structure of the steel; theoretically they could also be metallic oxides that form but that was not suspected and it was not confirmed with additional analysis.

With the current laser cladding method and ruthenium enriched powder, an even coating thickness was obtained of approximately 800 μm but lacking in homogeneity at higher ruthenium concentrations. On some samples 'stratification' was observed, in the form of ruthenium-rich stringers, where the ruthenium was well mixed with the stainless steel powder, in those areas the ruthenium concentration was very close to the initial powder composition (Figure 25, Figure 26, Figure 27 and Figure 28). In other areas ruthenium islands were observed where the ruthenium concentration was up to 100% (white spots in Figure 25, Figure 26 and Figure 28). These structures formed in the cladded layer as can be seen clearly in Figure 29. The cladding process also introduced porosity which was identified as small areas where air was trapped during the application, these show up as dark spots in Figure 24 to Figure 28. This is especially evident at the interface of the alloy to the stainless steel base plate and also seems to be more prominent at the higher ruthenium compositions.

The islands of ruthenium that formed could have been improved or reduced by using a more homogeneous powder. One could have pre-melted the ruthenium and stainless steel powder in the targeted concentrations to make an alloy from that mixture and then produced a fine powder from that to be used in the laser cladding application rather than using the premixed powder as was done in this case. If this type of application is selected for further investigation, an improved method of applying a homogeneous alloyed layer of the ruthenium onto the stainless steel should be looked at.

The heterogeneity of the samples, therefore every time exposing a slightly different surface composition to the media being tested, could have led to the variability in the electrochemical tests. If a fresh surface area was exposed for Figure 145 as per the lines marked 1 to 5, different results could be obtained as each is slightly different. Testing exposed surface area 5 would probably give very accurate results for the actual ruthenium composition desired as the area was cut where strings of ruthenium are observed and a more uniform distribution of the alloyed metals was observed. Testing with surface area 4 being exposed might give slightly better results as three ruthenium clusters were exposed and some strings of ruthenium. Surface area 3 test results could give some variability as ruthenium islands were exposed, quite a large area of stratified bulk is exposed but also a rather large pore. When surface area 2 is exposed for testing two large ruthenium islands are exposed, some stratification and porosity is encountered as the cladded layer is reduced. When surface area 1 is exposed for testing, the ruthenium content is probably lower; three areas of extended pores are exposed so

that results might be less favourable even when tested in the same medium as surface 4, for example. This has to be considered when looking at the test results.

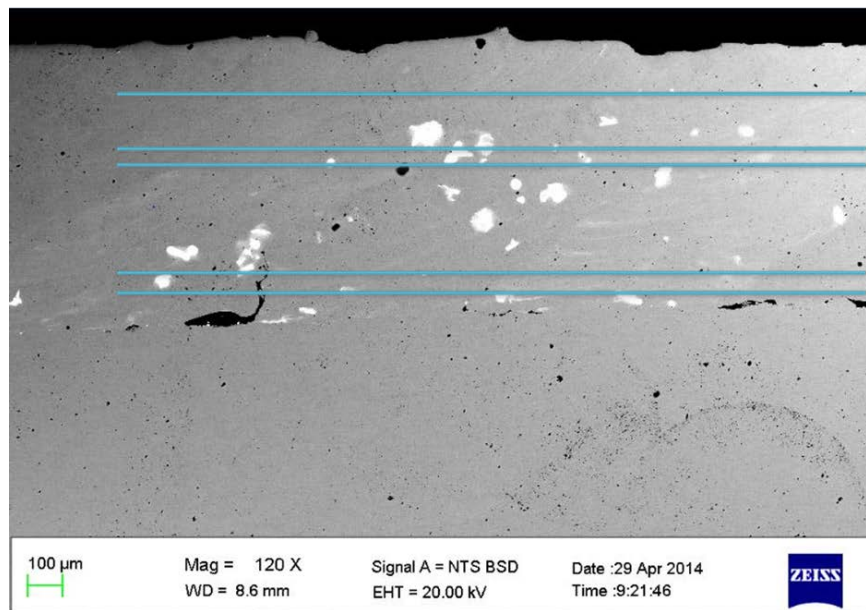


Figure 145: Cross sectional view of the 2.92 wt% Ru sample indicating different surface exposure possibilities

It is believed that the different runs with the laser over the surface of the base plate introduced variability with an increase in ruthenium composition. That does seem to indicate that, as ruthenium concentrations increases, the need for a different application is required, one that is able to uniformly distribute the ruthenium within the alloy in the cladded layer.

Some literature, e.g. Tjong (1989), Jones (1996) and Higginson et al. (1989) suggested that during corrosion, ruthenium accumulates at the surface. Presumably this occurs as chromium and iron are oxidised, leaving behind higher concentrations of ruthenium directly on the surface layer. This was not observed as all SEM tests were performed before the corrosion testing started. Before and after images could support this.

5.2 Microstructural Analysis

Corrosion resistance is closely linked to chemical composition (such as the amount of chromium, molybdenum and in this research, ruthenium) but might appear to be “almost independent from the microstructure” (Charles et al., 2007). This is of course not correct for such specific cases as in stress corrosion cracking and localised corrosion but might apply to general corrosion resistance. These authors have conducted various experiments in saline solutions and at elevated temperatures and reported no clear effect linking the microstructure to corrosion resistance, only its composition. They did observe that the most sensitive

structure for intergranular corrosion is the heat affected zone (HAZ) of welded structures. This they attributed to carbides precipitating at the grain boundaries. Since a 304L stainless steel was used the free carbon would have been sufficiently low to ensure that chromium carbide formation was minimal. The cladding process applied can be compared to a welding application and it was most certainly found in all the media studied that the cladded sample without ruthenium additions was the most severely affected by corrosion.

During any process whereby metals are heated to such temperatures that they melt so that other elements can be alloyed to them, such as in fusion welding or laser cladding, the original microstructure of the fused zone is destroyed and a new structure develops. According to Woollin (1994) “The resulting room temperature structure depends upon the phases developing during solidification and the extent of subsequent solid state transformations”. He also observed that residual stresses, as a result of the contraction during the cooling process, contribute to the changes in microstructure. It can thus be said that the difference in microstructure observed between the 304L base plate and the alloy even with a small amount of ruthenium, are attributed only to the cladding process and not to the addition of the precious metal.

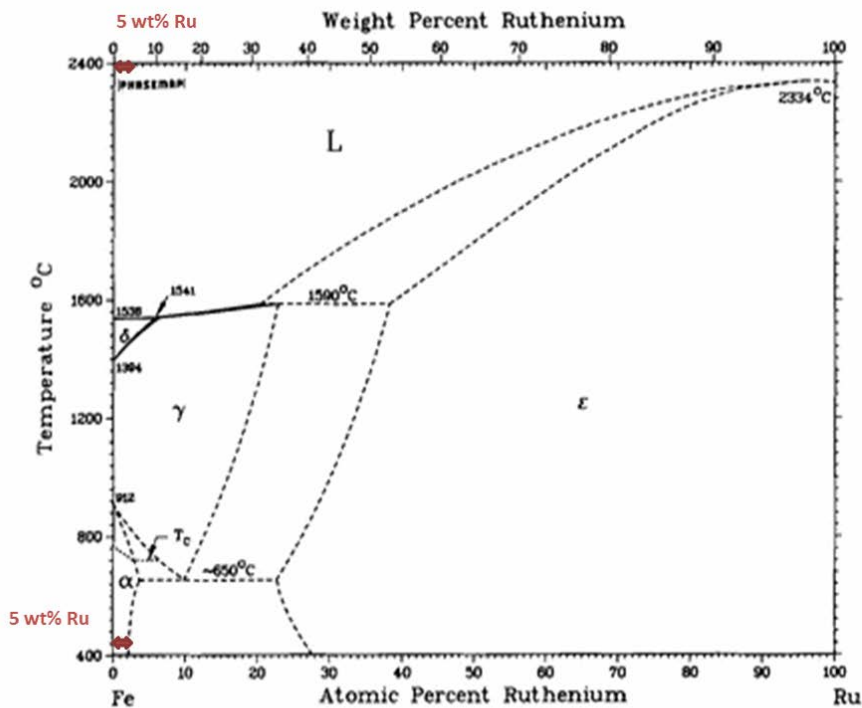
It is known from previous work that small amounts of ruthenium, the authors used up to 0.6 wt% Ru, seemed to have no detrimental effect on the microstructure which results from alloying it with a duplex stainless steel (Banda and Van der Merwe, 2014). McGill (1990) observed that palladium additions to stainless steel did not alter its microstructure and he found an alternative explanation for its effect on the corrodibility of the stainless steel. No adverse effects were thus expected when the ruthenium was alloyed with the 304L stainless steel which was confirmed during the microstructural analysis carried out. The austenitic structure is maintained and no detrimental phases were introduced during the cladding process or from the ruthenium. For the cladded samples a cellular dendritic grain structure was observed, Figure 30 and Figure 35 serve as examples, this confirms what Liang et al. (2010) had observed in their Ni-Cu-Ru button welded sample. Porosity is low but can be observed mostly on the boundary to the base plate and between the welded beads but no links/routes have been observed which would suggest that the exposed media could directly penetrate through to the base plate which is important for corrosion protection. The cladded layer seems very well adhered to the base plate which is also important for any application; this is one of the primary benefits of the laser cladding. As ruthenium concentrations

increase, so does the formation of ruthenium rich islands which introduced variability as the precious metal is not as evenly distributed within the grain structure. As ruthenium increases, it is suspected that a large portion of the ruthenium is situated on the edge of the crystal lattice thus possibly affecting the shape of the crystals and distribution of the ruthenium throughout the cladded layer. Olubambi et al. (2009) also observed in their ruthenium containing superferritic stainless steel samples that “the grain sizes are refined as the amounts of ruthenium increased”. This suggests that a different application method is required when ruthenium concentrations of 5 wt% or higher are required in the surface layer, preferably a method even for smaller amounts of ruthenium. This confirms what was observed by the EDS and looking at SEM images. Olubambi et al. (2009) testwork indicated the formation of a second-phase ruthenium particle in the alloys which increased with an increase in ruthenium content and that this “would correspond to an increase in the corrosion resistance of the alloy”.

The cladding process at high temperatures followed by a rapid cooling cycle introduced a very fine microstructure to the alloyed material which is very similar to a welding application under those conditions. This statement is based on visually observing the samples under the microscope (various Figures in section 4.2) and is not supported by an assessment of the grain size and grain refinement. The fine nature of the phases of the ruthenium containing stainless steel alloy was also observed in the testwork conducted by Olubambi et al. (2009) which they were able to link to “contribute to the fastness of its enrichment on the surface of the alloys, with a concomitant increase in the hydrogen reduction kinetics”. This implies that ruthenium promotes its enrichment on the metal surface and thus the formation of a more stable protective layer when exposed to corrosive environments.

Looking at a very simplified model, i.e. assuming that the steel only consists of iron so that the existing equilibrium diagrams for iron and ruthenium can be looked at to identify the individual phases, Figure 146 can be produced (Swartzendruber and Sundman, 1983). The laser heats the material (304L stainless steel powder with the selected amount of ruthenium) to a temperature where it is all in the liquid phase designated with the L in the top left hand corner of the diagram. This means that ruthenium is completely soluble in iron at these temperatures. As the sample is cooling down the sample goes through a variety of phases until finally an alpha iron phase is precipitated, i.e. ferrite. The remaining gamma phase, i.e. austenite, runs into the eutectic point at 650°C and just less than 10 wt% ruthenium and is

split into the ruthenium rich epsilon phase and more alpha iron. It still implies that for the ruthenium concentrations used to make up the samples studied, all the ruthenium was dissolved and a uniform distribution could have been expected. Ideally this analogy should be conducted using a phase diagram for 304L stainless steel with varying ruthenium content but this was not available. Olaseinde et al. (2012) characterised the microstructure exploring the various phases for a DSS mixture with ruthenium; this type of work is recommended to be carried out for the 304L stainless steel.



L. J. Swartzendruber and B. Sundman, 1983.

Figure 146: Equilibrium Phase Diagram of the Fe-Ru system

The diagram is however still helpful in understanding what is observed in the diagrams in Figure 30 to Figure 35. During the rapid cooling process following the laser cladding, perhaps not all the phases were encountered but at equilibrium conditions it is clear that austenitic steel is observed with a specific ruthenium concentration included.

5.3 Electrochemical Testing

Electrochemical analysis was carried out in a number of conditions to test the effectiveness of the samples in a variety of environments. As described in the Experimental Procedure the tests conducted consisted of:

1. Open Circuit Potential for 12 hours
2. Anodic scan from -500 mV to +1100 mV at a scan rate of 1 mV/sec
3. Polarisation at -500 mV for 5 min
4. Anodic scan from -500 mV to +1100 mV at a scan rate of 1 mV/sec

The following environments were selected for the electrochemical testing and the results obtained are discussed in the sections below:

1. 1 M sulphuric acid at 25°C
2. 1 M sulphuric acid with the addition of 1 wt% sodium chloride at 25°C
3. 1 M sulphuric acid at 45°C
4. 1 M sulphuric acid with the addition of 1 wt% sodium chloride at 45°C
5. 1 M hydrochloric acid at 25°C

5.3.1 1 M H₂SO₄ solution at 25°C

5.3.1.1 Repeatability of results

Repeatability of the results, having tested all the samples in a 1 M sulphuric acid solution, was very reasonable for the following compositions: the stainless steel blank, 0 wt% Ru, 0.44 wt% Ru from the cleaned surface scan and 0.82 wt% Ru; and it is expected that reliable conclusions can be drawn from them. Other results, however, showed some spread in the results: 0.44 wt% from the exposed surface scan, 2.92 wt% Ru, 2.44 wt% Ru and 4.67 wt% Ru. Where ruthenium was not consistent, a slightly different surface area composition after each 1200 grid paper grinding was allowed to be exposed. Therefore, during the next electrochemical testing, a slightly different ruthenium composition was tested. What exactly that composition was was not measured and therefore a direct link to exact surface composition for each electrochemical test cannot be made. Only average compositions are reported. The repeatability of the stainless steel blank and cladded sample without ruthenium was expected to be excellent as the exposed surface was very consistent which was confirmed by the testwork. Therefore the cladding process alone was not responsible for the variability; it seems that only the ruthenium distribution was causing the observed variability in the corrosion behaviour. The nature of the ruthenium content and dispersion of it in each alloy could possibly prevent one from seeing the expected results in all the test cases and environments; this will be particularly problematic where changes are subtle such as in the cathodic Tafel potential region. The variability observed is less for the low ruthenium compositions and increases with the amount of ruthenium which relates

directly to compositional variability at higher concentrations. This is especially noticeable during the fresh surface scans where the passive layer had not yet formed.

Only one example per ruthenium composition was selected to represent that composition when comparing them (as can be seen in Figure 42, Figure 43 and Figure 44) since the results were reasonably reproducible.

It must also be noted that the corrosion rate measurements were all carried out on the entire surface area of the sample; the actual corrosion activity measured was dominated by the most easily corroded part of that area. As can be observed from the EDS analysis described before, variability can be high and thus it is difficult to be absolutely sure what the ruthenium concentration is on each exposed surface. The variability in composition is a common problem for all types of coatings (Mills, 2014). Moreover, the test surface and the exact concentration of metal ions in the solution are changing during the measurement. These might not be the same for every single experimental run even when conducted under seemingly the same conditions. Other studies (Potgieter et al., 2011) have revealed that Tungsten carbide, WC-Co, surfaces did not behave equally active when exposed to sulphuric acid, but localised corrosion initiated at phase boundaries which dominated corrosion rates observed. This might have occurred in these samples to some extent causing fluctuations between the individual test runs. Variability of results is most likely also affected by the different phases present in the samples (austenite combined with ruthenium) which are then exposed during testing.

5.3.1.2 Current density vs potential responses

It is observed that in most cases (stainless steel blank, 0.44 wt% Ru, 0.82 wt% Ru, 2.92 wt% Ru, 2.44 wt% Ru and partly 4.67 wt% Ru), the corrosion protection from the exposed scan is better than that of the fresh surface scan, i.e. the current densities are significantly lower for the exposed surface scan. The stainless steel surface that was exposed for 12 hours in the sulphuric acid was able to form a passive film on the surface; it is assumed that it includes Cr_2O_3 and the added ruthenium, giving it corrosion protection in the acidic medium it is exposed to. After the exposed surface scan was completed, the surface was 'cleaned' during the polarisation step and immediately after a second scan was run where the sample did not have sufficient time to form the passive film on its surface to enhance its corrosion protection. This is a critical parameter for evaluation since it is important for the passive film

to form quickly so that the selected material can immediately withstand the corrosive environment and it is thus an important measure of corrosion protection.

The experiments conducted show that the ruthenium contributes to corrosion protection but it is the rate at which it can do so that is critical. Theoretically it might be said that with increasing amounts of ruthenium, more ruthenium atoms should be available for the formation of a more stable passive protective layer, however, the amount of ruthenium added was not observed to be directly proportional to the rate of passivation. Even so there is a strong correlation between the passivation rate and the ruthenium content as the data shows.

The breakdown of water as indicated in Figure 5 occurs at a higher potential, typically 1.23 V with reference to the Standard Hydrogen Electrode (SHE), and is not expected to have had any influence during the tests conducted for this report. It is interesting to note that all the potentials going into the trans-passive region were identical for all the samples. Typically on 304L stainless steel, pitting would occur in this trans-passive region which is visual on the steel surface but in the media studied, no evidence of pitting corrosion occurred.

The stainless steel sample with no cladding showed a typical $\log i$ vs E curve with an initial active region until a stable passive film was formed, presented by a stable current density with an increase in potential until the trans-passive region was reached. The cladded sample without ruthenium showed an increased corrosion rate with a much higher i_{crit} and a more active corrosion potential, indicative of more anodic dissolution. A higher but stable i_{pass} was reached before the trans-passive region where it then followed the same curve as the stainless steel sample. This confirms that a cladded or welded region would be more susceptible to corrosion as expected and is often observed in industry (Salgado-Lopez and Rubio-Gonzalez, 2015 and Charles et al., 2007). With a small addition of ruthenium, 0.44 wt%, the i_{crit} was reduced by almost an order of magnitude indicating significantly less anodic dissolution. The current density thereafter did increase slightly with an increase in the working potential indicating that a stable passive layer had formed and the ruthenium caused the corrosion potential to move into the passive region, ensuring improved corrosion protection. Observing the $\log i$ vs E curve (Figure 42) it was thus evident that adding small amounts of ruthenium to the stainless steel surface was protecting the surface in 1 M sulphuric acid. The ruthenium shifts the corrosion potential to a larger value but does not extend the passive region over a larger potential range. The trans-passive region is again similar to that of the stainless steel blank sample. The curves with higher ruthenium concentrations showed a different shape, i.e.

a transition compared to that was observed with stainless steel samples in this environment which indicates that a very stable passive film was formed over approximately the same range of working potentials. The much reduced i_{crit} values seen at higher potentials indicate improved corrosion protection in these samples.

The passive region in the ruthenium-containing samples extends approximately over the same potential range, i.e. over a 0.8 to 1.0 V range, compared to the blank and 0% Ru sample extending over a 1.2 V range. Relating this to Figure 15 in section 2.6 and the proposed effect that ruthenium would have on the shift in the hydrogen reaction, the results observed correspond with that assumption changing the shape of the curve. Clearly with a small amount of ruthenium added, i.e. the 0.44 wt%, only a slight shift in current density occurred reducing the traditional 'active nose' shape that formed but already at the next step increase in ruthenium composition, i.e. from 0.82 wt% onwards, the cathodic reaction (formation of hydrogen) line intersects the steel curve at above the 'active nose' in the passive region of the curve in order to display the transition at these ruthenium compositions, as per Figure 10. This indicates much reduced metal dissolution and therefore reduced corrosion rates as anticipated, which is confirmed by all the results. Increased passivation was induced in the samples analysed which leads to the conclusion that the passivation potential of the ruthenium-metal alloy is less than the over-potential of the hydrogen evolution reaction on the alloying ruthenium. Testwork conducted by Olubambi et al. (2009) also found that small additions of PGMs lowered the hydrogen over-potential and thus inhibited anodic dissolution in sulphuric acid and hydrochloric acid.

Potgieter and Brookes (1995) concluded that there was a maximum amount of ruthenium that can be added to stainless steel to improve corrosion resistance and that is exactly what was observed in this environment. The samples containing 0.82 wt% and 4.67 wt% Ru showed similar trends, i.e. the curves correspond with one another, while the samples containing 2.92 wt% and 2.44 wt% Ru too showed similar trends with a further improvement in corrosion protection; they had the highest i_{crit} of these samples. Troselius (1971) concluded that "the influence of an alloying element is not linear within a wider content range" and explained that this is due to the interaction between different alloying elements.

The cleaned surface scan is a true test of the benefit of the ruthenium for corrosion protection; this comparison can be seen in Figure 43. The stainless steel blank curve is the traditional curve as explained in detail and shown in Figure 5 which can be split into active, passive and

trans-passive regions but for the fresh surface scan the corrosion current density, i_{corr} , is larger than that of the sample from the exposed surface scan implying more active dissolution of the metal and thus higher corrosion rates as expected. The i_{pass} however is very similar. The surface layer clearly did not have a chance to form the protective chromium oxide layer as in the exposed media. The passive region is also not as stable over the potential range compared to, for example, the cladded sample with no ruthenium which showed only slightly higher corrosion activity. The passivation potential of the blank and 0% Ru was almost the same at just below 0 V and so was the corrosion potential at -0.44 V. For all the samples containing ruthenium the E_{corr} numbers were almost the same and had increased to -0.24 V. In this condition the distinctive shape is maintained for all the samples tested but not always can one observe stable current densities in that region. Some small spikes were observed in the passive region of these curves, this normally represents instability but it can be explained as the hydrogen line shifts upwards into the passive region, going through the 'active nose', as per Figure 9, Figure 11, Figure 12 and sometimes Figure 13. Depending on the actual shape it can be predicted how far the hydrogen line has actually been shifted. The passive current density is surprisingly spread over a relatively small range for all the samples containing ruthenium compared to the spread during the exposed surface scan. The 0.44 wt% Ru sample log i vs E curve was close to the one for the 0 wt% Ru indicating that small amounts of ruthenium do not seem to improve corrosion protection during the fresh surface scan. The samples with 0.82 wt% Ru and 2.92 wt% Ru however showed higher current densities than the cladded sample without ruthenium. Only the 2.44 wt% and 4.67 wt% Ru showed marginally lower current densities in the low working potential range, i.e. below 0.4 V; thereafter they also showed higher current densities before going into the same trans-passive region.

5.3.1.3 Open Circuit Potential vs time responses

Samples that exhibit high corrosion potentials have a thermodynamically lower tendency to corrode since a high potential energy is required to break-down or corrode the alloy. Noble potentials are an indication of spontaneous passivation of the surface of the sample; this effect is known as cathodic modification or cathodic alloying. From the OCP values indicated in Table 6, the most noble potential was observed for the 2.92 wt% Ru sample, closely followed by the 0.82 wt% Ru which both indicate rapid passivation, then 4.67 wt% Ru, 2.44 wt% Ru, 0.44 wt% Ru, the stainless steel blank and then cladding with no ruthenium. The attained potentials with ruthenium addition are in the more noble, positive, potential

region compared to the stainless steel reference; this was immediately evident by the starting potentials of the OCP graph. Even at the 0.44 wt% Ru the benefit of corrosion protection could be observed and at higher ruthenium concentrations this became clearer by the more noble corrosion potentials, generally indicating the formation of a more stable passive layer. A direct comparison of the average OCP values can be seen in Figure 50 showing the highest positive value at 2.92 wt% Ru. A definite optimum ruthenium concentration in the stainless steel exists for this environment and adding more ruthenium does not seem to improve its corrosion resistance; confirmed via the OCP values. In the case of tungsten carbide corrosion resistance in sulphuric acid, the highest OCP value was obtained at the 3 wt% Ru addition (Potgieter et al., 2011); similar to these test results.

The initial gradients of the OCP curves in Figure 44 indicate how quickly the sample reached a stable value aiming towards its OCP value, the steepest gradient was observed in the stainless steel blank sample. The next fastest increase in potential was observed in the 2.44 wt% Ru sample, followed by 2.92 wt% Ru, 0.82 wt% Ru, 0.44 wt% Ru and the most sluggish curve was in fact observed for the 4.67 wt% Ru sample. In practice it would be important to reach the OCP value quickly; as generally, the sample would be more active before equilibrium is reached. The 0 wt% Ru sample showed erratic behaviour but a distinct downward trend in OCP indicating active dissolution.

Figure 44 shows that a stable potential was achieved over a short period of time; most notably for the 2.44 wt% Ru sample. The OCP values were expected to increase with time as the formation of a passive region occurs by the dissolution of oxides that accumulate into a protective layer. The ruthenium ions were expected to concentrate on the surface, as the other components oxidise, and therefore stabilise the protective layer by preventing break-down. It was thus expected that increasing the ruthenium content would increase that stabilising effect and consequently improve the resistance of the corroded material. It must however be remembered that higher OCP values only give reduced corrosion rates if it means passivity has been reached; without passivity at higher OCP value actually gives an increased corrosion rate. Higher, positive OCPs were obtained with increasing ruthenium this time peaking at 0.82 wt% Ru, followed by 2.92 wt% Ru, 4.67 wt% Ru, 0.44 wt% Ru and 2.44 wt% Ru. Both the stainless steel blank sample and the clad sample without ruthenium were in the lower potential region, even though these also indicated negative OCP values, implying that corrosion is less possible with the ruthenium additions.

Ideally the OCP values should equal to the E_{corr} values as this is where the corroding surface activity is at equilibrium, however, disturbing that equilibrium will in practice cause the two not to be identical for this type of test. It is believed that in this case the scan rate of 1 mV/sec was too fast for equilibrium to be reached whereas the OCP values better represent equilibrium (allowing the test to be run without interference). Another contributing factor is that the test was started cathodic to E_{corr} . The two potentials were different also due to the fact that changes occur on the electrode surface during the scan.

In all test results the OCP values were larger than E_{corr} and E_{pass} values indicating passivation occurred but at a higher potential, i.e. in the passive region of the metal and therefore a transition is observed in this region; as showed in Figure 8 and Figure 10. However, passivation did not occur over a large potential range at low current densities.

5.3.1.4 Corrosion Rates summary

Increasing the ruthenium concentration within the cladded layer was expected to improve corrosion resistance on an exposed surface. Ranking the observed corrosion potential in Table 6, the calculated corrosion rate, the polarisation resistance, etc. shows a similar trend as already described above. The corrosion rate, for example, was significantly higher for the cladded sample without ruthenium while adding even a small amount of ruthenium makes a significant positive difference to the corrosion protection of the sample. 0.44 wt% Ru reduced the corrosion rate more than three times and adding 0.82 wt% Ru improved the corrosion rate 61 times in this environment. The polarisation resistance showed a similar trend as it gave an indication of charge transfer across the double layer. The 0.0 wt% Ru sample had by far the lowest resistance, the stainless steel blank was better and adding just 0.44 wt% Ru doubled the resistance and adding 0.82 wt% Ru improved the resistance 28 times. The current density at 0.2 V was selected to give an idea of passive current density at one specific passive potential and again it showed the lowest value, i.e. least corrosion taking place, for the 2.92 wt% sample. The table clearly highlights that the 4.67 wt% Ru sample does not show the best corrosion resistance for any of the criteria looked at. It indicates that under these conditions, the best corrosion resistance is observed with a stainless steel cladding targeting 2 to 3 wt%. For samples containing ruthenium cladding, the current density increased in the passive region, however, the expected directly proportional step increase with increasing ruthenium concentration was not evident. Olubambi et al. (2009) observed that in sulphuric

acid (and hydrochloric acid) corrosion decreased with increasing ruthenium contents but the samples tested in their study included only up to 0.2 wt% Ru.

Graphically these results are shown in Figure 45 to Figure 50. The E_{corr} values were positive, i.e. more noble when compared to the reference stainless steel blank, for the ruthenium compositions from 0.82 wt% to 4.67 wt% Ru with the highest two values being between 2 to 3 wt% ruthenium. The i_{corr} values were smallest for the ruthenium concentrations between 2 to 3 wt% Ru indicating its most beneficial addition range for this environment. The current density at 0.2 V also indicates the lowest range from 0.8 wt% Ru onwards. The corrosion rate demonstrated rates below 0.01 mm/year only for the samples containing 0.8 wt% Ru or more. Polarisation resistances increased significantly for higher than 0.5 wt% Ru samples peaking at 2.44 wt% Ru. The OCP comparison indicates that the highest positive value was obtained at 2.92 wt% Ru. This is exactly as Potgieter et al. (1995) reported that with the addition of ruthenium the E_{corr} values would increase while both the i_{crit} and i_{pass} values would decrease in comparison to the stainless steel alone. Their testwork was carried out using a DSS but the same effect was observed during this testwork on 304L stainless steel where anodic dissolution was inhibited and a stable passive film formed.

Performing the same comparison on the fresh surface scans, summarised in Table 7 and Figure 51 to Figure 54, it is very clear that the ruthenium had a definite beneficial effect on the corrosion protection of the steel surface. E_{corr} values immediately increase with the addition of ruthenium; however, the spread of results for the ruthenium containing samples is small and definitely peaking at 4.67 wt% Ru. This is also observed for the other parameters, such as corrosion rate, that there is a significant improvement with the addition of ruthenium. However, more corrosion activity is observed on a fresh surface in comparison to a surface where equilibrium has been established on the surface and this includes the built-up of a passive layer.

Ruthenium, being a noble metal, is thermodynamically stable in the presence of aqueous solutions of almost any pH. In general the addition of ruthenium to the samples added the benefit of corrosion protection and at higher ruthenium concentrations this became clearer by the observed more noble corrosion potentials, OCP values larger than E_{corr} and larger than E_{pass} . This indicates the formation of a more stable passive layer thus shifting the corrosion potential into the more noble and passive region. Averaging all the results and looking at a combination of all the above mentioned parameters for corrosion protection, a very clear

ranking order is observed. The order of decreasing corrosion resistance in 1 M sulphuric acid at 25°C is: 2.44%, 0.82%, 2.92%, 4.67%, 0.44%, stainless steel blank and 0% Ru. The combined effect of very low current densities for the alloys containing ruthenium and noble open circuit corrosion potentials explains why the ruthenium containing samples have pronounced lower corrosion rates than the 304L stainless steel base metal. In summary, it is clear that in this environment one can demonstrate the beneficial effect of ruthenium; however, the variation in ruthenium concentration within a single sample may be preventing one from seeing firm trends with regards to actual ruthenium composition.

5.3.1.5 Comparison of different stainless steels

No OCP scans were performed for the 316 stainless steel, the SAF2205 and the Hastelloy C276 materials. The samples were exposed to the media for 12 hours after which the first potentiodynamic scan was run to establish the current density over a potential range after exposure; and after polarisation, the scan would be re-run, as with all the previous samples for the 304L stainless steel and its alloys to establish the current density over the same potential range on a freshly cleaned surface. This serves to give an initial idea of how the ruthenium containing samples compare against commercially available steels. The conclusions drawn thus reflect the limited testwork conducted and certainly would require further investigation if economically viable. In this environment it can be seen that the 316 stainless steel formed a passive film but displayed a higher E_{pass} value than the ruthenium containing alloys of 304L stainless steel thus reducing the passive region and that at higher current densities. This implies that the 3-5 wt% Ru alloys would offer more corrosion protection in this case. What makes one stainless material more corrosion resistant than another is however not only indicated by the polarisation current density but the robustness of the passivity. The SAF and Hastelloy displayed much larger passive ranges at current densities similar to that of the 304L stainless after exposure; by this measure at least they are more corrosion resistant especially since no OCP values were obtained. For the fresh scans, all the samples behaved very similarly in the passive region implying that in this case, the ruthenium alloys can compete with these materials from a corrosion point of view. The passivation ranges were similar except for the Hastelloy which has a reduced range. It is definitely worthwhile to continue the investigation into an alloy of ruthenium with 304L stainless steel for this environment, it can have significant benefits.

5.3.2 1 M H₂SO₄ + 1% NaCl solution at 25°C

5.3.2.1 *Repeatability of results*

Repeatability concerns regarding the variations in ruthenium concentration in individual samples were also observed during the testing in sulphuric acid and salt solution at ambient conditions. As with the tests conducted in 1 M sulphuric acid at 25°C, it is again observed that the repeatability of the stainless steel blank and cladded sample without ruthenium was very good so the cladding process alone is not responsible for the variability. It therefore can be said that mainly the quantity of ruthenium addition and distribution thereof are causing the observed variability. In this environment it was not clearly observed that variability increased with the amount of ruthenium but only that addition of ruthenium causes variability. Sample to sample variability has to be considered and that was investigated in this case where two of the 0.82 wt% Ru samples were tested in this environment. Two 5 mm by 5 mm sections were cut out of the cladded plate and mounted as described in section 3 so that a comparison could be made between the two. The results are drastically different as can be seen in Figure 147. The three blue curves are from the one 0.82 wt% Ru sample and the three orange curves are from the other 0.82 wt% Ru sample. The blue lines show the transition shape with varying steepness of the respective Tafel slopes implying that the hydrogen line has cut the metal at a point in the passive region creating a very stable protective layer with low corrosion rates. The orange lines illustrate a variety of small to larger active noses with a stable passive region at higher passive densities and thus higher corrosion rates but clearly implying that the hydrogen reaction is also shifted up to reduce the active nose. During each run the quantity of ruthenium exposed and its distribution on the surface are slightly different so that one can observe the variability of that hydrogen shift along the metal curve.

Of course, variability is not the only explanation for this vast difference; there could be another, such as the fact that crevice corrosion occurred on the one surface and not on the other. Crevice corrosion would immediately increase the corrosion rate and could result in the varied shape observed between the two curves. In crevice corrosion, the chloride ions would attack the formed crevice providing a localised high corrosion rate which then reflects on the overall corrosion rate as the weak points are measured. This was however not visually observed nor analytically tested for. The reason for testing two samples from the same coupon in the same environment was to illustrate the variability observed with corrosion testing. This must be kept in mind when discussing the results and when drawing conclusions about them.

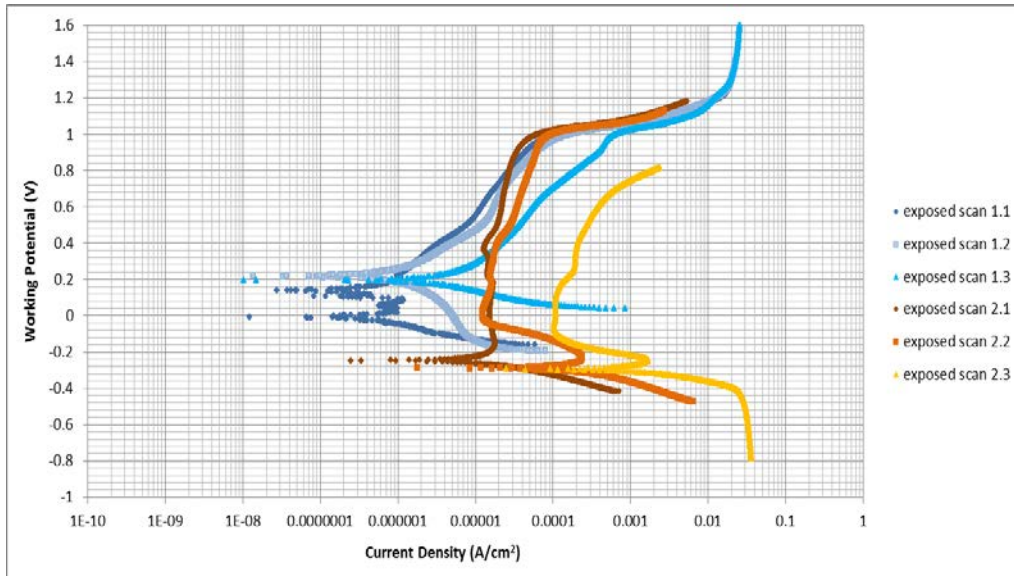


Figure 147: Log i vs E graphs for the two 0.82 wt% Ru samples in 1 M H_2SO_4 + 1% NaCl at 25°C

5.3.2.2 Current density vs potential responses

Adding sodium chloride to the sulphuric acid solution increased the corrodibility of the environment. The chloride ions attack the passive layer formed on the surface of the cladded material, their presence therefore accelerates the degree of damage to the oxides formed providing the passive layer. It is expected that stainless steel 304L does not perform well from a corrosion resistance point of view in an acidic environment containing chloride ions. This is observed in industry.

Small amounts of ruthenium (up to 0.28 wt%) have been added to DSSs and tested using 3.5 wt% NaCl solutions (Sherif et al., 2009) where their electrochemical measurements indicated that the Ru-DSS alloy surface passivated and it significantly decreased the corrosion and passivation currents with corrosion and pitting potentials shifting to more noble values. This effect was found to increase with increasing ruthenium content. They state that “the presence of Ru and the increase of its content, which reflects on decreasing the cathodic, i_{corr} , anodic currents and corrosion rates”. This lead to their observation that in NaCl environments, increasing amounts of ruthenium would improve the corrosion protection of the samples by kinetically slowing down both the iron dissolution and breakdown of water; i.e. reactions (1) and (2) in section 2.1. They proposed two mechanisms for the improvement in corrosion protection: they suggest that it is possible that the ruthenium interacts with the iron in such a way that allows the chromium atoms to freely diffuse to the surface which ensures improved passivation and thus increases its resistance against corrosion, in their case, in the NaCl solution. The other explanation offered is that the ruthenium “will be taken up in

the scale, resulting in a thin, compact film, which could decrease the general and pitting corrosion of the DSS alloy” (Sherif et al., 2009). The exact mechanisms were not investigated in detail for this report but both of these proposed methods by Sherif et al. (2009) are certainly a possibility to occur with the samples studied. A similar study conducted by Banda and Van der Merwe (2014) showed the same results where they observed that the PGMs act “as an active cathode in the alloy, hence retard the kinetics of the anodic process”. A clear trend developed in terms of the increasing ruthenium concentration providing better corrosion protection in sulphuric acid media with the introduction of chloride ions in the form of sodium chloride addition, as stated for the DSS. The scans in Figure 65, which were confirmed in Figure 67 by the OCP values, show that the corrosion protection increased with increasing ruthenium content. Trending the current density at the onset of passivation, i.e. at 0.1 V, the order with increasing current densities is 4.67 wt% Ru, 2.92 wt% Ru, 0.82 wt% Ru and thereafter the 304L stainless steel without ruthenium. The same trend is observed for the i_{corr} values. The curves from the exposed surface scan clearly indicate that ruthenium additions both reduce the i_{crit} and i_{pass} significantly. The shape of the curves suggests that the samples were able to form stable passive layers over a large potential range averaging 1.2 V. In fact, the first 0.82 wt% Ru sample shows the transition which suggests that the hydrogen line was able to intersect the passive region of the steel suggesting the formation of a stable passive film on its surface. For the fresh surface scan this is not the situation and almost all the ruthenium containing samples showed similar behaviour which was an improved corrosion resistance compared to the samples without ruthenium.

Relating this to Figure 15 in section 2.6, it is clear that the shift in hydrogen potential has only occurred minimally, i.e. reducing the nose but in most cases not able to shift entirely into the passive region. From the comparison using Figure 139 to Figure 142 and Figure 144, it can be observed that the chloride additions tend to extend the nose towards higher current densities, i.e. increase the i_{crit} values, and over a larger potential range. This is observed due to the increased dissolution of the metal in those environments. However, in the ruthenium containing samples, this large increase is not observed as prominently indicating (especially at high ruthenium concentrations as per Figure 143) that the ruthenium is contributing towards a reduction in the dissolution at that point and thus reducing overall corrosion activity. Both the mechanisms proposed by Sherif et al. (2009) could have contributed to this as well as the effect observed by Banda and Van der Merwe (2014).

For a surface area where equilibrium has been reached, i.e. after exposure to the environment for 12 hours, the 304L stainless steel sample exhibits the traditional shape as explained in Figure 5 except with a bigger active nose. The clad sample without ruthenium exhibits more dissolution and thus a larger active nose at higher current densities. For the samples containing small amounts of ruthenium, e.g. the 0.82 wt% Ru sample, the nose was much smaller and passivation current densities were an order of magnitude less indicating a stable passive layer with much lower corrosion activity. As the concentration of ruthenium is increased, the nose shrinks and longer passive ranges are observed with minor serrations at the onset of the passive region. This demonstrates how the hydrogen line is shifting further up and thus reducing corrosion activity. For the fresh surface area, the samples without ruthenium behaved similarly compared to the exposed surface scans. The ruthenium containing samples also behaved similarly with reduced dissolution and lower current densities especially during the passive region compared with the samples without the precious metal. The active noses were not significantly reduced though indicating that this shift in hydrogen over-potential was not as effective on the fresh surface. The current densities, which are directly proportional to corrosion rates as per equation (G), are higher than the ones observed on an exposed surface. The formation of a stable passive film for stainless steel is critical to the reduction in corrosion rates and thus is it important for the metal to form this passive layer as quickly as possible.

For the 1 M sulphuric acid with 1% sodium chloride solution the results for the exposed and fresh surface scans were not orders of magnitude different as observed in the 1 M sulphuric acid media; they were in a more similar current density range. It is noticed that a passive region exists, i.e. similar i_{pass} over a large potential range, except for one of the 0.82 wt% Ru samples where a transition is observed for the exposed sample. In the 304L stainless steel sample (Figure 57) and clad sample without ruthenium (Figure 158) it was observed that corrosion resistance improved marginally from the exposed to the cleaned surface scan. With some ruthenium addition (Figure 59 and Figure 63), however, the corrosion resistance was improved significantly from the fresh surface scans compared to the exposed surface scans. This is verified by the observation that the passive range increases slightly from 1.0 V to 1.2 V when comparing fresh results to exposed ones. This implies that the ruthenium enhances the build-up of a stable passive layer and increases the rate at which it does so. In order to achieve this, the surface of the alloy must be enriched with ruthenium which promotes passivity as observed. The exposed samples do on average still show lower current

densities especially for the higher ruthenium containing samples as can be seen when comparing Figure 65 to Figure 66. This suggests that the exposure time of 12 hours allowed equilibrium to be reached which included the formation of a passive layer on the surface of the steel to protect it from the environment. As explained in section 5.3.1.2, pitting would occur in the trans-passive region which would have been visual on the steel surface but even with the addition of chloride ions, no evidence of pitting corrosion occurred in this environment.

5.3.2.3 Open Circuit Potential vs time responses

Observing the Open Circuit Potential over time curve carefully (Figure 67) confirms what has been discussed above. For the two 0.82 wt% Ru samples very different results were observed, i.e. they were not confirming each other's results, and thus they provided contradicting information especially in relation to the other ruthenium compositions. The fact that variability of samples taken from the same coupon is this large has to be taken into consideration when drawing conclusions for all the test results.

It is clearly observed that the stainless steel blank and cladded sample without ruthenium behaved very similarly and have almost identical OCPs which were large negative numbers. These were lower than the OCPs for the ruthenium containing samples, implying that corrosion is less possible with ruthenium additions. Without considering the first 0.82 wt% Ru sample (orange line in Figure 67), again a clear trend is observed which shows that the OCP values increase, i.e. become more noble and less active, with an increase in ruthenium. This is as expected.

The 304L stainless steel curve is a flat and very stable curve where the initial OCP value is similar to that observed after 12 hours, the cladded sample without ruthenium initially decreases drastically before levelling off to a value similar to that of the stainless steel blank sample while the ruthenium containing samples all initially increase quickly by a small amount and at the same rate before also levelling off but at a higher value than the samples without ruthenium. This gives an indication of how quickly equilibrium is reached and confirms the above statement regarding the effect of increasing amounts of ruthenium enhancing the rate at which the passive layer is built-up and thus passivation occurs.

The OCP values followed exactly the same trend as the E_{corr} values, as theoretically these should be the same value. Values that quickly go to more noble values are desired for

maximum corrosion protection and all samples containing ruthenium tested in this experiment shifted the OCP into the more noble region. For the stainless steel samples without ruthenium, the E_{corr} values are almost the same as the OCP values but as ruthenium is added there is a significant difference between the numbers with the E_{corr} values constantly being lower than the OCP values.

Various studies, referred to by Banda and Van der Merwe (2014), tested ruthenium alloyed with stainless steel and found that spontaneous passivation occurred on the surface of the ruthenium containing steels. Their testwork was conducted with a high strength sodium chloride solution at 25°C and found that small amounts of ruthenium reduced current densities to maintain passivity and increased the passive range of the LDX2101 stainless steel. For the samples tested in 1 M sulphuric acid with 1% sodium chloride solution at 25°C without ruthenium, the OCP values are less than the E_{pass} values for both the fresh and exposed surface scans implying active corrosion is taking place under these conditions. With the addition of ruthenium this is reversed and the OCP values increase and are positive numbers implying passivation as they are larger than the E_{pass} values. This really demonstrates the power of the ruthenium additions. Again, it is assumed that one or both of the methods described by Sherif et al. (2009) are causing this behaviour.

5.3.2.4 Corrosion Rates summary

Table 9 highlighted the already established trend after exposure and in fact confirmed it with regards to other corrosion protection indicators: the observed corrosion potential, the corrosion current density, current density at 0.1 V, corrosion rate and polarisation resistance. The various parameters highlighted that cladding alone, without any ruthenium, significantly reduced the corrosion protection of that sample while increasing the ruthenium content improved the corrosion protection significantly in 1 M sulphuric acid with 1% sodium chloride at 25°C. The table compares all the actual values calculated per sample and then averaged for the tests ran. These therefore highlight the massive and consistent improvement that the ruthenium addition demonstrates. For example, the corrosion rate and corrosion current density improved 35 times each when comparing the 4.67 wt% Ru sample to the one cladded without ruthenium; for the same comparison it is observed that the OCP values after 12 hours and the corrosion potential were doubled and corrosion resistance had increased by over 100 times! It also indicates that under these conditions, the best corrosion resistance is

observed with an increase in the ruthenium concentration; i.e. for the samples tested a stainless steel cladding targeting 5 wt% Ru.

Figure 68 to Figure 73 illustrate graphically the same trend: improved corrosion with an increase in ruthenium concentration as well as large variability between the two 0.82 wt% Ru samples. For a freshly cleaned surface the actual results indicated that corrosion activity is higher when no passive film is formed making the surface vulnerable to corrosion attack. The trend however is the same as for the exposed surface area; the ruthenium additions have a significant positive effect on corrosion protection and corrosion rates decrease with an increase in ruthenium concentration. This suggests that both the anodic and cathodic kinetics are altered by the presence of the ruthenium atoms on the surface. If ruthenium were only acting by increasing the hydrogen exchange current density, one would expect the ruthenium to have a beneficial effect once a threshold value was exceeded, but for there to be no further benefit as ruthenium increased further. However, as is clearly observed with these results, the beneficial effect improves as ruthenium composition increases (at least under these conditions described in this section) which suggests that both anodic and cathodic kinetics are altered.

In general, and as already observed with the samples in the 1 M sulphuric acid solution, the addition of ruthenium to the samples adds the benefit of corrosion protection and at higher ruthenium concentrations this becomes clearer by the observed lower current densities and more noble corrosion potentials indicating the formation of a more stable passive layer and the move of the corrosion potential into the positive, more passive region. Averaging all the results and looking at a combination of all the above mentioned parameters for corrosion protection, a very clear ranking order was observed. The order of decreasing corrosion protection in 1 M sulphuric acid with 1% sodium chloride added at 25°C is: 4.67 wt% Ru, 2.92 wt% Ru, 0.82 wt% Ru, stainless steel blank and 0 wt% Ru clad sample.

5.3.2.5 Comparison of different stainless steels

The large improvement in corrosion protection on the surface of an exposed alloy of ruthenium has already been described when compared to 304L stainless steel. The 316 stainless similarly showed good corrosion resistance and so did the Hastelloy material but the best performer in terms of lowest current density throughout the entire scan was the SAF2205. The 4.67 wt% Ru sample performed very similar and would make an excellent substitute in this environment if required. On a fresh surface the ruthenium containing

samples also performed well whereas the 316 stainless definitely was not as suitable. The Hastelloy behaved similarly to the ruthenium containing samples but with a much reduced active nose. Again, the SAF2205 showed a reduced nose, the longest passive region and the lowest current densities during the scan. This performance is critical as small material scratches etc. could leave a portion of the material unprotected damaging the metal structure if exposed to such a corrosive environment as this one. Existing materials are available that are suitable in chloride environments and in 1 M sulphuric acid with 1% sodium chloride at 25°C, it seems that the ruthenium cannot add as much benefit as during exposure to the sulphuric acid alone. It is thus suggested that this might be re-checked or higher ruthenium concentrations used but no further studies are required to investigate ruthenium enriched austenitic stainless steel for this environment. A cost analysis will also be helpful in making a final decision.

5.3.3 1 M H₂SO₄ solution at 45°C

5.3.3.1 Repeatability of results

Repeatability of the samples was observed under these conditions and some variability must be taken into account when analysing and comparing the results. The results for the log *i* vs *E* curves were very consistent and in fact greater variances were observed for the stainless steel blank sample than the samples with ruthenium. The differences between the exposed surface test results and fresh surface test results were minor in terms of repeatability, i.e. in the case of testing the samples in 1 M sulphuric acid at 45°C there was no greater fluctuations testing after exposure compared to before. For the OCP results, variability was excellent for the samples without ruthenium as the graphs for the repeat runs were coinciding with the first run but some variability occurred for the 0.82 wt% Ru, the 2.92 wt% Ru and 4.67 wt% Ru samples where fluctuations were observed. Final values were reasonable and it is thus expected that accurate conclusions can be drawn from the results obtained. In this environment it can certainly not be said that the ruthenium addition caused any variability of the surface area and thus the test results.

Comparing the variability of these test results to the variability of the tests at ambient conditions, they revealed that the higher temperature testing did not introduce any additional variability in this media. It might be thought that as reaction kinetics are increased at elevated temperatures, repeatability of results would be reduced but that was not observed in this case.

5.3.3.2 *Current density vs potential responses*

Increasing the temperature of the 1 M sulphuric acid environment to which the samples were exposed, increased the corrodibility of the samples by increasing the rate of the reactions taking place on the surface of the metal and thus the rate of corrosion observed. Activity increased with an increase in temperature.

For the exposed surface scan at 1 M sulphuric acid at 45°C the cladded sample without ruthenium follows the same trend, i.e. displays the same shape of the $\log i$ vs E curve, as the stainless steel blank sample but at higher corrosion densities suggesting more activity at the surface where corrosion is taking place. This is as expected since the cladding process introduces porosity to the area and stresses from the heating and cooling cycle. In industry, it is very commonly observed that a welded portion corrodes first when exposed to an acidic media or elevated temperatures (Salgado-Lopez and Rubio-Gonzalez, 2015 and Charles et al., 2007). In this environment both were tested. It is thus important to compare the ruthenium containing samples to both the 304L stainless steel blank sample and the cladded sample without ruthenium. In order to be technically viable, the effect of the ruthenium must be such that it overcomes the negative effect of the cladding process as well as improves the corrosion protection of the 304L stainless steel.

Comparing the samples in the different environments it is very obvious that the increase in temperature caused a massive increase in activity which is observed by a two orders of magnitude increase in current densities throughout the scan; Figure 139 and Figure 140 for the stainless steel. This difference is reduced to one order of magnitude shift in current densities with the addition of ruthenium but it remains significant for all the samples. Besides such a big increase in overall activity, it is also observed at higher temperatures that instability is introduced in the passive region. On some occasions this is reflected in a 'second active nose' as in Figure 141 or wavy behaviour as in Figure 140. This reduces the passive region and is thus the ideal suitable range of the material under these conditions.

For the anodic scan on an exposed surface the cladded sample showed the highest current densities suggesting the most active corrosion taking place as already discussed. The stainless steel sample and the 0.82 wt% Ru sample behaved very similarly suggesting that a small amount of ruthenium added does not seem to have much if any benefit under these conditions. The 2.44 wt% Ru will be excluded here as it is believed that the actual surface cladding was ground off at this stage of the testing but no further samples were available for

re-testing. The three tests run with this sample showed very consistent results but these certainly did not follow any trend! It is possible that crevices were present on the sample configuration, which was not specifically observed before the testing started. Crevice corrosion could thus have occurred and was possibly aggravated by the higher temperature. The two samples containing the largest amounts of ruthenium behaved very similarly with the 4.67 wt% Ru sample not always showing lower current densities especially in the passive region. This would suggest that an addition of 3 or 5 wt% Ru makes no difference from a corrosion point of view, i.e. corrosion protection cannot be further improved by the addition of more ruthenium, and thus an optimum amount of ruthenium has been detected at 2.9 wt%.

At higher temperatures no graphs displaying transitions were observed, they all however follow the traditional curve of having distinct active, passive and trans-passive regions. This implies that the added ruthenium was not able to sufficiently shift the hydrogen reaction into the passivation region. The ruthenium has however caused a drop in the current densities increasing corrosion resistance. The instability within the active region is not caused by this shift. Anodic loop formation was only observed for the 4.67 wt% Ru sample (after exposure to the media) implying that the hydrogen line was shifted the most for the highest amount of ruthenium, illustrated in Figure 9.

The fresh surface scan confirmed this general trend: the cladded sample showed the highest dissolution activity with a specifically elongated active nose, the stainless steel blank had slightly reduced current densities but showed instability in the passive region, the 0.82 wt% Ru was marginally improved compared to the blank stainless sample for most of the active region whereas the two samples with the highest amounts of ruthenium showed the most corrosion protection and are again very similar to each other. The improvement of the ruthenium additions is not as evident on a fresh surface as on the exposed surface but it is significant. The ruthenium is therefore not only improving the stability and speed of building up the passive layer but also reduces the activity on a fresh surface. In this situation it would be valid to suggest that further additions of ruthenium would have no significant benefit to the corrosion protection.

Comparing the curves with each other, a clear trend was observed, which is the same for both the exposed and fresh surface scans and was already discussed. The ranking order obtained from Figure 86 and Figure 87 in order of reducing corrosion protection is 4.67 and 2.92 wt% Ru are very close to each other, followed by 0.82, 0 wt% Ru and then the stainless

steel blank but last being the 2.44 wt% Ru sample. This order is especially prominent in the passive region. In terms of i_{crit} and i_{pass} only, the 2.44 wt% sample could actually be ranked between the 0.82 and 0 wt% Ru samples. Besides small variations which increased or decreased results for the various ruthenium compositions, the large difference in current densities that was observed for the sulphuric acid at ambient conditions was not observed at 45°C but a much narrower band in results was obtained. This implies that a fresh surface reacts very similar to a surface which had a chance to build up a protective oxide layer which would imply that the protective layer is formed extremely fast. This can be attributed to the influence that ruthenium additions have on the cladded alloy layer and it can also be assumed that the increased temperature assisted in that behaviour.

5.3.3.3 *Open Circuit Potential vs time responses*

Table 14 compares the average OCP values that were calculated from all the repeat runs. The lowest and only positive result was obtained for the 2.92 wt% Ru sample. The trend observed for increasing potentials is as follows: the cladded sample without ruthenium, the stainless steel blank, the 0.82 wt% Ru sample, the 4.67 wt% Ru sample and the best results were obtained for the 2.92 wt% Ru sample. The 2.44 wt% Ru was the outlier as discussed before. All the OCP values in this environment were smaller than the passivation potential. This indicates that even as equilibrium is established and a passive film is formed to reduce corrosion activity, the passivation potential is on average still larger and is thus not reached, even after 12 hours. This indicates active corrosion is taking place. The only exception is the 2.92 wt% Ru sample (after the 12 hour exposure) where the OCP is slightly larger than the E_{pass} value. The difference between the two values is reducing as ruthenium content increases suggesting that active corrosion is reduced by the presence of the ruthenium atoms in the surface layer of the alloy. The passivation potentials are generally slightly higher on the fresh surface compared to the value on an exposed surface. This means that a higher potential energy is required for corrosion to take place on the fresh surface, even though no passive film exists as a barrier between the metal and the media. This could possibly be explained by a drift of the whole curve to higher potentials.

Observing potentials over time, as in Figure 88, the trend is the same as what was discussed before: the 4.67 wt% Ru sample has the highest OCP value at the end of the 12 hour period, closely followed by the 2.92 wt% Ru sample; both of which are in the positive region. The remaining results are all close to each other and all in the negative region suggesting that

significant improvement of corrosion resistance at higher temperatures is only achieved with ruthenium compositions at close to 3 wt% Ru and above. The results were all relatively stable except for the 2.92 wt% Ru sample which displayed some erratic behaviour throughout the test.

The initial gradients of all the OCP curves showed a downward trend, steepest for the stainless steel blank followed by the 0.82 wt% Ru sample and the two gentlest slopes were observed for the highest ruthenium containing samples which took almost three hours to stabilise. As mentioned previously, it would be beneficial to reach equilibrium as quickly as possible since active dissolution is prominent before. When applying the potential over a relatively large range during the potentiodynamic scans, the open circuit conditions will be disturbed and the sample thus has to 'recover' from this disturbance. A gentler curve indicates a slower recovery from exposure.

It has been discussed before in section 5.3.1.3 that during such an anodic scan as was performed, it is not likely that the OCP value would be equal to the E_{corr} value as it theoretically should be. For the sulphuric acid at increased temperatures, the E_{corr} values were generally slightly lower than the OCP values while that difference was widening with an increase in ruthenium content. At ambient conditions the difference was also observed where E_{corr} values were less than OCP values but the difference could not be linked to ruthenium composition.

The temperature increase from 25°C to 45°C has not only affected the increase in current densities but also caused the drastic reduction in OCP values as can be observed when comparing Table 8 with Table 14. E_{pass} values on the other hand have drastically increased from spontaneous passivation at ambient conditions for the high ruthenium containing samples to them experiencing active dissolution at elevated temperatures.

5.3.3.4 Corrosion Rates summary

The general trend after exposure to the media for 12 hours was that most studied indicators of corrosion (such as corrosion current density, corrosion rate and polarisation resistance) suggest that increased amounts of ruthenium improve the corrosion protection of the material. This is as expected since more ruthenium atoms in the surface layer would imply a more stable passive film could be established more quickly reducing corrosion rates. Previous indicators have however already suggested that there is no direct benefit after an addition of

3 wt% Ru. This was observed for the other parameters looked at (such as corrosion potential, current density at 0.1 V and OCP values after 12 hours) the effectiveness of the ruthenium was levelling off before or at the 4.67 wt% composition and thus the best composition for maximum corrosion protection would be around 3 - 5 wt% Ru. The additional 2 wt% Ru certainly does not seem to have any detrimental effect on corrosion. In fact, the corrosion current density is reduced by approximately 1000 times at 4.67 wt% Ru, compared to the stainless steel blank sample. Similar numbers are obtained for the improvement in corrosion rate and polarisation resistance. While this number was closer to the 3 wt% in 1 M sulphuric acid at 25°C, the elevated temperatures seemed to require additional ruthenium to optimise corrosion resistance. It should also be acknowledged that the actual cladding process did not cause any additional weakness in terms of corrosion at higher temperatures.

On a fresh surface area corrosion rates were significantly higher but did follow the same trend as already described. The ruthenium addition had a significant effect on reducing corrosion potentials, decreasing corrosion current densities and thus reducing corrosion rates as well as increasing the polarisation resistance. The best results for all the parameters were obtained for the 2.92 wt% Ru sample followed by the 4.56 wt% Ru sample emphasising the optimum range of ruthenium in this environment. The much higher corrosion rates indicate active corrosion on the surface of a fresh metal alloy implying that the ruthenium additions reduce the corrosion rate but cannot induce true passive behaviour.

No tests were carried out comparing the various steels to the ruthenium containing 304L stainless steel alloys under these conditions.

5.3.4 1 M H₂SO₄ + 1% NaCl solution at 45°C

5.3.4.1 Repeatability of results

Considering repeatability of the results, having tested all the samples in a 1 M sulphuric acid and 1% sodium chloride solution at 45°C, it can be said to be very reasonable. The stainless steel blank showed some variability when observing the log *i* vs *E* graphs, which was unexpected but had been observed for the same scans in 1 M sulphuric acid at 45°C; the OCP graphs for the stainless steel were however consistent. The cladded sample without ruthenium showed almost the same variability as the stainless steel blank sample confirming that the cladding process did not add any variability. The 0.82 wt% Ru sample showed very consistent results but thereafter variability did increase as the ruthenium content was

increased. The 4.67 wt% Ru sample had one outlier but the other results were reasonable and one result that did not confirm the other three test scans conducted could be left out when determining averages. The 2.44 and 4.67 wt% Ru samples showed the greatest variability, the 4.67 wt% Ru being worst; perhaps again suggesting that variability is introduced with an increase in ruthenium content. No significant differences in repeatability were observed when looking at the exposed surface scans compared to the fresh surface scans. It was not observed that the repeatability reduced with the increase in temperature (this was not observed either in the 1 M sulphuric acid solution when temperatures were increased from 25°C to 45°C). It can thus be concluded that the results obtained in this environment can be used for comparisons.

5.3.4.2 Current density vs potential responses

Increasing the temperature of the 1 M sulphuric acid and 1% sodium chloride environment, to which the samples were exposed, increased the corrodibility of the samples. The chloride ions attacked the passive layer formed on the surface of the clad material and the temperature increase allowed the metal dissolution reactions to take place faster. The presence of chloride ions in the solution must have accelerated the degree of damage to the passive oxide layer formed (no stable passive region observed in Figure 105 and Figure 106) which was further accelerated by increasing the rate of reactions taking place. It is therefore not expected that stainless steel 304L performs well in an acidic environment with chloride ions present at elevated temperatures from a corrosion resistance point of view; as is observed in industrial applications. For this study it was the harshest environment and the true potential of the ruthenium for corrosion protection was tested.

As observed when increasing the temperature of the 1 M sulphuric acid to 45°C, in this solution at elevated temperatures the active nose was extended over a longer current density and potential range and thus shortening the passive region and the overall scan exhibited an increase in current density by over an order of magnitude. This implies a significant increase in corrosion activity on the surface. With ruthenium additions it was clear that the nose was significantly reduced, as can be observed for example in Figure 141. However, the current densities throughout the anodic scan are approximately two orders of magnitude larger than when testing the samples in this solution at ambient conditions. This is the case for both the exposed surface scans and the fresh surface scans. The passive region is characterised by a slight increase in current density with potential and not one stable i_{corr} value. The difference in shape of the log i vs E curve and current density value at a specific potential is smaller

comparing the 1 M sulphuric acid at 45°C to the 1 M sulphuric acid with the addition of the 1% sodium chloride at 45°C. That indicates that the increase in temperature by 20°C is a harsher condition for the 304L stainless steel than the addition of the 1% chloride ions. The addition of both really is the harshest condition with the highest current density values obtained compared to all the media tested.

The stainless steel blank as well as the 0 wt% Ru sample behaved similarly and all other samples containing ruthenium behaved very similarly as can be seen from Figure 105 and Figure 106. The samples without the ruthenium have large active noses before going into the passive region and current densities are much higher than in any other environment. The scans are actually very similar on an exposed surface compared to the fresh surface. It is assumed in this case that perhaps the constant chloride attack and increased activity due to the elevated temperatures, never allowed the proper build-up of a stable passive layer and thus corrosion activity was high and did not vary significantly even after, or because of, exposure to the environment for 12 hours. Equilibrium might have been reached but that included active dissolution of the metal. The ruthenium containing samples all displayed much higher corrosion potentials than the samples without ruthenium, very much reduced active noses and a passive region where current densities increased with an increase in potential. No additional transition was observed. For the exposed surface scan the 0.82 wt% Ru sample and the 2.92 wt% Ru sample results almost coincided and so did the scans for the 2.44 wt% Ru and 4.67 wt% Ru samples. There is a slight but consistent difference in current density all throughout the passive region, the higher ruthenium containing samples having the lower current densities. On a fresh surface the same trend is observed but with much less of a difference between all the ruthenium containing samples and at slightly lower current densities. This implies less corrosion activity on the fresh surface and would point again towards the fact that no passive film was able to form in this environment. In chlorine rich environments it is sometimes observed that the chloride ions displace the oxygen molecules on the metallic surface to bond with the metal producing metallic chlorides instead of metallic oxides (Jones, 1996). The metallic oxides, such as chromium oxide, passivate the surface in the form of a stable film which is not the case when metallic chlorides are present; instead the surface starts to corrode faster. This appears to be a valid explanation for what has been observed. The exposed surface had 12 hours during which the chloride ions attacked the surface and thus increased corrosion rates were observed during the scan; when compared to a fresh surface where the chlorides had not had a chance to form metallic chlorides. The i_{pass}

of the ruthenium containing samples is more than an order of magnitude smaller when compared to the samples without ruthenium. This clearly shows that the ruthenium is taking part in reducing the active nose by significantly reducing the active dissolution of the metal and assisting in providing a stable passive film on the surface. The passivation range is much longer (by at least 0.4 V) for the ruthenium containing samples compared to the samples without the PGM.

In summary, it can be said that at the increased temperature the test results showed that there was corrosion activity on the surface layer of the metal; this activity was stable at equilibrium. Even a small amount of ruthenium added to the cladded surface showed a significant improvement in corrosion resistance and a further improvement with an increase in the ruthenium content occurred but was not directly proportional. A notable improvement in corrosion protection was observed with the addition of ruthenium under these conditions but adding more ruthenium does not show any additional benefit for the ruthenium range observed. However, active corrosion is observed in this environment for all the samples tested. It is expected that the passive layer could be more degraded over time in the presence of chlorides.

5.3.4.3 Open Circuit Potential vs time responses

The OCP was expected to increase with time as the formation of a passive region occurs by the dissolution of oxides that accumulate into a protective layer. The presence of ruthenium is expected to concentrate on the surface, as the other components oxidised, and therefore stabilise the protective layer by preventing its break-down. It was thus expected that increasing the ruthenium content would increase that stabilising effect and consequently the resistance of the corroded material. As discussed above, this was not observed for the $\log i$ vs E graphs and also not for the OCP graphs.

OCP values of samples containing ruthenium increased slightly and consistently by over 0.1 V compared to the two samples without ruthenium. All the samples containing ruthenium behaved very similarly and all showed a stable OCP value almost right throughout the 12 hours. For the samples without ruthenium, there was an initial quick drop in voltage to the OCP value while the ruthenium samples varied in this regard with the lower concentrations of ruthenium being stable from the start and the 4.67 wt% Ru sample dropping gently before levelling off. Therefore the OCP values did not simply increase with increasing ruthenium content. It appears in this case that any ruthenium addition (at least 0.82 wt% Ru) achieves

the slight improvement in increasing the OCP value, any further addition seems not to have any additional effect which confirms what was discussed above and observed for the Evans diagrams. Stabilisation was still achieved at active potentials which was due to the breakdown of the passive film as dissolution takes place.

Table 17 presents the average results from the various scans while the graph in Figure 107 only shows one representative curve. The table shows the clad sample without ruthenium having the lowest OCP value closely followed by the stainless steel blank sample and the general trend for the ruthenium containing samples is that the OCP value is increased with an increase in ruthenium content. This is what one would expect. The table also clearly shows that the OCP values are consistently lower than the E_{pass} values, for the exposed surface and the fresh surface as well as for all ruthenium levels indicating active corrosion. No passivity was reached. The difference between the two values is decreasing with an increase in ruthenium which demonstrates that as more ruthenium is available the natural system potential is heading towards passivation. This trend does not show a levelling off at the 4.67 wt% Ru suggesting that adding more ruthenium to the cladding could allow passivation to be reached and provide corrosion protection with a stable and passive film.

Ideally the OCP values should be equal to the E_{corr} values and in this environment they are almost identical. They are both large negative values and very close to each other, for example, the OCP for the stainless steel sample is -317 mV while its E_{corr} value is -315 mV. The exception is the 4.67 wt% Ru sample where the OCP value is significantly higher than the E_{corr} value.

5.3.4.4 Corrosion Rates summary

Testing a sample after 12 hours exposure to the media allows a measurement that indicates equilibrium behaviour for the sample. The observed corrosion potentials had the lowest value at 0.82 wt% Ru, the corrosion current density was lowest at 2.44 wt% Ru, the current density at 0.1 V was lowest at 0.82 wt% Ru and the corrosion rate at 2.44 wt% Ru. This indicates the optimum ruthenium range which provides the most corrosion protection. Results with higher ruthenium content in fact showed reduced corrosion protection under these severe conditions. Testing a sample on a freshly cleaned surface allows the response to be tested when the metal had no time to build up a protective layer and gives a good indication of corrosion protection from the start of exposure. Corrosion rates are reduced on the fresh surface meaning that less corrosion activity is occurring compared to the exposed surface area. The corrosion potential

is highest for the 0.82 wt% Ru sample, the corrosion current density lowest for the 2.44 wt% Ru and the corrosion rate lowest for the 4.67 wt% Ru. Corrosion rates are high, however, which does not indicate passivity for any of the samples tested.

A definite optimum ruthenium concentration alloyed with the stainless steel exists for a particular environment which, in this case, is confirmed by all the corrosion parameters. Under these conditions, the trend indicates improved corrosion protection with an increase in ruthenium but that trend is not directly proportional but on average is best in the range of 1 to 3 wt% Ru. All parameters were definitely levelling off at or before the 4.67 wt% Ru composition. The only exception is the average OCP value which is highest at the highest ruthenium composition. It seems that in this environment the ruthenium does not have the significant beneficial effect it had in the 1 M sulphuric acid at 25°C. The ruthenium containing samples show less corrosion activity than the equivalent 304L samples regarding corrosion rate but all are still in the active region, passivity was not achieved.

5.3.4.5 Comparison of different stainless steels

As discussed above, the 304L stainless steel sample showed a large active nose when tested after exposure to the media for 12 hours. The ruthenium samples showed higher E_{corr} values, much reduced current densities but these increased as the potential was increased and thus crossing the more stable passive region of the stainless steel at potentials around 0.7 V. In this environment the 316 and SAF2205 behaved similarly only observing small active noses but stable passive regions at significantly lower current densities than the ruthenium containing samples especially as potentials are increased. The Hastelloy showed its true potential in this environment having the most stable passive region at the lowest current density. It would be the preferred material in this case. On the fresh surface the 304L stainless and ruthenium alloys behaved similarly to the scan after exposure but the remaining three steels showed slightly increased corrosion potentials and orders of magnitude lower current density throughout the scan. The passive region was however not stable but characterised by variability and anodic loops at various potentials. It actually demonstrates the severity of this environment but these still performed better from a corrosion point of view than the ruthenium containing samples. It is very clear from this comparison that technically more suitable materials already exist but a cost analysis would reveal if there is any economic benefit to continue investigating ruthenium alloyed with 304L stainless steel.

At ambient temperatures, the ruthenium containing samples showed an equivalent corrosion rate to the SAF2205 and Hastelloy C276 but as temperatures increase, the ruthenium is certainly not as beneficial as existing materials. This has to be considered for any application.

5.3.5 1 M HCl solution at 25°C

5.3.5.1 Repeatability of results

Repeatability of results in the hydrochloric acid media has not been good at all including the stainless steel blank sample; variability did not seem to increase with an increase in ruthenium however. The log i vs E graphs are particularly affected showing three to four orders of magnitude difference between the three scans conducted but also the OCP graphs show large variability which was not common for the testing in the sulphuric acid media. Troselius (1971) has already observed the increased variability for hydrochloric acid when he conducted tests using various stainless steels in 1 M sulphuric acid and 1 M hydrochloric acid. Therefore, when a representative sample had to be selected, the one showing the most average value was selected but in fact that might not always give the best representation for that sample.

Hydrochloric acid, being acidic chloride, is extremely aggressive and thus severely damaging to, especially, 304 stainless steel. After all, acidic ferric chloride is used to rank the pitting resistance of stainless steels in ASTM G48. Pitting was observed on the surface of the ruthenium containing samples; this could of course alter the corrosion behaviour making it more erratic if pits start forming. During pitting corrosion the initially formed pits are then attacked by the chloride ions causing severe localised corrosion which could produce very different corrosion results depending on when the pit formation started, where it is positioned, the number of pits formed etc. This most certainly could have contributed to the variability of the results. In the presence of chlorides, it could have also been crevice corrosion which caused the variability, this was suspected to have occurred when the sodium chloride was added and could have played a role in these tests as well.

5.3.5.2 Current density vs potential responses

The 304L stainless steel sample in hydrochloric acid had a low corrosion potential, a long nose and extremely high current densities throughout the entire scan, both on a fresh surface and on a surface which has been exposed to the media for 12 hours. It has the shortest passive region and the highest passivation current density when comparing the sample in the various

environments studied in this research report as can be observed in Figure 139 and Figure 140; it is an extremely harsh environment. Previous research (Troselius, 1971) had already indicated that for austenitic stainless steel exposed to 1 M hydrochloric acid “no real passive region was formed before the onset of passivation”.

As ruthenium is added, even at 0.82 wt% Ru, the scan exhibits the transition shape with much reduced corrosion potentials, E_{corr} , and drastically reduced current densities. In fact the E_{corr} values seem to decrease with the increase in ruthenium content, steeper Tafel slopes are observed and a stable and long passive region is seen at very low current densities which were observed only for the 1 M sulphuric acid at 25°C; as per Figure 143 and Figure 144 for the 4.67 wt% Ru sample. Testwork conducted by Olubambi et al. (2009) showed that minor additions of ruthenium improved the corrosion resistance in sulphuric acid and hydrochloric acid; they however studied the additions for superferritic stainless steels. The results observed indicated that the ruthenium lowered the hydrogen over-potential and inhibited anodic dissolution which was also observed for these tests in, for example, achieving the transition shape implying direct passivation of the ruthenium containing steel.

During the exposed surface scan, it is observed that the 304L stainless steel has a long active nose but a stable passive region is occurring at potentials just below 0.2 V which is similar to the behaviour of the clad sample with only the 304L stainless; for that sample slightly higher current densities are observed. With the addition of ruthenium a drastic change is observed in the shape of the curve by forming a transition and orders of magnitude reduced current densities. The ranking order in terms of decreasing current density (i.e. improved corrosion protection) in the passive region is as follows: 0.82 wt% Ru, 2.92 wt% Ru, 2.44 wt% Ru and 4.67 wt% Ru. It can thus be said that corrosion rates decrease with an increase in ruthenium concentration in the 1 M hydrochloric acid solution. The 4.67 wt% Ru sample also showed the lowest E_{corr} values. The i_{corr} values, for example, were orders of magnitude higher in comparison with the samples tested in sulphuric acid at 25°C implying much higher corrosion rates. In the sulphuric acid environment with sodium chloride added at 25°C, i_{corr} values were similar for the non-ruthenium containing samples but for the ruthenium containing samples, in general, they were lower than in this environment. This points towards the harshness of these conditions for the metals tested.

Investigating the corrosion behaviour on a fresh surface is important as it indicates corrosion behaviour when no time has been given to build up the passive film. On a fresh surface area it

was observed, just like during the exposed surface scan, that all the ruthenium containing samples showed orders of magnitude lower current densities than the samples without ruthenium even though the actual values were in a much narrower current density range than the samples from the exposed surface scan. Both the samples without ruthenium behaved similarly even though the cladded surface showed greater corrosion activity on the fresh surface than on the exposed surface implying that no protective film was able to form. The ranking order is however not the same as during the exposed surface scans but has changed as follows, in order of decreasing current density in the passive region: 0.82 wt% Ru, 2.92 wt% Ru, 4.67 wt% Ru and 2.44 wt% Ru. This implies that considering both scans, the range of 2 – 5 wt% ruthenium is the most optimal in this severe environment.

Observing the scans carefully, it is very noticeable that jagged lines were dominant in the passive region during the anodic polarisation of the ruthenium containing samples; the samples without ruthenium did not observed this behaviour. This would suggest that the ruthenium, even though it shifts the entire scan to much reduced current densities, also causes this instability and in that way, promoting corrosion. For any application, it is important that the corrosion activity is stable and passivation is achieved in the exposed environment, materials showing instability are a big risk factor and would thus not be recommended for the application. The role of ruthenium is understood to promote passivity by depolarising the cathodic reaction but that is not entirely what can be observed in this environment. One possibility may be that the jagged appearance of the anodic plot is caused by a competition between passive film formation and destruction thereof, so that at any given potential the current fluctuates widely. As discussed in the previous section, chloride ions could be adsorbed onto the surface and replace the oxygen ions on the metallic surface layer forming a soluble metal chloride instead of metal oxide, destroying the passive film which causes additional corrosion instead of providing protection. This mechanism was described by Olubambi et al. (2009).

Visible damage was observed on the surfaces of all the ruthenium containing samples in the form of small indents or pits. It can be concluded that severe pitting corrosion, possibly also crevice corrosion, occurred on the ruthenium containing alloys in hydrochloric acid environments.

5.3.5.3 Open Circuit Potential vs time responses

The potential vs time graph showed that all OCP values were very close to each other in this environment: the highest values were obtained for the 0.82 wt% Ru sample as well as the 2.92 wt% Ru sample. All the values however, were large negative numbers. Stable values were observed for most of the duration of the scan which does imply that equilibrium was reached and for all the samples the stable values were reached quickly, i.e. within just over an hour. The initial slopes do vary, however, but no specific trend was observed to correlate their slope or shape to ruthenium content. This might seem to be in contradiction with the point raised about the passive layer instability but that instability might not be reflected in the measured current without any interference, as is the case with the polarisation scans.

The ranking order of the average OCP values after 12 hours of exposure confirmed that all the values were very close to each other as follows, in order of increasing value: 304L stainless steel blank sample, 2.44 wt% Ru, the cladded sample with 0 wt% Ru, 4.67 wt% Ru, 0.82 wt% Ru and the highest value was calculated for the 2.92 wt% Ru sample. This would also hint at the trend observed in 5.3.5.2 that the optimum amount of ruthenium in this environment is between 2 to 5 wt% Ru.

As discussed previously, if the ruthenium is unable to promote passivity it may increase the corrosion rate and would in that case certainly not be beneficial to corrosion protection. In the 1 M hydrochloric acid at 25°C it was observed that all the OCP values were smaller than the E_{pass} values, this statement is true for both the exposed and fresh surface scans. In all the samples, except the 4.67 wt% Ru sample, the E_{pass} value was smaller for the exposed surface scan compared to the fresh surface scan. There does not appear to be a trend in this environment with regards to the difference between the values. This implies that there is no passivity for any of the samples in the hydrochloric acid environment, irrespective of the presence of ruthenium. In the $\log i$ vs E graphs it was observed that jagged lines occurred which pointed towards the instability of the passive layer and in these results, active behaviour was observed.

5.3.5.4 Corrosion Rates summary

Due to the exceptionally inconsistent test results obtained, it is very difficult to draw conclusions about the average results obtained and comparing them to establish any trends. During the exposed surface scans, corrosion rate analysis is interesting as the lowest rate was

observed for the stainless steel blank sample, followed by the 2.44 wt% Ru and then the 4.67 wt% Ru sample. Polarisation resistance was highest for the 2.44 wt% Ru, and then the 4.67 wt% Ru followed by the 304 stainless steel sample. This would imply that the addition of a small amount of ruthenium is detrimental to the corrosion behaviour of the austenitic steel and only once at least 2.4 wt% of the precious metal is added do corrosion rates improve. On the fresh surface area corrosion rates are extremely high, lowest again for the stainless steel blank but all observed parameters are very inconsistent as can graphically be seen in the Results section (Figure 127 to Figure 135).

As suspected above, pitting corrosion and/or crevice corrosion might be responsible for this phenomenon as pits were actually observed on the surface of the ruthenium samples after testing. Both pitting and crevice corrosion are localised forms of corrosion. Pitting is considered to be more dangerous than uniform corrosion damage because it is more difficult to detect, predict and thus design against; this is mainly due to its inconstancy. The mechanism of pitting corrosion is the same as that for crevice corrosion, they occur due to the depassivation of a small localised area on the surface of the sample which becomes anodic while the remaining area becomes cathodic, leading to very localised galvanic corrosion. The ions taking part in the corrosion reactions penetrate into the metal with limited diffusion creating deep visible pits or crevices.

5.3.5.5 Comparison of different stainless steels

After exposure to the hydrochloric acid for 12 hours, it was observed that the 304L stainless steel had the highest current densities and thus the highest corrosion rates illustrating the harshness of this environment for this type of steel. The 316 stainless proved not to be much more suitable under these conditions with similarly high current densities and no passive region able to form. The two ruthenium containing samples had much lower corrosion potentials than the remainder of the samples, displayed the lowest current densities throughout the scan with a transition shape and seemingly instability occurring in the passive regions. The SAF2205 displayed a small active nose, slight instability at the onset of passivation but thereafter a stable passive region with current densities similar to the ones observed from the ruthenium containing samples. The Hastelloy had the highest E_{corr} value and a stable passive region with similar current density values compared to the SAF material.

On a fresh surface a similar trend is observed except that the ruthenium containing samples, the SAF2205 and Hastelloy C276 samples had results within a narrow current density range which was much lower than the remaining sample results. From a technical point of view the ruthenium samples certainly could compete with existing types of steel suitable for this environment. It must be noted however, that the Hastelloy had the most stable passive region from all the samples tested. The 304L and 316 stainless steels behaved similarly showing that they are not the materials of choice in this environment from a corrosion point of view. It is suggested that a ferritic stainless steel be tested in this environment as these have specifically outstanding corrosion resistance properties especially with regards to reducing pitting and crevice corrosion (Olubambi et al., 2009).

The open circuit potential observed for all these samples over a 12 hour period indicated that these potentials stabilised very quickly. All the sample results obtained were around the same value, a relatively large negative number, except the Hastelloy C276 which did not show as stable a line but at significantly higher values. In this case the OCP value was greater than the E_{corr} value indicating passivity. No other samples showed clear passive behaviour during this comparison. This seems to suggest that the most suitable material in this environment is the C276 and should be used if possible and economics permit it.

5.3.6 Cost analysis of the ruthenium alloys

It is important in the development of any new product or alloy to ensure that it is cost effective, else there will be only very limited scope for application. In this case, the various compositions of ruthenium in the stainless steel need to be evaluated for cost-effectiveness and compared to other existing materials offering similar corrosion protection. A comparison was made using an average 304L stainless steel price, allowing only for an 8 mm sheet with a specified ruthenium and stainless alloy cladded onto that sheet. Only material costs (AK Steel, 2014 and SMT, 2014) were taken into account for this exercise and no handling or processing costs; the purpose was just to identify any merit in continuing to investigate such claddings. The findings are represented in Table 21. All costs given are per m^2 of the sheet.

Table 21: Cost analysis of only the material costs for the different ruthenium claddings in Rand

	304L + 1 wt% Ru	304L + 2 wt% Ru	304L + 3 wt% Ru	304L + 4 wt% Ru	304L + 5 wt% Ru
with 800 μm coating	R 3996.23	R 5295.82	R 6595.42	R 7895.02	R 9194.61
with 500 μm coating	R 3416.95	R 4229.20	R 5041.44	R 5853.59	R 6665.94
with 400 μm coating	R 3223.86	R 3873.65	R 4523.45	R 5173.25	R 5823.05
with 200 μm coating	R 2837.67	R 3162.57	R 3487.47	R 3812.37	R 4137.27
with 100 μm coating	R 2664.58	R 2807.08	R 2969.47	R 3131.92	R 3294.37
with 50 μm coating	R 2548.08	R 2629.25	R 2710.48	R 2791.70	R 2872.93

- A 304L blank stainless steel sheet, 8 mm thick, costs R 2451.48
- A 316 stainless steel sheet, 8 mm thick, costs R 3223.25; i.e. approx. 31.5% more
- A SAF2205 stainless steel sheet, 8 mm thick, costs R 4388.46, i.e. approx. 79.0% more and
- A Hastelloy C276[®] sheet, 8 mm thick, costs R 68 640.00, i.e. approx. 2700% more

Therefore, if a 5 wt% Ru coating was required, it could only be 100 – 200 μm thick if it were to replace a 316 stainless steel or SAF2205; such thickness is impossible to achieve at this stage with the laser cladding process. If a 3 wt% Ru coating was sufficient, it could be up to 500 μm thick to compete with a SAF2205 on the material costs only, which is the minimum thickness that can be achieved with the laser cladding. A different technique needs to be looked at in order to reduce the applied ruthenium alloy thickness. The Hastelloy is so expensive that almost any quantity of ruthenium alloyed with 304L stainless steel would be cost effective providing that it can demonstrate equivalent corrosion protection.

In the 1 M sulphuric acid at 25°C, the ruthenium containing alloys indicated good corrosion protection, certainly a marginal improvement compared to the 316 stainless steel but seemed not be able to compete with the SAF2205 or Hastelloy materials. Therefore comparing the cost from Table 21 against the SAF2205 material or the Hastelloy, it would remain beneficial to use the existing material in this environment unless a 200 μm coating or less would be

sufficient in the application. This however, is also only true if the actual application costs for the alloyed layer were minimal and such a thin layer was technically achievable.

When chloride ions were added, i.e. in the 1 M sulphuric acid with 1% sodium chloride at 25°C, the ruthenium containing samples performed well on both the fresh and exposed surfaces. The 316 stainless steel can certainly not compete with them from a corrosion point of view, but the Hastelloy behaves similarly and the SAF2205 duplex demonstrated lower current densities and thus corrosion rates; at least for the limited testwork conducted. From a technical point of view it does not seem necessary to investigate the ruthenium option further. From an economic point of view, however, it might still be worth looking at them if a layer of less than 200 µm could be applied and application costs are low.

No tests were carried out to compare the various steels with the ruthenium containing 304L stainless steel in the 1M sulphuric acid media at 45°C.

In a solution consisting of 1 M sulphuric acid with the addition of 1% sodium chloride at 45°C, the ruthenium samples did show improved corrosion resistance compared to the 304L stainless steel but still demonstrated active corrosion on a fresh surface and after equilibrium was reached. The 316 stainless steel and SAF2205 behaved similarly showing improved corrosion protection compared to the ruthenium containing materials but by far the best material in this harsh environment is the Hastelloy C276. No cost comparison would provide different results except if higher concentrations of ruthenium were to be tested and revealed further improvement in corrosion rates which could compete with the existing materials. The trend however showed that this is unlikely as corrosion parameters were levelling off even before the 5 wt% Ru and further increases in ruthenium addition would also increase the cost of the material.

The 1 M hydrochloric acid is a harsh environment for the 304L stainless steel for which it is not ideally suited, neither is the 316 stainless steel. The 2 – 5 wt% Ru range seems to be optimal for corrosion protection showing a significant improvement in current density values but instability in the passive range. In fact, lower amounts of ruthenium seemed to have a detrimental effect on corrosion rates. The SAF2205 is compatible with the high ruthenium samples in this environment but the most ideal material, from the limited range tested, to be used in this environment is Hastelloy C276. Due to its absorbent cost, it is always specified with caution, therefore further ruthenium concentrations alloyed with the 304L stainless steel

should be tested in this environment to observe if it can be technically as well as economically effective. There is certainly scope for it.

6. Conclusion

It is well reported in the literature (Sherif et al., 2009) that “the corrosion resistance of virtually all stainless steels can be remarkably increased by alloying them with minor additions of platinum group metals”. It is suggested that the PGMs retard the anodic dissolution of the stainless steel alloy and increase the effectiveness of the cathodic processes due to the reduced overvoltage of hydrogen on them. It was the aim of this report to investigate varying ruthenium additions (targeting 0.0, 1.0, 2.0, 3.0, 4.0 and 5.0 wt% Ru) to 304L stainless steel, applied by laser cladding the alloy onto the stainless steel surface, and monitoring their corrosion properties in acidic media as well as comparing that to other commercially available stainless steels. The microstructure and chemical composition of the produced alloys was investigated in order to relate them to the corrosion resistance observed, in terms of OCP and fresh as well as exposed surface anodic scans. The media studied were 1 M sulphuric acid, 1 M sulphuric acid with the addition of 1% sodium chloride and 1 M hydrochloric acid at both 25°C and 45°C. This was meant to improve the existing knowledge in this field and decide on future research and possible industrial applications.

The laser surface cladding method was able to add small amounts of ruthenium to clad stainless steel but with significant variability. A layer of consistent thickness of approximately 770 µm was obtained but the variability introduced by the addition of ruthenium powder caused inconsistencies in the results. Ruthenium-rich islands and strings were observed throughout the alloyed layer causing the bulk concentration to be less than the targeted value. The inconsistency of the cladded layer increased with an increase in the ruthenium composition. It is assumed that for every test, a slightly different ruthenium composition was exposed which caused the variability of the electrochemical results obtained. Sufficient testing was conducted, however, to be able to average results and compare representative curves to each other so that technically sound conclusions could be drawn which are presented in this research report.

In general, the addition of ruthenium to the 304L stainless steel improved its corrosion protection in 1 M sulphuric acid, 1 M sulphuric acid with the addition of 1% sodium chloride as well as in 1 M hydrochloric acid. This was observed looking at a number of parameters such as current densities and thus corrosion rate, corrosion potential, OCP value and polarisation resistance. Increasing ruthenium content would seem to improve passivation, however, the amount of ruthenium added was not directly proportional to the rate of

passivation. There exists an optimum ruthenium concentration to be added for a specific environment.

For the 1 M sulphuric acid solution at 25°C the overall best corrosion protection is obtained in the range of 0.8% Ru to 3% Ru by weight, thereafter it seems to be levelling off for most parameters. All the samples, including the 304L blank and cladded layer without ruthenium, showed passive behaviour in this environment while the ruthenium was able to reduce the active dissolution of the metal and stabilise the passive film formation. Other commercially available steels such as SAF2205 and Hastelloy C276 showed equally good corrosion protection in this environment and thus the ruthenium coating at the optimum composition would only be commercially beneficial if less than 200 µm thin.

Environments contaminated with chloride ions are destructive to the formation of a passive layer in stainless steel increasing their corrosion rate; this was still applicable to the ruthenium cladded samples even though corrosion protection was substantially improved. In the 1 M sulphuric acid with 1% sodium chloride at 25°C, the observed corrosion parameters showed a clear trend of reduced corrosion activity with an increase in ruthenium additions. There was a big step increase in corrosion protection with even a small addition of ruthenium. As observed before, SAF2205 and Hastelloy C276 showed equivalent or improved corrosion protection in this environment and a ruthenium cladding would only be considered financially viable if much less than 200 µm thin.

Increasing the temperature of the 1 M sulphuric acid environment to which the samples were exposed to, to 45°C, increased the corrodibility of the samples by increasing the rate of the reactions taking place on the surface of the metal and thus the rate of corrosion observed. All samples tested in this environment experienced active corrosion; passivity had not been achieved at elevated temperatures. The ruthenium additions, however, significantly reduced corrosion activity on the surface of the metal which was most evident for the range of 3 to 5 wt% Ru.

Tests conducted in 1 M sulphuric acid with 1% sodium chloride at 45°C was an exceptionally harsh environment for the 304L stainless steel and even the additions of ruthenium could not achieve passivity for any of the samples tested. A notable improvement in corrosion protection was observed with the addition of ruthenium under these conditions but adding more ruthenium did not show any additional benefit for the ruthenium range observed, in fact, most parameters started levelling off at/or before the 4.67 wt% Ru. The 316 stainless

steel as well as the SAF2205 provided improved corrosion protection compared to the ruthenium containing 304L stainless steel but by far the best corrosion protection is observed in the Hastelloy. Its great cost is a deterrent in specifying it more often and thus the ruthenium coating is being investigated for such conditions as these.

Hydrochloric acid is extremely aggressive to stainless steel and pitting, possibly crevice corrosion, were observed on the sample surfaces after each test. Variability of the samples tested was a concern only in this environment. The 2 – 5 wt% Ru range seems to be optimal for corrosion protection showing a significant improvement in current density values but instability in the passive region which is most evident at the smaller additions of ruthenium. It seemed that the chlorides displaced the oxygen on the surface layer forming metallic chlorides which had the opposite effect that a protective layer normally has. The SAF2205 is compatible with the samples containing the most amount of ruthenium but technically, by far the most preferred material to use in this environment is the Hastelloy. It is suggested that more tests are conducted, at higher ruthenium concentrations to find and optimise the conditions in which it is most beneficial.

The addition of ruthenium to the 304L stainless steel did not indicate to have had any negative effects on its microstructure, in fact the rapid cooling process introduced a fine microstructure which is assumed to have had a beneficial effect on the ruthenium distribution and thus enhance its ability to shift the hydrogen over potential. The methods in which the ruthenium is achieving improved corrosion resistance when alloyed with 304L stainless steel point towards two mechanisms already described in the literature (Potgieter et al., 1995). They attributed the corrosion resistance of the ruthenium alloys to a combined effect of cathodic modifications causing improved hydrogen evolution efficiencies which shift corrosion potentials towards more noble values and the inhibition of anodic dissolution (a decrease in the i_{crit} values). It seems, as per Tjong et al. (1997), that ruthenium accumulates on the surface of the alloy and there promotes the efficiency of hydrogen evolution moving the corrosion potential into the noble direction and in some cases, resulting in spontaneous passivation. Ruthenium additions enhance the passivating layer that is formed in corrosive environments; however, ruthenium clad samples behaved differently in different environments and hence their application should be carefully selected.

7. Recommendations

7.1 Further testwork with the available samples

The testwork conducted has been interesting and most valuable; the ruthenium alloyed with 304L stainless steel can have great benefit in some of the media studied. It is suggested that the samples remaining can be used for further investigations: nitric acid could be tested to verify how these samples can protect the steel in such a harsh environment, it is also suggested that temperatures are increased to perhaps 70°C to determine how ruthenium can reduce the active dissolution at such high temperatures and higher concentrations should be tested of the media already studied, i.e. an increase from the 1 molar solutions to perhaps 2 molar. All these recommendations are common industrial concerns and could establish ruthenium as the preferred alloying material for all the three big acid applications, at elevated temperatures and high concentrations. Often materials are selected for risk scenarios which include contact with other materials used in the facility, exposure to elevated temperatures and if compositions are made up incorrectly. Having performed such extensive testwork on this material would potentially make it suitable for a wide range of applications.

Where testwork indicated that the ruthenium concentrations are not sufficient, it might be worthwhile to find an application process to accurately alloy a larger concentration of ruthenium with the 304L stainless steel for comparisons.

As the applicability of the material is established for certain conditions in industry, further research into better and cheaper application methods can be conducted. Initially it is critical to establish what corrosion related improvements ruthenium is capable of achieving and under what conditions.

7.2 Application method

This research aimed at testing if the laser cladding technique with ruthenium was feasible and how corrosion resistant the stainless steel could become with the addition of small amounts of ruthenium. It was established that ruthenium does significantly improve the corrosion resistance of the material in certain environments, more economical methods of applying the ruthenium onto/ into the stainless steel can be investigated in future research. Higher than 5 wt% concentrations of ruthenium have not given good distribution of the ruthenium during the cladding process (Masiu, 2013), these have therefore not been investigated but with a

different method, this could be reevaluated. The laser cladding method has introduced significant variability, even at very low concentrations of ruthenium; this is not ideal for consistent corrosion protection in industrial applications and therefore the method of introducing the ruthenium into the stainless steel should be further investigated. If laser cladding is preferred however, a more accurate method of application with the laser must be investigated. It is suggested to pre-melt the ruthenium and stainless steel powders in the targeted concentrations to alloy the metals before application to the base plate. A fine powder can then be obtained from that alloy to be used in the laser cladding application rather than using a premixed powder from raw stainless steel powder and ruthenium powder.

Another option is to use the ruthenium only in the welding applications of stainless steel to ensure that, this normally weak spot for corrosion, does not remain the weak point. Testwork has been conducted with different types of welding techniques using Ni-Cu-Ru welding consumables where these have improved the corrosion performance for 300-series austenitic stainless steels, Liang et al. (2010).

In addition to that, it is recommended to investigate a variety of other existing surface applications, for example, electroplating ruthenium only onto the stainless steel surface, so that large surfaces could be covered. This way the ruthenium would be creating a corrosion resistant barrier between the environment and the stainless steel. This should be investigated further to establish industrial applications. The method to be sought must not only include consistency of the ruthenium distributed throughout the stainless steel, it also has to consider the complexity of the process with regards to labour and machinery requirements, its flexibility in terms of where and how it can be applied even looking at retrofitting and refurbishing existing equipment or structures; the cost of application and how time consuming it will be. All these need to be optimised in order to compete with existing types of materials.

7.3 Alternative corrosion prevention to be tested

Pickle and passivation of the stainless steel as well as the ruthenium and stainless steel samples could be considered for additional corrosion protection. This process is a very common method to treat stainless steel and it should be analysed to confirm what effect it will have on the obtained corrosion prevention. It is assumed to add some benefit but that will have to be tested if that is possible with the stainless steel alloyed with ruthenium.

In practice, many corrosion protection activities involve simply the application of a permanent over-potential, measured and calculated as per the specific conditions, to the steel structure or equipment. For further research, it would be advisable to test this, i.e. to check the application of an over-potential to stainless steel and comparing its corrosion protection with that of the ruthenium containing stainless steel. The continual cost for electricity must then be weighed against the initial cost of the ruthenium and its application to the stainless steel. It is understood that the application of the potential is not always effective because one might have a crevice that forms where the potential is not controlled, skewing the results. It is however something that needs to be considered and investigated for a complete solution to the problem.

7.4 Industrial applications

In order to find actual applications in industry the economic evaluation must be favourable compared to other materials used and industrial requirements and concerns must be addressed in the research. There are many processes where equipment is exposed to acidic solutions such as the pulp and paper as well as the chemical processing industries. In the oil and gas industry, for example, it is of real interest to investigate the material's effect on resistance to seawater (304L is significantly affected by pitting corrosion in seawater) and, of course, resistance to chloride-induced stress corrosion cracking (SCC). There are also standard tests for determining the critical crevice temperature (CCT) and critical pitting temperature (CPT) which have not formed part of this research but should be looked at for the ruthenium and stainless steel alloy for future industrial applications.

It is already known that ruthenium doped standard 304 austenitic stainless steel is less susceptible to intergranular SCC than the standard 304 austenitic stainless steel in high temperature water (Scenini et al., 2012). This was observed by a greater strain to failure.

The marine environment often uses duplex stainless steels which are known to have good corrosion resistant properties against chloride ion attack. The ruthenium doped 304L stainless steel should be tested in these conditions, i.e. using aerated sodium chloride solutions, as well. Often the sodium chloride content of the sea water is 3 – 4 wt% and tests conducted during this research only included an acidic media with a 1 wt% sodium chloride solution.

Wear and abrasion resistance are two critical parameters and one of the reasons why stainless steel is selected in certain applications. It must be thoroughly tested to ensure that these are

not negatively affected by the introduction of the ruthenium. A research report by Masiu (2013) considered hardness tests on these samples indicating that they were of the same hardness as 304L stainless steel: there was no improvement nor was there deterioration in the hardness of the material with the introduction of the ruthenium. It is known that the hardness of cemented tungsten carbide (WC-Co) increases and the toughness decreases with increasing the ruthenium content (Shing et al., 2001). During the same experimentation they also found that ruthenium improved the abrasion resistance of the material which was, however, attributed to the hardening of the binder phase. It is therefore assumed that the abrasiveness of 304L stainless steel would improve with the ruthenium addition but this has not been established yet and should be investigated in future research. This is important for any industrial applications such as in the usage of pumps and centrifuges.

7.5 Analytical questions

The lack of XRD analysis has been recognised for this report but was considered beyond the scope investigated. It is suggested to be considered in future research in this field.

It is suggested to analyse where the ruthenium actually sits within the crystal structure, for example with an Electron Probe Microanalyser (EPMA). A more detailed analysis should be conducted to reveal ruthenium concentrations at the grain boundaries, on the surface and perhaps more uniform distribution apart from the isolated large islands mentioned already. This is absolutely relevant when explaining corrosion behaviour but was beyond the scope of this report. It is especially critical to perform these tests before the sample is exposed to a certain environment and then again immediately afterwards as this will provide insight into the method of metal dissolution occurring at the surface and establish exactly how the ruthenium is contributing towards the corrosion protection of the base metal. The surface analytical techniques commonly used to determine the surface chemistry of passive films are Auger Electron Spectroscopy (AES) and X-ray Photoelectron Spectroscopy (XPS) which is even able to distinguish between the oxidation states of the passivating species. This could lead to the determination of the mechanism for passivation.

8. References

Ahmad Z. (2006) 'Principles of Corrosion Engineering and Corrosion Control', 1st edition, Oxford, UK, Butterworth-Heinemann is an imprint of Elsevier Ltd.

'AK Steel Specialty Stainless Sheet & Strip Stainless Price Schedule' (2014), [Electronic], Available: <http://www.aksteel.com> [23 July 2014]

Allen L.C. (1989) 'Electronegativity is the average one-electron energy of the valence-shell electrons in ground-state free atoms', Journal of the American Chemical Society, vol. 111, no. 25, pp. 9003-9014

Al Subai S., Barai K., Esteban M. and Murillo E.M. (2014) 'Failure analysis of firewater pipeline', presented at EuroCorr 2014, P-7738, pp. 549

Aoki A., Sasaki K.M., Watanabe H. and Ishikawa I. (2004), 'Lasers in nonsurgical periodontal therapy', Periodontology 2000, vol. 36, issue 1, pp. 59-97, [Electronic], Available: <http://www.wiley.com> [23 July 2014]

Asteman H., Svensson J.E., Johansson L.G. and Nrell M. (1999) 'Indication of Chromium Oxide Hydroxide Evaporation During Oxidation of 304L at 873 K in the Presence of 10% Water Vapor', Oxidation of Metals, vol. 52, pp. 95-111

Australian Stainless Steel Development Association (ASSDA) homepage (2014) [Online], Available: <http://www.assda.asn.au> [3 Oct 2014]

Banda S.C.K. and van der Merwe J. (2014) 'Effects of small additions of ruthenium on pitting corrosion resistance of LDX2101 duplex stainless steel', Corrosion Engineering, Science and Technology, vol. 49, no. 1, pp. 32-38

'Basics of Corrosion Measurements' (2014), Princeton Applied Research, Application Note CORR-1, [Electronic], Available: www.princetonappliedresearch.com [11 Dec 2014]

Beyer E.H., Brenner B. and Nowotny S. (2004) Proceedings of the 1st Pacific International Conference on Application of Lasers and optics, pp. 1-6

Bradford S.A. (2001) 'Corrosion Control', 2nd edition, Edmonton, Alberta T5H 3J7, Canada, CASTI Publishing Incorporation

British Stainless Steel Association homepage (2014) [Online], Available: <http://www.bssa.org.uk> [26 Nov 2014]

Butler J. (2011) 'Platinum 2011', Johnson Matthey PLC, England, pp. 5, [Electronic], Available: www.platinum.matthey.com [15 Sep 2014]

Butler J. (2012) 'Platinum 2012', Johnson Matthey PLC, England, pp. 45, [Electronic], Available: www.platinum.matthey.com [15 Sep 2014]

Charles J., Mithieux J.D., Santacreu P.O. and Peguet L. (2007) 'The Ferritic Stainless Steel Family: The Appropriate Answer to Nickel Volatility?' [Electronic], Available: <http://www.outokumpu.com/en/stainless-steel/grades/ferritic> [16 Sep 2014]

'Corrosion and Corrosion Properties of Stainless Steels: Part Three' (2008), [Online], Available: <http://www.keytometals.com> [17 Dec 2014] Exeter: Author.

Crawford G. (2014) 'No Sacred Cows: Mice, Men, Marketing and Metallurgy', Stainless Steel, second quarter, quoting the May 2014 report by the International Stainless Steel Forum (ISSF)

Davis J.R. (1994) 'Stainless Steels' 3rd edition, ASM International

De la Fuente D., Morcillo M., Ivanshechkin P., Colla V., Branca T.A., De Sanctis M., Vivas B.P., Cabanas M., Rassow A. and Lucca C. (2014) 'Sustainable water and facility management in the steel industry: influence of saline streams on pipeline corrosion', presented at EuroCorr 2014, P-7566, pp. 210

Diminich M., Mari F., Bazzoni B., Lecardi G., Caglioni T. and Duranti F. (2014) 'Cathodic protection assessment of oil storage tank farm', presented at EuroCorr 2014, O-7754, pp. 493

'Duplex Stainless Steels: Part One' (2007), [Online], Available: <http://www.keytometals.com> [3 Dec 2014] Exeter: Author.

Ebbing D.D. (1990) 'General Chemistry', 3rd edition, Houghton Mifflin

Facts and Figures (2012) Chamber of Mines, Johannesburg, South Africa, [Electronic], Available: www.chamberofmines.org.za, [15 Sep 2014]

Fontana M.G. (1986) 'Corrosion Engineering', 3rd edition, McGraw-Hill Book Company, New York USA

Govender K., Scenini F., Lyon S. and Sherry A. (2012) 'Influence of Pd and Ru additions on stress corrosion cracking of austenitic stainless steels', Corrosion Engineering, Science and Technology, vol. 47, no. 7, pp. 507-515

Henkel G. and Henkel B. (2003) 'Information on Passivation Layer Phenomena for Austenitic Stainless Steel Alloys', Technical Bulletin provided by Henkel, Essay No 45, pp. 1-12

Higginson A., Newman R.C. and Procter R.P.M. (1989) 'The passivation of Fe-Cr-Ru Alloys in Acidic Solutions', Corrosion Science, vol. 29, pp. 1293-1318

Hoyle R.A.S. and Taylor D.E. (1993) 'Effects of chlorinated hydrocarbons on the corrosion resistance of austenitic stainless steels in chloride solutions', quoted by Datta P.K. and Gray

Ibrahim M.A.M., Abd El Rehim S.S. and Hamza M.M. (2009) 'Corrosion behavior of some austenitic stainless steels in chloride environments', Materials Chemistry and Physics, vol. 115, pp. 80-85

Jones D.A. (1996) 'Principals and Prevention of Corrosion', 2nd edition, Upper Saddle River, New Jersey, Prentice Hall Inc.

Kajiyama F. (2014) 'Electrochemical phenomenon of a.c. corrosion likelihood of cathodically protected steel pipelines', presented at EuroCorr 2014, O-7148, pp. 486

Kelly E.J. (1965) 'The active iron electrode: Iron dissolution and hydrogen evolution reactions in acidic sulphate solutions', Journal of International Money and Finance, vol. 33, pp. 306-326

Kittel J., Bonis M. and Perdu G. (2014) 'Mitigating corrosion in sweet gas units: a comparison between laboratory data and field survey', presented at EuroCorr 2014, O-7811, pp. 608

Koetz E.R. and Stucki S. (1987) 'Ruthenium dioxide as a hydrogen-evolving cathode', Journal of Applied Electrochemistry, vol. 17, pp. 1190-1197

Koch G.H, Brongers M.P.H., Thompson N.G., Virmani Y.P. and Payer, J.H. (2014) 'Corrosion Costs and Preventative Strategies in the United States', published by NACE International for the US Department of Transport, Federal Highway Administration, Publication number FHWA-RD-01-156

Kotz J.P. and Purcell K.F. (1991) 'Chemistry and Chemical Reactivity', 2nd edition, Saunders College Publishing, Pub., Philadelphia, USA

Kuroda S., Kawakita J., Watanabe M. and Katanoda H. (2008) 'Warm spraying-a novel coating process based on high-velocity impact of solid particles', Science and Technology of Advanced Materials, vol. 9, pp. 17-33

Laurence R. (2014) April 14, discussion regarding welding techniques

Lekala M.B., van der Merwe J.W. and Pityana S.L. (2012) 'Laser Surface Alloying of 316L Stainless Steel with Ru and Ni Mixtures', International Journal of Corrosion, pp. 1 - 4

Liang D., Sowards J.W., Frankel G.S., Alexandrov B.T. and Lippold J.C. (2010) 'Corrosion resistance of welds in type 304L stainless steel made with a nickel-copper-ruthenium welding consumable', Corrosion Science, vol. 52, pp. 2439-2451

London Metal Exchange homepage (2014) [Online], Available: <http://www.LondonMetalExchange.co.uk> [3 Feb 2014]

Lorenz W.J. and Mansfeld F. (1981) 'Determination of corrosion rates by electrochemical DC and AC methods', Corrosion Science, vol. 21, pp. 647-672

Lu Y.C. and Ives M.B. (1995) 'Chemical treatment with cerium to improve the crevice corrosion resistance of austenitic stainless steels', Corrosion Science, vol. 37, issue 1, pp. 145-156

Maass P. (2013) 'Corrosion and Corrosion Protection', Wiley-vch Books, [Electronic], Available: www.wiley-vch.de/books [13 Oct 2014]

MacSteel homepage (2014) [Online], Available: <http://www.MacSteel.co.za> [10 Jan 2014]

Martinez S. and Stern I. (2001) 'Inhibitory mechanism of low-carbon steel corrosion by mimosa tannin in sulphuric acid solutions', *Journal of Applied Electrochemistry*, vol. 31, pp. 973-978

Masiu P. (2013) 'The Corrosion Analysis of Stainless Steel Laser Surface Alloyed with Ruthenium', submitted as her final year laboratory project to the University of Witwatersrand, School of Chemical and Metallurgical Engineering, not published

Maskall K.A., White D. (1986) 'Vitreous Enamelling: A Guide to Modern Enamelling Practice', *The Pergamon Materials Engineering Practice Series*, 1st edition, Pergamon Press, on the behalf of The Institute of Ceramics, ISBN 0-08-0334288

McGill I.R. (1990) 'Platinum Metals in Stainless Steels – A Review of Corrosion and Mechanical Properties', *Platinum Metals Review*, vol. 34, pp. 85-97

Myburg G., Varga K., Barnard W.O., Baradlai P., Tomcsányi L., Potgieter J.H., Louw C.W. and van Staden M.J. (1998) 'Surface composition of Ru containing duplex stainless steel after passivation in non-oxidising media', *Applied Surface Science*, vol. 136, pp. 29-35

Noren D.A. and Hoffman M.A. (2005) 'Clarifying the Butler–Volmer equation and related approximations for calculating activation losses in solid oxide fuel cell models', *Journal of Power Sources*, vol. 152, pp. 175-181

Oerlikon Metco homepage (2014) [Online], Available: <http://www.oerlikon.com/metco> [15 Oct 2014]

Olaseinde O.A., van der Merwe J.W., Cornish L.A., Chown L.H and Olubambi P.A. (2012) 'Electrochemical studies of Fe-21Cr-1Ni duplex stainless steels with 0.15 wt% ruthenium at different temperatures', *Journal of the Southern African Institute of Mining and Metallurgy*, vol. 112, supplement 1, pp. 535-538

Olubambi, P.A., Potgieter, J.H. and Cornish, L. (2009) 'Corrosion behaviour of superferritic stainless steels cathodically modified with minor additions of ruthenium in sulphuric and hydrochloric acids', *Materials and Design*, vol. 30, pp. 1451-1457

Outokumpu Stainless Steel Oy (2004) 'Outokumpu Stainless Corrosion Handbook', 9th edition, Espoo, Finland, Outokumpu Stainless Steel Oy

Pardo A., Feliu Jn. S., Merino M.C., Arrabal R. and Matykina E. (2010) 'Electrochemical Estimation of the Corrosion Rate of Magnesium/Aluminium Alloys', International Journal of Corrosion, article ID 953850

Pawlowski L. (2008) 'The Science and Engineering of Thermal Spray Coatings', 2nd edition, John Wiley & Sons, Ltd [Online], Available: <http://onlinelibrary.wiley.com> [13 August 2014]

Perry R.H. and Green D. (1984) 'Perry's Chemical Engineers' Handbook', 6th edition, McGraw-Hill Book Co., Singapore

Potgieter J.H. and Brookes H.C. (1995) 'Corrosion Behavior of a High-Chromium Duplex Stainless Steel with Minor Additions of Ruthenium in Sulfuric Acid', Corrosion Engineering, pp. 312-320

Potgieter J.H., Ellis P. and van Bennekom A. (1995) 'Investigation of the Active Dissolution Behaviour of a 22% Chromium Duplex Stainless Steel with Small Ruthenium Additions in Sulphuric Acid', ISIJ International, vol. 35, pp. 197-202

Potgieter J.H., Heyns A.M. and Skinner W. (1990) 'Cathodic modification as a measure of improving the corrosion resistance of alloys', Journal of Applied Electrochemistry, vol. 20, pp. 711-715

Potgieter J.H., Thanjekwayo N., Olubambi P., Maledi N. and Potgieter-Vermaak S.S. (2011) 'Influence of Ru additions on the corrosion behaviour of WC-Co cemented carbide alloys in sulphuric acid' Int. Journal of Refractory Metals and Hard Materials, vol. 29, pp. 478-487

Princeton University homepage (2014) [Online], Available: <http://www.princeton.edu> [13 Oct 2014]

Rao C., Trivedi D. (2005) 'Chemical and electrochemical depositions of platinum group metals and their applications', Coordination Chemistry Reviews, 249 (5–6), pp. 613

Rebak R.B. and Dolley E.J. (2014) 'Effect of Superheated Steam on the Corrosion Behaviour of Advanced Steels proposed as Accident Tolerant Fuel Cladding', presented at EuroCorr 2014, O-7283, pp. 85

Roberge P.R. (2006) 'Corrosion Basics: An Introduction' 2nd edition, NACE Press Book

Roymech company homepage (2014) [Online], Available: <http://www.roymech.co.uk> [13 Oct 2014]

Salgado-Lopez J.M. and Rubio-Gonzalez C. (2015) 'Handbook of Materials Failure Analysis and Case Studies from the Oil and Gas Industry', 1st edition, The Boulevard, Langford Lane, Kidlington, Oxford OX5 1GB, UK, Butterorth Heinemann (inprint of Elsevier)

Scenini F., Govender K., Lyon S. and Sherry A. (2012) 'Stress corrosion cracking of Ru doped 304 stainless steel in high temperature water', Corrosion Engineering, Science and Technology, vol. 47, no. 7, pp. 498-515

Shepeleva L., Medres B. and Kaplan W.D. (2000) 'Laser cladding of turbine blades', Surface and Coatings technology, vol. 125, no. 1, pp. 45-48

Sherif E.M. (2012) 'Corrosion of Duplex Stainless Steel Alloy 2209 in Acidic and Neutral Chloride Solutions and its Passivation by Ruthenium as an Alloying Element', International Journal of Electrochemical Science, pp. 2374-2388

Sherif E.M., Potgieter J.H., Comins J.D., Cornish L.A., Olubambi P.A. and Machio C.N. (2009) 'Effects of minor additions of ruthenium on the passivation of duplex stainless-steel corrosion in concentrated hydrochloric acid solutions', Journal of Applied Electrochemistry, vol. 39, pp. 1385-1392

Sherif E.M., Potgieter J.H., Comins J.D., Cornish L.A., Olubambi P.A. and Machio C.N. (2009) 'The beneficial effect of ruthenium additions on the passivation of duplex stainless steel corrosion in sodium chloride solutions', Corrosion Science, vol. 51, pp. 1364-1371

Shing T.L., Luyckx S., Northrop I.T. and Wolff I. (2001) 'The effect of ruthenium additions on the hardness, toughness and grain size of WC-Co', International Journal of Refractory Metals & Hard Materials, vol. 19, pp 41-44

Stefanov P., Stoychev D., Stoycheva M. and Marinova T.S. (2000) 'XPS and SEM studies of chromium oxide films chemically formed on stainless steel 316 L', Materials Chemistry and Physics, vol. 65, issue 2, pp. 212-215

Stern M. and Geary A.L. (1957) 'Electrochemical Polarization: I. A Theoretical Analysis of the Shape of Polarization Curves', *Journal of Electrochemical Society*, vol. 104, no. 1, pp. 56-63

Strafford K.N., Subramanian C. and Wilks T.P. (1993) 'Characterisation and quality assurance of advanced coatings', quoted by Datta P.K. and Gray J.S. (ed.) (1993b) 'Surface Engineering Volume 2: Engineering Applications', pp. 259-284, Royal Society of Chemistry, Cambridge, UK

Streicher M.A. (1977) 'Alloying Stainless Steels with the Platinum Metals: Increased resistance to corrosion in acids', *Platinum Metals Review*, vol. 21, pp. 51-55

Sun Y., Li X. and Bell T. (1999) 'Low temperature plasma carburising of austenitic stainless steels for improved wear and corrosion resistance', *Surface Engineering*, vol. 15, issue 1, pp. 49-54

Swartzendruber L.J. and Sundman B. (1983) 'The Fe-Ru (Iron-Ruthenium) System', *Bulletin of Alloy Phase Diagrams*, vol. 4, no. 2, pp. 155-165

Talbot D.E.J. and Talbot J.D.R. (2007) 'Corrosion Science and Technology', 2nd edition, CRC Press

The Stainless Steel Information Centre (2014) [Online], Available: <http://www.ssina/overview/alloyelements-intro.html> [3 Nov 2013]

The Thermal Spray Depot home page (2014) [Online], Available: <http://thermalspraydepot.com/Laser-Cladding.html> [20 Nov 2014]

Tjong S.C. (1989) 'Electrochemical and Surface Analysis of the Fe-Cr-Ru System in non-oxidizing Acid Solutions', *Applied Surface Science*, vol. 44, pp. 7-15

Tjong S.C., Ku J.S. and Ho N.J. (1997) 'Laser surface alloying of ferritic Fe-40Cr alloy with ruthenium', *Surface and Coatings Technology*, vol. 90, pp. 203-209

Trimpin S., Inutan E.D., Herath T.N. and McEwen C.N. (2009) 'Laserspray Ionization, a New Atmospheric Pressure MALDI Method for Producing Highly Charged Gas-phase Ions of Peptides and Proteins Directly from Solid Solutions', *Molecular & Cellular Proteomics*, vol. 9, pp. 362-7

Triwiyanto A., Husain P., Haruman E. and Ismail M. (2012) 'Low Temperature Thermochemical Treatments of Austenitic Stainless Steel Without Impairing Its Corrosion Resistance', Corrosion Resistance, vol. 14, pp. 317-338; available from www.intechopen.com

Troselius L. (1971) 'Polarization Performance of Stainless Steels in H₂SO₄ and HCl', Corrosion Science, vol. 11, pp. 473-484

Van der Merwe J.W. (2012) CHMT7031: course notes and assignments for the course on Electrometallurgy, University of the Witwatersrand

Varga K., Baradlai P., Barnard W.O., Myburg G., Halmos P. and Potgieter J.H. (1997) 'Comparative study of surface properties of austenitic stainless steels in sulphuric and hydrochloric acid solutions', Electrochimica Acta, vol. 42, no. 1, pp. 25-35

Wang X., Shi S. and Zheng Q. (2004) 'Wear resistance of laser cladding and plasma spray welding layer on stainless steel surface', Chinese Optics Letters, vol. 2, no. 3, pp. 151-153

Webb N. (2011) 'Field Joint Repair Coatings of Pipelines' address at Petro.t.ex Africa 2011, 9th June 2011 at Gallagher Convention Centre in Midrand, for the Corrosion Institute of Sothern Africa (CorrISA), [Online], Available: <http://www.mears.net/horizontal-directional-drilling/index.php/media/press-releases/pipeline-corrosion-highlights-petro-t-ex-africa-2011/> [20 Nov 2014]

Woollin P. (1994) 'Developments in fusion welding of stainless steels', Welding and Metal Fabrication, vol. 62, no. 1, pp. 18-26

Wright G. (2014) 'Corrosion Protection of Metals', published on line for the Chemistry Department, University of Auckland [Online], Available: <https://www.auckland.ac.nz/en.html> [August 2014]

Yang B.L. and Gasworth S.M. (2000) for the General Electric Company, US patent number US 6110544A

Yu F. and Bennett T.D. (2005). 'A nondestructive technique for determining thermal properties of thermal barrier coatings', Journal of Applied Phycs, vol. 97

Zhu F. and Wang Y. (2009) 'Study on the Laser Hybrid Cladding Technology on the Surface of Copper Substrate', Applied Physics Research, vol. 1, no. 2, pp. 68-70

Appendices

Appendix A – Publications and Presentations

Refereed Publication

Van der Merwe, J., Tharandt, D. and Masiu, P. (2014) ‘Corrosion resistance of laser-cladded 304L stainless steel surfaces enriched with ruthenium additions in sulphuric acid media’, *The 6th International Platinum Conference, Platinum–Metal for the Future*, The Southern African Institute of Mining and Metallurgy (SAIMM)

Conference Presentation

This research was presented at the European Corrosion Conference, Pisa, Italy, 9th September 2014, O-7757, and at The 6th International Platinum Conference, Sun City, South Africa, 21st October 2014

Appendix B - Calculations

As per equation (G), the following was calculated:

For the alloys containing ruthenium it was assumed that the chromium levels remained unchanged at 19 wt%, the nickel also remained unchanged at 9.5 wt% but that the ruthenium content increased as targeted from 1 wt% to 2 wt%, 3 wt%, 4 wt% and 5 wt% and therefore decreasing the remaining iron concentration from 70.5 wt% to 69.5 wt% down to 66.5 wt%. Other, minor elements were ignored. For the SAF2205, chromium was taken as 22 wt%, nickel as 5 wt% and the remaining 73 wt% were taken to be iron.

The number of electrons transferred each time, n , was taken as Cr = 3, Ni = 2, Fe = 2 and Ru = 2 and the atomic weights were used as per Perry and Green (1984).

$$N_{eq\ 1\%Ru} = \frac{1}{\left(\frac{(0.19)(3)}{52.00} + \frac{(0.095)(2)}{58.71} + \frac{(0.01)(2)}{101.07} + \frac{(0.705)(2)}{55.85}\right)} = 22.23$$

$$N_{eq\ 2\%Ru} = \frac{1}{\left(\frac{(0.19)(3)}{52.00} + \frac{(0.095)(2)}{58.71} + \frac{(0.02)(2)}{101.07} + \frac{(0.695)(2)}{55.85}\right)} = 22.33$$

$$N_{eq\ 3\%Ru} = \frac{1}{\left(\frac{(0.19)(3)}{52.00} + \frac{(0.095)(2)}{58.71} + \frac{(0.03)(2)}{101.07} + \frac{(0.685)(2)}{55.85}\right)} = 22.43$$

$$N_{eq\ 4\%Ru} = \frac{1}{\left(\frac{(0.19)(3)}{52.00} + \frac{(0.095)(2)}{58.71} + \frac{(0.04)(2)}{101.07} + \frac{(0.675)(2)}{55.85}\right)} = 22.54$$

$$N_{eq\ 5\%Ru} = \frac{1}{\left(\frac{(0.19)(3)}{52.00} + \frac{(0.095)(2)}{58.71} + \frac{(0.05)(2)}{101.07} + \frac{(0.665)(2)}{55.85}\right)} = 22.64$$

$$N_{eq\ 2205} = \frac{1}{\left(\frac{(0.22)(3)}{52.00} + \frac{(0.05)(2)}{58.71} + \frac{(0.73)(2)}{55.85}\right)} = 24.67$$

Appendix C - EDS analysis of all samples

Table 22: EDS Analysis obtained for the 2nd batch of tested samples

XRD Sample	Location	Fe%	Ni%	Cr%	Si%	Mn%	Ca%	Ru%	average Ru%
<u>area analysis</u>									
3% Ru targeted	cross section	65.91	9.76	18.84	0.74	1.53	0.00	3.22	
	surface	66.26	9.81	18.91	0.79	1.58	0.00	2.65	
	surface	66.09	9.79	18.88	0.77	1.56	0.00	2.90	2.92
4% Ru targeted	cross section	65.44	9.68	18.85	0.77	1.56	0.00	3.70	
	surface	66.06	9.20	20.06	1.28	1.60	0.00	1.81	
	surface	65.75	9.44	19.46	1.03	1.58	0.00	1.80	2.44
5% Ru targeted	cross section	64.41	9.53	18.39	0.83	1.60	0.00	5.24	
	surface	65.29	9.75	18.46	0.73	1.57	0.00	4.19	
	surface	64.85	9.64	18.43	0.78	1.59	0.00	4.57	4.67
average		65.56	9.62	18.92	0.86	1.57	0.00		
stainless steel base plate #1		70.97	7.99	19.11	0.50	1.42	0.00	0.00	
stainless steel base plate #2		71.03	8.02	19.13	0.47	1.36	0.00	0.00	
average		71.00	8.01	19.12	0.49	1.39	0.00	0.00	
std deviation		0.030	0.015	0.010	0.015	0.030	0.00	0.00	
<u>point analysis</u>									
from sample 3% Ru targeted		39.38	5.90	10.93	0.47	0.93	0.00	42.38	at Ru cluster
from sample 3% Ru targeted		0.00	0.00	0.00	0.00	0.00	0.00	100.00	at Ru cluster
from sample 3% Ru targeted		9.68	1.16	3.04	0.00	0.00	0.00	86.13	at Ru cluster
from sample 3% Ru targeted		12.70	1.85	3.60	0.00	0.42	0.00	81.43	at Ru cluster
from sample 4% Ru targeted		27.27	3.87	7.60	0.36	0.64	0.26	60.00	at Ru cluster
from sample 4% Ru targeted		4.02	0.52	1.13	0.00	0.00	0.00	94.33	at Ru cluster
from sample 4% Ru targeted		0.47	0.00	0.00	0.00	0.00	0.00	99.53	at Ru cluster
from sample 4% Ru targeted		27.93	4.21	7.51	0.32	0.66	0.00	59.38	at Ru cluster
from sample 4% Ru targeted		31.44	4.81	8.39	0.40	0.69	0.00	54.27	at Ru cluster
from sample 4% Ru targeted		66.11	9.92	18.71	0.66	1.56	0.00	3.04	stratification section
from sample 5% Ru targeted		38.73	5.58	10.54	0.42	0.87	0.00	43.86	at Ru cluster
from sample 5% Ru targeted		48.90	7.92	14.28	0.67	1.22	0.00	27.01	at Ru cluster
from sample 5% Ru targeted		0.53	0.00	0.00	0.00	0.00	0.00	99.47	at Ru cluster
from sample 5% Ru targeted		0.35	0.00	0.00	0.00	0.00	0.00	99.65	at Ru cluster
average		21.97	3.27	6.12	0.24	0.50	0.02	67.89	
std deviation		20.428	3.145	5.779	0.253	0.504	0.067	30.093	

Appendix D - 1 M H₂SO₄ solution at 25°C

For the laser cladded sample with stainless steel powder only as per Figure 148, the curves corresponded with one another indicating very consistent results, that was why the test was only repeated once. There was no real difference between the samples from the exposed and fresh surface scans. The E_{corr} values were close to -0.4 V and i_{crit} was between 3.0×10^{-4} and 7.0×10^{-4} A/cm² whereas the i_{pass} was between 1.0 and 2.0×10^{-5} A/cm².

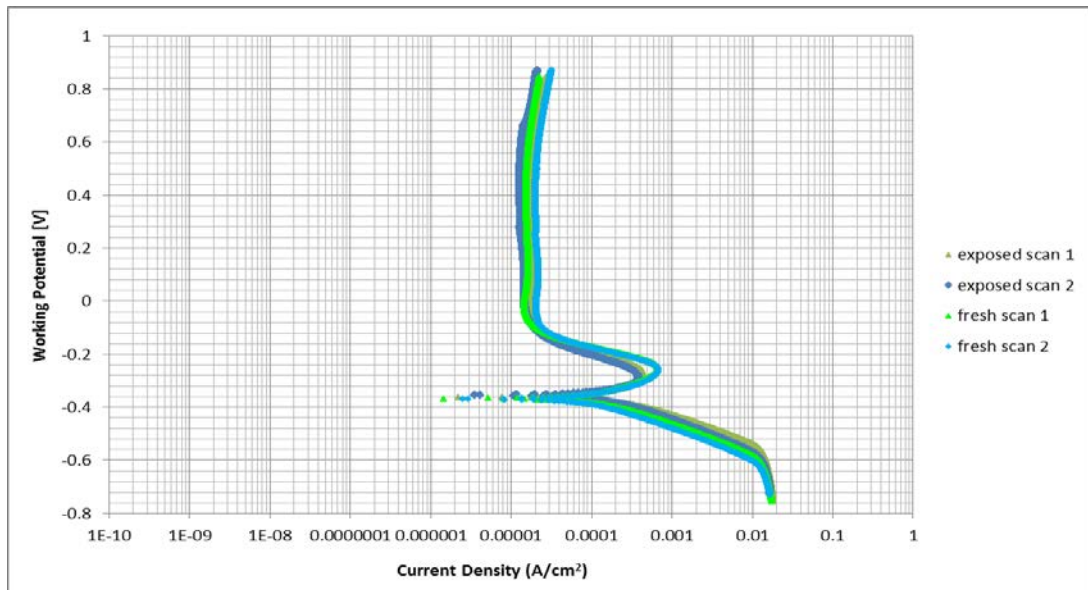


Figure 148: Log i vs E graphs for the 0 wt% Ru sample in 1 M H₂SO₄ at 25°C

The OCP experiments did not show such a consistent trend for the duration of the experiment, as can be observed in the potential over time graph, even though the final values showed excellent consistency both being just less than -0.2 V. They started off with a large difference, showed different trends throughout the experiment but had some consistencies as can be observed in Figure 149.

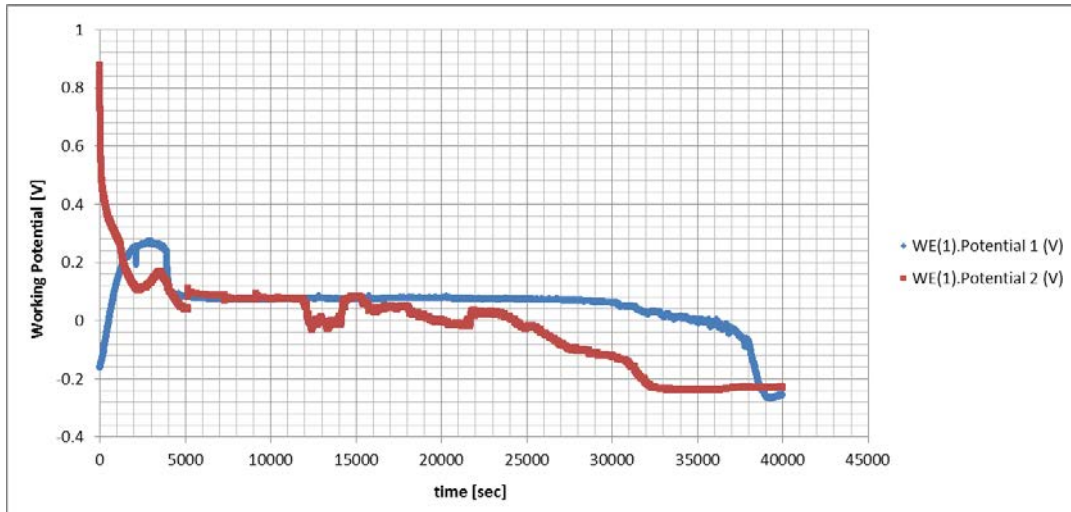


Figure 149: E vs time graphs for the 0 wt% Ru sample in 1 M H₂SO₄ at 25°C

For the sample containing the smallest amount of ruthenium, i.e. at 0.44 wt% Ru as can be seen in Figure 150, the repeatability of the exposed samples was starting to become a concern for the results from the exposed surface scan. The Tafel slopes for the cathodic reaction were the same but the critical current density had a large range extending over almost an order of magnitude. i_{crit} was one of the important aspects of assessing corrosion activity and therefore the evaluation of the results must take this variability into account. The current density increased with an increase in working potential and in the passive region the curves were similar again as well as going into the trans-passive region. The curves from the fresh surface scan were much more consistent but showing higher current densities at a specific potential. The Tafel slopes were flatter and a more linear stable passive region was observed before going into the same trans-passive region. Consistency of the samples during the fresh surface scan was excellent.

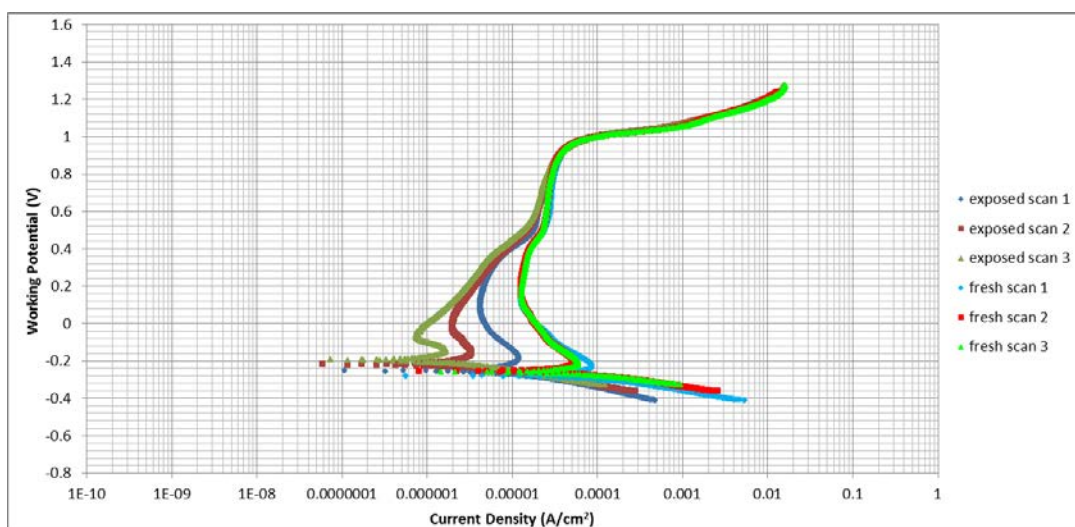


Figure 150: Log i vs E graphs for the 0.44 wt% Ru sample in 1 M H₂SO₄ at 25°C

Observing OCP values for consistency, a small variance was observed, the curves all had the same shape and final values differed by less than 0.1 V settling at around 0.15 V. This can be observed in Figure 151.

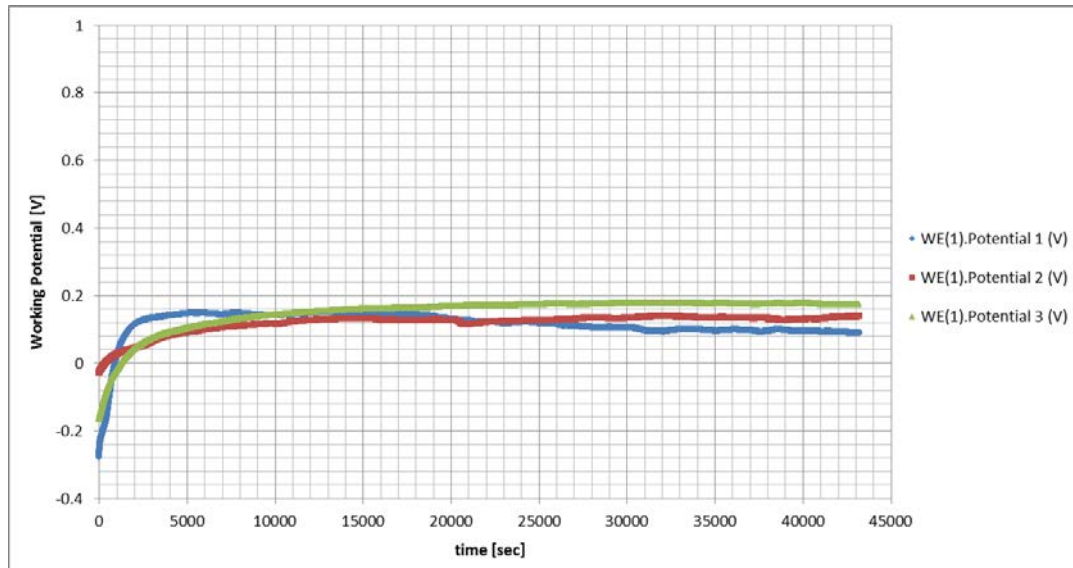


Figure 151: E vs time graphs for the 0.44 wt% Ru sample in 1 M H₂SO₄ at 25°C

At the next highest ruthenium composition, i.e. at 2.92 wt% Ru, it was clearly observed that for the samples from the exposed surface scan, only two of the three samples had the characteristic transition shape and one still exhibited the otherwise standard graph for steels with the passive region which was almost vertical. Figure 152 clearly shows that the two graphs exhibiting transition did so at slightly different passivation potentials both just above 0 V. The passive region was reduced to stretch over 0.8 V. Consistency was poor in this case, i.e. for the samples during the exposed and fresh surface scans. The distinct difference previously observed between behaviour from the exposed and fresh surface scans was starting to reduce. The samples from the cleaned surface scan showed a stable passive current density with increasing potential at larger current densities than the samples from the exposed surface scan before they combined going into the trans-passive region almost coinciding. The passive region for the fresh samples was extended over approximately 1.0 V and E_{corr} values of less than -0.2 V were observed.

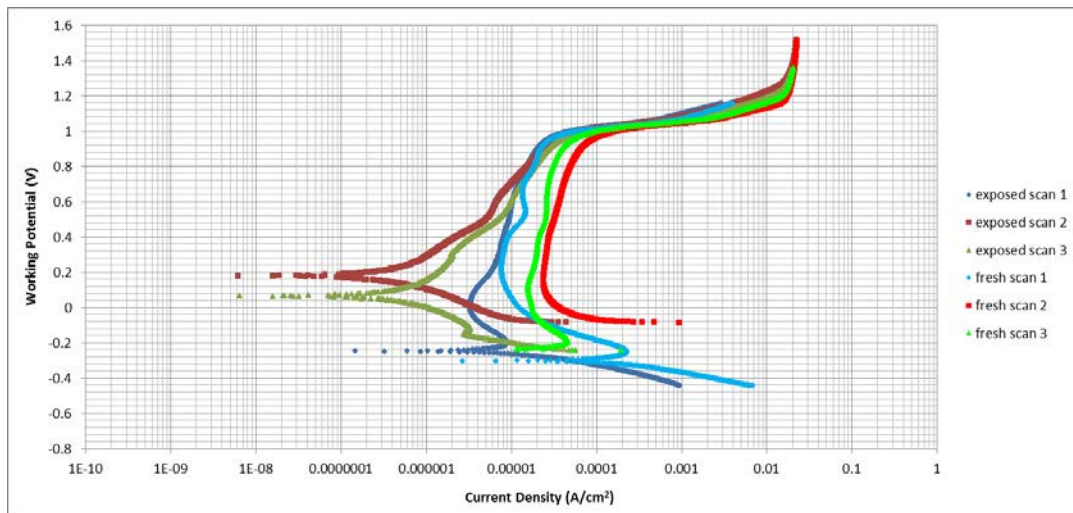


Figure 152: Log i vs E graphs for the 2.92 wt% Ru sample in 1 M H_2SO_4 at 25°C

The OCP test showed extremely inconsistent results for the 2.92 wt% Ru so comparative results must be viewed with this in mind, as can be seen in Figure 153. Stable values were reached after the 12 hours of exposure for each of the tests but results varied between 0.4 V and 0.04 V.

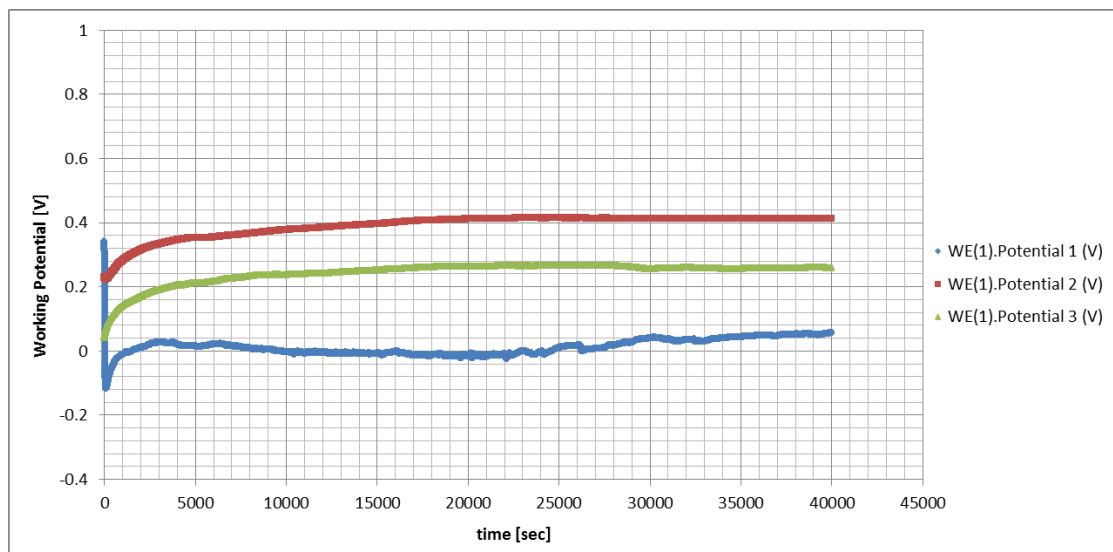


Figure 153: E vs time graphs for the 2.92 wt% Ru sample in 1 M H_2SO_4 at 25°C

The sample containing 2.44 wt% Ru was only tested twice and these showed very different results, unfortunately this sample was not able to be used for repeat experiments. The variance and off target values were large for this sample, observed from Table 3. This is clearly evident in the lack of consistency in the electrochemical tests as can be seen in Figure 154. The results from the exposed surface scan indicated low current densities and the transition shape for test 1 and cathodic loops were observed during test 2, while during the fresh surface scan, the 2.44 wt% Ru sample showed a more stable passive current density

with increasing potential at larger current densities than the samples from the exposed surface scan before they combined going into the same trans-passive region. Again, it can be noted that the distinct difference between the exposed and fresh surface scans behaviour was reducing. The passivation potential range for both scans was between 0.8 and 1.0 V.

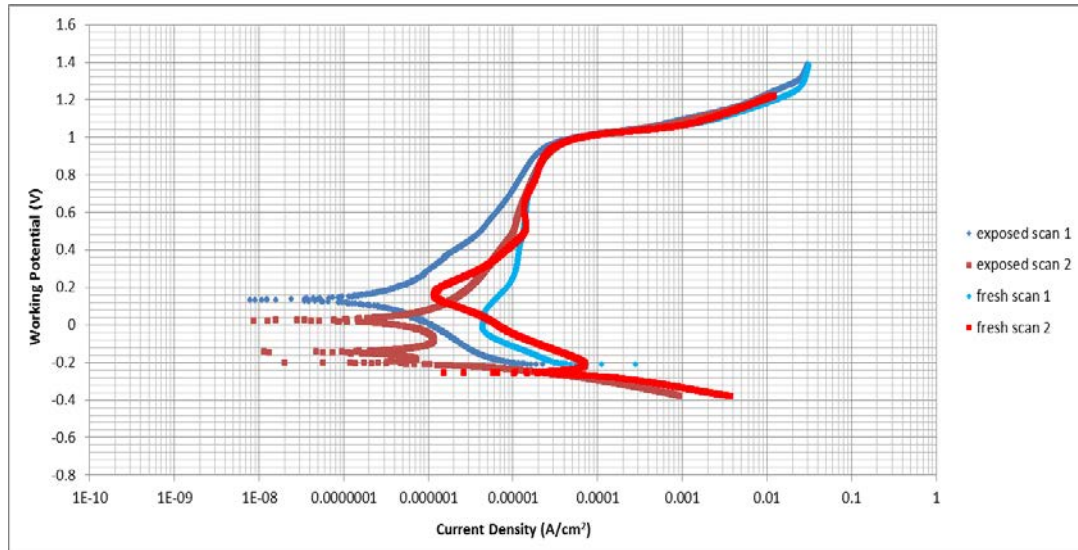


Figure 154: Log i vs E graphs for the 2.44 wt% Ru sample in 1 M H_2SO_4 at 25°C

The inconsistency of the log i vs E graphs is carried over to the OCP tests, the test started off similarly but quickly diverged and the final values showed a difference of over 0.16 V and it actually looked like a stable value had not yet been reached, especially for test 1. This is observed in Figure 155.

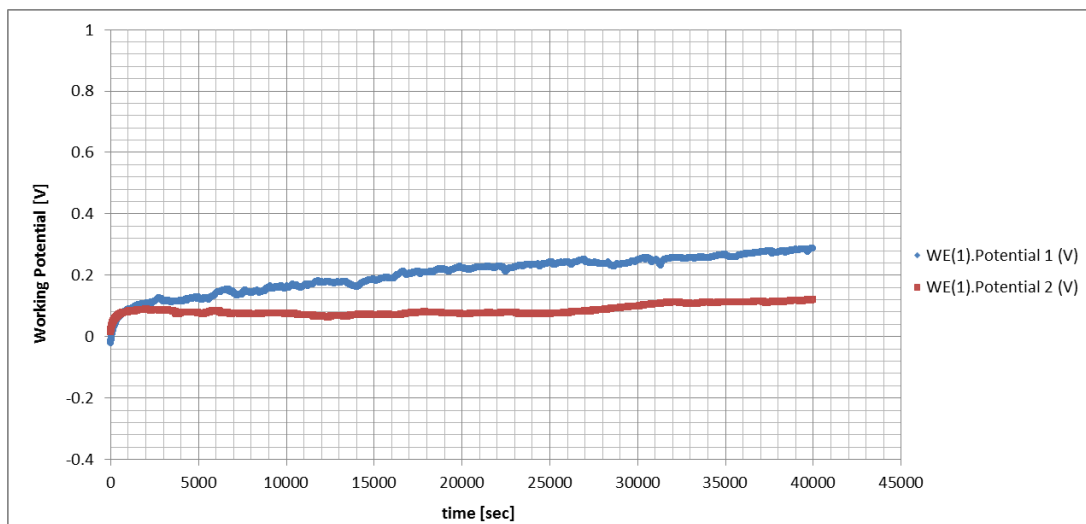


Figure 155: E vs time graphs for the 2.44 wt% Ru sample in 1 M H_2SO_4 at 25°C

Appendix E - 1 M H₂SO₄ + 1% NaCl solution at 25°C

The reproducibility of results in the cladded sample without ruthenium was good as can be seen in Figure 156, one of the reasons that this test only needed to be repeated once. The E_{corr} values for both scans were around -0.35 V with a large active nose and passivation only really achieved at 0.4 V and upwards for the exposed surface scan while passivation occurred earlier at 0 V for the fresh surface scan. The i_{pass} values were between 1×10^{-4} and 3×10^{-4} A/cm². The trans-passive region was not reached during this set of tests. In this case there was no great difference between the results from the exposed and fresh surface scans, similar to that of the samples exposed to only 1 M sulphuric acid.

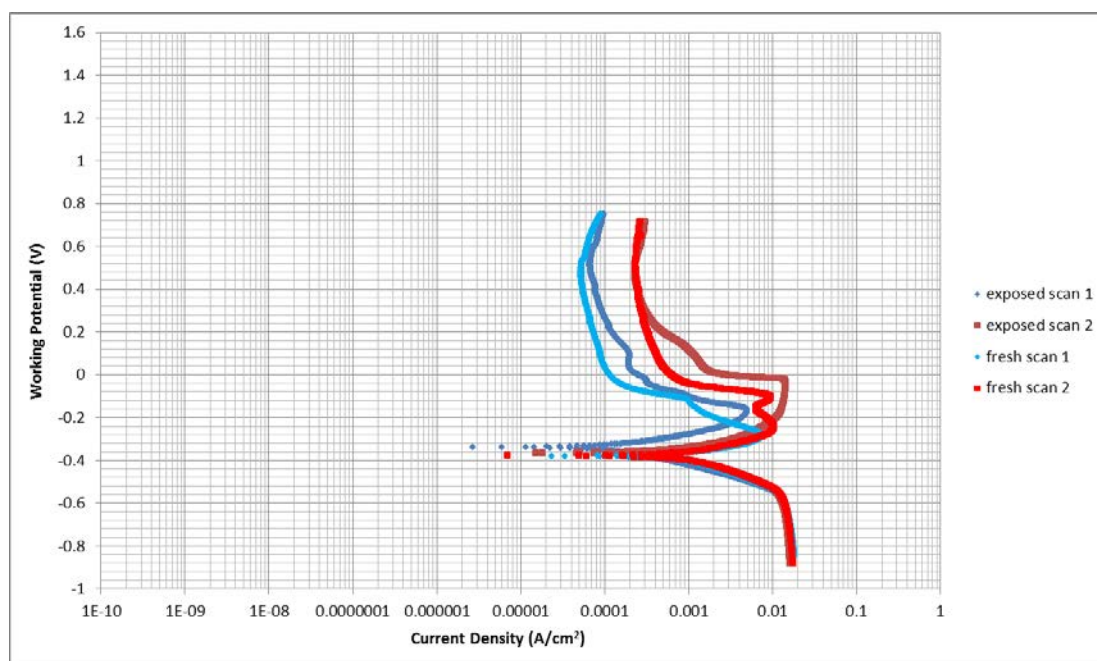


Figure 156: Log i vs E graphs for the 0 wt% Ru sample in 1 M H₂SO₄ + 1% NaCl at 25°C

Good repeatability was also observed looking at the potential over time in Figure 157 where the starting potentials perhaps were very inconsistent but both curves quickly converged and gave very good agreement. Final OCP results were around -0.36 V and only differed marginally where a stable value was reached after the 12 hour period.

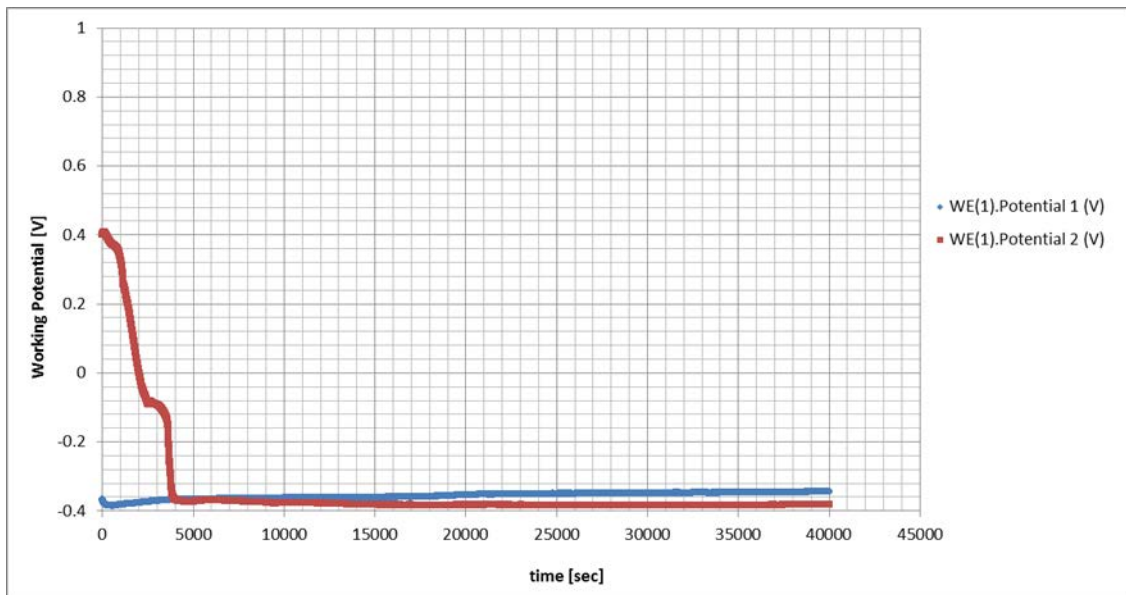


Figure 157: E vs time graph for the 0 wt% Ru sample in 1 M H₂SO₄ + 1% NaCl at 25°C

Looking at the three 2.92 wt% Ru tests conducted there was significant variability that could be observed during both scans; this time test 2 being the largest outlier. The exposed surface scan showed more variability between results: a much lower i_{crit} which was around 1×10^{-5} A/cm² and almost an order of magnitude lower i_{pass} . The E_{corr} values were, however, very consistent around -0.24 V and a small active nose was displayed. The passive range extended over 1.0 V before moving into the expected and common trans-passive region. The curves for tests 1 and 3 of the fresh surface scan showed good repeatability but the E_{corr} values were lower at -0.32 V, had a large active nose before achieving passivity and E_{pass} of approximately 0.1 V and at i_{pass} of around 1×10^{-5} A/cm² which thus reduced the passive range to 0.9 V; as can be seen in Figure 158. The test 2 result for the cleaned surface scan showed incomplete passivity as explained in Figure 9 showing cathodic loops which reduce the passive range significantly. In general however, the test results from the exposed surface scan were only slightly less corrosion resistant in this medium than the test results show for the fresh surface scan.

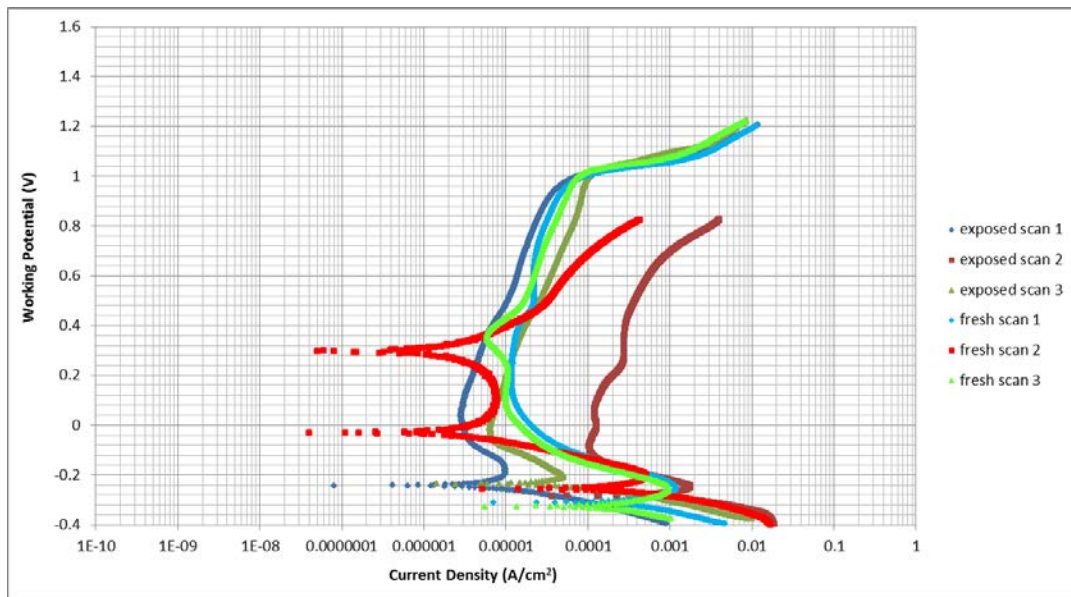


Figure 158: Log i vs E graphs for the 2.92 wt% Ru sample in 1 M H_2SO_4 + 1% NaCl at 25°C

As observed in Figure 158, test 2 was not consistent with test results 1 and 3; this is again observed in the potential vs time curve seen in Figure 159. Test 1 potentials increased quickly before leveling off, test 2 results remained relatively stable throughout the 12 hours and test 3 potentials decreased gently before levelling off. Stable OCP values were obtained this time at 0.11 V for tests 1 and 3 while -0.23 V was reached for test 2.

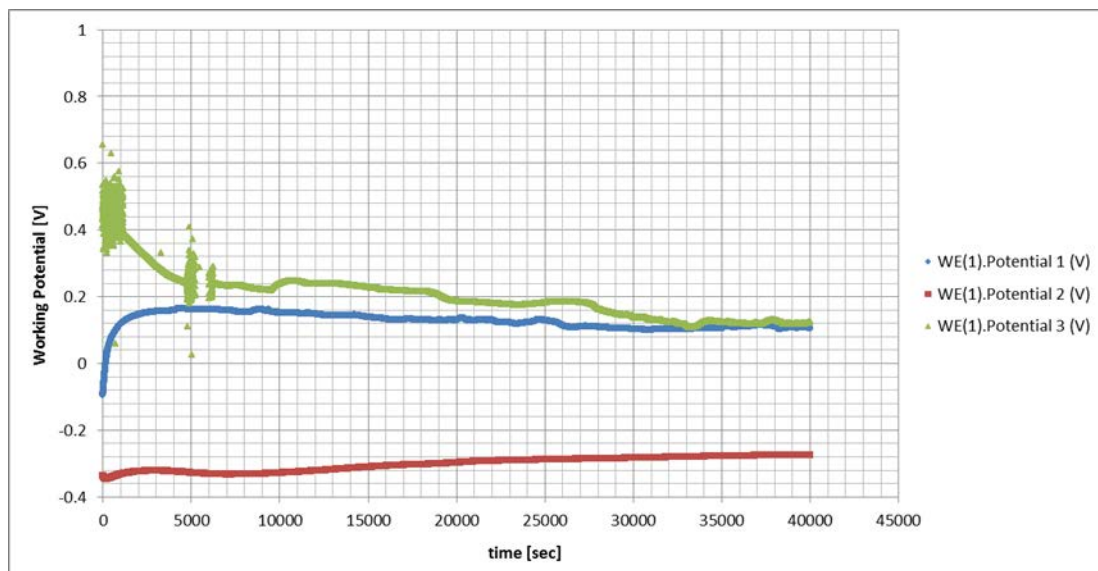


Figure 159: E vs time graphs for the 2.92 wt% Ru sample in 1 M H_2SO_4 + 1% NaCl at 25°C

Tests for the 2.44 wt% Ru sample only needed to be repeated once as the results showed very good repeatability. The exposed surface scan had a slightly higher E_{corr} (-0.32 V versus -0.39 V) and i_{pass} compared to the fresh surface scan results even though this difference was also marginal. The results can be seen in Figure 160.

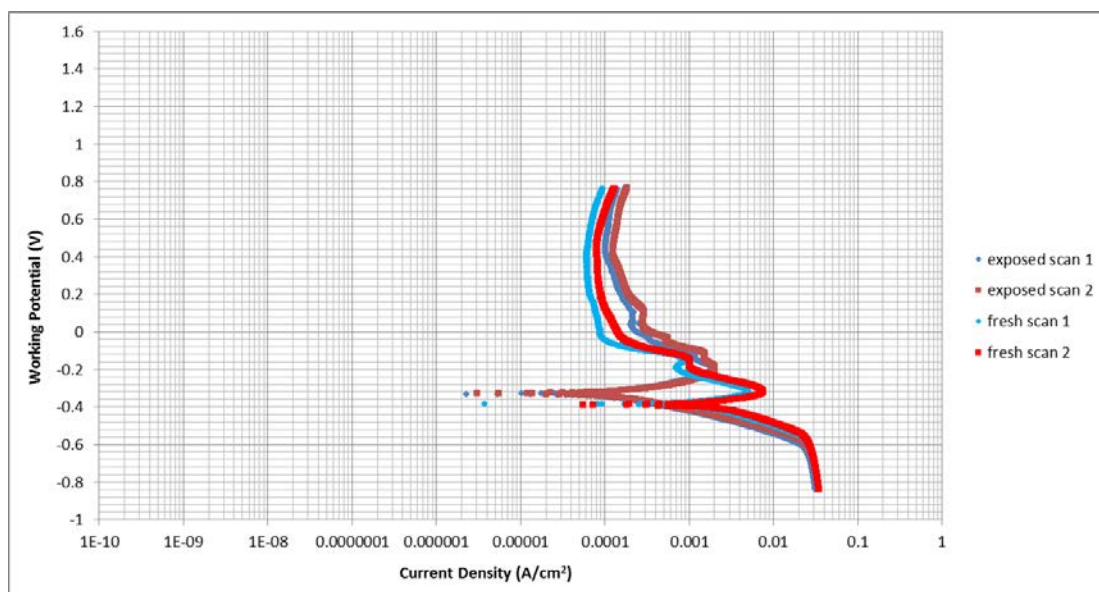


Figure 160: Log i vs E graphs for the 2.44 wt% Ru sample in 1 M H_2SO_4 + 1% NaCl at 25°C

The excellent repeatability is confirmed during the OCP results, they are very close to each other throughout the period tested, as per Figure 161. The trend, however, was still slightly in an upwards direction towards the positive after the 12 hours and it seemed that in this case an equilibrium value had not yet been reached but would be very close to the 0.338 V value obtained after 12 hours.

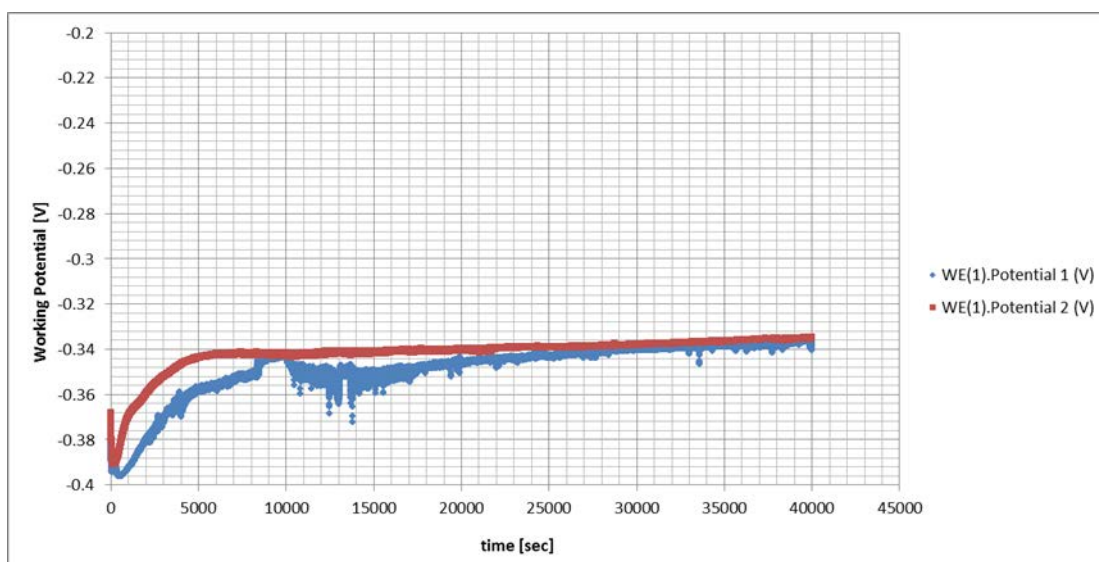


Figure 161: E vs time graphs for the 2.44 wt% Ru sample in 1 M H_2SO_4 + 1% NaCl at 25°C

Appendix F - 1 M H₂SO₄ solution at 45°C

Contrary to the stainless steel blank sample, the cladded sample without any ruthenium addition shows very good repeatability, observed in Figure 162. The shape of the curves did not display consistent passivity after the active nose and as the potential was increased which was not something that was observed in previous experiments at ambient conditions but the two test results are in agreement. The E_{corr} values were almost identical to the results of the exposed and fresh surface scans at around -0.32 V. The active noses were prominent and in that region the curves were starting to show their variability; overall though the current densities for the first anodic scan (i.e. after exposure) had higher values than the current densities for the second anodic scan (i.e. on a fresh surface). The results from the fresh surface scan followed the same shape as the results from the exposed surface scan and were also reasonably close to each other, good for a comparison.

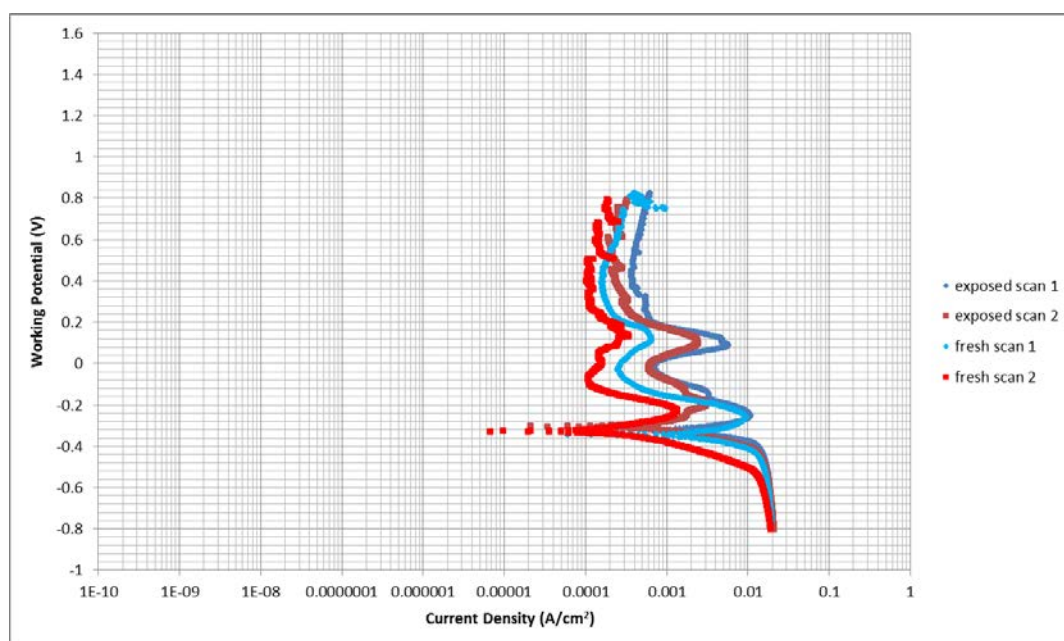


Figure 162: Log i vs E graphs for the 0 wt% Ru sample in 1 M H₂SO₄ at 45°C

Again, this consistency is reflected in the E vs time graph in Figure 163 where the two curves followed a similar trend of initially decreasing quickly and then levelling off after some time to almost the same OCP value after 12 hours. Stable values were obtained at -0.29 V.

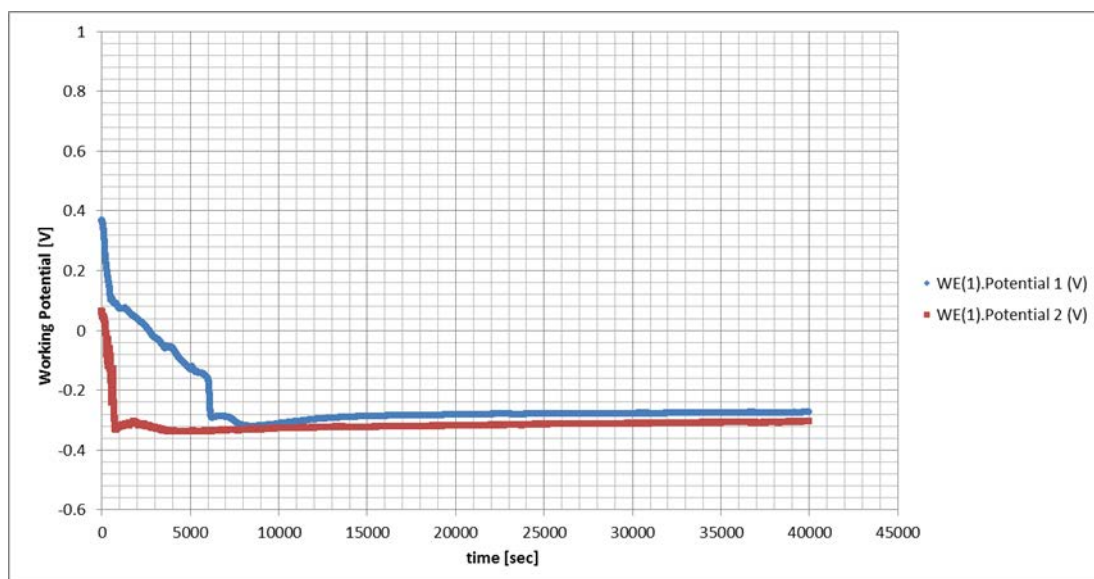


Figure 163: E vs time graphs for the 0 wt% Ru sample in 1 M H₂SO₄ at 45°C

The graphs at an increased ruthenium composition of 2.92 wt% were very consistent; they all followed very similar trends except the 1st test of the fresh surface scan as can be observed in Figure 164. For the exposed surface scan the Tafel slopes of the tests conducted showed good repeatability, the E_{corr} value of -0.21 V was reached for tests 1 and 2 while test 3 was slightly lower at -0.27 V, the active noses were small and passivation was reached at close to 0 V even though the current densities still increased with increasing potential until the trans-passive region was reached at 1 V; the passive region ranging therefore over 1 V. The tests conducted during the fresh surface scan showed that the parameters were very similar to those of the exposed surface scan, there was some variability in the passive region but then the curves coincided again going into the trans-passive region. The first test from the fresh surface scan showed the same E_{corr} value as the other tests but then a cathodic loop was observed before following the other graphs into a stable passive region at just above 0 V.

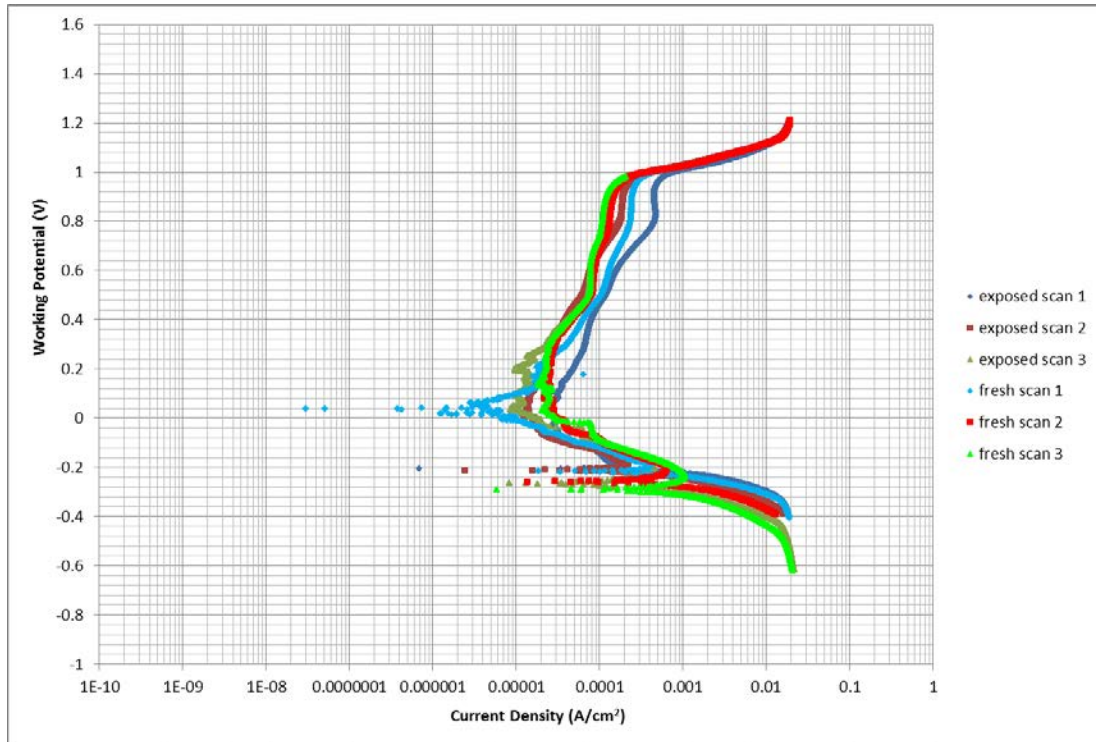


Figure 164: Log i vs E graphs for the 2.92 wt% Ru sample in 1 M H_2SO_4 at 45°C

Figure 165 indicates that the consistency in the E vs time curves was not as great as before, especially the test 3 result showed some difference with a significantly lower OCP value after 12 hours than the other two tests. OCP values for tests 1 and 2 were very close reaching 0.1 V and therefore these results were acceptable. The curves look as if they are still on a slight downward trend and might not have stabilised completely yet.

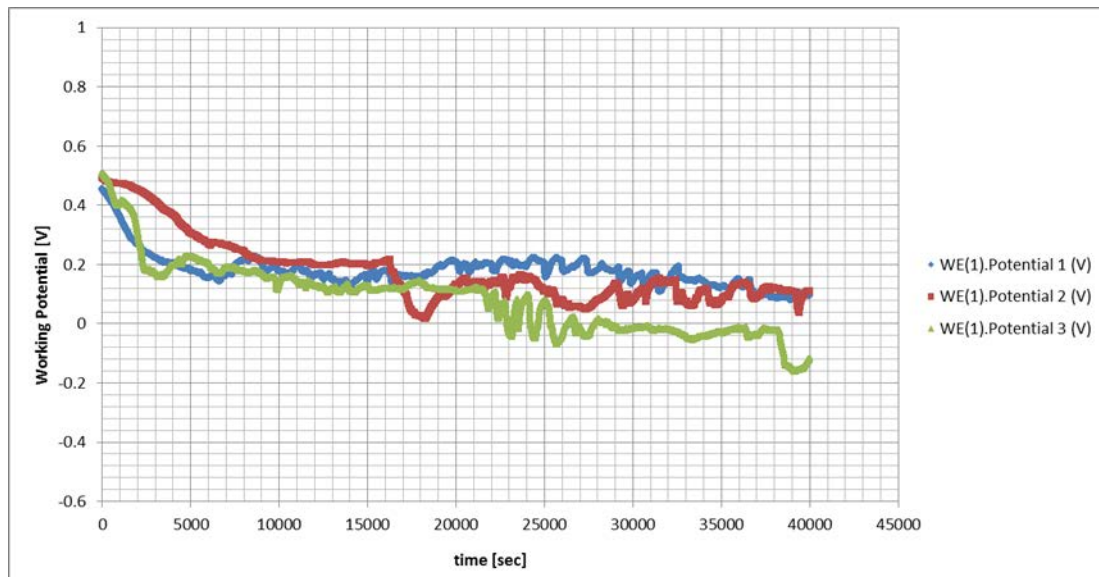


Figure 165: E vs time graphs for the 2.92 wt% Ru sample in 1 M H_2SO_4 at 45°C

For the 2.44 wt% Ru sample, repeatability of the tests is excellent as can be viewed in Figure 166. All the curves from the exposed surface scan coincided with one another and so did the

curves for the three tests conducted for the fresh surface scan. The Tafel slope for the fresh surface scan was not as steep as for the exposed surface scan, all E_{corr} values averaged around -0.3 V, the i_{crit} was slightly reduced for the fresh surface scan and so was the i_{pass} which started at 0 V. This indicates that corrosion resistance was better during the fresh surface scan but thereafter the passive region was identical: initially it was observed that the current densities increased with an increase in potential but then stabilised at 0.4 V and above.

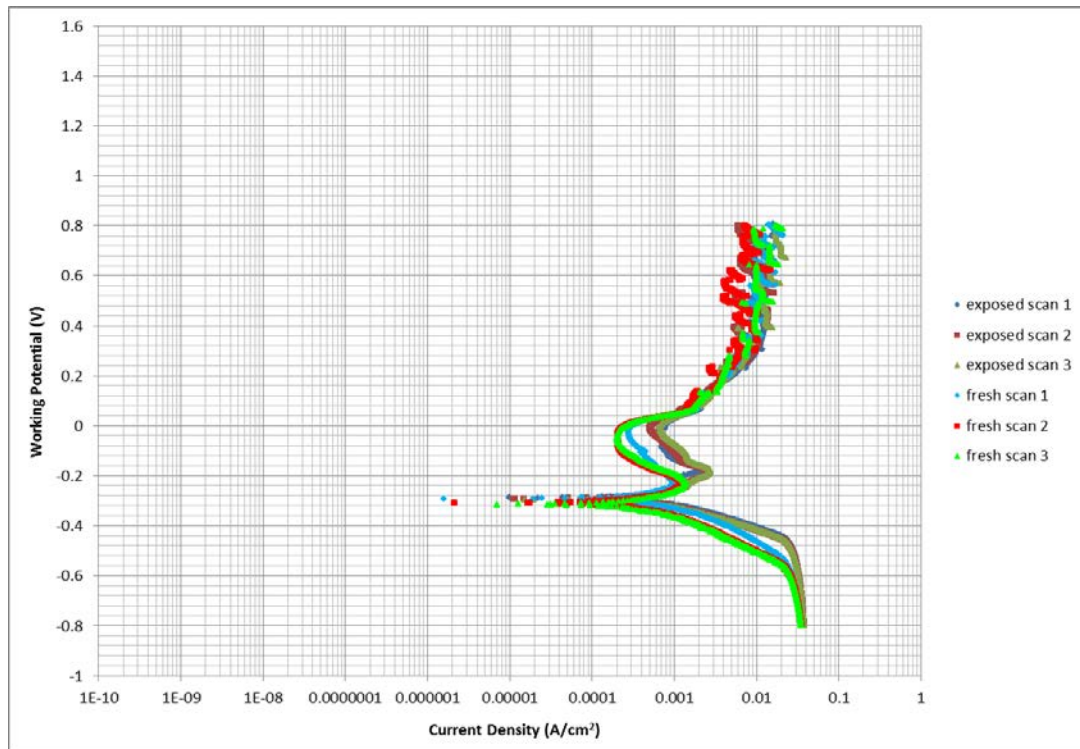


Figure 166: Log i vs E graphs for the 2.44 wt% Ru sample in 1 M H_2SO_4 at 45°C

The potential is very stable over time as per Figure 167, showing an initial step downward trend before levelling out; all three curves were reasonably comparable with all tending towards the same OCP value after 12 hours which was -0.29 V.

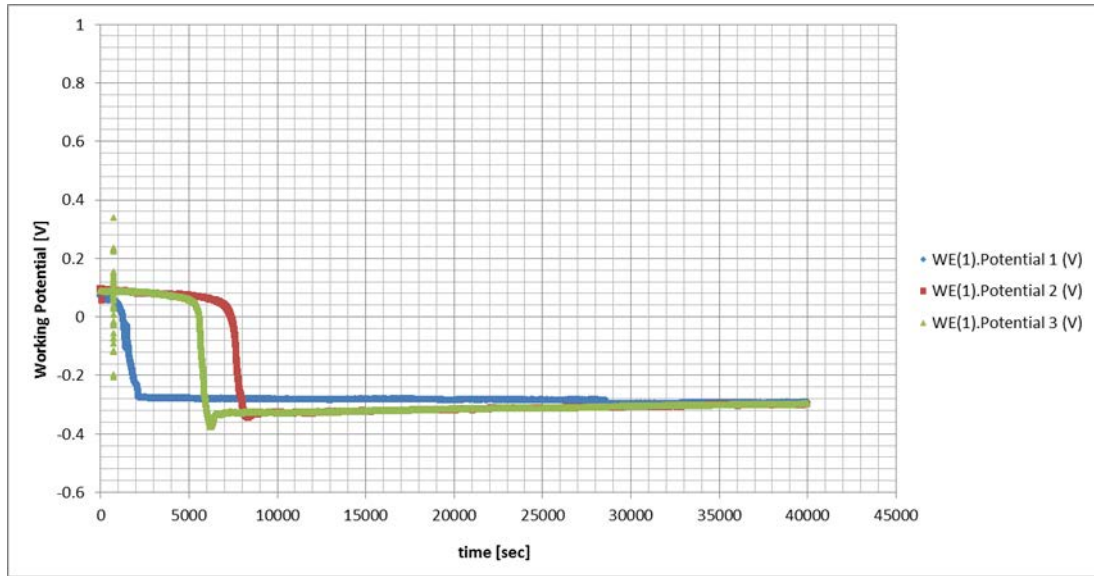


Figure 167: E vs time graphs for the 2.44 wt% Ru sample in 1 M H₂SO₄ at 45°C

Table 27: Results from the exposed surface scan in 1 M H₂SO₄ at 45°C

Sample	β _a [mV/dec]	β _c [mV/dec]	E corr Calc [mV]	E corr Obs [mV]	j corr [A/cm ²]	Current Density at 0.1V [A/cm ²]	i corr [A]	corrosion rate [mm/year]	polarisation resistance [Ω]	OCP after 12 hours [mV]
SS blank (1)	62.572	98.225	-319.660	-318.650	2.580E-03	1.173E-02	6.847E-04	26.851	24.24	-279.816
SS blank (2)	88.690	90.800	-284.480	-291.940	7.896E-05	6.530E-04	2.618E-05	0.82119	744.38	-265.900
SS blank (3)	91.382	78.345	-282.640	-291.940	6.837E-05	4.220E-04	2.266E-05	0.71098	808.34	-259.247
SS blank average	80.88	89.12	-295.59	-300.84	9.09E-04	4.27E-03	2.45E-04	9.461	525.7	-268.32
0 wt% Ru (1)	65.140	71.790	-325.940	-324.330	1.813E-03	4.955E-03	6.883E-04	18.858	21.55	-273.346
0 wt% Ru (2)	89.222	100.830	-298.270	-305.120	7.188E-04	2.426E-03	2.729E-04	7.4752	75.34	-304.565
0 wt% Ru average	77.18	86.31	-312.11	-314.73	1.27E-03	3.69E-03	4.81E-04	13.167	48.4	-288.96
0.82 wt% Ru (1)	67.159	85.562	-224.480	-228.600	2.583E-04	5.668E-04	5.162E-05	2.3883	316.58	-229.248
0.82 wt% Ru (2)	47.464	288.610	-269.570	-267.390	8.588E-05	2.057E-05	1.716E-05	0.7939	1031.70	73.944
0.82 wt% Ru (3)	101.600	87.445	-285.720	-297.990	4.533E-04	1.736E-03	9.057E-05	4.1905	225.36	-310.059
0.82 wt% Ru average	72.07	153.87	-259.92	-264.66	2.66E-04	7.75E-04	5.31E-05	2.458	524.5	-155.12
2.92 wt% Ru (1)	N/A	N/A	N/A	N/A	N/A	3.161E-05	N/A	N/A	N/A	95.612
2.92 wt% Ru (2)	73.430	134.860	-194.550	-211.320	2.084E-04	1.489E-05	6.296E-05	1.9352	327.97	109.436
2.92 wt% Ru (3)	45.293	97.664	-266.680	-264.480	1.466E-04	1.080E-05	4.429E-05	1.3613	303.44	-118.378
2.92 wt% Ru average	59.36	116.26	-230.62	-237.90	1.77E-04	1.91E-05	5.36E-05	1.648	315.7	28.89
2.44 wt% Ru (1)	102.340	110.980	-278.220	-287.960	5.671E-04	2.216E-03	1.157E-04	5.2921	199.86	-293.945
2.44 wt% Ru (2)	102.240	179.200	-295.840	-293.560	6.352E-04	1.896E-03	1.296E-04	5.927	218.20	-299.286
2.44 wt% Ru (3)	97.163	111.700	-291.910	-297.080	5.360E-04	2.437E-03	1.094E-04	5.0021	206.38	-298.523
2.44 wt% Ru average	100.58	133.96	-288.66	-292.87	5.79E-04	2.18E-03	1.18E-04	5.407	208.1	-297.25
4.67 wt% Ru (1)	N/A	N/A	N/A	N/A	N/A	3.182E-05	N/A	N/A	N/A	70.038
4.67 wt% Ru (2)	465.610	382.360	-283.120	-299.400	9.827E-07	7.224E-06	2.579E-07	0.0092106	353620.00	228.516
4.67 wt% Ru (3)	N/A	N/A	N/A	N/A	N/A	3.389E-04	N/A	N/A	N/A	179.321
4.67 wt% Ru (4)	N/A	N/A	N/A	N/A	N/A	9.723E-06	N/A	N/A	N/A	-299.316
4.67 wt% Ru (5)	N/A	N/A	N/A	N/A	N/A	3.360E-03	N/A	N/A	N/A	-305.267
4.67 wt% Ru average	465.61	382.36	-283.12	-299.40	9.83E-07	7.50E-04	2.58E-07	0.009	353620.0	-25.34

Table 28: Results from the fresh surface scan in 1 M H₂SO₄ at 45°C

Sample	β_a [mV/dec]	β_c [mV/dec]	E corr Calc [mV]	E corr Obs [mV]	j corr [A/cm ²]	i corr [A]	corrosion rate [mm/year]	polarisation resistance [Ω]
SS blank (1)	50.213	145.530	-353.140	-343.960	1.674E-02	4.440E-03	174.12	3.652
SS blank (2)	142.690	173.410	-323.000	-329.570	4.369E-04	1.448E-04	4.5439	234.710
SS blank (3)	143.170	176.940	-327.110	-333.150	1.418E-04	1.418E-04	1.475	242.330
SS blank average	112.02	165.29	-334.42	-335.56	5.77E-03	1.58E-03	60.046	160.2
0 wt% Ru (1)	86.878	207.830	-366.170	-347.840	8.600E-03	3.265E-03	89.44	8.150
0 wt% Ru (2)	118.980	66.208	-305.680	-328.850	6.528E-04	2.478E-04	6.7892	74.549
0 wt% Ru average	102.93	137.02	-335.93	-338.35	4.63E-03	1.76E-03	48.115	41.35
0.82 wt% Ru (1)	94.677	103.950	-232.870	-258.270	5.575E-03	1.114E-03	57.975	19.320
0.82 wt% Ru (2)	52.779	54.046	-314.340	-314.060	2.385E-03	4.765E-04	22.046	24.339
0.82 wt% Ru (3)	138.720	112.750	-295.410	-310.900	1.283E-03	2.564E-04	11.863	105.360
0.82 wt% Ru average	95.39	90.25	-280.87	-294.41	3.08E-03	6.16E-04	30.628	49.67
2.92 wt% Ru (1)	70.712	65.483	-201.050	-217.810	3.900E-04	1.178E-04	3.6216	125.330
2.92 wt% Ru (2)	110.220	248.430	-227.370	-258.910	5.788E-04	1.748E-04	5.3743	189.650
2.92 wt% Ru (3)	106.510	83.504	-274.470	-290.410	1.812E-03	5.475E-04	16.828	37.133
2.92 wt% Ru average	95.81	132.47	-234.30	-255.71	9.27E-04	2.80E-04	8.608	117.37
2.44 wt% Ru (1)	168.900	100.060	-261.500	-291.980	3.106E-03	6.336E-04	28.981	43.074
2.44 wt% Ru (2)	154.330	158.130	-303.520	-309.110	2.485E-03	5.070E-04	23.192	66.905
2.44 wt% Ru (3)	151.090	105.810	-302.800	-314.260	2.198E-03	4.484E-04	20.511	60.275
2.44 wt% Ru average	158.11	121.33	-289.27	-305.12	2.60E-03	5.30E-04	24.228	56.75
4.67 wt% Ru (1)	N/A	N/A	N/A	N/A	N/A	N/A	N/A	N/A
4.67 wt% Ru (2)	115.550	171.210	-322.860	-330.670	3.838E-03	1.007E-03	35.971	29.754
4.67 wt% Ru (3)	N/A	N/A	N/A	N/A	N/A	N/A	N/A	N/A
4.67 wt% Ru (4)	N/A	N/A	N/A	N/A	N/A	N/A	N/A	N/A
4.67 wt% Ru (5)	80.454	66.363	-206.380	-220.930	3.330E-04	1.062E-04	3.1213	148.680
4.67 wt% Ru average	98.00	118.79	-264.62	-275.80	2.09E-03	5.57E-04	19.546	89.22

Appendix G - 1 M H₂SO₄ + 1% NaCl solution at 45°C

For the cladded sample without ruthenium variability is reasonable except that the values differed slightly at higher potentials in the passive region, as observed in Figure 168. During the exposed surface scan E_{corr} values were at -0.33 V followed by a large active nose and the passive region starting at just above 0 V with a seemingly stable passive region. During the fresh surface scan E_{corr} values were slightly lower at -0.37 V followed by a longer nose with the same i_{crit} value as the exposed surface scan and a passive region which was a little inconsistent ranging in current densities between 4.0×10^{-3} and 1.5×10^{-2} A/cm². The test results from the exposed and cleaned surface scan were almost identical in the active region, the Tafel slope for the oxidation reaction was more gentle thus increasing the E_{crit} for the results obtained from the exposed surface scan even though they did seem to be going into the passivation region together before spreading out again as they reached passivation. In general, however, the results from the exposed surface scan showed better corrosion protection in this region compared to the results from the fresh surface scan.

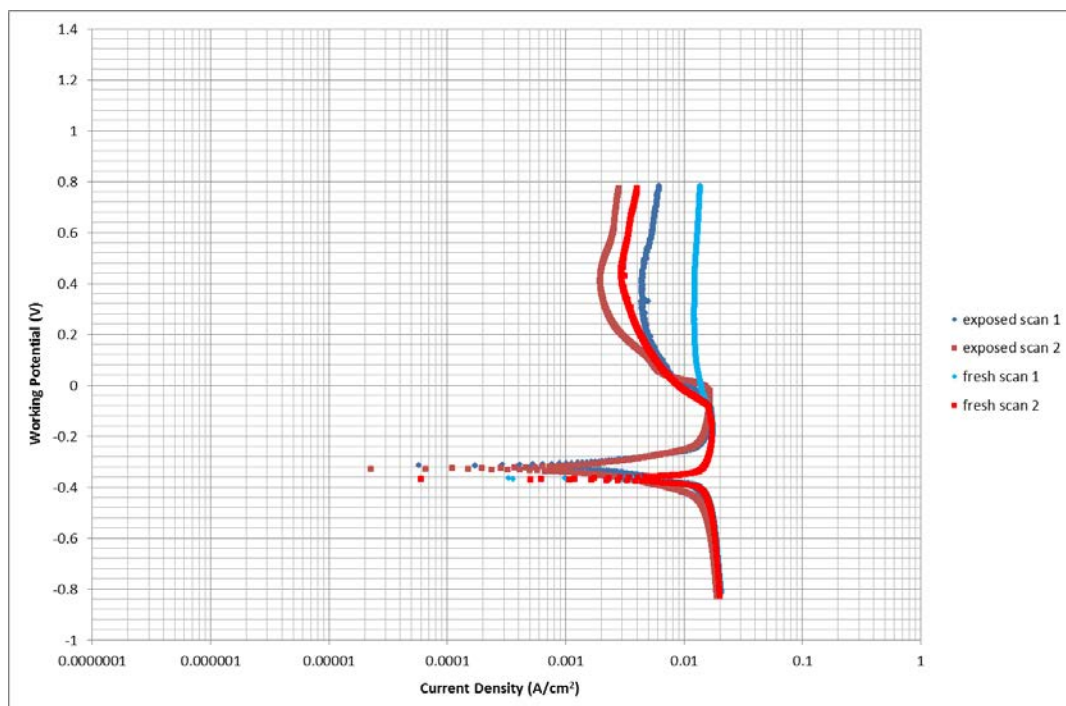


Figure 168: Log i vs E graphs for the 0 wt% Ru sample in 1 M H₂SO₄ + 1% NaCl at 45°C

The potential observed over time in Figure 169 confirmed the good consistency between the two tests conducted. The OCP values did not vary significantly and had definitely reached a stable value after the 12 hours, i.e. -0.32 V.

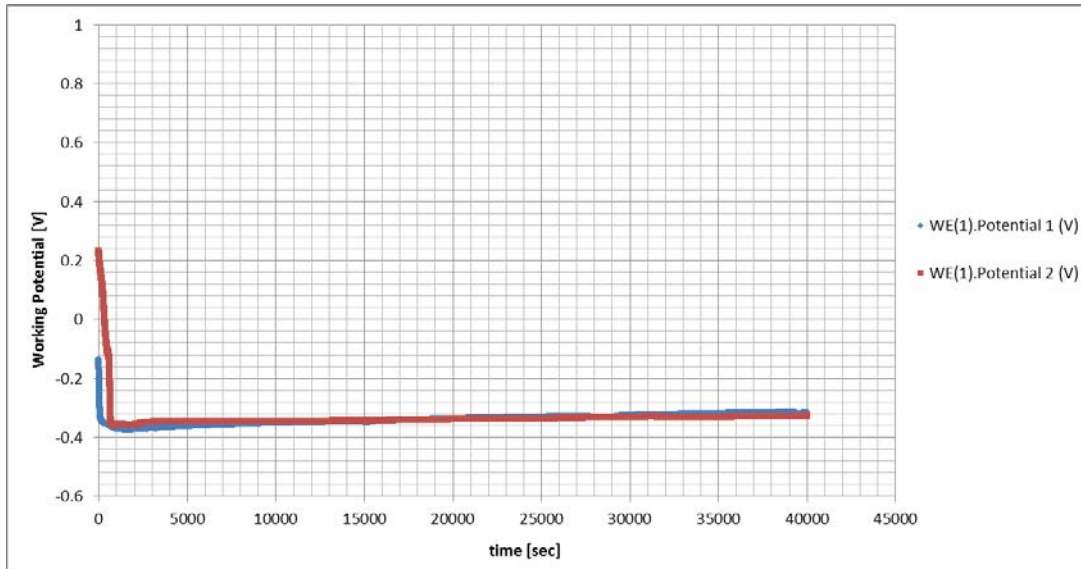


Figure 169: E vs time graphs for the 0 wt% Ru sample in 1 M H₂SO₄ + 1% NaCl at 45°C

The tests conducted at the 2.92 wt% Ru composition shown in Figure 170 indicated reasonable repeatability, the curves behaved very similarly with very steep Tafel slopes, E_{corr} values at just below -0.2 V, small noses were observed and in the passive region the current density was increasing with an increase in potential. In that region the two tests conducted differed by a significant amount even though they followed the same shape. The E_{corr} value for the repeat test during the cleaned surface scan was lower at -0.27 V but then followed the same trend again. The test results from the exposed surface scan showed less corrosion resistance, indicated by the higher current densities, compared to those from the fresh surface scan in the passive region.

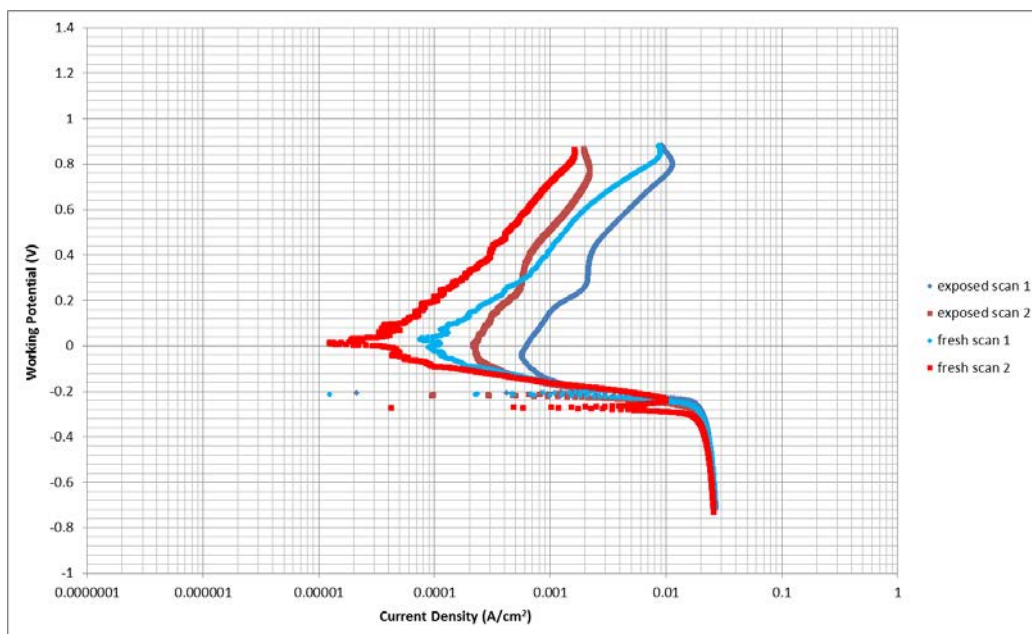


Figure 170: Log i vs E graphs for the 2.92 wt% Ru sample in 1 M H₂SO₄ + 1% NaCl at 45°C

The potential versus time graphs showed large variability between the two tests during the first nine hours, as can be observed in Figure 171 but the two curves then almost join and good repeatability of the two test results was observed at the OCP value of -0.21 V until 12 hours.

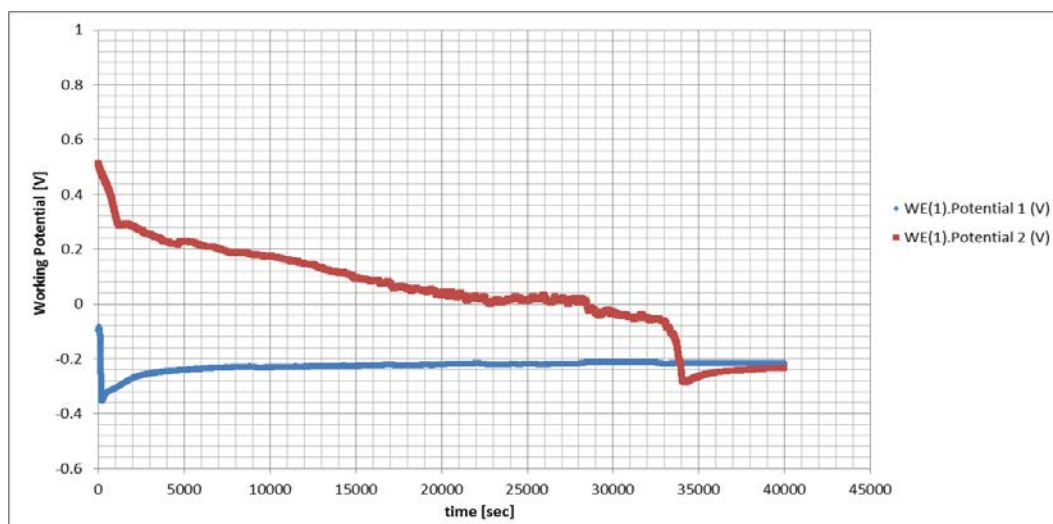


Figure 171: E vs time graphs for the 2.92 wt% Ru sample in 1 M H₂SO₄ + 1% NaCl at 45°C

The active region of the log *i* vs E graphs for the 2.44 wt% Ru sample as per Figure 172 was very consistent but as some critical parameters were reached, such as E_{corr} at between -0.20 V and -0.24 V and very stable Tafel slopes, the curves separated. Test results from the exposed surface scan were more consistent than results for the fresh surface scan but they all did follow the same trend. Passivity was reached but throughout current densities increased with an increase in potential. The trans-passive region was not reached for any of these tests. On average in the passive region, the current densities were higher during the exposed surface scan compared to those of the cleaned surface scan indicating less corrosion protection after exposure to this environment compared to a fresh surface.

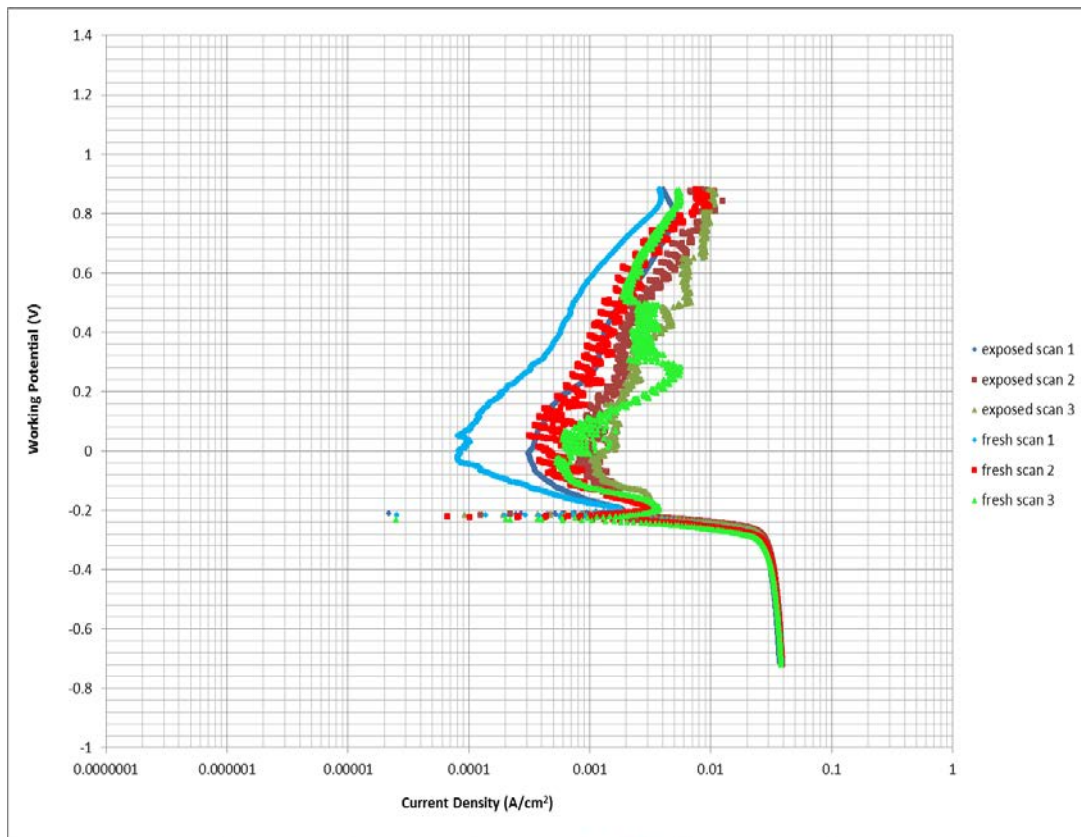


Figure 172: Log i vs E graphs for the 2.44 wt% Ru sample in 1 M H_2SO_4 + 1% NaCl at 45°C

Figure 173 indicates that tests 2 and 3 were very consistent with test 1 starting out on a different trend but with time coming all together and levelling out at the OCP value of -0.21 V. The E vs time graph followed almost a straight line from the start.

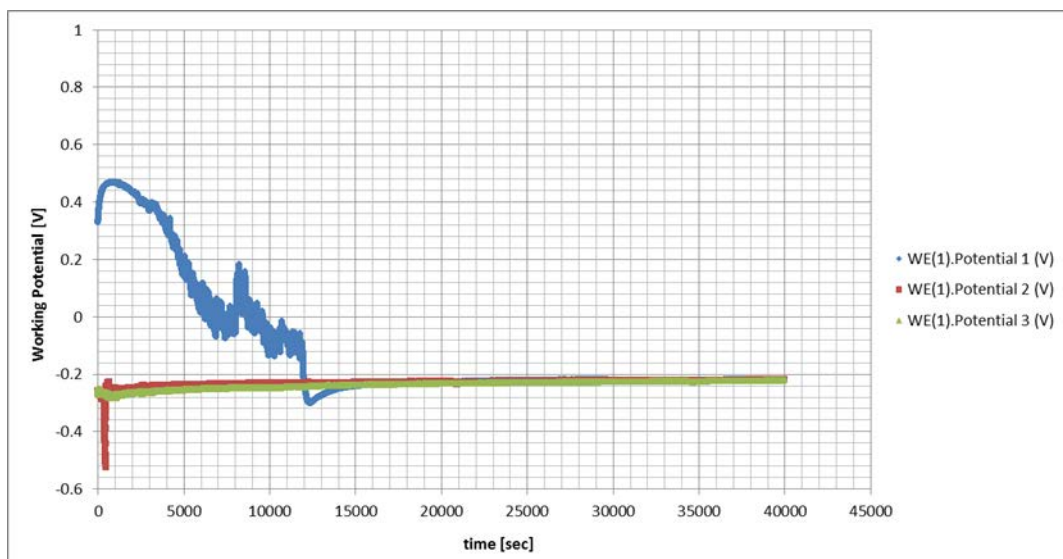


Figure 173: E vs time graphs for the 2.44 wt% Ru sample in 1 M H_2SO_4 + 1% NaCl at 45°C

Appendix H - 1 M HCl solution at 25°C

There was a significant variability observed with the cladded samples in the hydrochloric acid with the consistency being better between the exposed and fresh surface scans than between the three tests carried out. The results can be seen in Figure 174. All of them did however follow the transition shape and seem to reach a passive region, even though the results stretched over a large current density range. During the exposed surface scan the E_{corr} values obtained were spread from -0.35 V (for test 3) to -0.55 V (for test 1) and the passive region was reached from approximately 0 V upwards for all three tests but they were in a large current density range from 3×10^{-6} (for tests 1 and 2) to 2×10^{-2} A/cm² (for test 3) which made any of these tests difficult to use during a comparison with other ruthenium containing samples. The results for the fresh surface scan were equally variable with E_{corr} values ranging from -0.23 V (for test 2) to -0.45 V (for test 1) and achieving passivity in similar current density ranges as the tests during the exposed surface scan even though test 1 results were substantially different almost lying in between the current density values from test 2 and 3 results. No trans-passive region was reached with these tests.

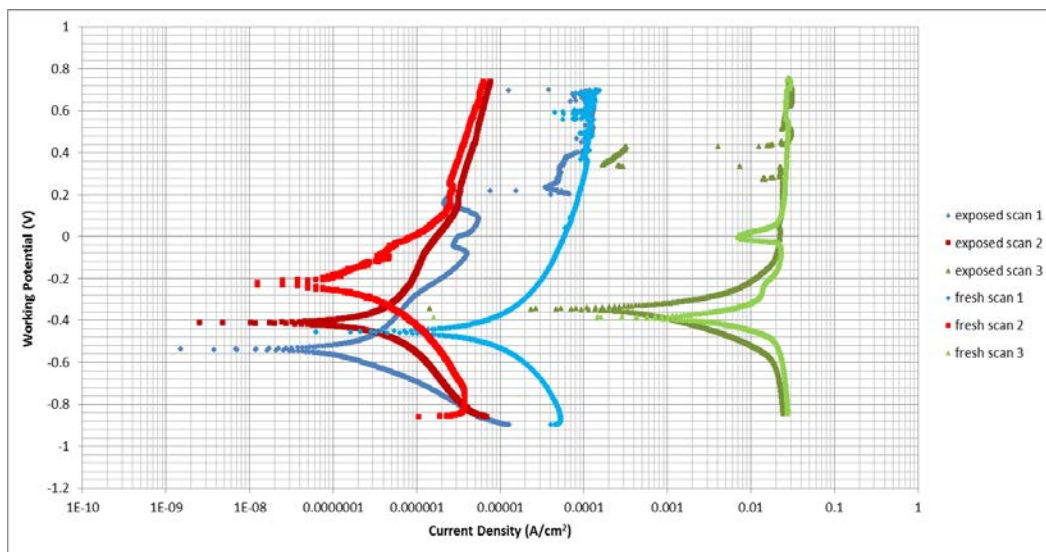


Figure 174: Log i vs E graphs for the 0 wt% Ru sample in 1 M HCl at 25°C

The potential versus time graphs indicated good consistency for all three tests with a variability of 0.06 V and both tests 2 and 3 being close to -0.35 V after the 12 hour period. Stable results were reached with an initial sharp drop to the final OCP value as can be viewed in Figure 175.

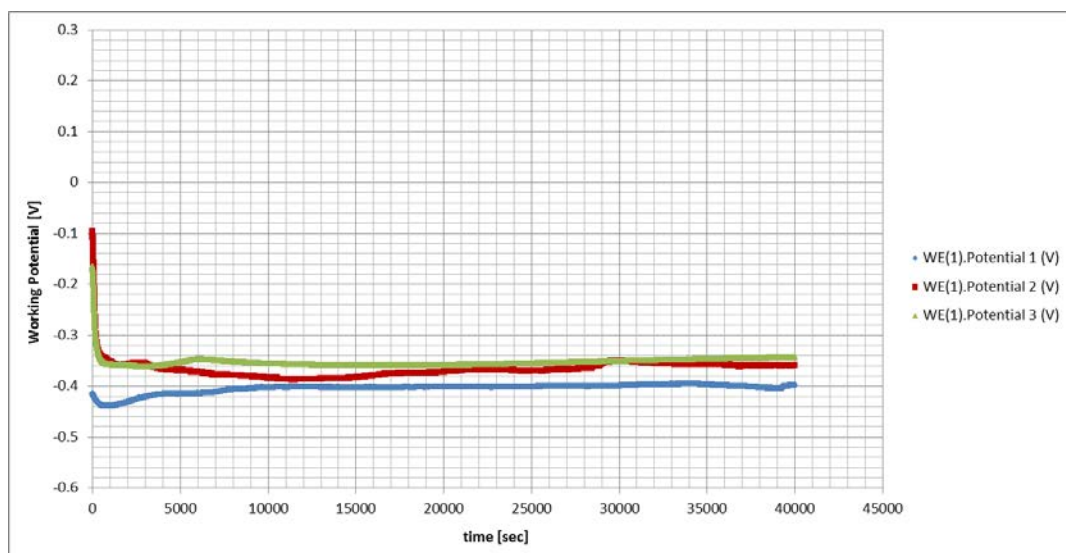


Figure 175: E vs time graphs for the 0 wt% Ru sample in 1 M HCl at 25°C

For the 2.92 wt% Ru samples, test 1 appears to be an outlier as both scans showed values far lower than for tests 2 and 3 which were reasonably comparable which can be seen clearly in Figure 176. During the exposed surface scan, for tests 2 and 3, the results were very consistent having steep Tafel slopes, an E_{corr} value of -0.27 V followed by a reasonably large nose which then turned back to lower current densities at just below 0 V before reaching a passive region starting between 0.14 V (for test 3) and 0.28 V (for test 2) at i_{pass} of $2.5 \times 10^{-2} \text{ A/cm}^2$. Test 1 results during the exposed surface scan showed the transition shape with a broken curve at just above -0.8 V, an E_{corr} value of -0.36 V after which the curve continued to increase in current densities with an increase in potential while variability was again observed at potential above 0.4 V. During the fresh surface scan variability was slightly more pronounced for tests 2 and 3: they followed the same curve in the active region, had a similar E_{corr} value as during the exposed surface scan of -0.25 V which was followed by an active nose and for test 3, a curve back similar to the ones observed during the exposed surface scan before joining that curve going into the passive region while for test 2, cathodic loops were observed in the potential range of the kink back so that it also joined its curve from the exposed surface scan into the passive region. The fresh surface scan for test 1 also exhibited the transition shape with an E_{corr} of -0.23 V which was closer to the ones for tests 2 and 3, it then followed its curve during the exposed surface scan which implies the passive region was at much lower current densities between 1×10^{-5} and $5 \times 10^{-5} \text{ A/cm}^2$.

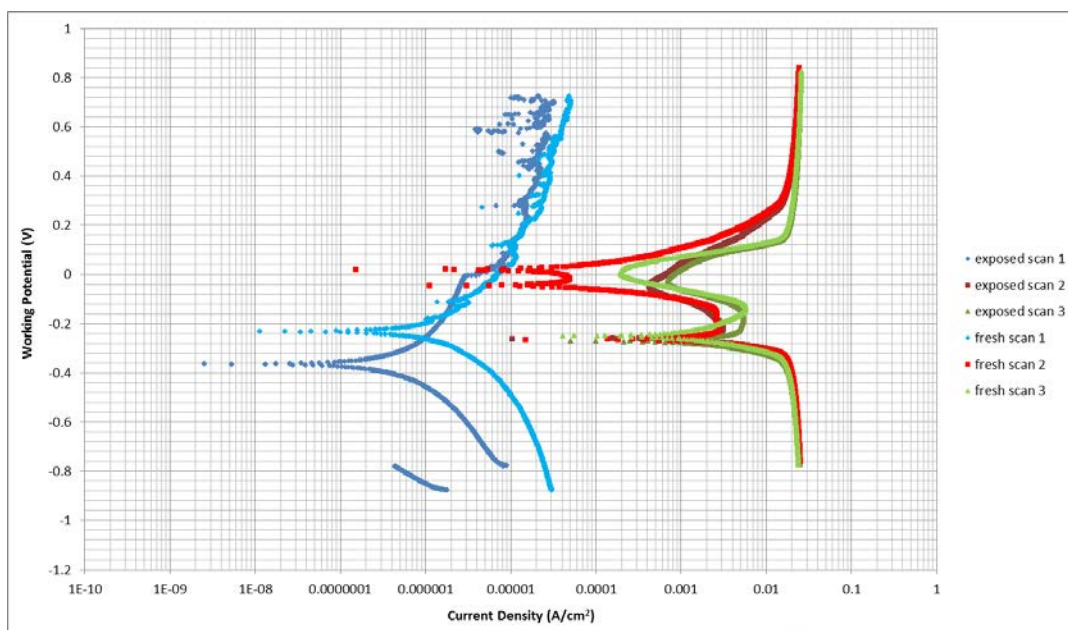


Figure 176: Log i vs E graphs for the 2.92 wt% Ru sample in 1 M HCl at 25°C

The potential over time graphs in Figure 177 also indicated that test 1 was an outlier and tests 2 and 3 curves correspond well with each other, they slowly increased in potential since the start but seemed to have leveled out after the 12 hour period to a value of -0.27 V. Test 1 behaved quite differently dropping quickly in the beginning and levelling off but with some waviness until stabilising at a much lower OCP value of -0.38 V.

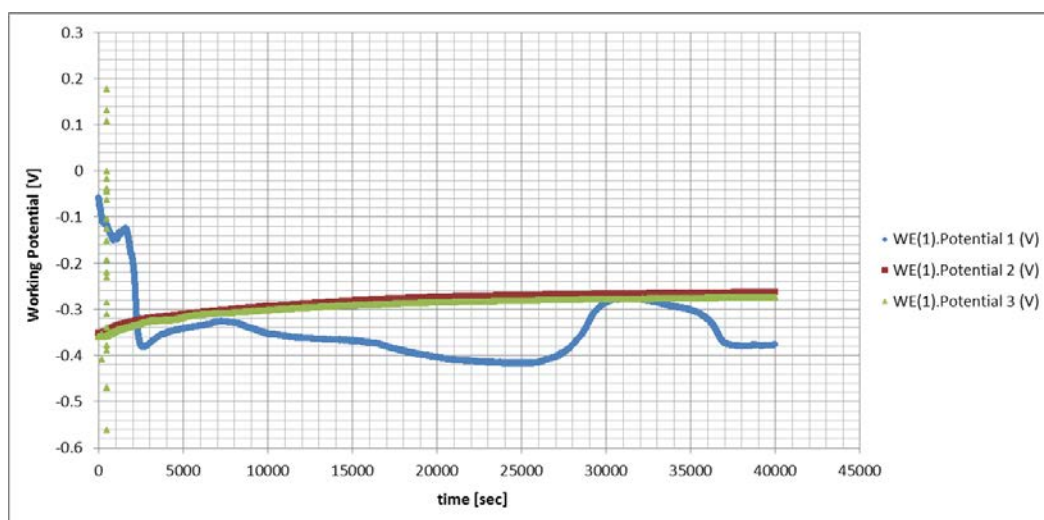


Figure 177: E vs time graphs for the 2.92 wt% Ru sample in 1 M HCl at 25°C

As with the cladded sample without ruthenium, the 2.44 wt% Ru sample showed no great consistency during the anodic scans, in fact, the consistency was better between the exposed and fresh surface scans than between the three tests carried out. The general trend can be observed in Figure 178 and was that they follow a transitional shape and they did seem to reach a passive region, even though the results stretched over a large current density range.

During the exposed surface scan the E_{corr} values obtained were close to each other at -0.41 V (for tests 1 and 2) and -0.34 V (for test 3) but then the shapes did change: test 1 displayed a transition but the values broke up going into the passive region from 0 V and above between 2.5×10^{-6} and 5.5×10^{-6} A/cm², test 2 had the transition shape with its passive region being at the lowest current densities while increasing with increasing potential never going higher than 4×10^{-7} A/cm² and test 3 had an active nose with a small kink back and reaching the passive region at just before 0.2 V at a value of i_{pass} of 3×10^{-2} A/cm². This variability would make any of these tests difficult to use during a comparison with any other samples. The results for the cleaned surface scan were equally variable with E_{corr} values ranging from -0.18 V (for test 1) to -0.38 V (for test 3) and achieving passivity in similar current density ranges as the tests during the exposed surface scans even though test 2 was just a straight vertical line and therefore meaningless for further analysis. No trans-passive region was reached with these tests.

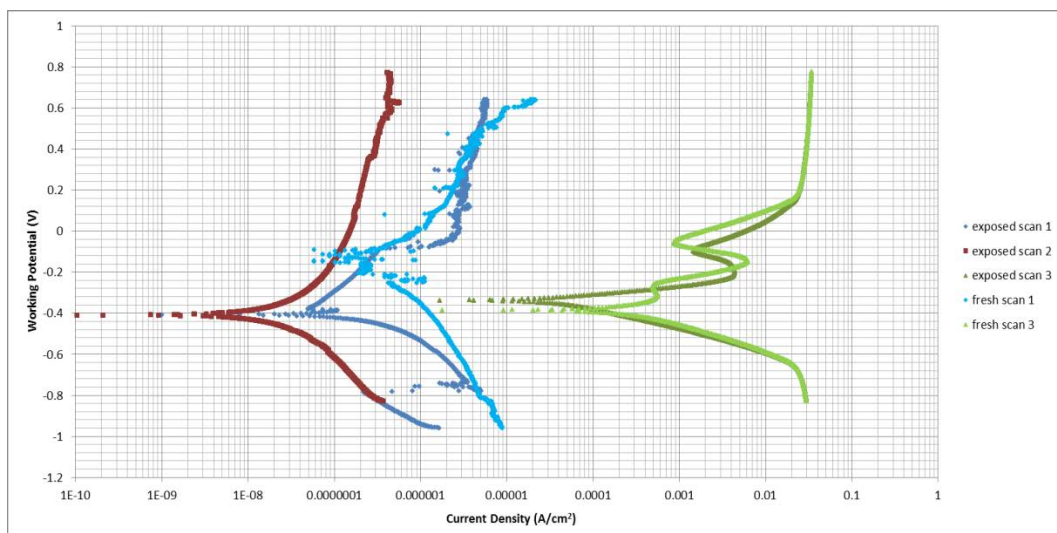


Figure 178: Log i vs E graphs for the 2.44 wt% Ru sample in 1 M HCl at 25°C

The three curves of potential over time in Figure 179 were also variable with the final OCP values of tests 2 and 3 being identical at -0.35 V and the test 1 result being substantially lower. The curves did level out over the 12 hours and stable values were reached.

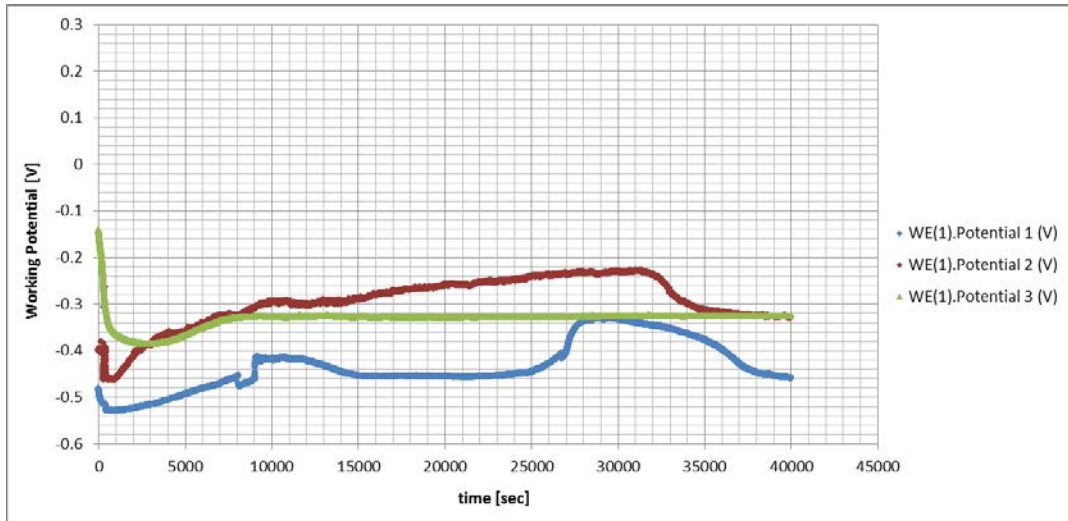


Figure 179: E vs time graphs for the 2.44 wt% Ru sample in 1 M HCl at 25°C

Table 31: Results from the exposed surface scan in 1 M HCl at 25°C

Sample	β_a [mV/dec]	β_c [mV/dec]	E corr Calc [mV]	E corr Obs [mV]	j corr [A/cm ²]	current density at 0.2V [A/cm ²]	i corr [A]	corrosion rate [mm/year]	polarisation resistance [Ω]	OCP [mV]
SS blank (1)	257.820	145.090	-503.370	-518.220	4.214E-08	2.144E-06	1.873E-05	0.00043819	2152300.0	-397.83
SS blank (2)	194.180	116.590	-661.200	-683.230	3.977E-08	1.276E-06	1.768E-08	0.00041358	1789400.0	-516.21
SS blank (3)	105.310	40.810	-326.450	-322.850	2.720E-05	1.197E-02	1.209E-05	0.28287	1056.3	-327.21
SS blank (4)	83.521	44.560	-326.290	-314.240	3.703E-05	1.333E-02	1.646E-05	0.38509	766.5	-328.61
SS blank average	160.21	86.76	-454.33	-459.64	1.61E-05	6.33E-03	1.18E-05	0.167	985881	-392.5
0 wt% Ru (1)	139.810	48.851	-526.010	-539.090	6.831E-08	2.588E-06	1.660E-08	0.00071044	947120.0	-399.81
0 wt% Ru (2)	102.120	76.048	-405.410	-413.120	9.457E-08	3.255E-06	2.298E-08	0.00098349	823780.0	-359.25
0 wt% Ru (3)	123.040	63.131	-343.380	-344.450	4.419E-04	2.424E-02	1.074E-04	4.596	168.7	-345.31
0 wt% Ru average	121.66	62.68	-424.93	-432.22	1.47E-04	8.08E-03	3.58E-05	1.533	590356	-368.1
0.82 wt% Ru (1)	114.890	137.840	-323.540	-328.900	7.286E-07	2.524E-05	2.160E-07	0.0067355	126020.0	-416.05
0.82 wt% Ru (2)	166.560	174.580	-332.000	-346.590	9.521E-08	2.240E-06	2.822E-08	0.00088018	1311800.0	-281.16
0.82 wt% Ru (3)	64.923	100.500	-244.130	-253.630	1.528E-03	1.288E-02	4.529E-04	14.127	37.8	-254.94
0.82 wt% Ru average	115.46	137.64	-299.89	-309.71	5.10E-04	4.30E-03	1.51E-04	4.712	479286	-317.4
2.92 wt% Ru (1)	271.680	279.650	-355.620	-364.880	4.309E-07	1.357E-05	1.165E-07	0.0040013	513830.0	-376.22
2.92 wt% Ru (2)	49.791	84.196	-259.880	-262.840	1.415E-03	7.906E-03	4.275E-04	13.139	31.8	-262.82
2.92 wt% Ru (3)	72.988	71.176	-270.620	-272.320	1.668E-03	1.925E-02	5.038E-04	15.486	31.1	-274.63
2.92 wt% Ru average	131.49	145.01	-295.37	-300.01	1.03E-03	9.06E-03	3.10E-04	9.543	171298	-304.6
2.44 wt% Ru (1)	N/A	N/A	N/A	-407.501	6.492E-09	3.510E-06	N/A	N/A	N/A	-458.65
2.44 wt% Ru (2)	228.050	331.300	-423.530	-411.440	1.870E-08	2.053E-07	3.815E-09	0.00017452	15376000.0	-328.22
2.44 wt% Ru (3)	102.460	46.264	-335.440	-336.990	3.928E-05	2.541E-02	7.950E-06	0.36655	1741.1	-325.84
2.44 wt% Ru average	165.26	188.78	-379.49	-385.31	1.31E-05	8.47E-03	3.98E-06	0.183	7688871	-370.9
4.67 wt% Ru (1)	170.710	127.620	-506.040	-519.210	4.335E-08	1.450E-06	8.774E-09	0.00040633	3614600.0	-397.92
4.67 wt% Ru (2)	230.530	213.400	-299.420	-304.430	2.390E-08	3.500E-07	4.837E-09	0.000224	9949900.0	-249.12
4.67 wt% Ru (3)	237.960	167.740	-305.440	-319.080	7.128E-05	1.080E-02	1.443E-05	0.66811	2961.8	-319.61
4.67 wt% Ru average	213.07	169.59	-370.30	-380.91	2.38E-05	3.60E-03	4.81E-06	0.223	4522487	-322.2

Table 32: Results from the fresh surface scan in 1 M HCl at 25°C

Sample	β_a [mV/dec]	β_c [mV/dec]	E corr Calc [mV]	E corr Obs [mV]	j corr [A/cm ²]	i corr [A]	corrosion rate [mm/year]	polarisation resistance [Ω]
SS blank (1)	152.700	68.401	-441.160	-457.760	2.324E-06	1.033E-06	0.02417	19855.0
SS blank (2)	198.360	292.780	-278.280	-277.100	6.292E-08	2.797E-08	0.00065433	1835800.0
SS blank (3)	114.640	65.546	-358.200	-373.360	9.275E-05	4.124E-05	0.96454	439.2
SS blank (4)	108.380	48.891	-290.690	-338.830	2.200E-05	9.780E-06	0.22877	1496.1
SS blank average	143.52	118.90	-342.08	-361.76	2.93E-05	1.30E-05	0.305	464398
0 wt% Ru (1)	93.685	70.788	-451.170	-456.010	6.671E-06	1.621E-06	0.069375	10803.0
0 wt% Ru (2)	79.576	141.920	-230.690	-226.360	2.089E-07	5.075E-08	0.0021722	436290.0
0 wt% Ru (3)	88.996	76.873	-383.980	-387.100	1.821E-03	4.425E-04	18.938	40.5
0 wt% Ru average	87.42	96.53	-355.28	-356.49	6.09E-04	1.48E-04	6.337	149044
0.82 wt% Ru (1)	N/A	N/A	N/A	-316.772	1.030E-08	N/A	0.00012	N/A
0.82 wt% Ru (2)	133.500	206.940	-179.050	-780.030	2.606E-07	7.725E-08	0.0024094	456210.0
0.82 wt% Ru (3)	49.540	88.318	-252.540	-257.200	4.322E-03	1.281E-03	39.958	10.8
0.82 wt% Ru average	91.52	147.63	-215.80	-451.33	1.44E-03	6.41E-04	13.320	228110
2.92 wt% Ru (1)	208.300	128.640	-206.880	-232.800	2.911E-06	7.869E-07	0.027034	43892.0
2.92 wt% Ru (2)	48.687	79.033	-260.710	-264.940	4.307E-03	1.301E-03	39.994	10.1
2.92 wt% Ru (3)	68.044	125.830	-250.180	-250.860	3.767E-03	1.138E-03	34.978	16.9
2.92 wt% Ru average	108.34	111.17	-239.26	-249.53	2.69E-03	8.13E-04	25.000	14640
2.44 wt% Ru (1)	N/A	N/A	N/A	-89.264	1.795E-07	N/A	0.00209	N/A
2.44 wt% Ru (2)	N/A	N/A	N/A	N/A	N/A	N/A	N/A	N/A
2.44 wt% Ru (3)	125.500	73.353	-371.440	-385.920	1.002E-03	2.029E-04	9.3529	99.1
2.44 wt% Ru average	125.50	73.35	-371.44	-237.59	5.01E-04	2.03E-04	4.677	99
4.67 wt% Ru (1)	235.700	274.380	-346.540	-335.690	2.015E-06	4.079E-07	0.018887	135010.0
4.67 wt% Ru (2)	N/A	N/A	N/A	N/A	N/A	N/A	N/A	N/A
4.67 wt% Ru (3)	147.410	66.646	-345.260	-364.060	3.02E-03	6.11E-04	28.292	32.6
4.67 wt% Ru average	191.56	170.51	-345.90	-349.88	1.51E-03	3.06E-04	14.155	67521